Ascl1 and MyT1 transcriptional networks in vertebrate neurogenesis

Francisca Ferreira de Vasconcelos

Dissertation presented to obtain the Ph.D degree in Developmental Biology

Instituto de Tecnologia Química e Biológica António Xavier | Universidade Nova de Lisboa

Research work coordinated by:

FUNDAÇÃO CALOUSTE GULBENKIAN
Instituto Gulbenkian de Ciência

Oeiras, July, 2015

INSTITUTO
DE TECNOLOGIA
QUÍMICA E BIOLÓGICA
ANTÓNIO XAVIER/UNL

Knowledge Creation

Ascl1 and MyT1 transcriptional networks in vertebrate neurogenesis

Supervisor

Dr Diogo S. Castro (Instituto Gulbenkian de Ciência, Oeiras, Portugal)

Jury members

Dr. Vijay Tiwari (Institute of Molecular Biology, Mainz, Germany)

Dr. Domingos Henrique (Instituto de Medicina Molecular, Lisboa, Portugal)

Dr. Sólveig Thorsteinsdóttir (Faculdade de Ciências da Universidade de Lisboa, Lisboa, Portugal)

Dr. José Bessa (Instituto de Biologia Molecular da Universidade do Porto, Porto, Portugal)

Funding

This dissertation was sponsored by Fundação para a Ciência e Tecnologia fellowships SFRH/BI/33840/2009 and SFRH/BD/51178/2010 and by Instituto Gulbenkian de Ciência.

Aos meus pais

Declaração

Declaro que esta dissertação de candidatura ao grau de Doutor é da minha autoria e que os dados aqui incluídos são o resultado de trabalho original por mim desenvolvido entre Julho de 2010 e Julho de 2015 no laboratório de Neurobiologia Molecular liderado pelo Dr. Diogo S. Castro no Instituto Gulbenkian de Ciência em Oeiras, Portugal. Todas as colaborações estão indicadas em cada capítulo, na secção de Acknowledgements.

Este doutoramento foi realizado no âmbito do Programa Doutoral do Instituto Gulbenkian de Ciência (PhD Programme in Integrative Biomedical Sciences, 2009).

Esta dissertação teve o apoio financeiro da FCT BI nº SFRH/BI/33840/2009 e BD nº SFRH/BD/51178/2010 e dos projectos PTDC/SAU-NEU/100208/2008 e PTDC/NEU-NMC/0315/2012.

Do trabalho desenvolvido durante este período resultaram as seguintes publicações:

Raposo, A.A.S.F.*, **Vasconcelos, F.F.***, Drechsel, D.*, Marie, C., and Johnston, C. (2015). Ascl1 Coordinately Regulates Gene Expression and the Chromatin Landscape during Neurogenesis Article Ascl1 Coordinately Regulates Gene Expression and the Chromatin Landscape during Neurogenesis. Cell Rep. 1544–1556. (* first co-authors)

Vasconcelos, F.F., and Castro, D.S. (2014). Transcriptional control of vertebrate neurogenesis by the proneural factor Ascl1. Front. Cell. Neurosci. *8*, 1–6.

Acknowledgments

I would like to thank to:

My supervisor Diogo Castro for sharing with me his knowledge, for his dedication, enthusiasm and for his time to discuss my work and to address all my doubts and questions; for giving many good ideas to the project and for helping me to mature my scientific reasoning throughout these years.

The molecular neurobiology present and past lab members Vera Teixeira, Alexandre Raposo, Cátia Laranjeira, Pedro Rosmaninho, Diogo Tomaz and Mário Soares and to the wing technician Sónia Rosa for fruitful discussions and enormous support, for being there with me every day, for making me feel I can count on you, for all our endless and funny conversations at lunch time and for the "word of the day" kind of things.

François Guillemot and the members of Guillemot lab, especially Daniela Drechsel, Ben Martynoga and Vydia Ramesh, for having me as a visitor for 4 months in London and for teaching me a lot. It was essential for a good start on the project.

Our collaborators on this project Alessandro Sessa and Vania Broccoli for their willingness on helping us by doing the *in utero* electroporation experiments.

Claudine Chaouiya for her support and helpful discussions as a thesis committee member.

The PhD program directors Thiago Carvalho for having helped me starting and Élio Sucena for having helped me finishing the PhD.

Manuela Cordeiro, Ana Portocarrero and Tatiana Rocha for having made my life much easier regarding bureaucracy.

My very good colleagues and friends at the IGC Leila Shirai, Maria Carvalho, Ana Teresa Avelar, Basia Jezowska, Gastón Guilgur, Maxi di Napoli, Ruben Abreu, Mariana Silva, Pedro Prudêncio, Paulo Navarro and Luís Valente for reagents, protocols,

helpful discussions and for making me feel at home at work. Everyone at the Zheng Ho wing and at the IGC for the good and collaborative environment.

Aos meus bons amigos Mariana Bártolo, Lara Carvalho, Maria Carvalho, Diana Duarte, Leila Shirai, Ana Teresa Avelar, Óscar Silva, Diogo Machado, Ricardo Carvalho e ao Vidro azul, ao Fala com ela, ao Tati, à Ana e ao Lindy hop por, de diferentes maneiras, me trazerem equilíbrio e muitas alegrias.

À minha mãe e ao meu irmão por todo o carinho e por saber que posso sempre contar convosco.

Muito obrigada!

Contents

Figures and tables

List of abbreviations

Act Notch	Activated Notch1
Ascl1	Achaete-scute homolog 1
ATP	Adenosine triphosphate
BAC	Bacterial artificial chromosome
BE	Binding event
bFGF	Basic fibroblast growth factor
bHLH	Basic helix-loop-helix
bp	Base-pair
BP	Basal progenitor
B-RARE	Beta-Retinoic acid response element
BS	Binding site
BSA	Bovine serum albumin
CAG	CMV immediate enhancer/B-actin
Cas9	CRISPR-associated protein-9 nuclease
CBP	CREB-binding protein
Cdk	Cyclin-dependent kinase
ChIP	Chromatin immunoprecipitation
CMV	Cytomegalovirus immediate early promoter
CNS	central nervous system
Co-IP	Co-immunoprecipitation
CoREST	REST corepressor 1
CRISPR	clustered regularly interspaced short palindromic repeats
CRM	Cis-regulatory module
DAPI	4',6-diamidino-2-phenylindol
DHS	Dnase Hypesentitivity site
Dll1	Delta-like 1
DMSO	Dymethyl sulfoxide
DNA	Deoxyribonucleic acid

DNAse-Seq	DNase I hypersensitive sites sequencing
dNTP	Deoxynucleotide mix
Dox	Doxycycline
DSG	Di-succinimidyl-glutarate
Dtx4	Deltex 4
E	Embryonic day
E(Spl)	Enhancer of split genes
EDTA	2-[2-[bis(carboxymethyl)amino]ethyl-(carboxymethyl)amino]acetic acid
EGF	Epidermal growth factor
eGFP	Enhanced green fluorescent protein
EMSA	Electromobility shift assay
EnR	engrailed repressor
FAIRE	Formaldehyde-assisted isolation of regulatory elements
Fbxw7	F-box and WD repeat domain containing 7
FDR	False discovery rate
FFL	Feed-forward loop
GABA	g-aminobutyric acid
GAPDH	Glyceraldehyde-3-phosphate dehydrogenase
GFP	Green fluorescent protein
GO	Gene ontology
GoF	Gain-of-function
HA	Hemagglutinin
HDAC1	Histone deacetylase 1
HDAC2	Histone deacetylase 2
Hes1	Hes Family bHLH Transcription Factor 1
Hes5	Hes Family bHLH Transcription Factor 5
Hes6	Hes family bHLH transcription factor 6
HRP	Horseradish peroxidase

ICC	Immunocytochemisty
INP	Intermediate neural progenitor
IP	Immunoprecipitation
IQR	Interquartile range
IRES	Internal ribosomal entry site
LEF1-B-CAT	fusion protein of LEF1 and B-catenin
LGE	Lateral ganglionic eminence
LoF	Loss-of-function
LSD1	Lysine-specific demethylase 1
Luc	Luciferase
LY	LY 411-575
Maml1	Mastermind-like protein 1
MCS	Multicloning site
mRNA	Messenger RNA
MyT1 (aka NZF2)	Myelin transcription factor (neural zinc finger 2)
MyT1Like (aka NZF1 or MyT1L)	myelin transcription factor 1-like (aka neural zinc finger 1)
MyT3 (aka NZF3 or St18)	myelin transcription factor 3 (aka neural zinc finger 3 or suppression of tumorigenicity 18)
MZ	Mantle zone
NaDOC	Sodium deoxycholate
NE	Neuroepithelium
NeuroD4	Neuronal differentiation 4
Neurog1	Neurogenin 1
Neurog2	Neurogenin 2
Neurog3	Neurogenin 3
NICD	Notch1 intracellular domain
NLS	Nuclear localization signal
NS/PC	Neural stem/progenitor cells
NSC	Neural stem cell

ON	Overnight
ORF	Open reading frame
PDGR	Platelet-derived growth factor
PEI	Polyethylenimine
PFA	Paraformaldehyde
Pit-1	POU domain, class 1, transcription factor 1
PLP	Protein Lipid protein
PNS	Peripheral nervous system
Prox1	Prospero homeobox 1
PWM	Positional weight matrix
qPCR	Real-time quantitative polymerase chain reaction
RBPJ	Recombination signal binding protein for immunoglobulin kappa J region
RG	Radial glia
RNA Pol II	RNA polymerase II
RNA-Seq	RNA sequencing (Whole Transcriptome Shotgun Sequencing)
RT	Room temperature
RT-qPCR	Reverse transcriptase quantitative real-time PCR
rtTA	Reverse tetracycline-controlled transactivator
SD	Standard deviation
SDS	Sodium dodecyl sulfate
Shh	Sonic hedgehog
shRNA	Short-hairpin RNA
Sin3B	SIN3 transcription regulator family member B
Su(H)	Suppressor of hairless
SVZ	Subventricular zone
TALEN	Transcription activator-like effector nucleases
TAM	4-hydroxy-tamoxifen
TATA	5’-TATAAAA-3’ core DNA sequences
TBP	TATA-binding protein

Tel	Telencephalon
TGF-B	Transforming growth factor beta
TIC	Transcription initiation complex
TRE	Tetracycline responsive element
TSS	Transcriptional start site
VP16	VP16 activation domain
VZ	Ventricular zone
WB	Western blot
XASH-3	Xenopus acheate-scute homolog 3
X-NGNR-1	Xenopus neurogenin 1
ZF	Zinc finger

Summary

Neurogenesis is a cell differentiation program in which neural stem cells undergo extensive and precise changes in gene expression on their way to become neurons. These changes are controlled to large extent by the activity of lineage-specific transcription factors. Of particular importance are classical proneural factors, such as Ascl1 (a.k.a. Mash1), that function as master regulators of the neurogenic program and are both required and sufficient to induce a complete program of neuronal differentiation.

In spite of its pivotal role during neurogenesis, relatively little is still known on how Ascl1 functions to regulate gene expression and, in particular, on how its activity is regulated by, and impacts the chromatin landscape. In the first part of this thesis (Chapter 2), we used a cellular model of neurogenesis to investigate the reciprocal interactions between Ascl1 and the chromatin landscape, when promoting neuronal differentiation. We found that Ascl1 functions as a pioneer transcription factor, targeting not only regions of accessible but also of closed chromatin. In addition, binding of Ascl1 to DNA precedes a local increase in chromatin accessibility at the regulatory regions of its target genes and consequent induction of gene expression during neuronal differentiation. Our work provides the first direct link between Ascl1 regulation of gene expression and local changes in chromatin landscape.

The induction of neuronal differentiation by Ascl1 requires the concomitant downregulation of Notch signalling in differentiating neural stem/progenitor cells, despite of incoming input signal from neighbouring cells. In the second part of this thesis (Chapter 3), we investigated the function of the zinc-finger transcription factor MyT1, an Ascl1 target gene previously implicated in the regulation of Notch signalling. For that, we combined functional assays in mouse NS cell cultures and in the developing mouse telencephalon, with the genome-wide characterization of its

transcriptional targets. We found that MyT1 potentiates Ascl1-driven neuronal differentiation by counteracting the inhibitory effect of Notch signalling. MyT1 functions globally as a repressor of gene expression and represses many canonical Notch target genes. In particular, MyT1 represses Hes1 expression in the presence of active Notch through a mechanism that involves direct DNA binding and competition with RBPJ. Our work provides the first molecular basis for MyT1 function during neurogenesis, revealing a regulatory step whereby Ascl1 functions to suppress Notch signalling in a cell-autonomous manner in differentiating neuronal progenitors.

Overall, our work contributed to a better understanding of the transcriptional and epigenetic mechanisms that control the progression of vertebrate neurogenesis.

Sumário

A neurogénese é um programa de diferenciação celular no qual as células estaminais do sistema nervoso sofrem alterações extensas e precisas na expressão genética para darem origem a neurónios. Estas alterações são controladas em grande medida pela actividade de factores de transcrição de linhagens celulares específicas. De particular importância são os factores de transcrição proneurais, tais como o Ascl1 (também conhecido por Mash1), que funcionam como reguladores mestre do programa de neurogénese e são necessários e suficientes para induzir um programa de diferenciação neuronal completo.

Apesar do seu papel essencial durante a neurogénese, sabe-se ainda relativamente pouco sobre como o Ascl1 regula a expressão genética e, em particular, como é que a sua actividade é regulada por e regula a conformação da cromatina. Na primeira parte da tese (Capítulo 2), utilizámos um modelo celular de neurogénese para investigar as interacções recíprocas entre o Ascl1 e a conformação da cromatina num contexto em que está a promover a diferenciação neuronal. Nós descobrimos que o Ascl1 funciona como um factor de transcrição pioneiro, sendo capaz de reconhecer os seus locais regulatórios não só em regiões acessíveis da cromatina mas também em regiões em que a cromatina está fechada. Além disso, a ligação do Ascl1 ao ADN precede um aumento local da acessibilidade da cromatina nas regiões regulatórias dos seus genes-alvo e consequente indução da expressão genética durante a diferenciação neuronal. O nosso trabalho revela, assim, a primeira ligação directa entre a regulação da expressão genética pelo Ascl1 e alterações locais na conformação da cromatina.

A indução da diferenciação neuronal pelo Ascl1 requer a repressão concomitante da via de sinalização Notch nas células em diferenciação, apesar de receberem sinais activadores das células vizinhas. Na segunda parte da tese (Capítulo 3) , investigámos

a função do factor de transcrição MyT1, um gene-alvo do Ascl1 previamente implicado na regulação da via de sinalização Notch. Para isso, combinámos ensaios funcionais em culturas de células estaminais do sistema nervoso e no telencéfalo em desenvolvimento do ratinho, com a caracterização à escala genómica dos seus genes-alvo. Nós descobrimos que o MyT1 potencia a diferenciação neuronal induzida pelo Ascl1 por contrariar o efeito inibitório da via de sinalização Notch. O MyT1 funciona globalmente como um repressor da expressão genética e reprime muitos genes-alvo da via de sinalização Notch. Em particular, o MyT1 é capaz de reprimir a expressão do Hes1 na presença de Notch activo através de um mecanismo que envolve ligação directa ao ADN e competição com o RBPJ. O nosso trabalho fornece, assim, a primeira base molecular para a função do MyT1 durante a neurogénese, revelando um passo regulatório no qual o Ascl1 suprime a via de sinalização Notch na célula em que é expresso durante a diferenciação neuronal de células progenitoras do sistema nervoso.

Globalmente, o nosso trabalho contribui para um conhecimento mais aprofundado dos mecanismos transcricionais e epigenéticos que controlam a progressão da neurogénese em vertebrados.

Chapter 1 – **General Introduction**

1. Vertebrate neurogenesis

The vertebrate central nervous system (CNS), which comprises the brain and the spinal cord, is built from three main cell types: neurons, oligodendrocytes and astrocytes. Neurons are electrically excitable cells that are connected through synapses and process and transmit information through electrical and chemical signals. Oligodendrocytes produce myelin and provide support and insulation to axons of neurons, contributing to efficient synaptic transmission. Astrocytes serve to maintain the chemical environment necessary for proper neurochemical signaling. These three cell types are assembled into intricate networks called neural circuits that encode and decode information for a wide variety of behaviors, including sensory perception, motor control, memory, attention, or language (Purves D, Augustine GJ, Fitzpatrick D, et al., 2001).

The development of the central nervous system in mouse starts at the end of gastrulation around E7.5 with the formation of the neural plate from a specialized region of the ectoderm. As development proceeds, the neural plate folds inward forming a groove (neural groove) and bringing the neural folds together. Upon complete fusion of the neural folds, a hollow-like structure is formed which constitutes the neural tube (Figure 1. 1). The neural tube is the structure that will give rise to the entire CNS. Three vesicles form at the rostral-most part of the neural tube: the prosencephalon mesencephalon and rhombencephalon (from rostral to caudal), which later will give rise to the forebrain, midbrain and hindbrain structures of the adult brain, respectively. Two of these three vesicles further subdivide into secondary vesicles: the prosencephalon originates the telencephalon and the diencephalon, and the rhombencephalon originates the metencephalon and the myelencephalon.

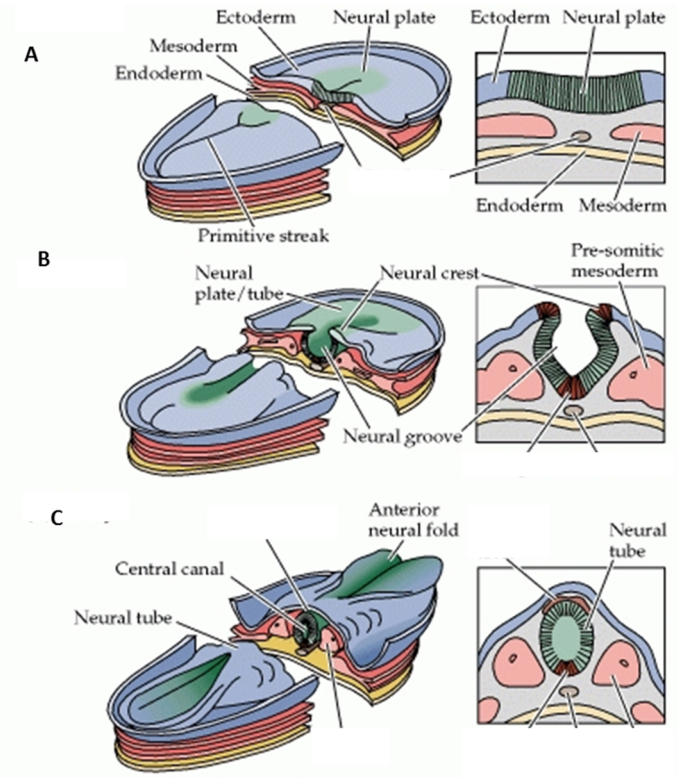

Figure 1. 1 Formation of the neural tube during embryonic development.

On the left side are dorsal views of the embryo at several different stages of early development; each boxed view on the right is a midline cross section through the embryo at the same stage. (A) During late gastrulation and early neurulation, the neural plate is formed from a specialized region of the ectorderm. (B) As neurulation proceeds, the neural plate begins to fold at the midline, forming the neural groove and ultimately the neural tube. (C) Once the edges of the neural plate meet in the midline, the neural tube is complete. Figure adapted from (Purves D, Augustine GJ, Fitzpatrick D, et al. 2001).

The telencephalon will generate the cerebral hemispheres; the diencephalon will consist of the thalamus, hypothalamus, in addition to other structures; the mesencephalon will originate the colliculi, tegmentum and cerebral peduncles; the metencephalon will become the pons; and the cerebellum and the myelencephalon the medulla. The caudal-most end of the neural tube will give rise to the spinal cord (Figure 1. 2) (Gilbert, 2000).

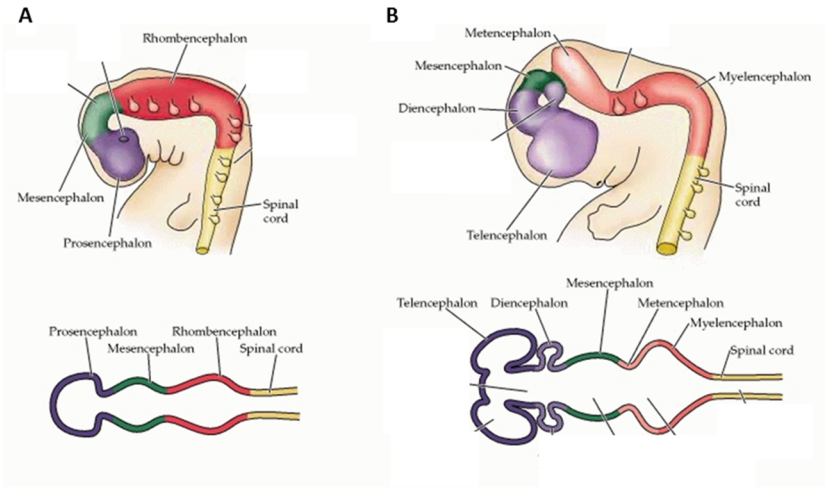

Figure 1. 2 Regional specification of the embryonic central nervous system.

(A) Early in gestation, the neural tube becomes subdivided into the prosencephalon (at the anterior end of the embryo), mesencephalon, and rhombencephalon. The spinal cord differentiates from the more posterior region of the neural tube. On the right is a longitudinal section of the neural tube, showing the position of the major brain regions. (B) Further development distinguishes the telencephalon and diencephalon from the prosencephalon; two other subdivisions — the metencephalon and myelencephalon — derive from the rhombencephalon. These subregions give rise to the rudiments of the major functional subdivisions of the brain, while the spaces they enclose eventually form the ventricles of the mature brain. At right is a longitudinal section of the embryo at the developmental stage shown in (B). Figure adapted from (Purves D, Augustine GJ, Fitzpatrick D, et al. 2001).

At the very early stage, the telencephalon is constituted by a mono-layer of epithelial cells called neuroepithelium. The neuroepithelium lines at the surface of the telencephalic ventricles and defines the first germinal layer of the telencephalon, the ventricular zone (VZ). Neuroepithelial (NE) cells are multipotent neural stem cells (NSCs) and have the capacity to, directly or indirectly, generate neurons, oligodendrocytes and astrocytes. These cells exhibit apical-basal polarity and extend processes to the apical (ventricular) and basal (pial) surfaces of the telencephalon. The nuclei of these cells migrate back and forth along the apical-basal axis, a stereotypical movement called interkinetic nuclear migration. This movement is

correlated with the progression of cell cycle: neuroepithelial cells migrate towards the basal surface during G1 and S phases, move apically during G2 phase and enter M phase at the apical surface. The asynchronous movement of the nuclei of neuroepithelial cells results in a pseudostratified epithelium (Götz and Huttner, 2005). At early stages of telencephalic development, these cells divide symmetrically, originating two daughter NE cells and, thus, contribute to the expansion of the NSC pool. At the onset of neurogenesis, around E11, NE cells switch to asymmetric cell division, originating one daughter NE cell and a radial glial (RG) cell. As NE cells, RG cells keep the epithelial and interkinetic nuclear migration characteristics but, contrary to NE cells, RG cells express glial markers and divide most of the times asymmetrically. In this asymmetric cell division, a RG cell gives rise to another RG cell and another type of neural progenitor cell, or, in a minority of the cases, directly to a post-mitotic neuron. This new type of progenitor cell is called intermediate neural progenitor (INP). The INPs lose the epithelial phenotype of their mother RG cells, retract their apical and basal processes, delaminate from the ventricular surface of the telencephalon and translocate their nuclei to the basal surface of the VZ (therefore they are often referred to as basal progenitors (BPs)), forming a new germinal layer, the subventricular zone (SVZ). INPs typically divide symmetrically and undergo either a limited number of proliferative cell divisions or a neurogenic division, originating two INPs or two neurons, respectively. Although more restricted in potential than RG cells, INPs, in addition to neurons, may also give rise to oligodendrocytes and astrocytes. Upon cell-cycle exit, newborn neurons migrate from the germinal layers towards the basal-most end of the telencephalon, constituting the mantle zone (MZ) (Figure 1. 3) (Franco and Müller, 2013; Götz and Huttner, 2005; Hevner, 2006; Kriegstein and Alvarez-Buylla, 2009).

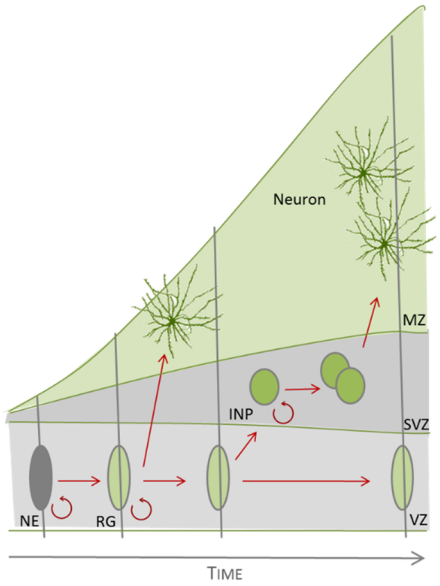

Figure 1. 3 Development of the neuronal lineage in the mouse embryonic telencephalon.

Neuroepithelial (NE) cells in early development divide symmetrically to generate more neuroepithelial cells. As the developing brain epithelium thickens, NE cells elongate and convert into radial glial (RG) cells. RG divide asymmetrically to, directly or indirectly through intermediate neural progenitor (INP) cells, generate neurons. Early post-mitotic neurons migrate radially to the MZ. NE, neuroepithelial cell; RG, radial glia; INP, intermediate neuronal progenitor cell; VZ, ventricular zone; SVZ, subventricular zone; MZ, mantle zone. Figure adapted from (Kriegstein & Alvarez-Buylla 2009).

More recently, new sub-types of neural progenitors have been identified both in the ventral and dorsal telencephalon. There are cases of radial glial cells that retain either the apical, the basal or both processes but divide sub-apically and are termed apical, basal or bipolar sub-apical radial glia, respectively. Also, there are intermediate progenitor cells that divide apically at the VZ and are termed apical intermediate progenitors or short neural precursors. These progenitor sub-types contribute to further amplification of the lineage or to direct generation of neurons at the VZ, respectively (Farkas and Huttner, 2008; Florio and Huttner, 2014; Haubensak et al., 2004; Miyata et al., 2004; Noctor et al., 2004; Pilz et al., 2013)

In the telencephalon, different populations of progenitor cells mature into specific subtypes of neurons. The majority of the dorsal progenitors develop into glutamatergic projection neurons that will populate the neocortex, while the majority of ventral progenitors (located in the medial, lateral and caudal ganglionic eminences) originate GABAergic inhibitory interneurons that will comprise the basal ganglia (striatum and globus pallidus) and the amygdala. The GABAergic interneurons that populate the neocortex, the hypothalamus and the olfactory bulb are also formed from ventral progenitors that reach those areas by tangential migration (Temple, 2001). As development proceeds, neural stem cells undergo temporal identity transitions and switch from a neurogenic phase to a gliogenic phase, first giving rise to astrocytes at late embryonic stages and later to oligodendrocytes at early post-natal stages (Rowitch and Kriegstein, 2010).

The proper number of cells and cell types within the CNS is, thus, ultimately dependent on the fine balance between proliferation and differentiation of neural stem cells during development (Götz and Huttner, 2005; Hevner, 2006; Kriegstein and Alvarez-Buylla, 2009).

2. Transcriptional regulation

Cell differentiation programs, such as neurogenesis, have been associated with extensive gene expression changes. These gene expression changes are tightly orchestrated both in space and time and involve intricate interactions between the transcriptional regulation machinery and DNA (Buecker and Wysocka, 2012; Macarthur et al., 2009; Ong and Corces, 2011). Below, we will focus on the general mechanisms of transcriptional regulation in metazoans.

The regulation of gene expression starts with the recruitment the transcriptional initiation complex (TIC) to the core promoter located approximately 50bp up- or downstream of the transcription start site (TSS) of a gene. The TIC is composed by

the pre-initiation and Mediator complexes and RNA polymerase II (RNA Pol II). The first member of this complex to be recruited recognizes a specific sequence in the core promoter region (in about 24% of the human genes, the TATAAA sequence - TATA-box - is bound by the member of the TIC complex TFIID) and promotes the subsequent recruitment of the other components of the TIC (Ong and Corces, 2011; Yang et al., 2007). The assembly of this TIC at the core promoter is the first pre-requisite for gene transcription, however, it is insufficient to elicit efficient and robust transcriptional events. For that to occur, the additional intervention of cis-regulatory modules (CRMs) and associated transcription factors (TFs) is required. CRMs can be located up- or downstream of the TSS, are typically 200-1000bp in length and contain multiple binding sites (BS) for sequence-specific TFs. They can be categorized according to their distance relative to the TSS of a gene: proximal promoters are usually located 20-200bp away from the TSS, while distal enhancers can be located up to 1 Mbp away from the TSS (Bulger and Groudine, 2011; Levine et al., 2014; Spitz and Furlong, 2012). Binding of an appropriate combination of sequence-specific TFs and additional co-activators to an enhancer region promotes looping of the enhancer to the core promoter regions (Ong and Corces, 2011). Sequence-specific TFs and co-activators stabilize Mediator complex proteins at the DNA and, hence, this DNA looping event facilitates the initiation and elongation of transcription, resulting in a net increase of the transcription rate (Levine, 2010). Alternatively, these sequence-specific TFs may also work as repressors and inhibit transcription. Therefore, enhancers function as information integration hubs of the input of multiple TFs. To add to this complexity, multiple enhancers can control the expression of a single gene at the same or at distinct cellular contexts (Buecker and Wysocka, 2012) (Figure 1. 4).

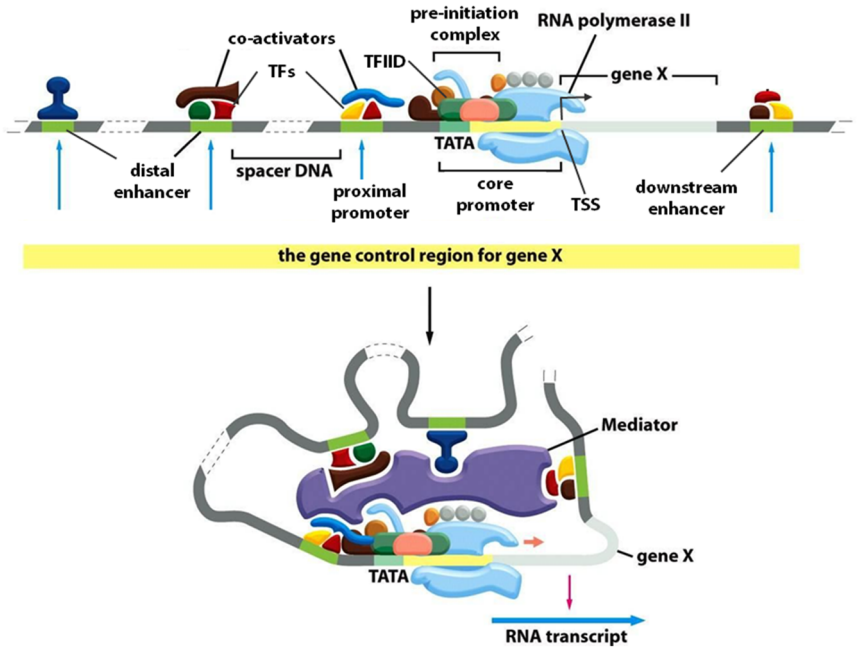

Figure 1. 4 Transcriptional regulation in metazoans.

Diagram of a typical metazoan gene illustrating the complex interactions among cis-acting modules and trans-acting factors regulating gene expression. TATA, 5'-TATAAAA-3' core DNA sequence; TF, sequence-specific transcription factor; TSS, transcription start site. Figure adapted from (Alberts B, Johnson A, Lewis J 2008).

During embryonic development, this uncoupling of TF activity on regulatory enhancers from transcription initiation machinery at core promoters greatly contributed to the multiplication of the possible modes of regulation of developmental genes and to the establishment of spatio-temporal specificity of gene expression by lineage-specific TFs (Buecker and Wysocka, 2012; Levine, 2010; Ong and Corces, 2011; Spitz and Furlong, 2012; Yang et al., 2007).

3. Chromatin accessibility and transcription factor binding

In eukaryotes, genomic DNA is tightly coiled around octamers of four core histones (H2A, H2B, H3 and H4), forming nucleosomes. Stretches of nucleosomes are the basic

components of chromatin. Chromatin can be further compacted and form higher-order structures. When in its most compact form, chromatin is defined as heterochromatin and is usually associated with gene silencing. When lightly packed, chromatin is defined as euchromatin and is usually associated with active gene expression. The chromatin structure is dynamic and is affected by the distribution of covalent modifications of histone tails (such as methylation and acetylation), the presence of specific histone variants at the nucleosomes and by DNA methylation. Within euchromatin domains, DNA may be more tightly bound to histones, in a compact state which is resistant to cleavage by enzymes such as DNAse I (often referred to as "closed chromatin"). CRMs within such regions may not be accessible for TF binding. Thus, chromatin conformation restricts TF activity. Conversely, TFs activity may also impact on chromatin structure by promoting the recruitment of histone modifying enzymes such as histone deacetylases (HDAC), acetyltransferases (HAT), methylases or methyltransferases (reviewed in (Calo and Wysocka, 2013; Ong and Corces, 2011)). In some cases, a TF can recognize its binding sites in the context of nucleosome-bound DNA, and is called a "pioneer TF". Pioneer TFs often initiate the targeting of a silent regulatory region and recruit histone modifiers, histone remodelers and histone variants (H2A.Z) that induce a higher turn-over rate of nucleosomes than canonical histones. This recruitment may be direct or indirect through the recruitment of additional intermediate TFs. These activities result in reduced nucleosomal occupancy and in the relaxation of the chromatin structure, originating "open chromatin" which is nuclease hypersensitive, facilitating subsequent activation of expression of the associated target genes (Calo and Wysocka, 2013; Iwafuchi-doi and Zaret, 2014; Zaret and Carroll, 2011). Alternatively, the binding of a pioneer factor may have no direct effect on chromatin structure or on the recruitment of other factors but may contribute for gene expression by simply reducing the number of subsequent TF binding events required for gene activation.

Some lineage-specific TFs have been shown to possess pioneering activity (the ability to bind to "closed" chromatin) such as GATA and FOXA during hepatocyte development, or Oct4, Sox2 and Klf4 during reprogramming of fibroblasts into induced pluripotent stem cells (Lupien et al., 2008; Takahashi and Yamanaka, 2006). Although pioneer factor activity has been shown to be dominant over chromatin structure, the pioneer factor binding to DNA is not completely independent of the state of chromatin at its target sites. Pioneer factor binding may be enhanced by the presence of H2A.Z at nucleosomes and by DNA hypomethylation, although these are not strictly necessary. On the contrary, pioneer factor binding may be blocked by epigenetic marks deposited in certain regions of heterochromatin, such as H3K9me2/3. Importantly, these features do not necessarily affect equally the binding of all pioneer factors (Iwafuchi-doi and Zaret, 2014).

Overall, the combination of the plethora of transcription factors available and their reciprocal interactions with the chromatin will determine which genes will be expressed or become or remain silent as cells progress through differentiation programs as neurogenesis.

4. Proneural transcription factors

Proneural genes have been first identified in Drosophila melanogaster and are divided into two families: the achaete-scute family (achaete, scute, lethal of scute, and asense) and the atonal family (atonal, amos and cato). They encode basic helix-loop-helix (bHLH) transcription factors and are both necessary and sufficient to promote the generation of committed neural precursors from ectodermal tissue in Drosophila melanogaster (neural specification). In this organism, the acheate-scute gene family induces the formation of neurons in the CNS and of external sensory organs in the peripheral nervous system (PNS), while the atonal family is required for

the formation of photoreceptor, chordotonal organs and olfactory sense organs (Bertrand et al., 2002).

In mouse, a large number of genes show homology to Drosophila achaete-scute and atonal families. Ascl1 (formerly known as Mash1) and Ascl2 are homologous to Drosophila achaete-scute genes. The atonal-related family has further diversified and is divided into distinct subclasses: Neurogenins (Neurog1, Neurog2, Neurog3), NeuroD (NeuroD, NeuroD2, Math2, Math3) and Math1-like (Math1, Math5, Math6) (Bertrand et al., 2002). It is important to note that, contrary to Drosophila melanogaster where proneural factors are required for neural specification, the proneural function in vertebrates is associated with the step of commitment of neural precursors towards the neuronal fate (Bertrand et al., 2002). Of the above listed neural bHLH genes, only a few are expressed in neural stem/progenitor cells (NS/PCs) and display such proneural function in vertebrates. Most significant are Ascl1 and Neurogenin1/2/3, while Math1/5 are expressed in a relatively small number of lineages. Members of the NeuroD family are only expressed in post-mitotic neurons, while Ascl2 is not expressed in the developing nervous system (Klisch et al., 2011; Nieto et al., 2001; Wang et al., 2001).

Vertebrate proneural TFs are pivotal regulators of neurogenesis, as they are both required and sufficient to induce a complete program of neuronal differentiation. Gain of function (GoF) of proneural factors in neural stem/progenitor cells typically results in cell-cycle exit and rapid neuronal differentiation (Berninger et al., 2007; Farah et al., 2000; Geoffroy et al., 2009; Nakada et al., 2004). In line with their master regulatory role in the neuronal lineage, recent studies have revealed the ability of Ascl1 to reprogram various non-neural somatic cells (e.g., fibroblasts) into induced neurons (Berninger et al., 2007; Chanda et al., 2014; Karow et al., 2012; Vierbuchen et al., 2010).

Proneural gene function has been particularly well studied in the developing telencephalon, where Ascl1 and Neurogenins are expressed in the germinal layers, in largely non-overlapping regions. Ascl1 is the only classical proneural gene expressed in the ventral telencephalon, while Neurog1/2 are exclusively expressed in the dorsal domain (Figure 1. 5).

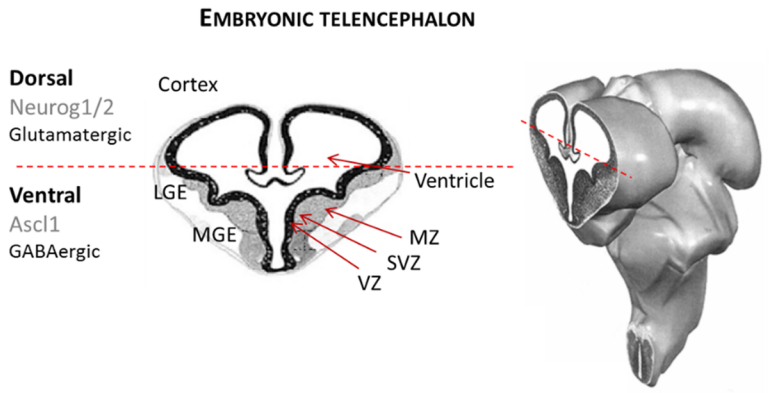

Figure 1. 5 The developing mouse telencephalon.

A coronal view of the embryonic telencephalon (~E14.5) showing its division into dorsal and ventral regions. The main neuronal type generated in the germinal layers of the ventral domain are GABAergic interneurons, while in dorsal domain are Glutamatergic projection neurons. Proneural transcription factors that are associated with dorsal (Neurog1, Neurog2) and ventral (Ascl1) cell fate specification are indicated. MZ, mantle zone; SVZ, subventricular zone; VZ, ventricular zone; LGE, lateral ganglionic eminence; MGE, medial ganglionic eminence.

The only exception is a subset of VZ and SVZ cortical progenitors in which Ascl1 and Neurog2 are transiently co-expressed (Britz et al., 2006). Loss of Ascl1 leads to depletion of GABAergic interneurons in the basal ganglia, cortex and olfactory bulb, all of which are derived from the ventral telencephalic progenitors where Ascl1 is expressed (Casarosa et al., 1999; Guillemot and Joyner, 1993; Horton et al., 1999). Neurog1 and Neurog2 expression pattern in the dorsal telencephalon are widely overlapping. Neurog1 mutant mice display mild defects on neurogenesis presumably due to functional redundancy with Neurog2. Single Neurog2 and double

Neurog1:Neurog2 mutant mice lack glutamatergic projection neurons in the dorsal telencephalon (Fode et al., 1998, 2000; Ma et al., 1998; Schuurmans et al., 2004).

In addition to their common proneural function, proneural factors play distinct roles in neuronal sub-type specification, an idea supported by several lines of evidence. Loss of Neurog1/2 in the cortex results in upregulation of Ascl1 and concomitant ectopic expression of GABAergic neuronal markers (Parras et al., 2002; Schuurmans et al., 2004). Accordingly, replacement experiments of Neurog2 by Ascl1 in the dorsal telencephalon lead to the re-specification of cortical progenitors into the GABAergic subtype (Parras et al., 2002). On the other hand, misexpression of Neurog2 in the ventral telencephalon via *in utero* electroporation instructs a glutamatergic identity, as assessed by the ectopic expression of various markers (Mattar et al., 2008). Therefore, these experiments suggests that Ascl1 contributes to the specification of GABAergic interneurons, while Neurog1/2 contribute the specification of the glutamatergic neurons. However, curiously, reprogramming of mouse embryonic fibroblasts by overexpression of a combination of 3 TFs which includes Ascl1 results in the generation of neurons mainly of the glutamatergic subtype (Vierbuchen et al., 2010). Overall, these data suggest that the neurogenic function of proneural genes can be uncoupled from its subtype specification function and that this latter function might be highly cell-context dependent.

Strikingly, mouse genetics also revealed that proneural factors promote neuronal cell fate commitment at the expenses of an alternative glial fate. Ascl1 single and Ascl1:Neurog2 double knock-out animals exhibit premature astrocytic differentiation at expense of neurons, suggesting that these proneural TFs have a role on the inhibition of the astrocytic fate (Nieto et al., 2001; Tomita et al., 2000). Neurog1 has been shown to actively suppress astrocyte differentiation via DNA-binding independent mechanisms. In one hand, Neurog1 has been shown to suppress the expression of the astrocyte differentiation gene GFAP by physically interacting and

sequestering CBP/p300/Smad1 activator complex and, on the other hand, by preventing the activation of the Jak-Stat3 pathway that functions upstream of this transcriptional complex (Sun et al., 2001). Finally, Ascl1 has also been implicated in the specification of oligodendrocyte progenitor cells in the ventral telencephalon by mechanisms that are still poorly understood (Nakatani et al., 2013; Parras et al., 2004).

Proneural genes encode basic helix-loop-helix (bHLH) transcription factors. The basic region is required for binding to DNA and confers specificity for binding site recognition. However, binding to DNA requires dimerization between two bHLH factors. This is mediated by the HLH domain which is constituted by two α-helices separated by a loop region. Ascl1 and Neurogenin1/2 typically form heterodimers with another class of bHLH proteins called E-proteins (E12/47, HEB, E2-2) and together recognize the core DNA binding motif CANNTG (E-box) (Bertrand et al., 2002; Johnson et al., 1992). Different dimers recognize distinct E-box sequences, with Ascl1/E-protein heterodimers preferentially binding to the CAGSTG E-box variant. Evidence mostly from transcriptional assays on individual target genes suggests proneural factors function as transcriptional activators (Bertrand et al., 2002; Borromeo et al., 2014; Castro et al., 2006).

5. The interplay between proneural factors and the Notch signaling pathway

While driving neuronal differentiation, proneural factors also activate the Notch signaling pathway in neighboring progenitors, transiently inhibiting their differentiation. This hallmark of proneural factors function is highly reminiscent of the “lateral inhibition” model initially described in invertebrates (Bertrand et al., 2002; Louvi and Artavanis-Tsakonas, 2006). In the mouse telencephalon, proneural factors directly activate the transcription of Notch ligands, such as Delta-like1 (Dll1) (Castro et al., 2006; Henke et al., 2009), which interact with a transmembrane Notch

receptor in neighboring cells. This event results in the proteolytic cleavage by gamma-secretase and in the release of the Notch intracellular domain (NICD) from the cell membrane into the nucleus. Once in the nucleus, NICD forms a transcriptional activator complex with the DNA-binding TF RBPJ (also known as RBPJk or CBF1) and additional co-activators, such as Mastermind-like protein 1 (Maml1). When Notch signaling is inactive, RBPJ is involved in a default repression mechanism by recruiting co-repressors (Kageyama et al., 2007). Interestingly, recent data portraits a more dynamic view of the association of RBPJ (or its Drosophila melanogaster homolog Su(H)) with many of its target genes, where this occurs exclusively or is enhanced in the presence of active NICD (Castel et al., 2013; Kopan and Ilagan, 2009; Krejčí and Bray, 2007). RBPJ preferentially binds to TGGGAA DNA binding motifs (TC-box). The most well established canonical Notch targets in vertebrate neurogenesis are the Hes genes Hes1 and Hes5 and Hes-related genes Hesr1 and Hesr2 (also known as Hey/Herp genes) (Iso et al., 2003; Jarriault et al., 1995; Kageyama et al., 2008; Louvi and Artavanis-Tsakonas, 2006). Hes1/5 genes encode bHLH transcriptional repressors that bind to the regulatory regions of proneural genes and repress their expression, thereby inhibiting neuronal differentiation (Kageyama et al., 2005) (Figure 1. 6). Thus, proneural and Notch networks are highly intertwined and mutually regulate each other in neural stem/progenitor cells. This allows proneural factors to induce neuronal differentiation and, in parallel, by activating Notch signaling on adjacent cells, keep them – even if only transiently – undifferentiated. Such lateral inhibition results in proneural factors being expressed in a “salt-and-pepper” pattern in the telencephalon and ensures the generation of appropriate numbers and subtypes of neurons during embryonic development (Kageyama et al., 2008; Vasconcelos and Castro, 2014).

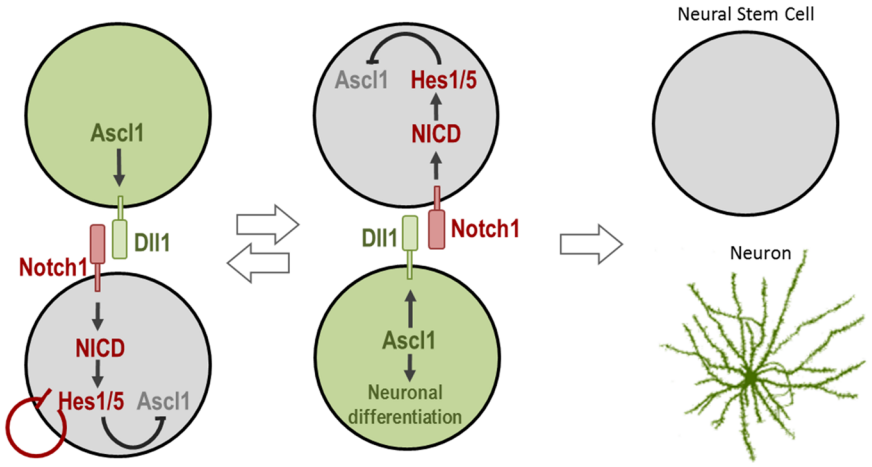

Figure 1. 6 An interplay between proneural and Notch signaling at the onset of neuronal differentiation.
Notch signaling is activated through cell-cell interaction, between Dll1 ligand-expressing and Notch receptor-expressing cells. Proneural factors (such as Ascl1) induce the expression of Dll1, which activate Notch signaling in neighboring cells. Upon activation, the Notch intracellular domain (NICD) is cleaved and translocated to the nucleus where it will form a complex with the TF RBPJ and induce the expression of downstream genes such as Hes1/5. Hes1/5 repress the expression of target genes including proneural genes, such as Ascl1, thereby inhibiting neuronal differentiation. At the onset of neurogenesis, Hes genes expression is permanently downregulated and Ascl1 expression remains sustained. Figure adapted from (Kageyama et al. 2008).

In mouse telencephalon, Hes1 is expressed from E7.5 onward while Ascl1, Dll1 and Hes5 are expressed only from E8-8.5. Therefore, initial expression of Hes1 seems to be independent of Notch signaling. It becomes dependent on Notch signaling only after Ascl1 induction of Dll1 expression. Contrarily, Hes5 expression in this region is dependent on Notch signaling from its start and is often used as a reporter of Notch signaling activity (Kageyama et al., 2008). Evidence from mouse genetics supports a role for Notch signaling in the maintenance of neural stem cells. In conditional RBPJ and Hes genes mutant mice, the NSCs in the neuroepithelium are normally formed but are not properly maintained and precociously upregulate proneural genes and differentiate into early-born neurons (Gao et al., 2009; Hatakeyama et al., 2004; Ishibashi et al., 1995; Ohtsuka et al., 1999; Tomita et al., 1996). Single Hes1 and Hes5

mutant animals exhibit a mild phenotype, while double Hes1/Hes5 mutant animals exhibit a more severe phenotype, suggesting functional redundancy. In accordance with the mouse mutant models, gain-of-function of Notch signaling by misexpression of Hes1, Hes5 or NICD by *in utero* electroporation in the mouse telencephalon results in the maintenance of radial glia and inhibition of neuronal differentiation (Gaiano et al., 2000; Ohtsuka et al., 2001).

Contrary to the wealth of knowledge on the cellular functions of Notch pathway in neural development, little is known on the identity of its downstream transcriptional program. Recently, a genome-wide study of Notch/RBPJ transcriptional program identified additional direct targets of the Notch/RBPJ complex in the mouse cortical tissues, highlighting its important role on the maintenance of the neural stem cell state (through regulation of Pax6, Sox2, Tlx, Msi1, Id4) and suggesting cross-regulatory interactions between Notch and members of the Wnt (Fzd2/8/9, etc), Shh (Smo, Gli2/3, Cdon) and Hippo (Tead2, Yap1) signaling pathways (Li et al., 2012).

6. A revised view of lateral inhibition in vertebrates

Hes1 can repress its own expression by directly binding to sequence-specific BSs (CACNAG aka N-box) in its own promoter, thus forming a negative feedback loop. This phenomenon, associated with short-lived Hes1 transcript and protein, and when in the presence of an activating signal, results in self-sustained oscillations of its expression (Kageyama et al., 2007). Oscillating expression of Hes1 was shown to occur in a variety of cell types (e.g. presomitic mesoderm, fibroblasts, myoblasts and embryonic stem cells) (Hirata et al., 2002; Kobayashi et al., 2009). In neural stem cells, it was recently shown that Hes1 and Hes5 also oscillate with a 2-3h periodicity and that these oscillations are asynchronous between neighboring progenitor cells and require mutual activation of Notch signaling (Imayoshi et al., 2013; Shimojo et al., 2008). Since Hes genes directly repress proneural genes expression, oscillation of

Hes1 results in oscillation in anti-phase of both Ascl1 and Neurog2, as shown by a variety of approaches (Imayoshi et al., 2013; Shimojo et al., 2008) (Figure 1. 7). Most notably was the generation of transgenic mice bearing a bacterial artificial chromosome (BAC) containing the Ascl1 regulatory regions upstream of Ascl1 fused to either luciferase or green fluorescent protein (GFP). In this system the activity of the reporter monitors the expression of the endogenous Ascl1 protein and inhibition of Notch signaling with a gamma-secretase inhibitor results in stable expression of Ascl1 (Imayoshi et al., 2013).

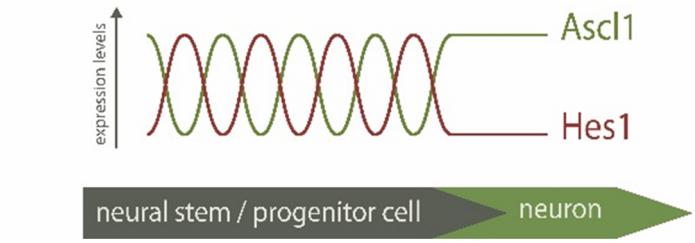

Figure 1. 7 Distinct modes of expression of Ascl1 and Hes1 during neuronal differentiation.

Hes1 and Ascl1 oscillate in NS/PCs. The inverse correlation of expression of Hes1 and Ascl1 proteins suggest these TFs oscillate out-of-phase. At the onset of neuronal differentiation, Hes1 expression is extinguished and Ascl1 expression becomes sustained. Figure from (Vasconcelos & Castro 2014).

In light of these recent findings, the "salt-and-pepper" expression pattern of proneural and Hes factors is perceived as a snapshot of a dynamic mode of expression in an asynchronous population of neural progenitors. According to these revised view, proneural factors are expressed in neural progenitors at different stages of differentiation, and not only in committed progenitors that will soon become post-mitotic, as was previously thought.

7. Consequences of oscillatory and sustained modes of expression

Time-lapse imaging of individual neural progenitors in culture revealed that, during neuronal differentiation, Ascl1 and Neurog2 switch from an oscillatory to a sustained

mode of expression after the last cell division, followed by the expression of the neuronal marker doublecortin 6-8h later (Imayoshi et al., 2013; Shimojo et al., 2008). This suggests that the ability of proneural factors to trigger differentiation may require their expression to be sustained. Such a causal link was established upon the use of an optogenetic approach where Ascl1 expression is regulated by a light-switchable transactivator (Imayoshi et al., 2013). This system was introduced in an Ascl1 null background to investigate the consequence of different dynamics of Ascl1 expression induced by different pulses of light. Sustained expression of Ascl1 for a minimum of 6h resulted in cell-cycle exit and neuronal differentiation. By contrast, an oscillatory mode of Ascl1 expression with periodicity of 3h increased NSCs proliferation, compensating the lower proliferation rate observed in Ascl1 null progenitors in culture. The same approach used in slice cultures of the dorsal telencephalon, where Ascl1 is usually expressed at very low levels, reached similar conclusions (Imayoshi et al., 2013). These findings explain why most evidence based on Ascl1 gain-of-function (sustained expression) points to a role in promoting differentiation (with concomitant cell cycle-exit) of progenitors (Castro et al., 2006; Geoffroy et al., 2009; Nakada et al., 2004) and only Ascl1 LoF analyses reveal its pro-proliferation function. Knock-down of Ascl1 levels upon expression of sequence-specific short-hairpin RNA (shRNA) and acute knock-out of Ascl1 in the ventral telencephalon decreased proliferation of NS cells in culture and caused premature cell-cycle withdrawal of both VZ and SVZ progenitors, respectively (Castro et al., 2011; Pilz et al., 2013). Taken together, all the above observations result in a model whereby different modes of Ascl1 expression sequentially promote proliferation and differentiation of progenitors along the neuronal lineage, with the concomitant activation of partially distinct transcriptional programs. This reconciles the classical view of Ascl1 as a differentiation factor with the fact that this proneural factor is expressed mostly in cycling cells.

The functional relevance of these TF oscillations in NS cells is still a matter of debate. One possibility is that the concerted Ascl1 and Hes1 oscillations regulate cell cycle progression. As above mentioned, Ascl1 oscillations induces proliferation of NS cells (Imayoshi et al., 2013). On the other hand, sustained high levels of Hes1 promote dormancy/quiescence of both neural stem cells located in the boundaries between different brain structures in the embryo and adult NSCs, while variable levels of Hes1 and Ascl1 are compatible with proliferation of NSCs (Andersen et al., 2014; Baek et al., 2006; Castella et al., 2000; Hartman et al., 2004; Parras et al., 2004; Sang et al., 2008). Thus, the two modes of expression may in principle allow for the activation of distinct sets of transcriptional targets by the same TF, allowing for the coordinate regulation of distinct cellular functions (e.g. proliferation vs. differentiation).

As opposed to steady-state expression mode, asynchronous oscillatory expression may generate heterogeneity of response of an apparently homogeneous progenitor cell population to a given input signal (Mengel et al., 2010) and, thus, another possibility is that Ascl1 and Hes1 oscillatory expression may provide means to prevent simultaneous differentiation of all NSCs upon an inductive signal and the exhaustion of the NSC pool. In addition, many more parameters of an oscillatory expression mode (e.g., period, amplitude) can in theory be subjected to regulation, as compared to steady-state expression mode, and that may be particularly suitable for the integration of multiple inputs that regulate cell fate determination.

In addition to Hes1 and proneural factors, Olig2 expression has also been shown to oscillate in NSCs, in a Hes1-dependent manner by a mechanism yet to be characterized. When expressed in a sustained manner, each of these three TFs induces a different cell fate: Ascl1 induces the generation of neurons; Hes1 induces quiescence of NSCs at early stages and the generation of astrocytes at later stages of development; and Olig2 induces the generation of oligodendrocytes (Imayoshi et al., 2013). It was suggested that variable expression of lineage-specific transcription

factors in hematopoietic progenitors may represent a state of plasticity or metastability in cell fate commitment that is progressively stabilized during the differentiation program, highlighting the possibility of multiple entry-points into lineage specification (Pina et al., 2012; Sequerra et al., 2013). Thus, a third possibility is that, as in hematopoiesis, the oscillatory expression of these lineage-specific TF in NS cells allow for the establishment of multipotency and, at the same time, allow a rapid upregulation of any of the three oscillating fate determinants upon inductive signals (Imayoshi and Kageyama, 2014).

It was proposed that sustained balanced expression of fate determinant TFs accounts for the establishment of pluripotency during induced pluripotent stem cell (iPSC) formation (Shu et al., 2013). Therefore, another way to maintain multipotency of NSCs could be through a similar mechanism. However, it has been proposed that oscillatory expression would be more robust to stochastic fluctuating stimuli when compared to a multipotent state based on a balanced coexpression of all three TFs ("seesaw" models based on oscillatory expression or on balanced coexpression of three cell fate determinants, respectively) (Imayoshi and Kageyama, 2014).

8. Neural stem cell cultures

Mammalian neurogenesis is not a synchronized process at a cell population level and studies investigating the mechanistic basis of TF function at a genome-wide scale are difficult to perform in the developing embryo. An alternative is the use of adherent cultures of multipotent neural stem cells derived from embryonic stem cells or embryonic neural precursors (Conti et al., 2005; Pollard et al., 2006). Different from *in vivo* NSCs, these NS cells in culture proliferate independently of the stem cell niche and undergo mainly symmetric cell divisions in the presence of the mitogens EGF and FGF2 and are, therefore, readily expandable in culture (Conti et al., 2005; Pollard et al., 2006). These cultures provide us reliable models to study neurogenesis, without

the confounding effects of cellular heterogeneity characteristic of other cellular models, such as neurospheres. NS-5 cells are clonogenic, genetically stable NS cells which were derived from mouse embryonic stem cells. After prolonged expansion in the presence of mitogens, they remain able to differentiate efficiently into neurons and astrocytes *in vitro* and upon transplantation into the adult brain (Conti et al., 2005). In proliferating culture conditions, endogenous Ascl1 regulates a progenitor program that functions to maintain cell proliferation, whereas overexpression of Ascl1 leads to efficient cell cycle exit and neuronal differentiation preferentially towards the GABAergic subtype (Castro et al., 2011).

9. Genome-wide techniques for the study of transcription factor binding, chromatin modifications and gene expression

In the last decades, there has been a profound change in the way regulation of gene expression is studied with the advent of genome-wide techniques for studying TF binding, epigenetic regulation and gene expression (reviewed in (Farnham, 2009; Furey, 2012; Schones and Zhao, 2008)) (Figure 1. 8). Transcription factor binding at a genome-wide scale can be studied by chromatin immunoprecipitation (ChIP) of TFs followed by identification of the associated genomic DNA fragments by microarrays (ChIP-on-chip) or by high-throughput sequencing (ChIP-Seq) or other variants of these techniques (Farnham, 2009; Park, 2009). Gene expression analysis can be performed at a genome-wide level by gene expression microarrays or by high-throughput sequencing of the total mRNAs (RNA-Seq). The combination of location analysis of a TF with expression profiling upon TF perturbation allow for the genome-wide identification of the direct targets of that TF in a given cellular context. Aspects of the chromatin state, such as DNA methylation or histone modifications can be assessed using bisulphite sequencing, ChIP of methylated DNA or of histone modifications. In addition, techniques such as formaldehyde-assisted isolation of

regulatory elements or DNase I hypersensitive assay followed by high-throughput sequencing (FAIRE-Seq and DNAse-Seq, respectively) allow for the genome-wide mapping of chromatin accessible regions (non-nucleosomal DNA).

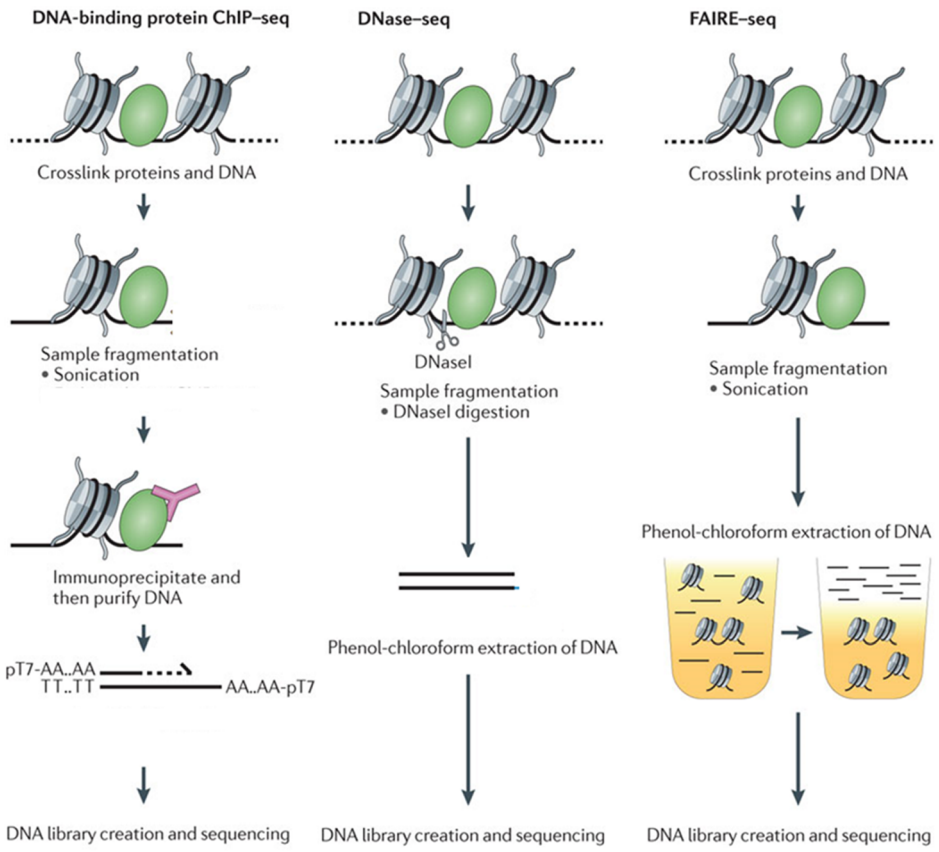

Figure 1. 8 An overview of ChIP-Seq, DNase-Seq and FAIRE-Seq experiments.

Simplified schematics of the main steps for each technique are shown. (A) Chromatin immunoprecipitation followed by sequencing (ChIP-Seq) for DNA-binding proteins, such as transcription factors. (B) DNase-Seq relies on digestion by the DNase I nuclease to identify regions of nucleosome-depleted (open) chromatin. (C) Formaldehyde-assisted identification of regulatory elements (FAIRE-Seq) similarly identifies nucleosome-depleted regions by isolating naked DNA that is not crosslinked to nucleosomes. Figure adapted from (Furey 2012).

Briefly, DNAse-Seq is based on the preference of DNAse I endonuclease to digest genomic DNA with low (as opposed to high) nucleosome occupancy. The 5‘ end of a sequence tag generated by DNase-Seq indicates the site of a DNase I digestion event

and regions of enrichment in digestion events are identified as DNAse hypersensitivity sites (DHS) (Song and Crawford, 2010). In FAIRE, the chromatin is cross-linked with the use of formaldehyde, cells are lysed and DNA is sonicated. The DNA fragments are then subjected to phenol-chloroform extraction and the fraction of DNA with low nucleosome occupancy is preferentially retained in the aqueous phase which is subsequently sequenced. Although distinct preferences have been described for each technique in the identification of distal or proximal regulatory regions, the two techniques have been shown to yield largely overlapping results on a genome-wide basis (Song et al., 2011) and both provide means of analyzing chromatin accessibility (reviewed in (Furey, 2012; Schones and Zhao, 2008)). Overall, the combined use of all these genome-wide approaches has been instrumental for the characterization of transcriptional regulatory networks.

10. Aims of this thesis

The main aim of the current thesis was to investigate the transcriptional mechanisms that regulate vertebrate neurogenesis. There are two major components to this work that are the subject of two results chapters:

First, we investigated the reciprocal interactions between Ascl1 and the chromatin landscape when promoting the neuronal differentiation of NS cells in culture (Chapter 2).

Second, we focused on one of the identified neurogenic targets of Ascl1, the zinc-finger TF MyT1. We combined functional and genomic approaches to characterize MyT1 function during neurogenesis, and understand how it interacts with the Notch signaling pathway to promote neuronal differentiation (Chapter 3).

Finally, we discuss the implications of our findings and present a general overview which includes ongoing work and an outlook of the future (Chapter 4).

References

Alberts B, Johnson A, Lewis J, et al. (2008). Molecular Biology of the Cell (New York: Garland Science).

Andersen, J., Urbán, N., Achimastou, A., Ito, A., Simic, M., Ullom, K., Martynoga, B., Lebel, M., Göritz, C., Frisén, J., et al. (2014). A Transcriptional Mechanism Integrating Inputs from Extracellular Signals to Activate Hippocampal Stem Cells. Neuron *83*, 1085–1097.

Baek, J.H., Hatakeyama, J., Sakamoto, S., Ohtsuka, T., and Kageyama, R. (2006). Persistent and high levels of Hes1 expression regulate boundary formation in the developing central nervous system. Development *133*, 2467–2476.

Berninger, B., Costa, M.R., Koch, U., Schroeder, T., Sutor, B., Grothe, B., and Götz, M. (2007). Functional properties of neurons derived from *in vitro* reprogrammed postnatal astroglia. J. Neurosci. *27*, 8654–8664.

Bertrand, N., Castro, D.S., and Guillemot, F. (2002). Proneural genes and the specification of neural cell types. Nat. Rev. Neurosci. *3*, 517–530.

Borromeo, M.D., Meredith, D.M., Castro, D.S., Chang, J.C., Tung, K.-C., Guillemot, F., and Johnson, J.E. (2014). A transcription factor network specifying inhibitory versus excitatory neurons in the dorsal spinal cord. Development 1–10.

Britz, O., Mattar, P., Nguyen, L., Langevin, L.M., Zimmer, C., Alam, S., Guillemot, F., and Schuurmans, C. (2006). A role for proneural genes in the maturation of cortical progenitor cells. Cereb. Cortex *16*.

Buecker, C., and Wysocka, J. (2012). Enhancers as information integration hubs in development: Lessons from genomics. Trends Genet. *28*, 276–284.

Bulger, M., and Groudine, M. (2011). Functional and mechanistic diversity of distal transcription enhancers. Cell *144*, 327–339.

Calo, E., and Wysocka, J. (2013). Modification of Enhancer Chromatin: What, How, and Why? Mol. Cell *49*, 825–837.

Casarosa, S., Fode, C., Guillemot, F., Inserm, C., Louis, U., Cédex, I., and Strasbourg, C.U. De (1999). Mash1 regulates neurogenesis in the ventral telencephalon. *534*, 525–534.

Castel, D., Mourikis, P., Bartels, S.J.J., Brinkman, A.B., Tajbakhsh, S., and Stunnenberg, H.G. (2013). Dynamic binding of RBPJ is determined by notch signaling status. Genes Dev. *27*, 1059–1071.

Castella, P., Sawai, S., Nakao, K., Wagner, J. a, and Caudy, M. (2000). HES-1 repression of differentiation and proliferation in PC12 cells: role for the helix 3-helix 4 domain in transcription repression. Mol. Cell. Biol. *20*, 6170–6183.

Castro, D.S., Skowronska-Krawczyk, D., Armant, O., Donaldson, I.J., Parras, C., Hunt, C., Critchley, J. a, Nguyen, L., Gossler, A., Göttgens, B., et al. (2006). Proneural bHLH and Brn

proteins coregulate a neurogenic program through cooperative binding to a conserved DNA motif. Dev. Cell *11*, 831–844.

Castro, D.S., Martynoga, B., Parras, C., Ramesh, V., Pacary, E., Johnston, C., Drechsel, D., Lebel-Potter, M., Garcia, L.G., Hunt, C., et al. (2011). A novel function of the proneural factor Ascl1 in progenitor proliferation identified by genome-wide characterization of its targets. Genes Dev. *25*, 930–945.

Chanda, S., Ang, C.E., Davila, J., Pak, C., Mall, M., Lee, Q.Y., Ahlenius, H., Jung, S.W., Südhof, T.C., and Wernig, M. (2014). Generation of Induced Neuronal Cells by the Single Reprogramming Factor ASCL1. Stem Cell Reports *3*, 282–296.

Conti, L., Pollard, S.M., Gorba, T., Reitano, E., Toselli, M., Biella, G., Sun, Y., Sanzone, S., Ying, Q.-L., Cattaneo, E., et al. (2005). Niche-independent symmetrical self-renewal of a mammalian tissue stem cell. PLoS Biol. *3*, e283.

Farah, M.H., Olson, J.M., Sucic, H.B., Hume, R.I., Tapscott, S.J., and Turner, D.L. (2000). Generation of neurons by transient expression of neural bHLH proteins in mammalian cells. Development *127*, 693–702.

Farkas, L.M., and Huttner, W.B. (2008). The cell biology of neural stem and progenitor cells and its significance for their proliferation versus differentiation during mammalian brain development. Curr. Opin. Cell Biol. *20*, 707–715.

Farnham, P.J. (2009). Insights from genomic profiling of transcription factors. Nat. Rev. Genet. *10*, 605–616.

Florio, M., and Huttner, W.B. (2014). Neural progenitors, neurogenesis and the evolution of the neocortex. Development *141*, 2182–2194.

Fode, C., Gradwohl, G., Morin, X., Dierich, A., LeMeur, M., Goridis, C., and Guillemot, F. (1998). The bHLH protein NEUROGENIN 2 is a determination factor for epibranchial placode-derived sensory neurons. Neuron *20*, 483–494.

Fode, C., Ma, Q., Casarosa, S., Ang, S.L., Anderson, D.J., and Guillemot, F. (2000). A role for neural determination genes in specifying the dorsoventral identity of telencephalic neurons. Genes Dev. *14*, 67–80.

Franco, S.J., and Müller, U. (2013). Shaping Our Minds: Stem and Progenitor Cell Diversity in the Mammalian Neocortex. Neuron *77*, 19–34.

Furey, T.S. (2012). ChIP–seq and beyond: new and improved methodologies to detect and characterize protein–DNA interactions. Nat. Rev. Genet. *13*, 840–852.

Gaiano, N., Nye, J.S., and Fishell, G. (2000). Radial glial identity is promoted by Notch1 signaling in the murine forebrain. Neuron *26*, 395–404.

Gao, F., Zhang, Q., Zheng, M.-H., Liu, H.-L., Hu, Y.-Y., Zhang, P., Zhang, Z.-P., Qin, H.-Y., Feng, L., Wang, L., et al. (2009). Transcription factor RBP-J-mediated signaling represses the

differentiation of neural stem cells into intermediate neural progenitors. Mol. Cell. Neurosci. *40*, 442–450.

Geoffroy, C.G., Critchley, J. a., Castro, D.S., Ramelli, S., Barraclough, C., Descombes, P., Guillemot, F., and Raineteau, O. (2009). Engineering of dominant active basic helix-loop-helix proteins that are resistant to negative regulation by postnatal central nervous system antineurogenic cues. Stem Cells *27*, 847–856.

Gilbert, S. (2000). Developmental Biology.

Götz, M., and Huttner, W.B. (2005). The cell biology of neurogenesis. Nat. Rev. Mol. Cell Biol. *6*, 777–788.

Guillemot, F., and Joyner, a L. (1993). Dynamic expression of the murine Achaete-Scute homologue Mash-1 in the developing nervous system. Mech. Dev. *42*, 171–185.

Hartman, J., Müller, P., Foster, J.S., Wimalasena, J., Gustafsson, J.-A., and Ström, A. (2004). HES-1 inhibits 17beta-estradiol and heregulin-beta1-mediated upregulation of E2F-1. Oncogene *23*, 8826–8833.

Hatakeyama, J., Bessho, Y., Katoh, K., Ookawara, S., Fujioka, M., Guillemot, F., and Kageyama, R. (2004). Hes genes regulate size, shape and histogenesis of the nervous system by control of the timing of neural stem cell differentiation. Development *131*, 5539–5550.

Haubensak, W., Attardo, A., Denk, W., and Huttner, W.B. (2004). Neurons arise in the basal neuroepithelium of the early mammalian telencephalon: a major site of neurogenesis. Proc. Natl. Acad. Sci. U. S. A. *101*, 3196–3201.

Henke, R.M., Savage, T.K., Meredith, D.M., Glasgow, S.M., Hori, K., Dumas, J., MacDonald, R.J., and Johnson, J.E. (2009). Neurog2 is a direct downstream target of the Ptf1a-Rbpj transcription complex in dorsal spinal cord. Development *136*, 2945–2954.

Hevner, R.F. (2006). From Radial Glia to Pyramidal-Projection Neuron. *33*, 33–50.

Hirata, H., Yoshiura, S., Ohtsuka, T., Bessho, Y., Harada, T., Yoshikawa, K., and Kageyama, R. (2002). Oscillatory expression of the bHLH factor Hes1 regulated by a negative feedback loop. Science *298*, 840–843.

Horton, S., Meredith, a, Richardson, J. a, and Johnson, J.E. (1999). Correct coordination of neuronal differentiation events in ventral forebrain requires the bHLH factor MASH1. Mol. Cell. Neurosci. *14*, 355–369.

Imayoshi, I., and Kageyama, R. (2014). bHLH Factors in Self-Renewal, Multipotency, and Fate Choice of Neural Progenitor Cells. Neuron *82*, 9–23.

Imayoshi, I., Isomura, A., Harima, Y., Kori, H., Miyachi, H., Fujiwara, T., Ishidate, F., and Kageyama, R. (2013). Oscillatory Control of Factors Determining Multipotency and Fate in Mouse Neural Progenitors.

Ishibashi, M., Ang, S.L., Shiota, K., Nakanishi, S., Kageyama, R., and Guillemot, F. (1995). Targeted disruption of mammalian hairy and Enhancer of split homolog-1 (HES-1) leads to

up-regulation of neural helix-loop-helix factors, premature neurogenesis, and severe neural tube defects. Genes Dev. *9*, 3136–3148.

Iso, T., Kedes, L., and Hamamori, Y. (2003). HES and HERP families: Multiple effectors of the Notch signaling pathway. J. Cell. Physiol. *194*, 237–255.

Iwafuchi-doi, M., and Zaret, K.S. (2014). Pioneer transcription factors in cell reprogramming. 2679–2692.

Jarriault, S., Brou, C., Logeat, F., Schroeter, E.H., Kopan, R., and Israel, A. (1995). Signalling downstream of activated mammalian Notch. Nature *377*, 355–358.

Johnson, J.E., Birren, S.J., Saito, T., and Anderson, D.J. (1992). DNA binding and transcriptional regulatory activity of mammalian achaete-scute homologous (MASH) proteins revealed by interaction with a muscle-specific enhancer. Proc. Natl. Acad. Sci. U. S. A. *89*, 3596–3600.

Kageyama, R., Ohtsuka, T., Hatakeyama, J., and Ohsawa, R. (2005). Roles of bHLH genes in neural stem cell differentiation. Exp. Cell Res. *306*, 343–348.

Kageyama, R., Ohtsuka, T., and Kobayashi, T. (2007). The Hes gene family: repressors and oscillators that orchestrate embryogenesis. Development *134*, 1243–1251.

Kageyama, R., Ohtsuka, T., Shimojo, H., and Imayoshi, I. (2008). Dynamic Notch signaling in neural progenitor cells and a revised view of lateral inhibition. Nat. Neurosci. *11*, 1247–1251.

Karow, M., Sánchez, R., Schichor, C., Masserdotti, G., Ortega, F., Heinrich, C., Gascón, S., Khan, M. a., Lie, D.C., Dellavalle, A., et al. (2012). Reprogramming of pericyte-derived cells of the adult human brain into induced neuronal cells. Cell Stem Cell *11*, 471–476.

Klisch, T.J., Xi, Y., Flora, A., Wang, L., Li, W., and Zoghbi, H.Y. (2011). *In vivo* Atoh1 targetome reveals how a proneural transcription factor regulates cerebellar development. Proc. Natl. Acad. Sci. U. S. A. *108*, 3288–3293.

Kobayashi, T., Mizuno, H., Imayoshi, I., Furusawa, C., Shirahige, K., and Kageyama, R. (2009). The cyclic gene Hes1 contributes to diverse differentiation responses of embryonic stem cells. Genes Dev. *23*, 1870–1875.

Kopan, R., and Ilagan, M.X.G. (2009). The Canonical Notch Signaling Pathway: Unfolding the Activation Mechanism. Cell *137*, 216–233.

Krejčí, A., and Bray, S. (2007). Notch activation stimulates transient and selective binding of Su(H)/CSL to target enhancers. Genes Dev. *21*, 1322–1327.

Kriegstein, A., and Alvarez-Buylla, A. (2009). The glial nature of embryonic and adult neural stem cells. Annu. Rev. Neurosci. *32*, 149–184.

Levine, M. (2010). Transcriptional enhancers in animal development and evolution. Curr. Biol. *20*, R754–R763.

Levine, M., Cattoglio, C., and Tjian, R. (2014). Looping back to leap forward: Transcription enters a new era. Cell *157*, 13–25.

Li, Y., Hibbs, M.A., Gard, A.L., Shylo, N.A., and Yun, K. (2012). Genome-wide analysis of N1ICD/RBPJ targets *in vivo* reveals direct transcriptional regulation of Wnt, SHH, and hippo pathway effectors by Notch1. Stem Cells *30*, 741–752.

Louvi, A., and Artavanis-Tsakonas, S. (2006). Notch signalling in vertebrate neural development. Nat. Rev. Neurosci. *7*, 93–102.

Lupien, M., Eeckhoute, J., Meyer, C. a., Wang, Q., Zhang, Y., Li, W., Carroll, J.S., Liu, X.S., and Brown, M. (2008). FoxA1 Translates Epigenetic Signatures into Enhancer-Driven Lineage-Specific Transcription. Cell *132*, 958–970.

Ma, Q., Chen, Z., Barrantes, I.D.B., De La Pompa, J.L., and Anderson, D.J. (1998). Neurogenin1 Is Essential for the Determination of Neuronal Precursors for Proximal Cranial Sensory Ganglia. Neuron *20*, 469–482.

Macarthur, B.D., Ma'ayan, A., and Lemischka, I.R. (2009). Systems biology of stem cell fate and cellular reprogramming. Nat. Rev. Mol. Cell Biol. *10*, 672–681.

Mattar, P., Langevin, L.M., Markham, K., Klenin, N., Shivji, S., Zinyk, D., and Schuurmans, C. (2008). Basic helix-loop-helix transcription factors cooperate to specify a cortical projection neuron identity. Mol. Cell. Biol. *28*, 1456–1469.

Mengel, B., Hunziker, A., Pedersen, L., Trusina, A., Jensen, M.H., and Krishna, S. (2010). Modeling oscillatory control in NF-κB, p53 and Wnt signaling. Curr. Opin. Genet. Dev. *20*, 656–664.

Miyata, T., Kawaguchi, A., Saito, K., Kawano, M., Muto, T., and Ogawa, M. (2004). Asymmetric production of surface-dividing and non-surface-dividing cortical progenitor cells. Development *131*, 3133–3145.

Nakada, Y., Hunsaker, T.L., Henke, R.M., and Johnson, J.E. (2004). Distinct domains within Mash1 and Math1 are required for function in neuronal differentiation versus neuronal cell-type specification. Development *131*, 1319–1330.

Nakatani, H., Martin, E., Hassani, H., Clavairoly, A., Maire, C.L., Viadieu, A., Kerninon, C., Delmasure, A., Frah, M., Weber, M., et al. (2013). Ascl1/Mash1 promotes brain oligodendrogenesis during myelination and remyelination. J. Neurosci. *33*, 9752–9768.

Nieto, M., Schuurmans, C., Britz, O., and Guillemot, F. (2001). Neural bHLH genes control the neuronal versus glial fate decision in cortical progenitors. Neuron *29*, 401–413.

Noctor, S.C., Martínez-Cerdeño, V., Ivic, L., and Kriegstein, A.R. (2004). Cortical neurons arise in symmetric and asymmetric division zones and migrate through specific phases. Nat. Neurosci. *7*, 136–144.

Ohtsuka, T., Ishibashi, M., Gradwohl, G., Nakanishi, S., Guillemot, F., and Kageyama, R. (1999). Hes1 and Hes5 as notch effectors in mammalian neuronal differentiation. EMBO J. *18*, 2196–2207.

Ohtsuka, T., Sakamoto, M., Guillemot, F., and Kageyama, R. (2001). Roles of the basic helix-loop-helix genes Hes1 and Hes5 in expansion of neural stem cells of the developing brain. J. Biol. Chem. *276*, 30467–30474.

Ong, C.-T., and Corces, V.G. (2011). Enhancer function: new insights into the regulation of tissue-specific gene expression. Nat. Rev. Genet. *12*, 283–293.

Park, P.J. (2009). ChIP-seq: advantages and challenges of a maturing technology. Nat. Rev. Genet. *10*, 669–680.

Parras, C.M., Schuurmans, C., Scardigli, R., Kim, J., Anderson, D.J., and Guillemot, F. (2002). Divergent functions of the proneural genes Mash1 and Ngn2 in the specification of neuronal subtype identity. 324–338.

Parras, C.M., Galli, R., Britz, O., Soares, S., Galichet, C., Battiste, J., Johnson, J.E., Nakafuku, M., Vescovi, A., and Guillemot, F. (2004). Mash1 specifies neurons and oligodendrocytes in the postnatal brain. EMBO J. *23*, 4495–4505.

Pilz, G.-A., Shitamukai, A., Reillo, I., Pacary, E., Schwausch, J., Stahl, R., Ninkovic, J., Snippert, H.J., Clevers, H., Godinho, L., et al. (2013). Amplification of progenitors in the mammalian telencephalon includes a new radial glial cell type. Nat. Commun. *4*, 2125.

Pina, C., Fugazza, C., Tipping, A., Brown, J., Soneji, S., Teles, J., Peterson, C., and Enver, T. (2012). Inferring rules of lineage commitment in haematopoiesis. Nat. Publ. Gr. *14*, 287–294.

Pollard, S.M., Conti, L., Sun, Y., Goffredo, D., and Smith, A. (2006). Adherent neural stem (NS) cells from fetal and adult forebrain. Cereb. Cortex *16 Suppl 1*, i112–i120.

Purves D, Augustine GJ, Fitzpatrick D, et al., editors (2001). Neuroscience (Sunderland (MA): Sinauer Associates;).

Rowitch, D.H., and Kriegstein, A.R. (2010). Developmental genetics of vertebrate glial-cell specification. Nature *468*, 214–222.

Sang, L., Coller, H.A., and Roberts, J.M. (2008). Control of the reversibility of cellular quiescence by the transcriptional repressor HES1. Science *321*, 1095–1100.

Schones, D.E., and Zhao, K. (2008). Genome-wide approaches to studying chromatin modifications. Nat. Rev. Genet. *9*, 179–191.

Schuurmans, C., Armant, O., Nieto, M., Stenman, J.M., Britz, O., Klenin, N., Brown, C., Langevin, L.-M., Seibt, J., Tang, H., et al. (2004). Sequential phases of cortical specification involve Neurogenin-dependent and -independent pathways. EMBO J. *23*, 2892–2902.

Sequerra, E.B., Costa, M.R., Menezes, J.R.L., and Hedin-Pereira, C. (2013). Adult neural stem cells: plastic or restricted neuronal fates? Development *140*, 3303–3309.

Shimojo, H., Ohtsuka, T., and Kageyama, R. (2008). Oscillations in notch signaling regulate maintenance of neural progenitors. Neuron *58*, 52–64.

Shu, J., Wu, C., Wu, Y., Li, Z., Shao, S., Zhao, W., Tang, X., Yang, H., Shen, L., Zuo, X., et al. (2013). Induction of pluripotency in mouse somatic cells with lineage specifiers. Cell *153*, 963–975.

Song, L., and Crawford, G.E. (2010). DNase-seq: A high-resolution technique for mapping active gene regulatory elements across the genome from mammalian cells. Cold Spring Harb. Protoc. *5*, 1–12.

Song, L., Zhang, Z., Grasfeder, L.L., Boyle, A.P., Giresi, P.G., Lee, B.K., Sheffield, N.C., Gräf, S., Huss, M., Keefe, D., et al. (2011). Open chromatin defined by DNaseI and FAIRE identifies regulatory elements that shape cell-type identity. Genome Res. *21*, 1757–1767.

Spitz, F., and Furlong, E.E.M. (2012). Transcription factors: from enhancer binding to developmental control. Nat. Rev. Genet. *13*, 613–626.

Sun, Y., Nadal-Vicens, M., Misono, S., Lin, M.Z., Zubiaga, A., Hua, X., Fan, G., and Greenberg, M.E. (2001). Neurogenin promotes neurogenesis and inhibits glial differentiation by independent mechanisms. Cell *104*, 365–376.

Takahashi, K., and Yamanaka, S. (2006). Induction of Pluripotent Stem Cells from Mouse Embryonic and Adult Fibroblast Cultures by Defined Factors. Cell *126*, 663–676.

Temple, S. (2001). The development of neural stem cells. Nature *414*, 112–117.

Tomita, K., Ishibashi, M., Nakahara, K., Ang, S.L., Nakanishi, S., Guillemot, F., and Kageyama, R. (1996). Mammalian hairy and Enhancer of split homolog 1 regulates differentiation of retinal neurons and is essential for eye morphogenesis. Neuron *16*, 723–734.

Tomita, K., Moriyoshi, K., Nakanishi, S., Guillemot, F., and Kageyama, R. (2000). Mammalian achaete-scute and atonal homologs regulate neuronal versus glial fate determination in the central nervous system. EMBO J. *19*, 5460–5472.

Vasconcelos, F.F., and Castro, D.S. (2014). Transcriptional control of vertebrate neurogenesis by the proneural factor Ascl1. Front. Cell. Neurosci. *8*, 1–6.

Vierbuchen, T., Ostermeier, A., Pang, Z.P., Kokubu, Y., Südhof, T.C., and Wernig, M. (2010). Direct conversion of fibroblasts to functional neurons by defined factors. Nature *463*, 1035–1041.

Wang, S.W., Kim, B.S., Ding, K., Wang, H., Sun, D., Johnson, R.L., Klein, W.H., and Gan, L. (2001). Requirement for math5 in the development of retinal ganglion cells. Genes Dev. *15*, 24–29.

Yang, C., Bolotin, E., Jiang, T., Sladek, F.M., and Martinez, E. (2007). Prevalence of the Initiator over the TATA box in human and yeast genes and identification of DNA motifs enriched in human TATA-less core promoters. Gene *389*, 52–65.

Zaret, K.S., and Carroll, J.S. (2011). Pioneer transcription factors: Establishing competence for gene expression. Genes Dev. *25*, 2227–2241.

Chapter 2 – **Investigating the mutual interactions between Ascl1 and the chromatin landscape in neurogenesis**

Abstract

Ascl1 plays a pivotal role during neurogenesis by activating the expression of genes involved in multiple and sequential functions. Importantly, these genes exhibit different temporal kinetics of expression along the neuronal differentiation program. How the temporal pattern of expression of Ascl1 targets is molecularly established along the neuronal lineage is still unclear. Here, we investigated the reciprocal interactions between Ascl1 and the chromatin landscape when promoting neuronal differentiation of NS cells in culture. For that, we combined expression profiling, Ascl1 binding and chromatin accessibility analyses at a genome-wide level in a cellular model of neurogenesis driven by Ascl1. We found that the accessibility of Ascl1 to its target sites remains largely unchanged throughout differentiation, as Ascl1 targets regions both in accessible and closed chromatin in proliferating cells. Moreover, binding of Ascl1 often precedes the appearance of new regions of open chromatin associated with *de novo* gene expression during neuronal differentiation. Thus, our results reveal a function of Ascl1 in promoting chromatin accessibility during neurogenesis, linking the chromatin landscape at Ascl1 target regions with the temporal progression of its transcriptional program.

Introduction

1. Ascl1 transcriptional program

A major leap forward in our understanding of the molecular mechanisms underlying Ascl1 function has been the progressive characterization of its transcriptional program. The advent of genomic approaches based on chromatin immunoprecipitation allowed the characterization of a large number of genes directly controlled by Ascl1 in neurogenesis. Two studies have used chromatin immunoprecipitation followed by hybridization to DNA arrays (ChIP-chip) or high-throughput sequencing (ChIP-Seq) to characterize the Ascl1 transcriptional program in ventral telencephalon and dorsal spinal cord of the developing mouse embryo, respectively (Borromeo et al., 2014; Castro et al., 2011). A common theme was the diversity of biological functions of Ascl1 target genes, indicating Ascl1 directly controls various stages of neurogenesis, including cell fate specification, neuronal differentiation, migration, axon guidance and synapse formation (Figure 2. 1).

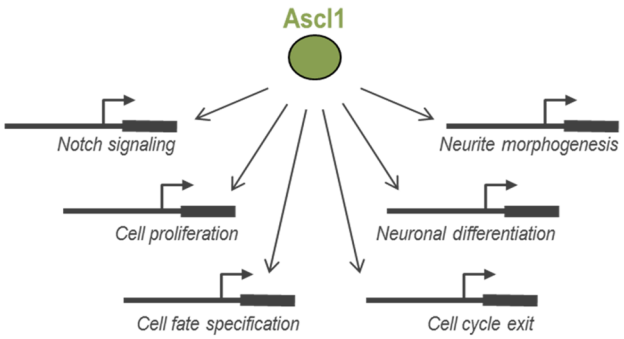

Figure 2. 1 Ascl1 direct target genes are associated with various steps of the neurogenic program.
Figure adapted from (Castro et al. 2011).

In the ventral telencephalon, the region of the murine brain with the largest SVZ during the neurogenic period, the pro-proliferation activity of Ascl1 extends beyond the maintenance of Notch/Hes1 oscillations through activation of Dll1, and includes

the activation of genes required for cell-cycle progression such as E2F1 and Foxm1. Interestingly, Ascl1 target genes exhibit distinct onsets of expression as indicated by their expression patterns along the neuronal lineage in mouse ventral telencephalon (Castro et al., 2011). The expression of the largest group of targets mirrors that of Ascl1 itself in both germinal layers and includes genes expected to promote cell proliferation (e.g., E2F1), whereas the expression of a smaller but significant group of targets is restricted to the mantle zone (e.g., MAP2) (Figure 2. 2).

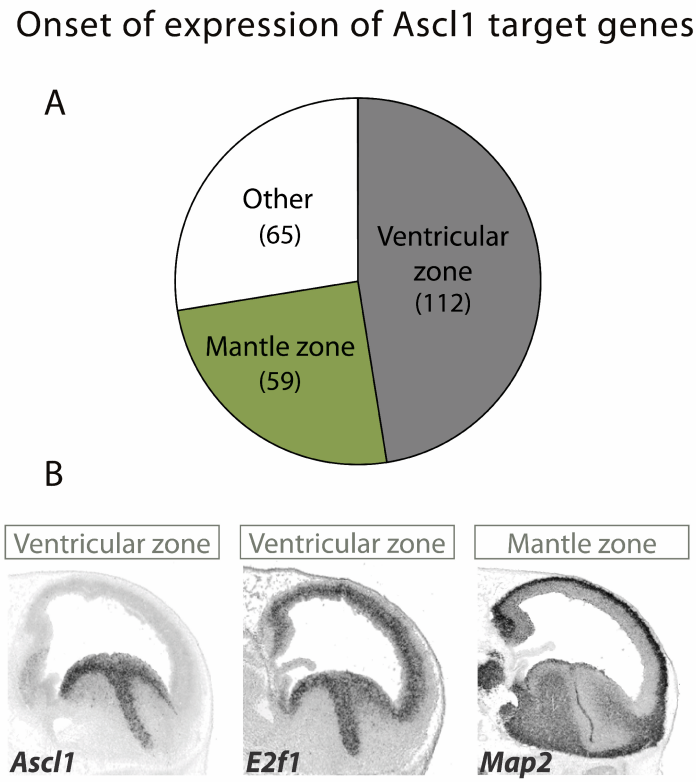

Figure 2. 2 Ascl1 targets exhibit different patterns of expression, suggesting distinct kinetics of activation downstream of Ascl1.

(A) A screening of expression patterns of Ascl1 direct targets in embryonic mouse ventral telencephalon revealed distinct patterns of expression (Castro et al., 2011). Genes in the largest set display an onset of expression at the VZ (which includes mostly neural stem cells), while in another the onset occurs at the mantle zone (here defined as including SVZ and all other outer layers, comprising intermediate progenitors and post-mitotic neurons). A third group includes genes with a uniform or more complex pattern of expression. Number of genes in each set is indicated in between brackets. (Continued on the next page.)

Figure 2. 2 (continued) **(B)** Examples of two Ascl1 direct targets with distinct patterns of expression revealed by *in situ* hybridization on sagittal sections of mouse telencephalon at E13.5 stage of embryonic development. Expression of the proliferation gene E2f1 in VZ/SVZ mirrors that of Ascl1. By contrast, the neuronal differentiation gene MAP2 is expressed in post-mitotic neurons. Images are from Allen Developing Mouse Brain Atlas. Figure from (Vasconcelos & Castro 2014).

Although it has not yet been clearly established, the different kinetics of Ascl1 targets may result from the integration of various mechanistic determinants discussed below.

2. Mechanisms underlying the onset of expression of Ascl1 targets

2.1. Ascl1 expression modes

A recent study has shown that distinct modes of Ascl1 expression are associated with opposing activities: oscillatory expression of Ascl1 promotes neural stem/progenitor cell proliferation whereas sustained expression promotes neuronal differentiation (Imayoshi et al., 2013). It is not yet clear how Ascl1 expression modes allow for differential activation of target genes involved in these distinct and sequential functions of neurogenesis. In other systems, TFs oscillations have been shown to differentially affect target gene expression, as compared to their sustained expression (Ashall et al., 2009; Hoffmann et al., 2002; Wee et al., 2012). For example, different modes of p53 expression (oscillatory vs. sustained) were showed to differentially activate different cohorts of genes involved in distinct functions as apoptosis and DNA repair (Weinberg et al., 2005). This ability has been shown to be a consequence of a differential p53 affinity to promoters: high affinity promoters are activated by oscillatory expression of p53, while low affinity promoters are activated only by p53 sustained expression (Ma et al., 2005; Wee et al., 2012).

Another possible mechanism invokes the function of a feed-forward-loop (FFL), a motif highly enriched in transcriptional networks. A variant of such motif called

coherent FFL (whereby one TF activates another TF, and both co-activate target genes) has been shown to allow for discriminated responses of the target gene triggered by transient or sustained input signals from the first TF (Mangan and Alon, 2003; Shen-Orr et al., 2002). Considering the large number of TFs found amongst Ascl1 targets, it would be of interest to investigate if any of these may establish with this proneural factor such a network motif.

In addition, differential mRNA stability of the target genes may contribute for further diversification of Ascl1 target genes expression dynamics. In response to the same TF oscillatory stimulus, it is expected that a short-lived mRNA or protein would display an oscillatory dynamics, while a long-lived mRNA or protein would accumulate progressively (hypothesis proposed on (Shimojo et al., 2008)). It remains to be determined if and how differential affinity of Ascl1 for subsets of its targets, feed-forward loops and/or differential stability of its target gene products account for the temporal patterning of its program.

2.2. Ascl1 protein levels

Some observations suggest that Ascl1 protein levels may also play a role on the selective activation of its targets. Ascl1 levels, which are dependent on its rate of production and degradation, directly impact on the likelihood of binding to a given promoter. It is formally possible that promoters with different affinities respond differentially to different levels of Ascl1. Time-lapse imaging of Ascl1/luciferase expressing neural progenitors in culture revealed that an increase in Ascl1 levels does occur both before the last cell division. An increase in Ascl1 levels before cell division occurs in 90% of the cells that undergo asymmetrical neurogenic cell division, but it also occurs in 30% of the cells that undergo a proliferative symmetric division, suggesting that, although not being strictly required or sufficient, an increase in Ascl1 protein levels before cell division does bias cells toward the neuronal fate (Imayoshi

et al., 2013). The same study also showed that, increasing the levels of Ascl1 oscillatory expression (increasing the amplitude of the oscillations) did not induce neuronal differentiation but increased the number of proliferating NSCs. By contrast, increasing the levels of Ascl1 sustained expression increased neuronal differentiation. These results indicate the expression mode, but not the levels of Ascl1, are important for a choice between proliferation and differentiation (Imayoshi et al., 2013), at least within the range tested.

A few signaling pathways (BMP/Id, PI3K/Akt) have been implicated in the regulation of Ascl1 protein levels in different cellular contexts (Oishi et al., 2009; Sriuranpong et al., 2002; Viñals et al., 2004), suggesting that the fine-tuning of Ascl1 protein levels may be important for its function. Varying Ascl1 protein levels induced by retinoic acid result in the generation of different subtypes of neurons at the p3 domains of the hindbrain and of the spinal cord (Jacob et al., 2013). However, it remains to be determined whether this depends on the activation of different sets of Ascl1 target genes. In summary, although it has been shown that various pathways converge to control Ascl1 protein levels, their relevance to the differential regulation of subsets of Ascl1 targets is not yet fully established.

2.3. Ascl1 post-translational modifications

Two recent studies provided evidence that Ascl1 function can be modulated by phosphorylation at multiple serine-proline sites. During cortical development, manipulating RAS/ERK signaling to abnormal high levels modifies Ascl1 activity by direct phosphorylation. As a result, Ascl1 promotes the specification of proliferating glial precursor cells, while, at moderate levels of RAS/ERK signaling, Ascl1 promotes GABAergic neuronal differentiation (Li et al., 2014). Another work showed that Ascl1 phosphorylation is regulated by levels of Cdk/Cdk inhibitors and affects its ability to drive primary neurogenesis in Xenopus embryos (Ali et al., 2014). It is currently not

known how phosphorylation allows Ascl1 to discriminate different targets. Possible mechanisms include differential protein stability, differential affinity for E-proteins and/or differential promoter affinity, as was previously shown for Neurog2 phosphorylation (Ali et al., 2011; Hindley et al., 2012). Strikingly, phosphorylation differentially affects the ability of Ascl1 to upregulate the late/differentiation targets X-MyT1 and neural B-tubulin, while having little effect on the induction of the early target X-Delta (Ali et al., 2014). Moreover, a differential effect is also observed on the ability of Ascl1 to transactivate the promoters of various target genes (Li et al., 2014). Therefore, it is possible that differential sensitivity of promoters to Ascl1 phosphorylation may be one important mechanism determining which targets Ascl1 regulates in proliferating vs. differentiating progenitors.

2.4. Functional interactions with other transcriptional networks

Few studies have so far identified functional interactions between Ascl1 and other TFs. The forkhead factor FOXO3 regulates neural stem cell maintenance and is required to preserve the neural stem cell pool in adult mice (Renault et al., 2009). Recently, it has been shown that FOXO3 inhibits Ascl1-driven neuronal differentiation of cultured adult neural progenitors and direct neuronal conversion of fibroblasts (Webb et al., 2013). Although not yet fully defined how, it was suggested that Ascl1 and FOXO3 bind to common regulatory regions and antagonistically regulate the expression of common target genes associated with the Notch signaling pathway (Webb et al., 2013).

A crosstalk between Ascl1 and Notch signaling, through its downstream effector RBPJ, has also been suggested to occur at the transcription of common target genes. Within the large number of Ascl1 targets identified in ventral telencephalon, the RBPJ DNA binding motif is significantly enriched at the vicinity of Ascl1 bound genes with pro-proliferation functions (Castro et al., 2011). Previous studies of neurogenesis in

Drosophila melanogaster provide important clues on how the two factors may interact at the molecular level (Cave et al., 2005; Nellesen et al., 1999). In co-bound regulatory regions with a specific cis-architecture, efficient transactivation is only achieved upon the simultaneous activation of both proneural and Notch pathways (Nellesen et al., 1999). A similar synergy between Ascl1 and RBPJ was also observed in transcriptional assays in murine cells (Cave et al., 2005). However, it remains to be shown whether such interaction does take place at gene regulatory regions. Radial glial cells can be distinguished from intermediate progenitor cells in the ventricular zone of the mouse telencephalon by their distinct high and low levels of canonical Notch signaling, respectively (Mizutani et al., 2007). Thus, in principle, the requirement for RBPJ and Ascl1 co-binding for activation of common promoter regions could be used to differentially activate Ascl1 targets in these two types of progenitors.

2.5. Chromatin landscape and Ascl1 binding

Distinct thresholds of response to Ascl1 may result from differences in requirements for chromatin remodeling across its target sites. However, very little is known on the impact that Ascl1 may have on the chromatin landscape when regulating gene transcription. It was recently found that Ascl1 is able to bind to close chromatin (high nucleosome occupancy) when ectopically expressed during reprogramming of fibroblasts into neurons (Wapinski et al., 2013), defining it as a pioneer factor. In particular, Ascl1 binding was shown to target specifically close chromatin that contains the trivalent chromatin signature consisting of enriched H3K4Me1, H3K27ac and H3K9me3 marks, a surprising observation considering the deterrent effect of H3K9me3 to other reprogramming factors (Soufi et al., 2012). In support of the importance of such trivalent mark, cell types that do not show this signature at bona fide Ascl1 targets revealed to be resistant to reprogramming (Wapinski et al., 2013).

In spite of this important observations, it remains to be shown whether Ascl1 binds to close chromatin in its native neurogenic context, and whether Ascl1 binding results in changes in the chromatin accessibility at target sites and affect the expression of the associated genes, as was shown to be the case for other pioneer TFs.

In this chapter, we aimed at understanding the importance of the chromatin accessibility for the temporal pattern of expression of Ascl1 target genes. For that, we investigated the interdependence between Ascl1 binding, chromatin accessibility and how that impacts on gene expression genome-wide, in a cellular model of neurogenesis driven by Ascl1.

Materials and methods

1. Animals

All experiments with C57BL/6 wild-type and Ascl1$^{-/-}$ mice (Casarosa et al., 1999) were carried out upon approval and following the guidelines of the ethics committee of Instituto Gulbenkian de Ciência.

2. NS-5 HA-Ascl1-ERT2 cell culture

NS-5 Ascl1-ERT2 cells (Raposo et al., 2015) were cultured in mouse Neurocult NSC basal medium supplemented with mouse Neurocult NSC proliferation supplement (Stem Cell Technologies), Penicillin-Streptomycin (100U/mL) (Gibco), EGF (10ng/mL) (Peprotech), bFGF (10ng/mL) (Peprotech), Puromycin (1µg/mL) (Calbiochem) and Laminin (1µg/mL) (Sigma-Aldrich) in T-flasks, plates or well plates (Corning). For differentiation, HA-Ascl1-ERT2 activity was induced with 4-hydroxytamoxifen (50nM) (Sigma-Aldrich), while reducing EGF concentration to 5ng/mL.

3. ChIP-Seq

For ChIP-seq, NS5 Ascl1-ERT2 cells were fixed sequentially with di(N-succimidyl) glutarate and 1% formaldehyde in PBS and then lysed, sonicated, and immunoprecipitated with anti-HA antibody (ab1424, Abcam), as previously described (Castro et al., 2011). DNA libraries were prepared from 10 ng of immunoprecipitated DNA according to the standard Illumina ChIP-seq protocol and sequenced with Illumina GAIIx. Raw reads were mapped to the mouse genome (NCBI37/mm9) with Bowtie 0.12.7 (Langmead et al., 2009). Uniquely mapped reads data (11.5 million for both Ascl1 ChIP and input chromatin samples) were then subsampled before peak calling with MACS 1.4.1 (Zhang et al., 2008).

4. ChIP-Seq peak visualization

To visualize the ChIP-Seq peaks, the bigwig files from each ChIP-Seq dataset were loaded onto the UCSC genome browser (http://genome.ucsc.edu/).

5. ChIP-seq data analysis and integration

Sequenced reads were processed after mapping with SAMTools for format conversion and removal of PCR duplicates (Li et al., 2009). Ascl1-ERT2 data sets were subsampled where necessary to balance each other for better comparison and peak-calling accuracy (Picard tools, http://picard.sourceforge.net/). Peaks for each sample were called against the input using MACS 1.4.1 (MACS 2.1.0 for histone datasets), with P value cutoff at 10^{-10} (Zhang et al., 2008). Subsampling of the data sets confirmed that peak calling saturation was achieved with approximately 90% of sequenced reads. Peaks were then annotated to the nearest TSS using PeakAnalyzer 1.4 (Salmon-Divon et al., 2010). Peak overlap with expression or DHS data calculated and plotted as heat maps with R/Bioconductor packages "genomeIntervals", "gplots", and in-house developed scripts.

6. Density plots

Overlapping (minimum 1 bp) and non-overlapping genomic regions between datasets were determined using BEDTools (Quinlan and Hall, 2010). ChIP-seq and DNase-Seq normalized tag signals were calculated using a 10bp sliding window over the ± 2kb region around each peak summit to generate the occupancy profiles (in-house developed algorithm). These were plotted as heat maps of signal density using R/Bioconductor packages (http://www.Rproject.org/ and http://CRAN.R-project.org/package=gplots) or used to determine the median of occupancy around peak summits.

7. ChIP-qPCR

The purified DNA retrieved from the ChIP was analyzed by qPCR using the standard mix protocol of PerfeCTa SYBR Green FastMix, ROX (Quanta Biosciences). Reaction was run under the following cycling conditions: 1 cycle (50ºC/ 2min; 95ºC/ 3min); 40 cycles (95ºC/ 15sec; 60ºC/ 1min); 1 cycle (95ºC/ 15sec; 60ºC/ 15sec; 95ºC/ 15sec) in ABI 7900HT (Applied Biosystems). Quantities of immmunoprecipitated DNA were calculated by comparison with a standard curve generated by serial dilutions of input DNA. Results are shown as mean ± SD of fraction of input chromatin for triplicate assays and Student's t test was applied for statistical significance. ORFs were used as negative control regions. The primers used in ChIP-qPCR are listed on Table 2. 1. Antibodies used for ChIP-qPCR, Ascl1 (556604, BD Pharmingen), HA-tag (ab1424, Abcam).

Table 2. 1 Primers used in ChIP-qPCR

Gene	Forward Primer	Reverse primer
Dll1_5'enh	ATGACACGCCTTTAGACG	AGCTGTGGGAGTATAGAGAC
Dll1_intr_enh	CCCAATTCTATGCACAAAGC	GGAGGGAAGACACAATGGAG
Dll1_ORF	GTCTCAGGACCTTCACAGTAG	GAGCAACCTTCTCCGTAGTAG
Fbxw7	CAGCTATGTTCCTGCTGTGC	CAACTTCTGCCTGCTTCCTC
Fbxw7_ORF	CTCGTCACATTGGAGAGTGG	CAGGAGCTTGGTTTCCTCAG
NeuroD4_2	CTTTCCTGATGCCCTCTTTC	GGAGCACTGCTGACATGTTT
NeuroD4_ORF	GCTGCAATAAGATGGACACAA	GGGTGAGGATACACCTCCAA
Stk33	ACAGCTGCTGGAGAGAGGAC	ACTTGTCCCAAGCCTCTGTG
Stk33_ORF	TTCAGCAAGACCAACCAATG	CATCCCTCCTACCTGCTTTG

8. DNase-Seq

DNAse-Seq samples from differentiating NS5 HA-Ascl1-ERT2 cells or proliferating NS-5 cells were prepared as previously described (Song et al., 2011). Libraries were generated as previously described (Boyle et al., 2008; Song and Crawford, 2010) with a slight modification to the linkers to increase ligation efficiency (Song et al., 2011)

and then sequenced with Illumina GAIIx. Mapping was done as for ChIP-Seq, resulting in 165.9 and 168.7 millions of unique reads for proliferating and differentiating conditions, respectively. Sequenced reads of 20bp for both conditions, proliferating and differentiating cells, were processed as for ChIP-seq, except subsampling. DHSs for each sample were defined with MACS 1.4.1 (P value cutoff at 10^{-5}) by extending mapped reads in 60bp as an estimation for the maximum distance between two nucleosomes (linker DNA). DHS annotation and overlap with expression data and clusters of deregulated genes were performed as described for ChIP-Seq.

9. FAIRE-qPCR

Chromatin preparation was done with a single fixation with 1% formaldehyde, from NS-5 cells infected with a doxycycline inducible lentivirus expressing WT Ascl1 (Wapinski et al., 2013). Three rounds of phenol/chloroform extraction were followed by isopropanol precipitation of the DNA. Quantification of genomic regions was done using a standard curve generated with de-cross-linked input chromatin by qPCR as above. The primers used in FAIRE-qPCR are listed on Table 2. 2.

Table 2. 2 Primers used in FAIRE-qPCR

Gene	Forward Primer	Reverse primer
Ap3b2	AGCAGAGGAGCCAACTAAGC	AGAGTGTGCTTTGCAGGTGA
Dll1_5'enh	ATGACACGCCTTTAGACG	AGCTGTGGGAGTATAGAGAC
Dll1_intr_enh	CCCAATTCTATGCACAAAGC	GGAGGGAAGACACAATGGAG
Dll1_ORF	GTCTCAGGACCTTCACAGTAG	GAGCAACCTTCTCCGTAGTAG
Fbxw7	CAGCTATGTTCCTGCTGTGC	CAACTTCTGCCTGCTTCCTC
Fbxw7_ORF	CTCGTCACATTGGAGAGTGG	CAGGAGCTTGGTTTCCTCAG
Mcf2l	GCAGAGCAGAAAGAACATGC	GCTGTTAGGAAAATGGGACAA
NeuroD4_1	CTAGGGCAAGCTAGGGAAGA	GGGTGGGAGTAGGATTTGAG
NeuroD4_2	CTTTCCTGATGCCCTCTTTC	GGAGCACTGCTGACATGTTT
NeuroD4_2	CTTTCCTGATGCCCTCTTTC	GGAGCACTGCTGACATGTTT
NeuroD4_3	GAGCCAGGGAATAGTCTGCT	GAGCCAAGCCAGATCCAG
NeuroD4_ORF	GCTGCAATAAGATGGACACAA	GGGTGAGGATACACCTCCAA

NeuroD4_TSS	CCCGCGAGTAGTTCTTTCA	TAGGAAGGGGAGGGGCTA
Nrxn3	CCTGGTTGCCCTCTACCTAC	GTCATGCTGAGTGGATGCTC
Stk33	ACAGCTGCTGGAGAGAGGAC	ACTTGTCCCAAGCCTCTGTG
Stk33_ORF	TTCAGCAAGACCAACCAATG	CATCCCTCCTACCTGCTTTG

10. Expression RT-qPCR

Expression analysis was performed on NS-5 Ascl1-ERT2 cells 0, 4, 12, 24 and 48h post tamoxifen addition to the culture and reduction of EGF concentration to 5ng/mL. RNA extraction, cDNA production and RT-qPCR were performed as described on the previous chapter. The primers used are listed on Table 2. 3. Triplicates of each biological replicate were used in the RT-qPCR. Values are normalized to β-actin expression levels and to untreated sample (0h). Results are shown as mean ± SD of triplicate assays.

Table 2. 3 Primers used in expression-qPCR

Gene	Forward Primer	Reverse primer
β-actin	CTAAGGCCAACCGTGAAAAG	ACCAGAGGCATAGGGACA
Ap3b2	AAGAATGTGGCCTGTAAGAACAT	GGACAGTAGAGCGAGGTCTTG
Mcf2l	TTGGAAACATGGAGGAAATCT	AGCTCTGGGCAGTCTATGC
Nrxn3	GAATGGGGGAAATGCTACAC	AGCCCAGAGAGTTGACCTTG

11. Other datasets used

The ChIP-Seq and gene expression microarrays datasets available used on this study are listed on Table 2. 4.

Table 2. 4 Datasets used generated by other studies

Dataset	Reference	Accession numbers
ChIP-seq Ascl1-ERT2, t=30min	(Raposo et al., 2015)	E-MTAB-2384.
ChIP-seq Ascl1-ERT2, t=18h	(Wapinski et al., 2013)	PMID:24243019
ChIP-seq Ascl1-ERT2, input	(Wapinski et al., 2013)	PMID:24243019
NS-5 HA-Ascl1-ERT2 microarrays (Ascl1 GoF)	(Raposo et al., 2015)	

Results

1. A cellular model of Ascl1-driven neurogenesis

It has been shown that Ascl1 overexpression promotes cell cycle exit and neuronal differentiation of neural progenitor cells (Castro et al., 2006). To study this process in controlled conditions, we have previously established a cellular model of Ascl1-driven neurogenesis by expressing Ascl1 fused to the modified ligand binding domain of the estrogen receptor (ERT2) (Figure 2. 3A) (Raposo et al., 2015). In this system, the activity of Ascl1-ERT2 fusion protein is inducible by 4-hydroxytamoxifen (herein referred to as tamoxifen or TAM) (Bergstrom et al., 2002; Burk and Klempnauer, 1991; Littlewood et al., 1995) and is accompanied by translocation of a small fraction to the nucleus (Figure 2. 3B), as previously reported in other cases of TFs fused to ERT2 (Burk and Klempnauer, 1991; Roemer and Friedmann, 1993). Upon activation, Ascl1-ERT2 induces neuronal differentiation of NS cells in culture with great efficiency as assessed by the expression of the neuronal marker TuJ1 (Figure 2. 3C).

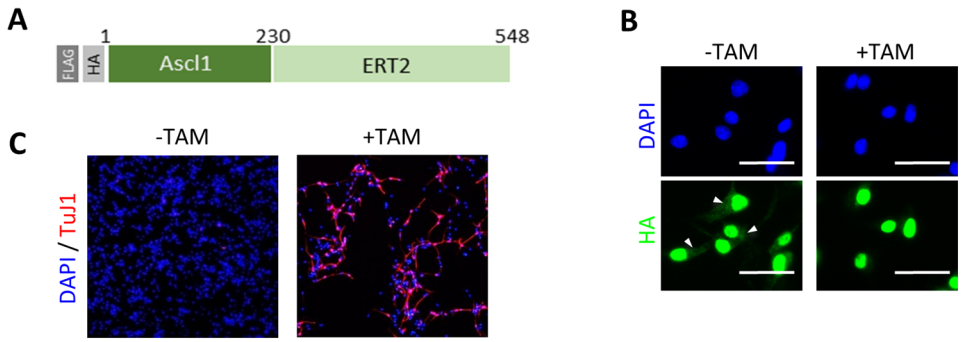

Figure 2. 3 A cellular model of neurogenesis driven by Ascl1.

(A) The ERT2 domain was fused in frame with full length Ascl1, at its carboxy-terminal end. Amino-terminally, HA- and FLAG-tags were inserted. Numbers refer to amino-acid residues. **(B)** Cellular localization of Ascl1-ERT2 in NS5 Ascl1-ERT2 cells before (-TAM) and 30min (+TAM) after the addition of tamoxifen, as assessed by immunocytochemistry using anti-HA antibody (green). White arrowheads mark cytoplasmic expression. Cell nuclei are labeled with DAPI (blue). Scale bar, 30µm. (Continued on the next page.)

Figure 2. 3 (continued) **(C)** State of differentiation of NS5 Ascl1-ERT2 cells before (-TAM) or 3 days after tamoxifen treatment (+TAM), as assessed by immunocytochemistry for the neuronal marker TuJ1 (red). Cell nuclei are labeled with DAPI (blue).

2. Ascl1 access to its target sites does not depend on the differentiation stage of NS cells

We hypothesized that Ascl1 accessibility to its target sites changes during neuronal differentiation and that can account for the differential onset of expression of Ascl1 target genes along the neuronal lineage. To investigate this, we compared the binding profile of overexpressed Ascl1-ERT2 before and after the onset of differentiation, at t=30min ("proliferating cells") and t=18h post TAM induction ("differentiating cells"), respectively, by ChIP-Seq on chromatin extracted from NS-5 Ascl1-ERT2 cells (Figure 2. 4A). Visual inspection of the genomic distribution of Ascl1 peaks finds a remarkable similarity between Ascl1 BEs in both conditions (Figure 2. 4B). Comparison of the two Ascl1 binding profiles in a bin-by-bin approach within high confidence limits ($p<10^{-18}$) (Figure 2. 4C, dashed line) shows an overlap of 86% between the two stages (Figure 2. 4C). Furthermore, the presence of normalized sequencing signal across both samples in genomic regions centered at putative sample-specific BEs suggests that the overlap of occupancies may have been underestimated by peak calling conditions (Figure 2. 4D). Overall, our results indicate that accessibility of Ascl1 to the full complement of its binding sites remains largely identical throughout neuronal differentiation.

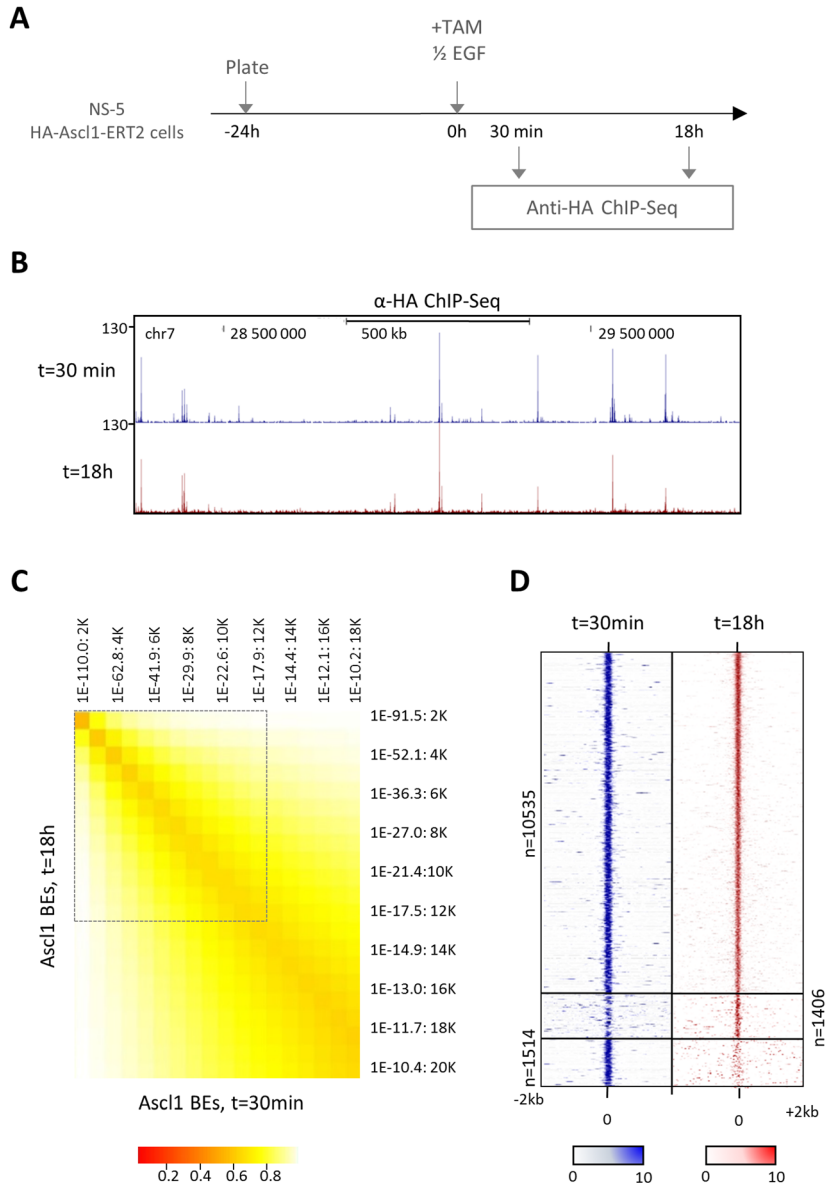

Figure 2. 4 Ascl1 binding to its target sites remains constant throughout differentiation.

(A) Scheme depicting the experiment in which Ascl1-ERT2 was induced by addition of TAM to NS-5 Ascl1-ERT2 cell cultures. HA-tagged Ascl1-ERT2 genome-wide binding analysis was performed t=30min and t=18h post TAM induction by ChIP-Seq using anti-HA antibody. **(B)** Visual representation of Ascl1 ChIP-Seq profiles at t=30min (blue) and t=18h (red) in a large genomic region centered on Dll3 gene. **(C)** Comparison of Ascl1 BEs at t=30min and t=18h ($p<10^{-10}$) by cumulative bins of increasing p value (bin=1007 BEs). (Continued on the next page.)

Figure 2. 4 (continued) The proportion of sites bound by Ascl1 in both conditions (overlapping peaks) is calculated in relation to the condition with the lowest number of BEs. Dashed lines represent high confidence lists defined by $p<10^{-18}$, analyzed in **(D)**. **(D)** Density plot of Ascl1 ChIP-Seq reads mapping to the genomic regions surrounding Ascl1 peak summits. The signal intensity represents the Ascl1 ChIP-Seq normalized tag count in the 4kb region surrounding the summit of each overlapping (top) and non-overlapping peak at t=30min (blue) and t=18h (red).

3. Characterization of chromatin accessibility changes during neuronal differentiation

We next wished to investigate how Ascl1 binding correlates with changes in chromatin accessibility during neuronal differentiation. For that, we started by characterizing the chromatin landscape of proliferating and differentiating NS cells using DNase I hypersensitivity assay coupled to massive parallel sequencing (DNase-Seq) (Figure 2. 5A). This technique identifies regions of decreased nucleosome occupancy (herein referred as ‘‘open chromatin’’) on a genome-wide scale, which correspond mostly to active regulatory elements such as promoters, enhancers, insulators, and silencers (Boyle et al., 2008; Natarajan et al., 2012; Thurman et al., 2012). The density of mapped reads for each genome position was computed to generate a comprehensive list of DNase I hypersensitivity sites (DHSs). Using a constant threshold of $p<10^{-5}$, we identified 87 000 and 94 000 DHSs in proliferating and differentiating NS cells, respectively, numbers with a magnitude consistent with those obtained in other cell types (Song et al., 2011). Although the majority of these sites is shared by both experimental conditions, each cell state exhibits a specific set of approximately 20 000 DHSs (Figure 2. 5B). To validate these differentiation-induced DHSs, we used formaldehyde-assisted isolation of regulatory elements (FAIRE), an alternative method to identify regions of open chromatin. Although distinct preferences have been described for each technique in the identification of distal or proximal regulatory regions, the two techniques have been shown to yield largely overlapping results on a genome-wide basis (Song et al., 2011). Indeed, 9 of

13 tested regions presented more than 2-fold enrichment by FAIRE-qPCR across samples collected before and 24h after addition of tamoxifen, as opposed to control regions (Figure 2. 5C).

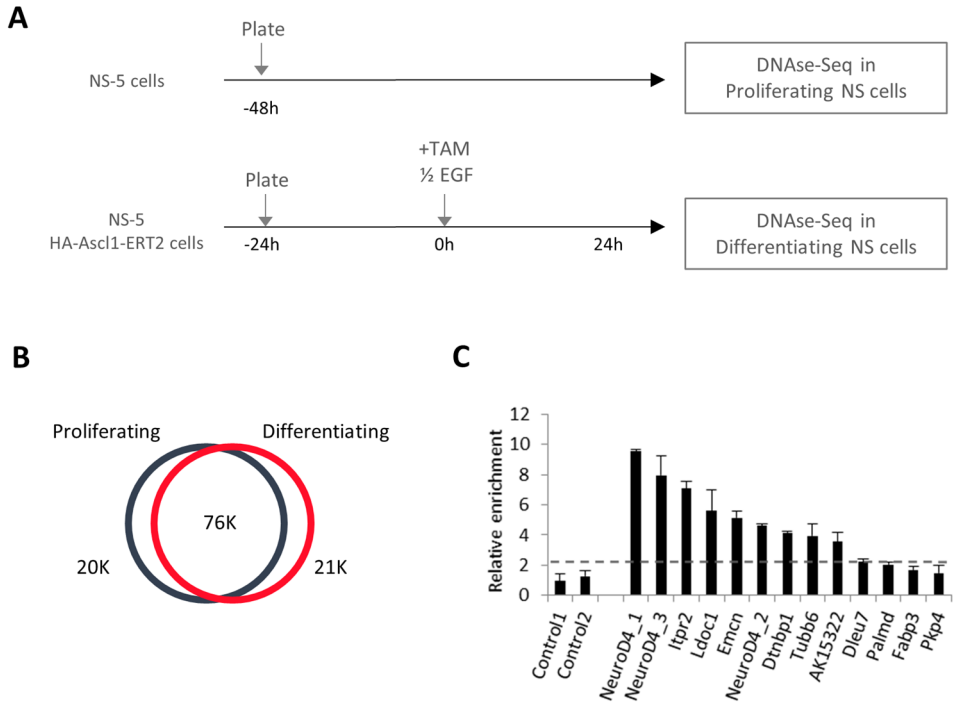

Figure 2. 5 Characterization of changes in chromatin accessibility during differentiation of NS cells

(A) Scheme depicting experiment in which analysis of chromatin accessibility was performed on proliferating (NS-5 cells) and differentiating (NS-5 Ascl1-ERT2 24h post TAM) NS cells by DNAse-Seq. **(B)** Number of DHSs common or specific in proliferating and differentiating NS cells. **(C)** FAIRE-qPCR validation of differentiation-induced DHSs. Bars show fold enrichment of genomic DNA obtained from NS cells 24h after induction over cells prior to addition of tamoxifen. Data are represented as mean ± SD.

4. Ascl1 promotes chromatin accessibility

To analyze the relation between Ascl1 and the changes in the chromatin landscape, we started by comparing the genomic distribution of Ascl1 BEs at the onset of neuronal differentiation (t=30min) with that of DHSs before and after neuronal differentiation. Ascl1 ChIP-Seq t=30min and DNase-Seq in proliferating NS cells data sets show a high degree of overlap. 80.3% of Ascl1 BEs at t=30min ($p<10^{-18}$) fall within

DHSs in proliferating cells, while 19.7% of the BEs fall within close chromatin regions (Figure 2. 6A). This indicates that, although a large fraction of Ascl1 BEs occurs in regions of open chromatin, in 1/5 of the cases Ascl1 binds to close chromatin regions in proliferating NS cells. Strikingly, this overlap increases significantly under differentiation conditions (to 91.1% of overlap between Ascl1 ChIP-Seq t=30min and DNase-Seq in differentiating NS cells; Figure 2. 6A). Accordingly, the overall DNase-Seq profile at Ascl1 peak summits is consistent with many BEs occurring in regions of already open chromatin at t=30min (Figure 2. 6B). Nevertheless, a significant increase is observed when comparing profiles before and after differentiation (2.33 fold increase of median read count) at Ascl1 peak summits genome-wide (Figure 2. 6B). When we focus on the Ascl1 peaks that fall within newly opened DHS sites (differentiation-induced DHSs), this increase is amplified (4.37 increase of median read count; Figure 2. 6B). On Figure 2. 6C are examples of genes in which Ascl1 binding is associated the appearance of new DHSs during differentiation. To validate changes in chromatin compaction at these selected sites, we performed FAIRE-qPCR. In addition, to exclude any possible artefacts generated by the Ascl1-ERT2 fusion protein, we used NS-5 cells expressing full-length Ascl1 under the regulation of a doxycycline inducible promoter (TetON) in this validation step. When comparing nucleosomal occupancy before and after Ascl1 induction, all selected regions were validated (Figure 2. 6D). Overall, our data suggest that (1) the Ascl1 binding profile remains constant at the two stages analyzed, (2) a large fraction of Ascl1 BEs occurs in regions of open chromatin in proliferating cells, with a subset falling within closed chromatin, and (3) binding of Ascl1 to closed chromatin precedes the appearance of new regions of decreased nucleosome occupancy (DHSs) during differentiation.

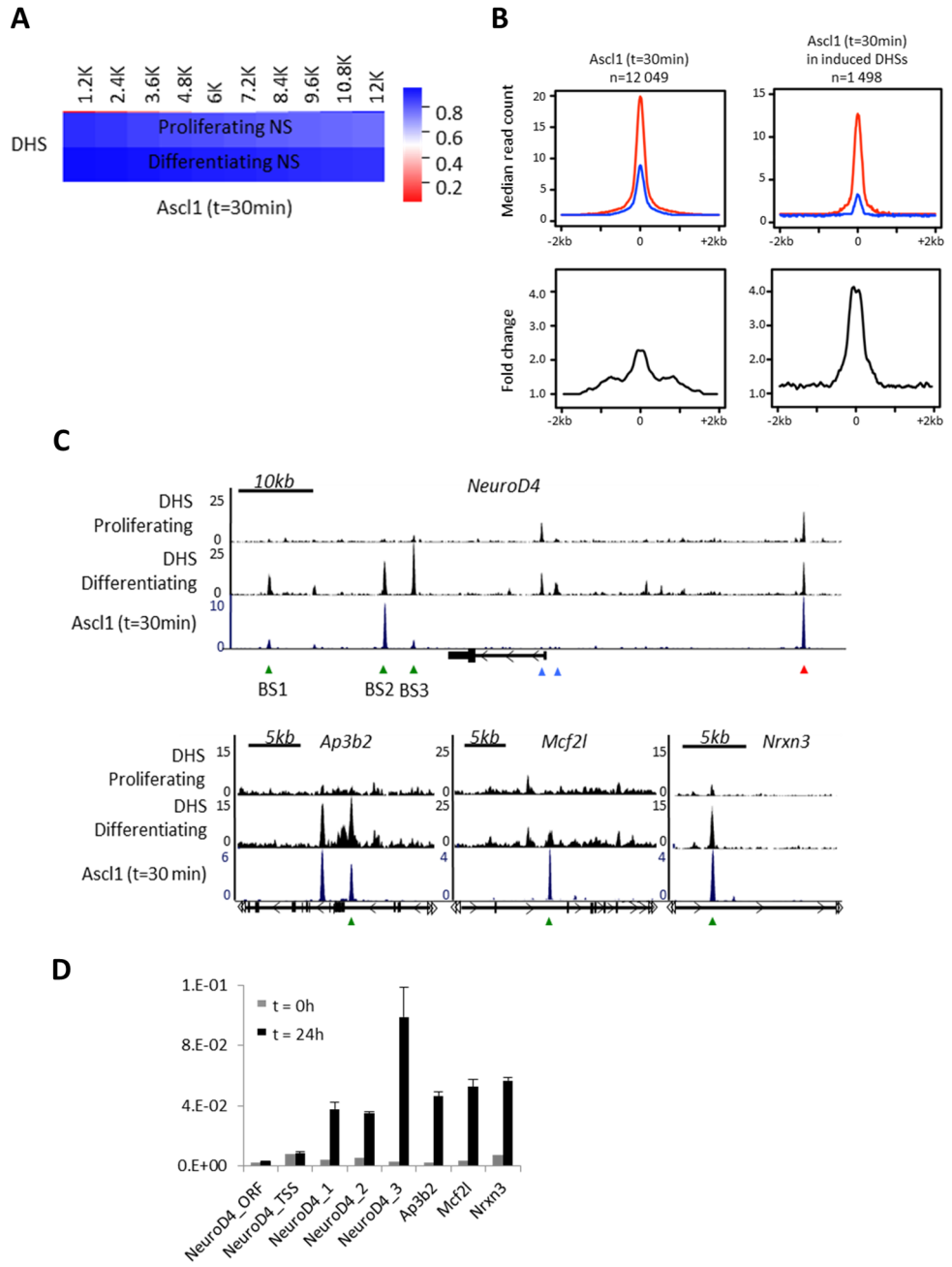

Figure 2. 6 Ascl1 binds closed chromatin and promotes chromatin accessibility.

(A) Proportion of Ascl1 BEs at t=30min, by cumulative bins of increasing p value (bin=1842 BEs), which fall within regions of open chromatin as determined by DNAse-Seq (DHSs) in proliferating (top) or differentiating (bottom) NS cells. (Continued on the next page.)

Figure 2. 6 (continued**) (B)** DNase-Seq signal distribution around all Ascl1 BEs at t=30min (left) or around those that fall within differentiation-induced DHSs (right).
Profile determined as the median read count of DNase-Seq reads mapped to the 4Kb regions centered at the peak summits in proliferating (blue) and differentiating cells (red). Corresponding fold change for the median profiles (bottom). **(C)** Visual representation of ChIP-Seq and DNase-Seq enrichment profiles in the vicinity of various Ascl1 targets. Examples shown are of differentiation-induced and constant DHSs localized at Ascl1 binding sites (green and red arrows, respectively) and DHSs with no apparent association with Ascl1 binding (blue arrows). **(D)** FAIRE-qPCR validation of differentiation-induced DHSs at Ascl1 binding sites (green arrows in **A**). Bars show quantification of nucleosome-depleted chromatin obtained from proliferating and differentiating NS cells (before and 24h after induction, respectively). Mean ± SD of triplicate assays are shown.

5. Ascl1 binds to close chromatin and promotes chromatin accessibility *in vivo*

To verify that Ascl1 can bind to closed chromatin *in vivo*, we focused on the Ascl1-bound regulatory region identified immediately downstream the NeuroD4 promoter (BS2 in Figure 2. 6C), a target gene of Ascl1 in our cellular system that is not expressed in ventral telencephalon. We reasoned that binding to closed chromatin on NeuroD4 regulatory region may still occur in this embryonic brain region at the neurogenic period, even in the absence of gene expression. Indeed, we detected strong binding of Ascl1 within the NeuroD4 locus, as compared with a negative control region, by ChIP-qPCR in chromatin extracted from mouse ventral telencephalon (Figure 2. 7A). However, in contrast to our previous findings in differentiating NS cells in culture, a lack of enrichment for nucleosome-depleted DNA assessed by FAIRE-qPCR shows this Ascl1 target site is found within closed chromatin in ventral telencephalon (Figure 2. 7B, compare with Ascl1 site in Dll1). Thus, our results with the NeuroD4 regulatory region demonstrate that endogenous Ascl1 can bind to closed chromatin in an *in vivo* context.

To provide loss-of-function evidence for a role of Ascl1 in promoting chromatin accessibility, we used chromatin extracted from the embryonic telencephalon of wild-type and Ascl1 null embryos. We analyzed nucleosomal occupancy at Ascl1 sites

associated with previously validated Ascl1 target genes (Dll1, Fbxw7, and Stk33) in this embryonic structure (Castro et al., 2006), by FAIRE-qPCR. Ascl1-null embryos show a significant reduction of signal relative to wild-type chromatin at all tested Ascl1 binding sites, as compared with pairwise control regions (Figure 2. 7C-D). These results support a role for Ascl1 on the promotion of chromatin opening *in vivo*.

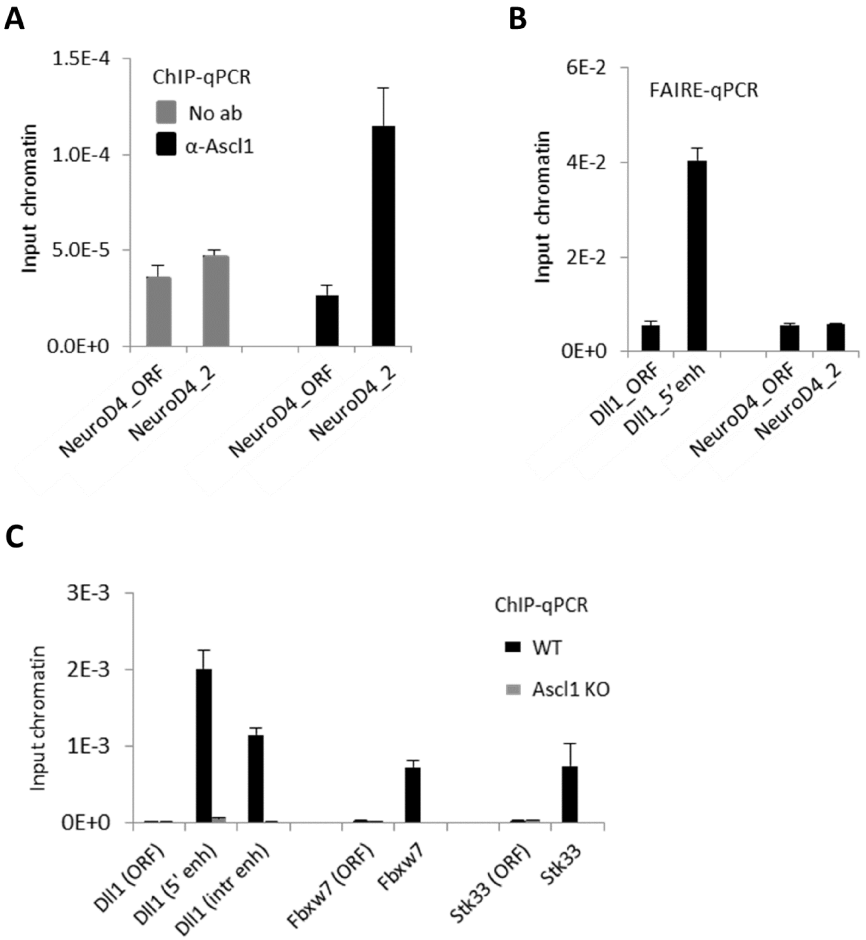

(figure continues on the next page)

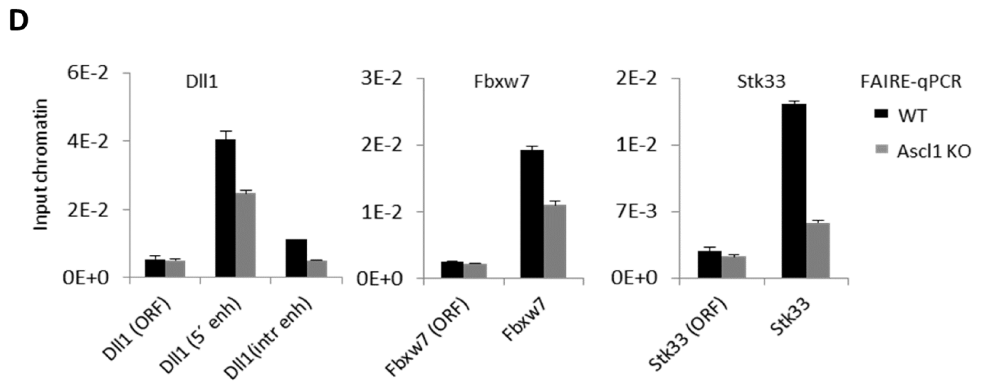

Figure 2. 7 Ascl1 binding is associated with chromatin opening *in vivo*.

(A) *In vivo* binding of Ascl1 to the NeuroD4 regulatory region (NeuroD4_2) assessed by ChIP-qPCR using chromatin extracted from E12.5 mouse ventral telencephalon. NeuroD4_ORF was used as negative control region. Mean ± SD of triplicate assays are shown. **(B)** Chromatin accessibility analysis by FAIRE-qPCR of NeuroD4 and Dll1 regulatory regions bound by Ascl1 in mouse ventral telencephalon. ORFs were used as negative control regions. Mean ± SD of triplicate assays are shown. **(C)** Analysis of Ascl1 binding to regions associated with Dll1, Fbxw7 and Stk33 genes by ChIP-qPCR, using chromatin extracted from ventral telencephalon of E14.5, wild type (WT) or Ascl1 null embryos (Ascl1 KO). ORFs were used as negative control regions. Mean ± SD of triplicate assays are shown. **(D)** Quantification of nucleosome-depleted chromatin at Ascl1-bound regions by FAIRE-qPCR using chromatin extracted from ventral telencephalon of E14.5 wild type (WT) or Ascl1 null embryos (Ascl1 KO). In parallel with Ascl1-bound sites, one negative control region within the gene open reading frame (ORF) was tested for each locus. Mean ± SD of triplicate assays are shown.

6. Induced DHSs are associated with genes expressed *de novo* during differentiation

We next asked if Ascl1 binding to close chromatin and subsequent opening is associated with changes in gene expression. To address that, we determined the number of newly opened chromatin regions (differentiation-induced DHSs) associated with up- or downregulation of genes along Ascl1-driven neuronal differentiation. Gene expression changes were identified by gene expression microarrays upon Ascl1-ERT2 GoF (Raposo et al., 2015). We find a statistically significant enrichment of differentiation-induced DHSs in the vicinity of upregulated genes, in sharp contrast with downregulated genes (Figure 2. 8A). Moreover, a large fraction of all upregulated genes (413 of 760) is associated with at least one

differentiation-induced DHS, suggesting the importance of these putative regulatory regions in activating gene expression during neurogenesis. Notably, upregulated genes associated with differentiation-induced DHSs are either not expressed in proliferating NS cells or expressed at low levels when compared with upregulated genes near constant DHSs (Figure 2. 8B). If we focus on differentiation-induced DHSs that co-localize with Ascl1 BEs, the association is maintained: differentiation-induced DHSs co-localizing with Ascl1 BEs are strongly associated with gene activation and not with gene repression ($p<6.8 \times 10^{-32}$, Figure 2. 8C). 98 of 413 genes associated with induced-DHSs and upregulated during differentiation are bound by Ascl1. Accordingly, the genes selected for validation of Ascl1 binding and newly opening of chromatin (Figure 2. 6C-D) are activated during differentiation (Figure 2. 8D).

Overall, the integration of Ascl1 location analysis, DNase-Seq and expression profiling demonstrates that: 1) Ascl1 can bind regions of "closed chromatin" as defined by high nucleosomal occupancy; 2) Ascl1 promotes chromatin opening at its target sites during neuronal differentiation, and 3) the appearance of new regions of open chromatin at Ascl1 target sites is associated with *de novo* gene expression during neuronal differentiation. These results suggest that the requirement for chromatin remodeling on Ascl1 targets associated with neuronal differentiation modulates the timing of activation of these target genes and, hence, contributes to the temporal pattern of Ascl1 targets.

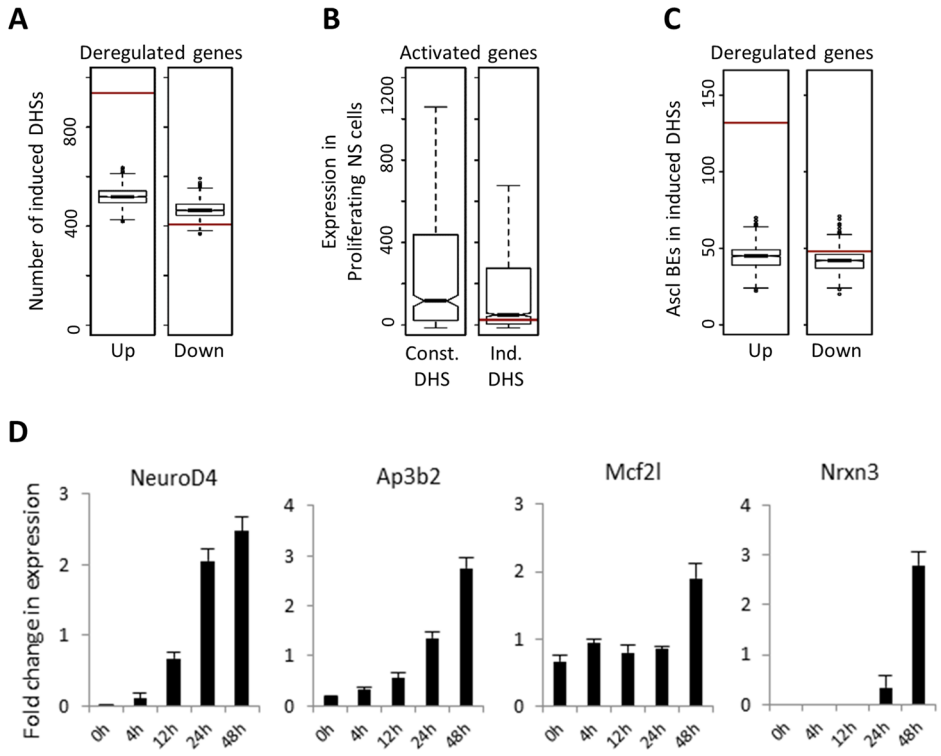

Figure 2. 8 Ascl1 binding and newly opening of chromatin are associated with upregulation of gene expression during differentiation.

(A) Differentiation-induced DHSs are significantly associated with activated genes (left) and not with repressed genes (right). Red bars, total number of DHSs annotated to each set of genes. Boxplots, distribution of DHSs associations with 1000 random sets of genes. Test data are represented as box with median of test and first and third quartiles; whiskers, ±1.5 x IQR. **(B)** Activated genes associated with differentiation-induced DHSs have low or no expression in proliferating cells. Gene expression levels in proliferating cells are significantly lower ($p<10^{-11}$, Wilcoxon test) for activated genes associated with induced DHSs (right) than for activated genes with no such association (left). Red bar, level of expression of NeuroD4 gene. Data distribution represented as box with median and first and third quartiles; whiskers, ±1.5 x IQR; notches, ±1.58 x $IQR/^{n1/2}$). **(C)** Ascl1 BEs located at differentiation-induced DHSs are significantly associated with activated genes (left) and not with repressed genes (right). Red bars, total number of Ascl1 BEs annotated to each set of genes; boxplots, distribution of Ascl1 BEs associations with 1000 random sets of genes. Test data represented as box with median of test and first and third quartiles; whiskers, ±1.5 x IQR. **(D)** Induction of expression of genes bound by Ascl1 and opened during differentiation as quantified by Real-time PCR. Values normalized to B-actin expression values. Mean ± SD of triplicate assays are shown.

Discussion

In spite of its pivotal role during neurogenesis, little is known on how Ascl1 regulates gene expression. Here, we investigated the reciprocal interactions between Ascl1 and the chromatin landscape when promoting neuronal differentiation of cultured NS cells. We found that Ascl1 binding to close chromatin precedes opening and activation of neuronal differentiation genes, establishing the first link between the chromatin accessibility and the temporal pattern of the Ascl1 program along the neuronal lineage (Figure 2. 9).

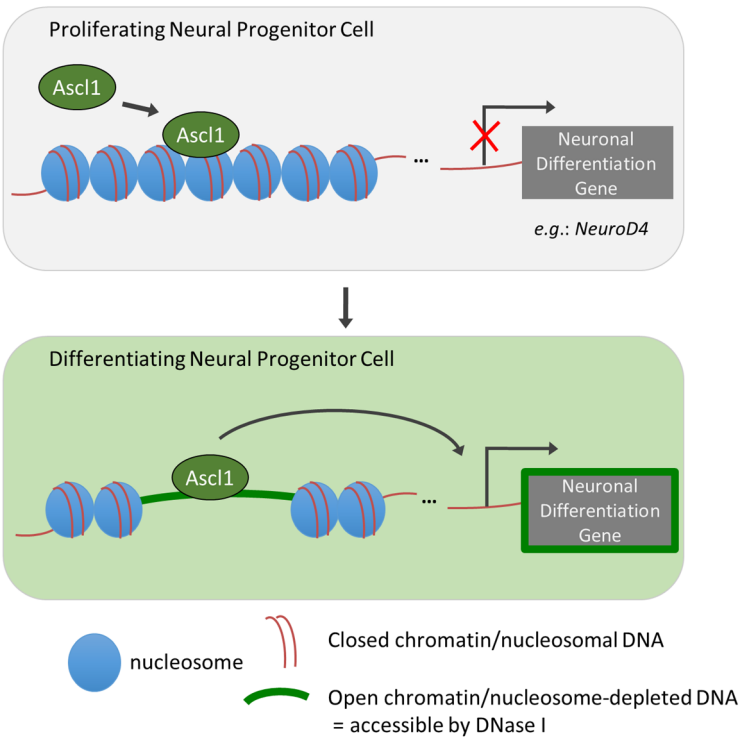

Figure 2. 9 Ascl1 coordinately regulates gene expression and the chromatin landscape during neurogenesis. Ascl1 sequentially activates target genes in proliferating and differentiating progenitors during neurogenesis. Ascl1 binds closed and open chromatin in proliferating cells. Binding to closed chromatin promotes accessibility and activation of expression of differentiation-specific genes. Thus, the dynamics of chromatin landscape at Ascl1 target genes regulates their onset of expression.

It was previously shown that Ascl1 can bind to closed chromatin when ectopically expressed in fibroblasts (as assessed by FAIRE-qPCR), defining it as a pioneer TF (Wapinski et al., 2013), results that the present study validates for the first time in a neural context. Moreover, our analysis of binding of Ascl1 to the NeuroD4 locus in ventral telencephalic progenitors that do not express this gene allowed for the dissociation between binding and opening of chromatin, revealing binding of endogenous Ascl1 to closed chromatin *in vivo* (Figure 2. 7). Altogether, our study supports the idea that Ascl1 displays pioneer activity when regulating gene expression in its native context.

It was shown that Ascl1 promotes sequentially the proliferation and differentiation along the neuronal lineage, with the concomitant activation of distinct target genes (Castro et al., 2011). More recently, different expression modes of Ascl1 have been associated with its different functions – Ascl1 oscillatory expression maintains proliferation, while Ascl1 sustained expression promotes differentiation of NPCs (Imayoshi et al., 2013). Our study focused on the transcriptional activity of Ascl1 when promoting neuronal differentiation upon a sustained mode of expression. It remains to be addressed how target gene specificity associated with both cellular functions (proliferation vs. differentiation) may relate to the differential need for its pioneer activity. Addressing this point will likely require the characterization of Ascl1 binding profile and chromatin accessibility in an oscillatory versus sustained mode of expression. Nevertheless, the observation that overexpressed Ascl1 can readily access the full complement of its differentiation sites at the onset of differentiation (t=30min) suggests these may already be accessible to this TF in proliferating cells when Ascl1 expression is oscillatory.

Another interesting question is why some TFs exhibit pioneer activity while others do not. Are there common features between the DNA binding domains of pioneer TFs? Interestingly, a recent report has shed some light into this issue. The TFs Oct4, Sox2,

Klf4 and c-Myc have been extensively used during reprogramming of fibroblasts into induced pluripotent stem cells (iPSCs) (Takahashi and Yamanaka, 2006). Oct4, Sox2 and Klf4, contrary to c-Myc, can access nucleosomal DNA in fibroblasts and, therefore, exhibit pioneering activity (Soufi et al., 2012). The biochemical, structural and genomic data of Oct4, Sox2, Klf4 and c-Myc during iPSC reprogramming were compared and, interestingly, the authors found that Oct4, Sox2 and Klf4, contrary to c-Myc, can access nucleosomal DNA because they possess highly flexible DNA binding domains that target partial motifs displayed on the nucleosome surface. This feature allows these TFs to recognize motifs that are not fully exposed in a close chromatin conformation, avoiding the need for extreme bending of their DNA binding domains that would otherwise be necessary for the recognition of the full motif (Soufi et al., 2015). Ascl1 belongs to the bHLH transcription factor family that interacts with the DNA through specific residues on the basic and HLH domains (Bertrand et al., 2002). Contrary to Ascl1, the bHLH TF c-Myc cannot access its sites within close chromatin (Soufi et al., 2012). The differential activity of these two bHLH TFs lies on the fact that Ascl1, like Oct4, Sox2 and Klf4 and contrary to c-Myc, also recognizes a partial motif when bound to close chromatin during reprogramming of fibroblasts into neurons. When bound to nucleosome-free DNA, Ascl1 recognizes the CAGCTG E-box motif, while, when bound to nucleosomal DNA, it recognizes a degenerate E-box motif (CANNTGG) (Soufi et al., 2015). The authors concluded that the basic helix1 of Ascl1 is considerably shorter compared to that of c-Myc, leaving more of the DNA surface solvent exposed and allowing Ascl1 to bind nucleosomal DNA more efficiently than c-Myc (Soufi et al., 2015). Interestingly, analysis by digital genomic footprinting of the motifs enriched on DHS-induced sites during neurogenesis induced by Ascl1 reveals the overrepresentation of various subtypes of E-boxes (E-box1 and E-box2 on Figure 2.S 1), suggesting that such mechanism of

recognition of partial E-box motifs within closed chromatin might also be valid in the neurogenic context.

Despite the ability of pioneer factors to bind nucleosomal DNA, they only bind to a small fraction of their putative binding sites in the genome (based on presence of binding motif). Histone modifications have been shown to modulate the access of pioneer factors to close chromatin. For example, the binding of Oct4, Sox2 and Klf4 is impaired by the presence of H3K9me3 (Soufi et al., 2012), while the binding of FoxA is stabilized by H3K4me1/2 (Lupien et al., 2008). Ascl1 is recruited to sites that possess a trivalent chromatin state, composed of H3K4me1, H3K27Ac and H3K9me3 marks, during reprogramming of fibroblasts into induced neurons. Cell types that lack this combination of marks are resistant to Ascl1-driven reprogramming. This mark is also described to be enriched on Ascl1 bound sites during neuronal differentiation (Wapinski et al., 2013). Future studies should investigate the dynamics of such trivalent mark during neurogenesis, and its contribution to the temporal pattern of the Ascl1 program.

We demonstrated that Ascl1 binding to close chromatin results in increased chromatin accessibility. It would be relevant to address how Ascl1 promotes opening of the chromatin structure. Other pioneer factors have been shown to induce loosening of the chromatin structure, directly or indirectly by recruitment of additional factors, recruiting histone modifying or chromatin remodeling enzymes that catalyze the introduction of histone modifications and histone variants (Iwafuchi-doi and Zaret, 2014; Zaret and Carroll, 2011). Little is known, however, on the identity of Ascl1 co-factors, namely those that could mediate its ability to promote chromatin accessibility.

It would also be of interest to investigate if the hierarchical model proposed for the reprograming paradigm (Wapinski et al., 2013) may also be representative of the neurogenesis process. According to this model, binding of Ascl1 precedes and

promotes the recruitment of Brn2 to its bona fide target sites during reprogramming. Specifically in the context of neurogenesis, it would be interesting to investigate which TFs may depend on Ascl1 binding for recognition of their target sites. Analysis of the motifs enriched on DHS-induced sites by digital genomic footprinting reveals enrichment the Neurog/NeuroD-type of E-box on those sites (E-box2 on Figure 2.S 1). One possibility is that NeuroD4, once activated by Ascl1, may work by co-regulating a subset of Ascl1 target genes.

Finally, it is tempting to speculate that the broad effect of Ascl1 in promoting chromatin accessibility described in this study will be important for the reprogramming capacity of this TF upon its ectopic expression in various cell types.

Supplemental data

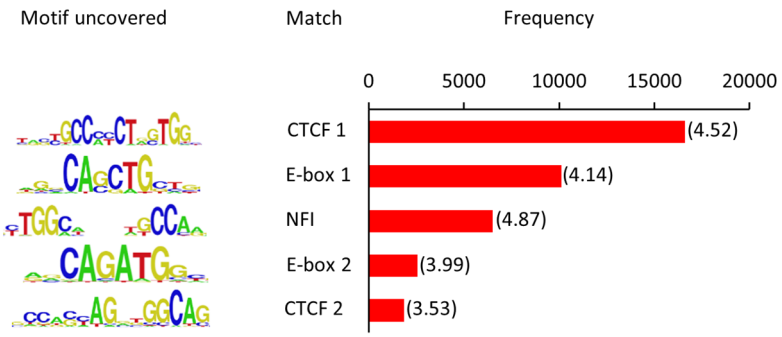

Figure 2.S 1 Variants of the E-box motif are enriched on regions opened *de novo* during neuronal differentiation.

Frequency of motif occurrence at high occupancy sites found within differentiation-induced DHSs by Digital Genomic Footprinting Overrepresentation ratio indicated between brackets.

References

Ali, F., Hindley, C., McDowell, G., Deibler, R., Jones, A., Kirschner, M., Guillemot, F., and Philpott, A. (2011). Cell cycle-regulated multi-site phosphorylation of Neurogenin 2 coordinates cell cycling with differentiation during neurogenesis. Development *138*, 4267–4277.

Ali, F.R., Cheng, K., Kirwan, P., Metcalfe, S., Livesey, F.J., Barker, R. a, and Philpott, A. (2014). The phosphorylation status of Ascl1 is a key determinant of neuronal differentiation and maturation *in vivo* and *in vitro*. Development *141*, 2216–2224.

Ashall, L., Horton, C.A., Nelson, D.E., Paszek, P., Harper, C. V, Sillitoe, K., Ryan, S., Spiller, D.G., Unitt, J.F., Broomhead, D.S., et al. (2009). Timing and Specificity of NF-kB – Dependent Transcription. *324*, 242–246.

Bergstrom, D. a, Penn, B.H., Strand, A., Perry, R.L.S., Rudnicki, M. a, and Tapscott, S.J. (2002). Promoter-specific regulation of MyoD binding and signal transduction cooperate to pattern gene expression. Mol. Cell *9*, 587–600.

Bertrand, N., Castro, D.S., and Guillemot, F. (2002). Proneural genes and the specification of neural cell types. Nat. Rev. Neurosci. *3*, 517–530.

Borromeo, M.D., Meredith, D.M., Castro, D.S., Chang, J.C., Tung, K.-C., Guillemot, F., and Johnson, J.E. (2014). A transcription factor network specifying inhibitory versus excitatory neurons in the dorsal spinal cord. Development 1–10.

Boyle, A.P., Davis, S., Shulha, H.P., Meltzer, P., Margulies, E.H., Weng, Z., Furey, T.S., and Crawford, G.E. (2008). High-Resolution Mapping and Characterization of Open Chromatin across the Genome. Cell *132*, 311–322.

Burk, O., and Klempnauer, K.H. (1991). Estrogen-dependent alterations in differentiation state of myeloid cells caused by a v-myb/estrogen receptor fusion protein. EMBO J. *10*, 3713–3719.

Castro, D.S., Skowronska-Krawczyk, D., Armant, O., Donaldson, I.J., Parras, C., Hunt, C., Critchley, J. a, Nguyen, L., Gossler, A., Göttgens, B., et al. (2006). Proneural bHLH and Brn proteins coregulate a neurogenic program through cooperative binding to a conserved DNA motif. Dev. Cell *11*, 831–844.

Castro, D.S., Martynoga, B., Parras, C., Ramesh, V., Pacary, E., Johnston, C., Drechsel, D., Lebel-Potter, M., Garcia, L.G., Hunt, C., et al. (2011). A novel function of the proneural factor Ascl1 in progenitor proliferation identified by genome-wide characterization of its targets. Genes Dev. *25*, 930–945.

Cave, J.W., Loh, F., Surpris, J.W., Xia, L., and Caudy, M.A. (2005). A DNA Transcription Code for Cell-Specific Gene Activation by Notch Signaling. Curr. Biol. *15*, 94–104.

Hindley, C., Ali, F., McDowell, G., Cheng, K., Jones, a., Guillemot, F., and Philpott, a. (2012). Post-translational modification of Ngn2 differentially affects transcription of distinct targets

to regulate the balance between progenitor maintenance and differentiation. Development *139*, 1718–1723.

Hoffmann, A., Levchenko, A., Scott, M.L., and Baltimore, D. (2002). The IkappaB-NF-kappaB signaling module: temporal control and selective gene activation. Science *298*, 1241–1245.

Imayoshi, I., Isomura, A., Harima, Y., Kori, H., Miyachi, H., Fujiwara, T., Ishidate, F., and Kageyama, R. (2013). Oscillatory Control of Factors Determining Multipotency and Fate in Mouse Neural Progenitors.

Iwafuchi-doi, M., and Zaret, K.S. (2014). Pioneer transcription factors in cell reprogramming. 2679–2692.

Jacob, J., Kong, J., Moore, S., Milton, C., Sasai, N., Gonzalez-Quevedo, R., Terriente, J., Imayoshi, I., Kageyama, R., Wilkinson, D.G., et al. (2013). Retinoid Acid Specifies Neuronal Identity through Graded Expression of Ascl1. Curr. Biol. 1–7.

Li, S., Mattar, P., Dixit, R., Lawn, S.O., Wilkinson, G., Kinch, C., Eisenstat, D., Kurrasch, D.M., Chan, J. a., and Schuurmans, C. (2014). RAS/ERK Signaling Controls Proneural Genetic Programs in Cortical Development and Gliomagenesis. J. Neurosci. *34*, 2169–2190.

Littlewood, T.D., Hancock, D.C., Danielian, P.S., Parker, M.G., and Evan, G.I. (1995). A modified oestrogen receptor ligand-binding domain as an improved switch for the regulation of heterologous proteins. Nucleic Acids Res. *23*, 1686–1690.

Lupien, M., Eeckhoute, J., Meyer, C. a., Wang, Q., Zhang, Y., Li, W., Carroll, J.S., Liu, X.S., and Brown, M. (2008). FoxA1 Translates Epigenetic Signatures into Enhancer-Driven Lineage-Specific Transcription. Cell *132*, 958–970.

Ma, L., Wagner, J., Rice, J.J., Hu, W., Levine, A.J., and Stolovitzky, G. a (2005). A plausible model for the digital response of p53 to DNA damage. Proc. Natl. Acad. Sci. U. S. A. *102*, 14266–14271.

Mangan, S., and Alon, U. (2003). Structure and function of the feed-forward loop network motif. Proc. Natl. Acad. Sci. U. S. A. *100*, 11980–11985.

Mizutani, K., Yoon, K., Dang, L., Tokunaga, A., and Gaiano, N. (2007). Differential Notch signalling distinguishes neural stem cells from intermediate progenitors. Nature *449*, 351–355.

Natarajan, A., Yardimci, G.G., Sheffield, N.C., and Frazer, K. a (2012). Predicting cell-type – specific gene expression from regions of open chromatin the genome. 1711–1722.

Nellesen, D.T., Lai, E.C., and Posakony, J.W. (1999). Discrete enhancer elements mediate selective responsiveness of enhancer of split complex genes to common transcriptional activators. Dev. Biol. *213*, 33–53.

Oishi, K., Watatani, K., Itoh, Y., Okano, H., Guillemot, F., Nakajima, K., and Gotoh, Y. (2009). Selective induction of neocortical GABAergic neurons by the PDK1-Akt pathway through activation of Mash1. Proc. Natl. Acad. Sci. U. S. A. *106*, 13064–13069.

Raposo, A.A.S.F., Vasconcelos, F.F., Drechsel, D., Marie, C., and Johnston, C. (2015). Ascl1 Coordinately Regulates Gene Expression and the Chromatin Landscape during Neurogenesis Article Ascl1 Coordinately Regulates Gene Expression and the Chromatin Landscape during Neurogenesis. Cell Rep. 1544–1556.

Renault, V.M., Rafalski, V. a., Morgan, A. a., Salih, D. a M., Brett, J.O., Webb, A.E., Villeda, S. a., Thekkat, P.U., Guillerey, C., Denko, N.C., et al. (2009). FoxO3 Regulates Neural Stem Cell Homeostasis. Cell Stem Cell *5*, 527–539.

Roemer, K., and Friedmann, T. (1993). Modulation of cell proliferation and gene expression by a p53-estrogen receptor hybrid protein. Proc. Natl. Acad. Sci. U. S. A. *90*, 9252–9256.

Shen-Orr, S.S., Milo, R., Mangan, S., and Alon, U. (2002). Network motifs in the transcriptional regulation network of Escherichia coli. Nat. Genet. *31*, 64–68.

Shimojo, H., Ohtsuka, T., and Kageyama, R. (2008). Oscillations in notch signaling regulate maintenance of neural progenitors. Neuron *58*, 52–64.

Song, L., Zhang, Z., Grasfeder, L.L., Boyle, A.P., Giresi, P.G., Lee, B.K., Sheffield, N.C., Gräf, S., Huss, M., Keefe, D., et al. (2011). Open chromatin defined by DNaseI and FAIRE identifies regulatory elements that shape cell-type identity. Genome Res. *21*, 1757–1767.

Soufi, A., Donahue, G., and Zaret, K.S. (2012). Facilitators and impediments of the pluripotency reprogramming factors' initial engagement with the genome. Cell *151*, 994–1004.

Soufi, A., Garcia, M.F., Jaroszewicz, A., Osman, N., Pellegrini, M., and Zaret, K.S. (2015). Pioneer Transcription Factors Target Partial DNA Motifs on Nucleosomes to Initiate Reprogramming. Cell *161*, 555–568.

Sriuranpong, V., Borges, M.W., Christopher, L., Nakakura, E.K., Watkins, D.N., Christine, M., Nelkin, B.D., Ball, D.W., Strock, C.L., and Blaumueller, C.M. (2002). Notch Signaling Induces Rapid Degradation of Achaete-Scute Homolog 1 Notch Signaling Induces Rapid Degradation of Achaete-Scute Homolog 1. Mol. Cell. Biol.

Takahashi, K., and Yamanaka, S. (2006). Induction of Pluripotent Stem Cells from Mouse Embryonic and Adult Fibroblast Cultures by Defined Factors. Cell *126*, 663–676.

Thurman, R.E., Rynes, E., Humbert, R., Vierstra, J., Maurano, M.T., Haugen, E., Sheffield, N.C., Stergachis, A.B., Wang, H., Vernot, B., et al. (2012). The accessible chromatin landscape of the human genome. Nature *489*, 75–82.

Vasconcelos, F.F., and Castro, D.S. (2014). Transcriptional control of vertebrate neurogenesis by the proneural factor Ascl1. Front. Cell. Neurosci. *8*, 1–6.

Viñals, F., Reiriz, J., Ambrosio, S., Bartrons, R., Rosa, J.L., and Ventura, F. (2004). BMP-2 decreases Mash1 stability by increasing Id1 expression. EMBO J. *23*, 3527–3537.

Wapinski, O.L., Vierbuchen, T., Qu, K., Lee, Q.Y., Chanda, S., Fuentes, D.R., Giresi, P.G., Ng, Y.H., Marro, S., Neff, N.F., et al. (2013). Hierarchical Mechanisms for Direct Reprogramming of Fibroblasts to Neurons. Cell *155*, 621–635.

Webb, A., Pollina, E., Vierbuchen, T., Urbán, N., Ucar, D., Leeman, D., Martynoga, B., Sewak, M., Rando, T., Guillemot, F., et al. (2013). FOXO3 shares common targets with ASCL1 genome-wide and inhibits ASCL1-dependent neurogenesis. Cell Rep. *4*, 477–491.

Wee, K.B., Yio, W.K., Surana, U., and Chiam, K.H. (2012). Transcription factor oscillations induce differential gene expressions. Biophys. J. *102*, 2413–2423.

Weinberg, R.L., Veprintsev, D.B., Bycroft, M., and Fersht, A.R. (2005). Comparative binding of p53 to its promoter and DNA recognition elements. J. Mol. Biol. *348*, 589–596.

Zaret, K.S., and Carroll, J.S. (2011). Pioneer transcription factors: Establishing competence for gene expression. Genes Dev. *25*, 2227–2241.

Acknowledgements

I would like to thank Daniela Drechsel (D.D.) and Diogo S. Castro (D.S.C.) for generating the NS-5 Ascl1-ERT2 cells (D.D.) and performing the Ascl1 ChIP-Seq on NS-5 Ascl1-ERT2 cells t=30min (D.S.C.) and t=18h (D.D.) post-TAM, the DNAse-Seq on proliferating and differentiating NS-5 cells (D.D.) and for ChIP-qPCR and FAIRE-qPCR analyses on Ascl1 knock-out and wild-type embryonic telencephalon (D.S.C) (Figure 2. 7). I would like to thank Alexandre Raposo for the ChIP-Seq and DNAse-Seq datasets pre-processing (alignment with the genome, peak calling) and downstream analyses (Figure 2. 4C-D, Figure 2. 5B, Figure 2. 6A-B, Figure 2. 8A-C, Figure 2.S 1). I would like to thank Corentine Marie and Carlos Parras for providing Ascl1$^{-/-}$ embryos. I would like to thank Abdul Sesay and the NIMR high-throughput sequencing facility for ChIP-Seq library preparation and sequencing and Daniel Sobral and the IGC Bioinformatics Unit for expert assistance. I was supported by a doctoral fellowship (SFRH/BD/51178/2010) from Fundação para a Ciência e a Tecnologia (FCT) and by Instituto Gulbenkian de Ciência.

Chapter 3 – **Function of the zinc-finger factor MyT1 and its transcriptional network in vertebrate neurogenesis**

Abstract

Notch signaling and proneural genes oppositely regulate vertebrate neurogenesis. One of the first hallmarks of the neurogenic transition is the stable downregulation of the Notch signaling effectors, Hes1/5 genes, and concomitant upregulation of proneural genes, such as Ascl1. However, how Hes genes expression become permanently downregulated during neurogenesis is still unclear.

We investigated the function of MyT1, a zinc-finger transcription factor previously linked to the regulation of Notch signaling in Xenopus neurogenesis. Using functional assays in cultured NS cells, complemented with *in utero* electroporation in the developing mouse telencephalon, we found that MyT1 is a direct target of Ascl1 and potentiates Ascl1-driven neuronal differentiation by counteracting the inhibitory effect of Notch signaling. We show that the expression of Hes1, a key downstream effector of the Notch pathway during neurogenesis, is directly controlled by MyT1. Transcriptional, *in vitro* and *in vivo* binding assays show that MyT1 abrogates Notch activation of the Hes1 promoter, by a mechanism based on mutually exclusive binding with RBPJ. A genome-wide search for additional MyT1 target genes indicates MyT1 functions globally as a repressor of gene expression, regulating many additional Notch targets, such as Hes5. Our work provides the first molecular basis for MyT1 function during neurogenesis, revealing a regulatory step whereby, Ascl1 functions to suppress Notch signaling in a cell-autonomous manner in differentiating progenitors.

Introduction

1. Mechanisms of regulation of Notch signaling

Notch signaling pathway has been extensively deployed during cell fate decisions along the metazoan phylogeny and ontogeny. How spatio-temporal specificity of Notch signaling is molecularly encoded is a topic of intensive research and has been suggested to be achieved by selective regulation of its components at multiple levels: from Notch receptor/ligand interaction, Notch receptor processing to target gene selection (Figure 3. 1) (reviewed in (Andersson et al., 2011; Cave, 2011; Fior and Henrique, 2009; Imayoshi and Kageyama, 2014; Kopan and Ilagan, 2009; Pierfelice et al., 2011)). The next subsections provide an overview of the diversity of mechanisms regulating Notch signaling activity in various cell types. Some of the examples mentioned below are described in more detail on Table 3. 1.

1.1. Notch receptor/ligand interaction

In mammals, there are 4 Notch receptors (Notch1,2,3,4) and 5 ligands (Jag1,2 and Dll1,3,4) that have been shown to take part in ligand/receptor interactions with different affinities. In principle, combinatorial expression of Notch receptor/ligand paralogs in interacting cells in different tissues could potentially generate different responses. However, there is very little evidence for differences in signaling output of the different receptor/ligand combinations (Andersson et al., 2011).

The expression of Notch1, 2 and 3 in the VZ of the mouse embryonic telencephalon suggest they may play a role during neurogenesis (Higuchi et al., 1995; Irvin et al., 2001). However, Notch3 deletion does not affect neuronal differentiation or CNS development (Krebs et al., 2003) and Notch2 mutants undergo widespread cell death in the CNS starting from E9, but it is unclear whether this phenotype is caused by a direct or indirect effect of Notch2 in the developing CNS (Hamada et al., 1999).

On the other hand, Notch1 mutant mice die around E11 and exhibit precocious neuronal differentiation in the CNS (de la Pompa et al., 1997).

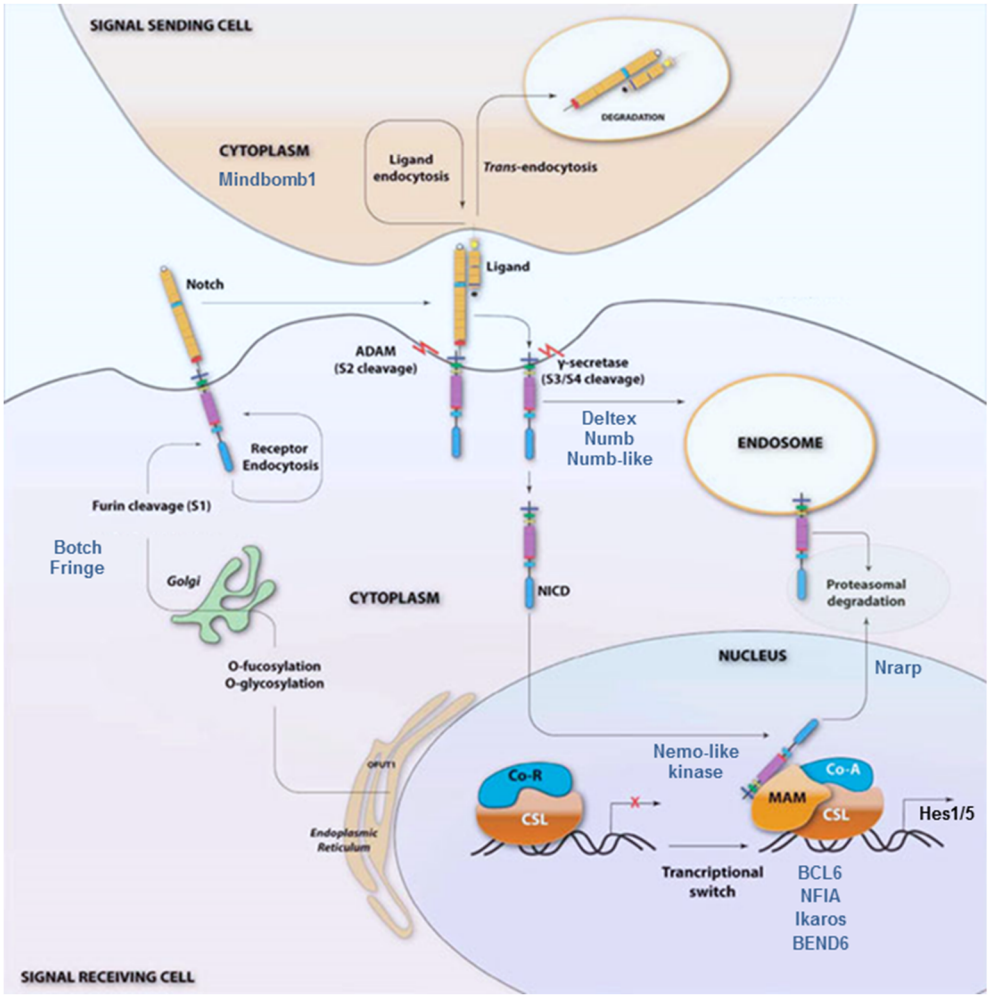

Figure 3. 1 The core elements and regulators of the Notch signaling pathway.

The newly translated Notch receptor protein is glycosylated, subsequently cleaved at site 1 (S1) and targeted to the cell surface. The Notch receptor is activated by binding to a ligand presented by a neighbouring cell. Endocytosis and membrane trafficking regulate ligand and receptor availability at the cell surface. G-Secretase cleaves the Notch transmembrane domain in site 3 and 4 (S3, S4) to release the Notch intracellular domain (NICD). NICD then enters the nucleus where it associates with the DNA-binding TF RBPJ, Maml1 and additional coactivators (Co-A) to activate transcription. In the absence of NICD, RBPJ may associate with corepressor (Co-R) proteins to repress transcription. Regulators of the pathway at various levels are highlighted in blue and their mechanism of action is described on Table 3.1. Figure adapted from (Yavropoulou & Yovos 2014).

Table 3. 1 Regulators of Notch signaling

Protein	Interferes with	Effect on Notch signaling activity	Mechanism	Reference
Mindbomb1	Dll1	Positive	Promotes endocytosis of Notch ligands.	(Yoon et al., 2008)
Nemo-like kinase	Notch receptors	Negative	Promotes phosphorylation of NICD which decrease the NICD-Maml1-RBPJ complex formation.	(Ishitani et al., 2010)
Botch	Notch receptors	Negative	Prevents cell surface presentation of Notch by inhibiting the S1 furin-like cleavage.	(Chi et al., 2012)
Numb, Numb-Like	Notch receptors	Negative/ Positive	Promotes Notch1 internalization and degradation.	(McGill and McGlade, 2003; McGill et al., 2009)
Nrarp	Notch receptors	Negative/ Positive	Binds to Notch transcriptional activator complex and increases NICD turnover.	(Lamar et al., 2001)
Deltex	Notch receptors	Negative/ Positive	Binds to Notch and promotes its ubiquitination and degradation.	(Hori et al., 2004; Matsuno et al., 1995)
Fringe (Lunatic, Manic, Radical)	Notch receptors	Negative	Introduce post-translational modification (fucosylation) on Notch receptor which decrease its stability and affinity for ligand binding.	(Moloney et al., 2000)
Prox1	Notch receptors	Negative	Promotes neurogenesis by binding to the regulatory region of Notch1 promoter and represses its expression by recruiting HDAC3.	(Kaltezioti et al. 2010)
NFIA	NICD/Maml1/RBPJ complex /Hes1	Negative	NFIA binds to Hes1 promoter and represses its expression, a step required for gliogenesis to occur in the telencephalon	(Piper et al. 2010)
Fezf1/2	NICD/Maml1/RBPJ complex /Hes5	Negative	Bind to and repress Hes5 promoter activity during neurogenesis in the forebrain.	(Shimizu et al., 2010)
BCL6	NICD/Maml1/RBPJ complex /Hes5	Negative	Binds to Hes5 promoter, excludes Maml1 from the activator complex and promotes the recruitment of Sirt1 and promotes deacetylation during cortical neurogenesis.	(Tiberi et al., 2012)
BEND6	NICD/Maml1/RBPJ complex /Hes1, Hes5, etc	Negative	Binds to RBPJ on target genes promoters (Hes1, Hes5, Hey1, Blbp). Competes with NICD for RBPJ binding.	(Dai et al., 2013)
Ikaros	NICD/Maml1/RBPJ complex /Hes1	Negative	Competes with RBPJ for binding to Hes1 promoter. Binds to RBPJ BSs directly and promotes H3K4me3. Confers non-responsiveness to active Notch signaling during T-cell development.	(Kleinmann et al., 2008)
Daughterless (Dros. homolog of E protein)	Su(H) / E(spl) (Dros. homologs of RBPJ and Hes genes)	Positive	Cooperates with Notch/Su(H) paired site-containing promoters of the *E(spl)* complex genes.	(Cave et al., 2005)
Grainyhead	Su(H) / E(spl) (Dros. homologs of RBPJ and Hes genes)	Positive	Cooperates with Notch/Su(H) paired site-containing promoters of the *E(spl)* complex genes.	(Furriols and Bray, 2001)
GATA	LIN-12 (C. elegans homolog of Notch)	Positive	Notch-GATA synergy promotes endoderm-specific expression of ref-1 gene.	(Neves et al., 2007)
Hes6	Hes1	Negative	Heterodimerizes with Hes1 and prevents it from binding to DNA.	(Bae et al., 2000)
Id1-3	Hes1	Negative	Heterodimerize with Hes1 and prevent it from binding to DNA.	(Bai et al., 2007)

Interestingly, Notch2 mutant mice do not show alterations either on distribution or intensity of Hes5 and Ascl1 expression, in striking contrast to Notch1 or RBPJ mutants. These results suggest that Notch1/2 receptors might have distinct functions in neurogenesis and points at Notch1, contrary to Notch2, as the main mediator of canonical signaling in the telencephalon (Hamada et al., 1999; Higuchi et al., 1995; de la Pompa et al., 1997).

The Notch ligands Dll1 and Dll3 are expressed at distinct stages along the neuronal lineage in the dorsal and ventral telencephalon. Dll1 expression peaks at the SVZ, an area highly enriched for INPs and newborn post-mitotic neurons. Dll3 expression starts after Dll1 expression, resulting in Dll1 and Dll3 expression in concentric layers in the telencephalon (Campos et al., 2001; Pierfelice et al., 2011). Jag1 expression is enriched on RG cells, while Jag2 expression is enriched on post-mitotic neurons. However, their function in neurogenesis in this brain region remains to be established (Nelson et al., 2013).

The distribution of Notch receptors and ligands is asymmetric within the progenitor types that comprise the germinal layers of the telencephalon. Notch receptors are mostly expressed in RG cells in the VZ, while the major sources of Notch ligand stimulation to RG cells *in vivo* are INPs and newborn neurons (Campos et al., 2001; Kawaguchi et al., 2008; Nelson et al., 2013). It was shown that INPs modulate Notch signaling on RG cells by expressing Dll1 on dynamic and transient elongate processes that can range from short distance (filopodia-like structures) or long distance, connecting INPs in SVZ with RG cells in VZ (Campos et al., 2001; Nelson et al., 2013).

Multiple proteins have been shown to modulate Notch ligand-receptor binding affinity by post-translational modifications of the receptor/ligand (e.g. Fringe molecules) (Moloney et al., 2000). Moreover, the availability of Notch receptor/ligands at the membrane depends not only on the expression/turnover rates of the ligand and the receptor but also on the intracellular trafficking of these

two membrane-bound proteins (regulated by Nrarp, Numb, Numb-Like and Botch, for example, Table 3. 1.) (Chi et al., 2012; Lamar et al., 2001; McGill and McGlade, 2003; McGill et al., 2009).

In addition to the classical trans-activating mechanism across adjacent cells, it has been shown that Notch ligands and receptors may also interact within the same cell (so called interaction "in cis"). This type of interaction has been shown to induce the internalization of the receptor/ligand complex and to result in inhibition of Notch signaling. Thus, the relative proportion and special distribution of Notch receptors/ligands within a cell and across adjacent cells, are important determinants for the cis/trans interaction that will, ultimately, modulate the quality and the intensity of the output signal generated (Del Álamo et al., 2011; Andersson et al., 2011; de Celis and Bray, 1997; Miller et al., 2009; Sprinzak et al., 2010). Dll3 lacks lysine residues in the intracellular domain and, because of that, cannot activate Notch signaling on the neighboring cells (in trans), suggesting that expression of this ligand may provide means of restricting the activation of this pathway.

1.2. Notch transcriptional activity

Upon activation of Notch signaling, NICD is translocated into the nucleus where it interacts with the DNA binding TF RBPJ and, together with the co-activator Maml1, makes part of a large multi-protein transcriptional activator complex (Kageyama et al., 2008). Although little is known on the Notch/RBPJ transcriptional program, the diversity of cellular functions elicited by the Notch pathway suggests that the regulation of at least some of its targets may be cell-context dependent. Below, we mention several reports that start to elucidate how tissue-specific expression of Notch targets is achieved.

Combinatorial interactions with tissue-specific transcriptional activators or repressors has been shown to result in target-specific activation or repression (e.g.

by interaction with the TFs NFIA, Fezf1/2, BCL6, BEND6, Daughterless, Ikaros, Grainyhead, GATA, etc. For details on the mechanisms see Table 3. 1) (Cave et al., 2005; Dai et al., 2013; Furriols and Bray, 2001; Kleinmann et al., 2008; Neves et al., 2007; Piper et al., 2010; Shimizu et al., 2010; Tiberi et al., 2012). In addition, the transcriptional activity of this complex can be regulated by alterations in the affinity between the members of the Notch/RBPJ complex introduced by post-translational modifications (e.g. phosphorylation of NICD by Nemo-like kinases affect its affinity for interacting with Maml1/RBPJ (Ishitani et al., 2010). Binding site architecture, namely the number of DNA binding sites and their relative orientation, may have a strong influence on the affinity of Notch/RBPJ activator complex or RBPJ/co-repressor complex to DNA. For example, inverted repeats of RBPJ binding sites separated by 15-17 nucleotides (called SPS elements) allow for cooperative assembly of dimeric Notch/Maml1/RBPJ complexes. These dimeric complexes exhibit differential threshold for activation by Notch signaling (Arnett et al., 2010; Cave et al., 2005; Nam et al., 2006).

The transcriptional activity of the Notch/RBPJ complex has also been shown to be restricted by epigenetic modifications on histones, the presence of specific histone variants and DNA methylation on its targets (reviewed in (Borggrefe and Liefke, 2012; Borggrefe and Oswald, 2009)). Cell-type specific epigenetic modifications may, therefore, restrict the activity of the Notch/RBPJ complex.

The specificity of Notch/RBPJ transcriptional activity might be achieved by a combination of the above-mentioned mechanisms.

1.3. Hes/E(spl) activity

1.3.1. Identity of Hes/E(spl) target genes

Both Hes and the Drosophila homolog E(spl) gene families encode basic helix-loop-helix (bHLH) transcriptional repressors. An WRPW motif at their C-terminus and an

Orange domain contribute to their repressive function by mediating protein-protein interactions with co-repressor proteins such as Groucho/TLE and other proteins, respectively (Fischer and Gessler, 2007; Kageyama et al., 2007).

Despite the importance of Hes/E(spl) as downstream mediators of Notch signaling in multiple cell types, the identity of their target genes is still poorly explored. In neurogenesis, the most well established Hes/E(spl) targets are the proneural genes. Hes/E(spl) TFs repress proneural genes expression by directly binding to their promoters (see Chapter 1 for more details) (Kageyama et al., 2008; Nakao and Campos-Ortega, 1996). In the absence of Hes/E(spl) genes, proneural genes are upregulated and trigger neuronal differentiation prematurely (Bertrand et al., 2002; Ishibashi et al., 1995). Intriguingly, overexpression of Hes1/E(spl) with proneural genes still results in a strong inhibitory effect on neurogenesis, suggesting that Hes1/E(spl) genes must have additional functions in neurogenesis downstream of proneural genes (Castella et al., 1999; Hinz et al., 1994; Nakao and Campos-Ortega, 1996).

1.3.2. Hes/E(spl) mechanisms of action

In addition to the previously described features of bHLH TFs, a proline residue within the basic domain is conserved in the vertebrate Hes1/5 and the Drosophila E(spl) proteins and is responsible for their DNA binding specificity. Hes/E(spl) bind to DNA via N-box (CACNAG) or C-site (CACGCG) motifs (Lin and Lee, 2012; Nakao and Campos-Ortega, 1996; Oellers et al., 1994; Sasai et al., 1992), while E(spl) transcription factors have been shown to also recognize variants of the E-box motif (CACNTG) (Jennings et al., 1999; Sasai et al., 1992). Mutation of the basic domain renders Hes/E(spl) proteins incapable of directly binding to DNA. Despite of that, they retain some ability to inhibit neurogenesis, suggesting that Hes/E(spl) proteins also act by a mechanism independent of direct DNA binding (Castella et al., 1999; Nakao

and Campos-Ortega, 1996). Consistent with this idea, both E(spl) and Hes1 have been shown to counteract the activity of overexpressed proneural/E-proteins on E-box-containing reporters by a mechanism that depends on protein-protein interactions (Akazawa et al., 1992; Alifragis et al., 1997; Giagtzoglou, 2003; Giagtzoglou et al., 2005). However, it is not yet consensual whether such interactions sequester E-proteins and prevent proneural/E-protein complex formation and subsequent DNA binding, (Lin and Lee, 2012; Sasai et al., 1992) or if this interaction occurs at the DNA and leads to direct repression by recruitment of Groucho (Giagtzoglou, 2003). It is possible that both mechanisms take place and may be determined by relative protein-protein/protein-DNA binding affinities in a promoter-specific fashion.

Hes1 transcriptional activity can be regulated by other bHLH proteins such as Hes6 or Id proteins. These proteins lack DNA binding ability and physically interact with Hes1, thereby sequestering it away from the DNA (Table 3. 1) (Bae et al., 2000; Bai et al., 2007).

2. Downregulation of Notch signaling at the onset of neuronal differentiation

One of the first hallmarks of the neurogenic transition is the stable downregulation of Hes genes and concomitant sustained expression of proneural genes. Proneural TFs induce neurogenesis and concurrently, by inducing the expression of Notch ligands, promote non-cell autonomous activation of Notch signaling on the neighboring cells. The activation of Notch signaling and consequent down-regulation of proneural genes maintain neighboring cells undifferentiated, in a process known as lateral inhibition (Kageyama et al., 2008). In the progenitors that have been instructed to become post-mitotic neurons, active Notch signaling has to be terminated (Kageyama et al., 2009; Louvi and Artavanis-Tsakonas, 2006). Although the reduced expression of Notch ligands by neighboring cells contributes to a decrease in Notch signaling, additional mechanisms should operate to protect

nascent neurons against Notch signals from neighboring cells and maintain neuronal fate. However, in vertebrate CNS, the molecular mechanisms that inactivate Notch signaling in cells destined to become neurons during the initial phases of differentiation remain largely unknown.

Several reports have recently shown that the response to Notch signaling activity is not uniform and is progressively reduced along the successive cellular states that comprise neurogenesis in the mouse telencephalon (Basak and Taylor, 2007; Kawaguchi et al., 2008; Mizutani et al., 2007; Nelson et al., 2013). Specifically, early intermediate neural progenitors (INP) present in the VZ of the dorsal telencephalon display attenuated Notch signaling response (lower RBPJ:GFP reporter activity) as compared to radial glial (RG) cells, despite of the presence of active Notch signaling (nuclear NICD) in both cell types and similar levels of RBPJ. This decreased responsiveness to Notch signaling is accompanied by lower Hes1/5 expression in INPs, as compared to RG cells (Kawaguchi et al., 2008; Mizutani et al., 2007). Inhibition of canonical Notch signaling (RBPJ-dependent) with a pharmacological inhibitor, with short-hairpin RNA (shRNA) for RBPJ or in RBPJ knock-out mice induces the conversion of RG cells into INPs, suggesting that canonical Notch signaling is required for maintenance of RG cells (Gao et al., 2009; Kawaguchi et al., 2008; Mizutani et al., 2007; Nelson et al., 2013) (Figure 3.2). The mechanisms regulating this decreased responsiveness of RBPJ-dependent transcription to active Notch signaling must have a pivotal role for the initiation of the neurogenic program. However, the precise mechanisms initiating and consolidating the inhibition of RBPJ-mediated transcription and the inhibition of Hes genes expression during neurogenesis remain to be elucidated.

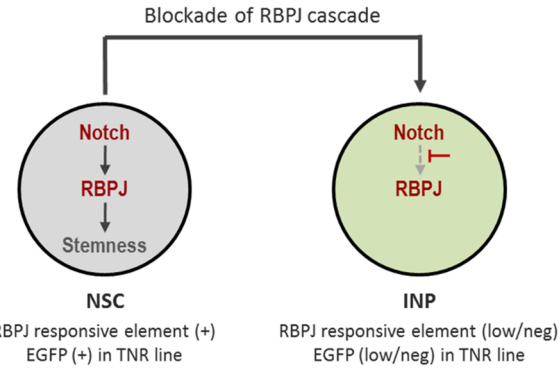

Figure 3. 2 Differential Notch signaling distinguishes NSCs from INPs.

Compared to NSCs, INPs exhibit reduced responsive to activation by Notch signaling, as assessed by reduced activity of RBPJ responsive element of transgenic mouse line and reduced EGFP expression in transgenic Notch reporter (TNR) mice (Mizutani et al. 2007). Figure adapted from (Mizutani et al. 2007).

Recent advances on the characterization of the Ascl1 transcriptional program suggest a cell-autonomous function of proneural factors in down-regulating Notch signaling (Borromeo et al., 2014; Castro et al., 2011; Raposo et al., 2015; Webb et al., 2013). Ascl1 targets mediating such putative function are, for example, Fbxw7 and Dtx4, which are part of ubiquitin ligase complexes and have been shown to promote Notch receptor degradation (Hoeck et al., 2010; Hori et al., 2004; Matsumoto et al., 2011; Matsuno et al., 1995). Other examples are genes encoding TFs previously linked to a relief of Notch inhibition by counteracting the activity of Hes1 (Hes6), by repressing Notch1 expression (Prox1) (Table 3. 1), or by yet unknown mechanisms (MyT1) (Bae et al., 2000; Bellefroid et al., 1996; Kaltezioti et al., 2010). This suggests that, while promoting neuronal differentiation, Ascl1 may concurrently promote a cell-autonomous inhibition of Notch signaling.

3. Myelin transcription factor (MyT1)

3.1. Myelin transcription factor family: structure, expression and function

Myelin transcription factor (MyT1) was identified through its ability to bind to the promoter of proteolipid protein (PLP), one of the essential constituents of myelin (Kim and Hudson, 1992). The MyT1 family comprises 3 members: MyT1 (NZF2), MyT1Like (NZF1 or MyT1L) and MyT3 (NZF3 or St18) that encode structurally related zinc-finger (ZF) TFs (Figure 3. 3). The MyT1 family members are highly homologous, especially within the DNA-binding ZF domains, and are conserved across vertebrate species (Bellefroid et al., 1996; Kim et al., 1997; Romm et al., 2005). All members possess various zinc-finger domains with an unusual C2HC arrangement of the zinc ion-coordinating residues (Jiang et al., 1996; Kim and Hudson, 1992; Yee and Yu, 1998). MyT1 and MyT1Like, unlike MyT3, possess an acidic N-terminal domain and a Serine/Threonine-rich central domain (Jiang et al., 1996; Kim and Hudson, 1992; Yee and Yu, 1998).

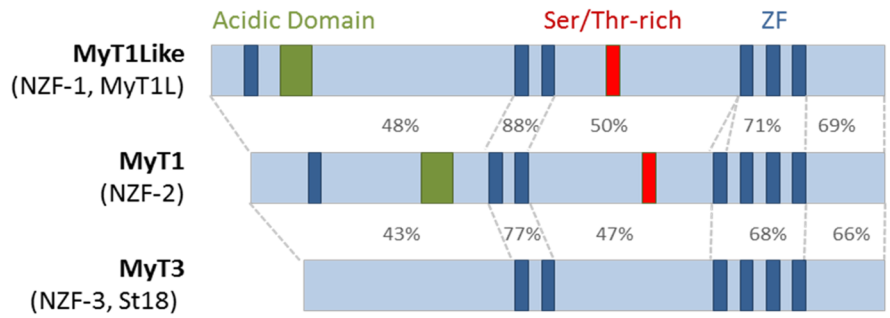

Figure 3. 3 MyT1 family members.

Structural comparison of members of the MyT1 family of transcription factors. MyT1Like (1188 amino acids), MyT1 (1127 amino acids) and MyT3 (1045 amino acids) proteins are schematically shown. The blue, green and red boxes indicate C2HC-type zinc finger units (ZF), the acidic domain and the Ser/Thr-rich region in the central domain, respectively. (Continued on the next page.)

Figure 3. 3 (continued) Percentages of the corresponding nucleotide identities of the zinc finger clusters and of the other portions (set apart by dashed lines) between MyT1 and each other members are shown. Figure refers to proteins encoded by mouse genes. Figure adapted from (Matsushita et al. 2013).

All MyT1 family members are expressed throughout the mouse developing central nervous system (CNS). Specifically in the telencephalon, *in situ* hybridization reveals that MyT1 is expressed in the dorsal and ventral domains in few VZ cells, SVZ cells, and post-mitotic neurons in the MZ; MyT3 expression is restricted to SVZ; and MyT1Like is expressed only in post-mitotic neurons in the MZ (Matsushita et al., 2002, 2013). Interestingly, expression profiling of different progenitor populations in the telencephalon showed that MyT1 expression is strongly induced in INPs, as compared to its expression in RG cells (Kawaguchi et al., 2008; Nelson et al., 2013). Therefore, MyT1 expression pattern is consistent with a role at the onset of neuronal differentiation. In addition to the neuronal lineage, MyT1 expression has been well documented in differentiating oligodendrocytes and in differentiating pancreatic endocrine islet cells (Armstrong et al., 1995; Gu et al., 2004; Nielsen et al., 2004; Wang et al., 2007). MyT1 is also upregulated in disease models of gliomas (Armstrong et al., 1995; Hu et al., 2013) and spinal cord injury (Sim et al., 2002; Wrathall et al., 1998).
First insights into MyT1 function in a neurogenic context were provided by studies in Xenopus embryos, where it was shown to counteract Notch inhibition of neurogenesis in the neural plate and retina, by a mechanism that involves synergy with the proneural factors X-NGNR1, XASH-3 and Xath5 (Bellefroid et al., 1996; Schneider et al., 2001). However, no molecular basis for such activity has been revealed. Interestingly, this synergy with proneural factors has also been observed in mammalian cells, during neuronal differentiation of P19 cells (synergy with Neurog1) (Kameyama et al., 2011) and during endocrine cell differentiation (synergy with Neurog3) (Gu et al., 2004). Another example of synergy between members of the proneural and MyT1 family has been recently described in reprogramming of mouse

and human fibroblasts into induced neurons by the use of defined TFs. In a variety of such protocols, MyT1Like has been shown to enhance the efficiency of Ascl1 in reprogramming and/or the morphological complexity and the electrophysiological properties of the induced neurons (Pang et al., 2011; Pfisterer et al., 2011; Vierbuchen et al., 2010; Yoo et al., 2011). Altogether, these results suggest that the interaction between MyT1 family and proneural TFs is conserved across evolution and deployed in various developmental contexts.

MyT1 germline and pancreas-specific knock-out mice and MyT1 eGFP/Cre knock-in mice have been generated to study MyT1 function during development (Hudson et al., 2011; Wang et al., 2007). Both MyT1 germline knock-out and knock-in animals die at birth presumably due to deficient enervation of the lungs. MyT1 knock-out animals possess abnormal multi-hormone expressing endocrine cells in the pancreas, suggesting defects on the differentiation and maturation of these cells. However, the relatively mild phenotype in pancreas may be due to genetic redundancy resulting from the concomitant upregulation of MyT1Like and MyT3 in the absence of MyT1 (Wang et al., 2007). Unfortunately, neither mouse model has contributed so far to a better understanding of MyT1 function in the nervous system. Gross analysis of neurogenesis in the spinal cord in MyT1 eGFP/Cre knock-in animals, did not detect any defects on the overall number of neurons formed, while an analysis of telencephalic development was not included in such study (Hudson et al., 2011). The description of compound mutants for MyT1 family members remains to be reported.

3.2. MyT1 transcriptional activity

MyT1 was first identified for binding to the proteolipid protein (PLP) promoter (Kim and Hudson, 1992), while MyT1Like was first identified for binding to the retinoic acid response element (B-RARE) on the pituitary specific TF Pit-1 promoter (Jiang et al., 1996). Both promoter regions contain one copy of AAGTT motif. This sequence

comprises the core MyT1 family binding motif identified by multiple rounds of selection/ amplification from a pool of randomized oligonucleotides or digested Xenopus laevis genomic DNA and validated by DNAse footprinting (Bellefroid et al., 1996) or electromobility shift assay (Jiang et al., 1996; Yee and Yu, 1998). The interaction of MyT1 and MyT1L with this motif has been the subject of several structural studies that revealed that efficient binding to DNA requires a pair of ZFs with a 2-fold symmetry (Gamsjaeger et al., 2008; Jiang et al., 1996). MyT1 family members possess two clusters of ZFs that can bind independently to DNA (Gamsjaeger et al., 2013; Jiang et al., 1996), suggesting that one MyT1 molecule, that contains 3 pairs of ZFs, can recognize simultaneously 2 or 3 distinct AAGTT motifs *in vivo* (Gamsjaeger et al., 2013).

Despite the high sequence homology of the ZF domains on MyT1 and MyT1Like, it appears that few non-conserved residues account for differential binding affinities of these two proteins to the AAGTT motif. MyT1Like binds with high affinity while MyT1 binds with low affinity to this sequence, suggesting that MyT1 and MyT1Like may exhibit different target gene selectivity *in vivo* (Besold et al., 2013).

In spite of the scarcity of information on the identity of target genes, few studies have associated MyT1 family members with both transcriptional activation and repression (Bellefroid et al., 1996; Hu et al., 2013; Jiang et al., 1996; Romm et al., 2005; Wang et al., 2007; Yee and Yu, 1998; Yokoyama et al., 2014). MyT1 and MyT1Like have been shown to physically interact with Sin3B in a repressor complex that contains HDAC1 and, to a lesser extent, HDAC2 (Romm et al., 2005). MyT1 also physically interacts with LSD1 demethylase in a complex that contains CoREST and together promote demethylation of H3K4 and concomitant transcriptional repression (Yokoyama et al., 2014). Both interactions with Sin3B or LSD1 are mediated by MyT1/MyT1L central domain (Romm et al., 2005; Yokoyama et al., 2014).

A role in mediating gene activation stems from reporter gene assays in which the Xenopus homolog of MyT1 (X-MyT1) induces the activity of a reporter construct that contains two copies of the MyT1 motif (AAGTT) (Bellefroid et al., 1996). In addition, this assay showed that the central domain and either one of the ZF clusters are required to induce the activity of this reporter. The activation function of MyT1 was further supported by GoF studies in which the activity of MyT1 ZF2-3 fused to VP16 activator or EnR repressor domains were compared to the activity of the full-length protein when inducing endocrine islet cell differentiation in mouse pancreas or primary neurogenesis in Xenopus (Bellefroid et al., 1996; Wang et al., 2008). Altogether, these results suggest that MyT1 activator/repressor function may be dependent on the cellular context and that, in addition to DNA binding through the ZF domains, protein-protein interactions through the central domain may be required for MyT1 function.

In this chapter, we investigate the mechanisms of MyT1 function in neurogenesis. For that we combined functional assays in mouse neural stem cell cultures and in the developing mouse telencephalon, with the genome-wide characterization of its target genes.

Materials and methods

1. Animals

All experiments with C57BL/6 wild-type and Ascl1$^{-/-}$ mice (Casarosa et al., 1999) were carried out upon approval and following the guidelines of the ethics committee of Instituto Gulbenkian de Ciência.

2. Molecular biology

2.1. Expression vectors

The expression vectors used are listed on Table 3. 2.

Table 3. 2 Expression vectors

Vectors	Reference
pCAG-LinkerA-IRES-NLS-GFP (aka pCAG-IRES- GFP)	(Guillemot et al.)
pMycMyT1-7ZF-IRES/Red	(Nielsen et al., 2004) (Addgene #22652)
pCAG-MyT1-IRES-GFP	(Vasconcelos et al. Unpublished)
pPyCAG-MCS-MyT1-FLAG2	(Vasconcelos et al. Unpublished)
pPyCAG-MCS-MyT1-V5	(Vasconcelos et al. Unpublished)
pME-FNIC	(Vasconcelos et al. Unpublished)
pME-FNIC Act Notch	(Kageyama et al.)
pCMX-VP16-RBPJ	(Blanpain et al., 2006)
pPyCAG-MCS-RFX4-FLAG2	(Vasconcelos et al. Unpublished)
pCAG-Sox2	(Bylund et al., 2003)
pCAG-Zeb1-IRES-GFP	(Rosmaninho et al. Unpublished)
LEF-bCTAD	(Vleminckx et al., 1999)
p3XFLAG-CMV-7-NICD1	(Ong et al., 2006) (Addgene #20183)
pFLAG-CMV-2-RBPJ	(Qin et al., 2004)
pFLAG-CMV-2-Maml1	(Wu et al., 2004)
pCAG-Ascl1-IRES-GFP	(Guillemot et al.)
pcDNA 3.1	
pcDNA 3.1 Hes1	

2.2. Luciferase reporter vectors

The luciferase reporter plasmids used are listed on Table 3. 3.

Table 3. 3 Luciferase reporter vectors

Vector	Genomic coordinates	Company / Reference
MyT1	chr2:181498673-181499078	(Vasconcelos et al. Unpublished)
Hes1:Luc	chr16:30064977-30065489	(Nishimura et al., 1998) (Addgene #41723)
Hes5:Luc	chr4 :154334233-154335105	(Nishimura et al., 1998) (Addgene #41724)
M50 Super 8x TOPFlash		(Veeman et al., 2003) (Addgene #12456)

2.3. Site directed mutagenesis

The mutations on the MyT1 BSs on the Hes1 promoter luciferase reporter were generated by site-directed mutagenesis using the plasmid pHes1:Luc and the primers listed on

Table 3. 4. The primers were designed according to the instructions of the QuickChange Site-Directed Mutagenesis Kit (Stratagene). PCR reactions were performed with 50nM of each primer, 100ng of each plasmid, 100µM dNTPs, 7.5U of Cloned Pfu polymerase and Pfu buffer with $MgSO_4$ (Stratagene).

Table 3. 4 Binding sites and primers for site-directed mutagenesis

pHes1:Luc		
MyT1 BS mutations		
Wild-type - TGAAAGTTACTGTGGGAAAGAAAGTTTGGGAAGTTTCA		
MyT1_BS1+2+3_mut - TGAACCCTACTGTGGGAAAGAACCATTGGGAACCTTCA		
MyT1_BS1_mut	FW	CTCTTCCTCCCATTGGCTGAACCCTACTGTGGGAAAGAAAGTTTG
	RV	CAAACTTTCTTTCCCACAGTAGGGTTCAGCCAATGGGAGGAAGAG
MyT1_BS2_mut	FW	GAAAGTTACTGTGGGAAAGAACCATTGGGAAGTTTCACACGAGCC
	RV	GGCTCGTGTGAAACTTCCCAATGGTTCTTTCCCACAGTAACTTTC
MyT1_BS3_mut	FW	GAAAGAAAGTTTGGGAACCTTCACACGAGCCGTTCG
	RV	CGAACGGCTCGTGTGAAGGTTCCCAAACTTTCTTTC
MyT1_BS1+2+3_mut	FW	GAAAGAACCATTGGGAACCTTCACACGAGCCGTTC
	RV	GAACGGCTCGTGTGAAGGTTCCCAATGGTTCTTTC

Reaction was run under the following cycling conditions: 1 cycle 95ºC/5min; 18 cycles (95ºC/50sec; 60ºC/50sec; 72ºC/10min); 1 cycle 72ºC/25min, followed by treatment with DpnI for 3-4h at 37ºC. DH5α bacteria were transformed with DpnI-treated DNA. Multiple mutations on pHes1:Luc were inserted by multiple rounds of site-directed mutagenesis.

2.4. Lentiviral vectors

The lentiviral vectors used are listed on Table 3. 5.

Table 3. 5 Lentiviral vectors

Vector	Company / Reference
TetON-FUW-V5-Ascl1	(Guillemot et al., Unpublished)
TetON-FUW-MyT1-V5	(Vasconcelos et al. Unpublished)
TetON-FUW-MyT1-HA	(Vasconcelos et al. Unpublished)
TetON-FUW-FLAG-Act Notch	(Vasconcelos et al. Unpublished)
TetON-FUW-eGFP	(Vierbuchen et al., 2010) (Addgene #30130)
TetON-FUW-M2rtTA	(Hockemeyer et al., 2008) (Addgene #20342)

2.5. Transformation into chemically competent E.coli

100µL of chemically competent E.coli DH5α were incubated with approximately 500ng of vector DNA for 15min on ice. After a 60sec heat shock at 37ºC the bacteria were chilled on ice for at least 2min, ~250µL LB was added. The bacteria were incubated for ~1h at 37ºC on a shaker incubator, subsequently plated on LB_{Amp} plates and placed overnight at 37ºC.

2.6. DNA purification

Plasmids were isolated from E.coli DH5α using Qiagen Mini, Midi or Maxi-Prep Kits. PCR-Products were purified with the Qiagen PCR Purification Kit, DNA bands from agarose gels were purified with the Qiagen Gel Extraction Kit. All steps were performed as recommended by the supplier.

Alternatively, DNA was separated by phenol-chloroform extraction. For that, one volume (relative to the sample volume) of phenol:chloroform:isoamyl alcohol 25:24:1 (Sigma-Aldrich) was added. The mixture was vortexed shortly and centrifuged for 5min at maximum speed in a tabletop microcentrifuge. The upper phase was recovered and 1/10 volume of 3M sodium acetate and 0.7 volumes of 100% ethanol (RNase free) were added to precipitate DNA. The sample was incubated for 30-60min at RT and centrifuged (10min at RT, 13000rpm). The supernatant was discarded and the pellet was washed with 70% ethanol. After air drying, the pellet was resuspended in an appropriate volume of RNAse and DNase free water (Sigma-Aldrich).

2.7. DNA restriction digestion

Analytical digestions were performed in 50µL total volume with 1-2µg DNA and ~ 2units enzyme overnight at 37ºC.

2.8. Vector dephosphorylation

The dephosphorylation of digested vectors usually decreases re-ligation of the vector. The dephosphorylation procedure was performed with purified pre-digested vector and 2µL of Antarctic phosphatase (New England Biolabs) to a total volume of 20µL for 15min at 37ºC. Heat inactivation of the enzyme was carried out by incubating the mixture for 5min at 65ºC.

2.9. Blunt End generation by Klenow DNA Polymerase

The large fragment of the DNA polymerase I from *E. coli* (also called Klenow fragment) was used to generate blunt ends from digested vectors and inserts. The purified pre-digested vector or insert fragments were incubated with dNTPs and Klenow polymerase (New England Biolabs) for 15min at 25ºC.

2.10. Ligation

Ligations were performed with a 10:1 or 3:1 molar ratio insert/vector, for blunt end or sticky end ligations, respectively, using the DNA and Takara Long ligation kit (Takara Bio) according to manufacturers' instructions. The samples were incubated at 16ºC overnight and transformed the next day. Colonies were selected and inoculated in LB medium with Ampicillin at 37ºC overnight. To confirm the correct insertion of the insert into the vector, digestion was performed at 37ºC for 1.5h and the resulting products were analyzed on a 1% agarose gel.

2.11. Subcloning

2.11.1. pCAG-MyT1-IRES-GFP

The full-length cDNA of mouse MyT1 was excised from pMycMyT1-7ZF-IRES/Red vector with EcoRI restriction enzyme and subsequently digested with Klenow (New England Biolabs) for blunt ends. MyT1 fragment was purified via agarose gel. The pCAG-LinkerA-IRES-NLS-GFP (aka pCAG-IRES-GFP) vector was digested with EcoRV and dephosphorylated with Antarctic phosphatase (New England Biolabs). Ligation of the vector with MyT1 fragment was carried out overnight at +16ºC. Bacteria were transformed and positive colonies were screened by digesting the purified DNA with BamHI and by subsequent analysis of the digestion pattern in agarose gel. The positive colonies were sequenced to confirm the lack of mutations.

2.11.2. pPyCAG-MCS-MyT1-V5

MyT1 sequence lacking the stop codon was amplified by PCR using pMycMyT1-7ZF-IRES/Red as template. The primers used annealed with the N-terminal end of MyT1 sequence and with C-terminal end of MyT1 sequence that precede the stop codon and have restriction sites for NheI or XhoI on the extremities, respectively. PCR was run under the following cycling conditions: 1 cycle 95ºC/3min; 30 cycles (95ºC/1min;

60ºC/1min; 72ºC/6.5min); 1 cycle 72ºC/10min. The PCR product was purified with the PCR Cleanup kit (Qiagen). The MyT1 sequence lacking the stop codon was excised from this vector by digestion with NheI and XhoI and purified via agarose gel.

The pPyCAG-MCS-V5 vector was digested with XhoI and NheI. The linearized backbone was purified via agarose gel.

MyT1 lacking the stop codon was cloned into pPyCAG-MCS-V5 upstream of V5 tag by ligation of the MyT1 fragment and pPyCAG-MCS-V5 backbone. Bacteria were transformed and positive colonies were screened by digesting the purified DNA with NotI and by subsequent analysis of the digestion pattern in agarose gel. The positive colonies were sequenced to confirm the lack of mutations.

2.11.3. pPyCAG-MCS-MyT1-FLAG2

The MyT1 cDNA lacking the stop codon was produced as described above.

The pPyCAG-MCS-FLAG vector was digested with XhoI and NheI. The linearized backbone was purified via agarose gel.

MyT1 lacking the stop codon was cloned into pPyCAG-MCS-FLAG upstream of FLAG tag by ligation of the MyT1 fragment and pPyCAG-MCS-FLAG backbone. Bacteria were transformed and positive colonies were screened by digesting the purified DNA with NotI and by subsequent analysis of the digestion pattern in agarose gel. The positive colonies were sequenced to confirm the lack of mutations.

2.11.4. pPyCAG-MCS-RFX4-FLAG2

RFX4 sequence lacking the stop codon was amplified by PCR using pCR4-TOPO-RFX4 as template. Primers used on the PCR annealed with the N-terminal end of RFX4 sequence and with C-terminal end of RFX4 sequence that precede the stop codon and have restriction sites for NheI or XhoI on the extremities, respectively. Reaction was run under the following cycling conditions: 1 cycle 95ºC/3min; 30 cycles

(95ºC/1min; 60ºC/1min; 72ºC/6.5min); 1 cycle 72ºC/10min. The PCR product was purified with the PCR Cleanup kit (Qiagen). The RFX4 sequence lacking the stop codon was excised from this vector by digestion with NheI and XhoI and purified via agarose gel.

The pPyCAG-MCS-FLAG vector was digested with XhoI and NheI. The linearized backbone was purified via agarose gel.

RFX4 lacking the stop codon was cloned into pPyCAG-MCS-FLAG upstream of FLAG tag by ligation of the RFX4 fragment and pPyCAG-MCS-FLAG backbone. Bacteria were transformed and positive colonies were screened by digesting the purified DNA with NotI and by subsequent analysis of the digestion pattern in agarose gel. The positive colonies were sequenced to confirm the lack of mutations.

2.11.5. pME-FNIC empty

Activated Notch1 (Act Notch) was excised from pME-FNIC Act Notch vector with EcoRI restriction enzyme. The pME-FNIC backbone was purified via agarose gel and re-ligated ON. The positive colonies were sequenced to confirm the lack of mutations.

2.11.6. MyT1-V5 TetON-FUW

MyT1-V5 fragment was excised from pPyCAG-MCS-MyT1-V5 vector using EcoRI restriction enzyme and purified via agarose gel.

The Ascl1-V5 TetON-FUW was digested with EcoRI and the TetON-FUW backbone was purified via agarose gel.

TetON-FUW backbone and MyT1-V5 fragment were ligated overnight. Bacteria were transformed and positive colonies were screened by digesting the purified DNA with SppI and ClaI and by subsequent analysis of the digestion pattern in agarose gel. The positive colonies were sequenced to confirm the lack of mutations.

2.11.7. MyT1-HA TetON-FUW

To generate MyT1 tagged C-terminally with HA-tag, an HA-tag oligonucleotide was inserted into the pPyCAG-MCS-MyT1-V5 vector and MyT1-HA fragment was excised and subcloned into TetON-FUW plasmid.

An HA-tag encoding oligonucleotide with restriction sites for XhoI and NotI in the extremities and additional EcoRI and AgeI restriction sites downstream of the HA-tag sequence was synthetized (Sigma-Aldrich). The pPyCAG-MCS-MyT1-V5 vector was digested with the restriction enzymes XhoI and NotI. The linearized vector and the HA-tag were ligated overnight. The HA-tag was cloned on the C-terminal end of MyT1 sequence upstream of V5-tag and stop codon. Bacteria were transformed and positive colonies were screened by digesting the purified DNA with AgeI and by subsequent analysis of the digestion pattern in agarose gel. The MyT1-HA fragment was excised using EcoRI and purified via agarose gel.

The Ascl1-V5 TetON-FUW was digested with EcoRI and the TetON-FUW backbone was purified via agarose gel.

TetON-FUW backbone and MyT1-HA fragment were ligated overnight. Bacteria were transformed and positive colonies were screened by digesting the purified DNA with SppI and ClaI and by subsequent analysis of the digestion pattern in agarose gel. The positive colonies were sequenced to confirm the lack of mutations.

2.11.8. FLAG-Act Notch TetON-FUW

Activated Notch1 tagged N-terminally with FLAG-tag was excised from pCAG-IRES-GFP-FLAG-Act Notch vector with BamHI and isolated via agarose gel purification. The Ascl1-V5 TetON-FUW was digested with EcoRI and the TetON-FUW was purified via agarose gel. TetON-FUW backbone and FLAG-Act Notch fragment were ligated overnight. Bacteria were transformed and positive colonies were screened by digesting the purified DNA with ApaI or EcoNI and by subsequent analysis of the

digestion pattern in agarose gel. The positive colonies were sequenced to confirm the lack of mutations.

3. Cell culture

3.1. NS-5 cells

NS-5 cells (Conti et al., 2005) were cultured in mouse Neurocult NSC basal medium supplemented with mouse Neurocult NSC proliferation supplement (Stem Cell Technologies), Penicillin-Streptomycin (100U/mL) (Gibco) EGF (10ng/mL) (Peprotech), bFGF (10ng/mL) (Peprotech) and Laminin (1µg/mL) (Sigma-Aldrich) in T-flasks, plates or well plates (Corning).

Notch signaling inhibition of NS-5 cell culture was performed by adding the g-secretase inhibitor LY-411575 (LY) (Lanz et al., 2004) to the culture to a final concentration of 10nM.

1.1. NS-5 Ascl1-ERT2 cells

NS-5 Ascl1-ERT2 cells were generated upon infection of NS-5 cells with pBABE-HA-Ascl1-ERT2 retrovirus, cultured and selected in NS-5 cell medium supplemented with puromycin (1µg/mL) (Calbiochem). For differentiation, HA-Ascl1-ERT2 activity was induced with 4-hydroxytamoxifen (50nM) (Sigma-Aldrich), while reducing EGF concentration to 5ng/mL. (Raposo et al., 2015)

3.2. NS-5 MyT1-V5 TetON cells (NS-5 MyT1-V5 inducible cells)

NS-5 MyT1-V5 TetON cells were generated upon infection of NS-5 cells with MyT1-V5 TetON-FUW and M2rtTA TetON-FUW lentiviruses on the proportion 1:1 and expanded for several passages in NS-5 cell medium. For induction of expression of the TetON-FUW construct, doxycycline hyclate (2µg/mL) (Sigma-Aldrich) was added to the culture.

3.3. NS-5 MyT1-HA/GFP TetON cells (NS-5 MyT1-HA inducible cells)

NS-5 MyT1-HA/GFP TetON cells were generated upon infection with MyT1-HA TetON-FUW, eGFP TetON-FUW and M2rtTA TetON-FUW lentiviruses on the proportion 1:1:1, expanded for several passages and cultured in NS-5 cell medium. For induction of expression of the TetON-FUW construct, doxycycline hyclate (2µg/mL) (Sigma-Aldrich) was added to the culture.

3.4. P19 and HEK293T cells

P19 embryonic carcinoma cells and human embryonic kidney cells (HEK293T) were maintained in Dulbecco's Modified Eagle's Medium (DMEM) / High glucose (Gibco) supplemented with Fetal Bovine Serum Heat Inactivated (10%) (PAA Laboratories, GE Healthcare), Penicillin-Streptomycin (100 U/mL) (Gibco) and L-Glutamine (2mM) (Gibco) in T-flasks, plates or well plates (Corning).

4. Transfection of P19 and HEK23T cells

On the previous day, P19 and HEK293T were plated to obtain a 75% confluency on the day of the transfection. Transfection was carried out with linear polyethylenimine (PEI) (Sigma-Aldrich) in the proportion of DNA:PEI (w/w) of 1:2.5 for P19 cells and 1:3 for HEK293T cells. Total amount of DNA/cm^2, 500 ng. Medium was replaced with fresh medium 4-6h after transfection.

5. MyT1 ShRNA validation

Mouse MyT1 MISSION shRNA vectors were purchased from Sigma-Aldrich (Table 3. 6). Each of the five MyT1 ShRNAs were cotransfected with MyT1 expression vector (pCAG-MyT1-IRES-GFP) in HEK293T cells in a proportion MyT1 ShRNA:MyT1 of 1:1 or 2:1. Cells were lysed and the efficiency of MyT1 protein knock-down was tested by Western blot. Only the analysis of the most efficient MyT1 ShRNA is shown.

Table 3. 6 ShRNA vectors

Vector	TRC Number	Company / Reference
pLKO.1 scramble shRNA	Addgene #1864	(Sarbassov et al., 2005)
pLKO MyT1 ShRNA	TRCN0000434193	Sigma-Aldrich
	TRCN0000081610 (the one shown in results)	Sigma-Aldrich
	TRCN0000081609	Sigma-Aldrich
	TRCN0000081610	Sigma-Aldrich
	TRCN0000081612	Sigma-Aldrich

6. Lentivirus production and infection of NS-5 cells

Replication-incompetent lentiviruses were produced by transient transfection of HEK293T cells with TetON-FUW vectors (Table 3. 5) cotransfected with the viral packaging vector psPAX2 and the viral envelope vector pCMV-VSVG. Medium was replaced with fresh medium 6-8h post transfection. 48h after medium replacement, lentiviral particles were concentrated from supernatant by ultracentrifugation at 90000g for 4h and resuspended in 0.1% BSA PBS.

7. Dual luciferase reporter gene assay

P19 cells were seeded into 48-well plates at a density of 70 000 cells/cm^2. Cells were transiently cotransfected with expression plasmids (Table 3. 2), firefly luciferase reporter plasmid (Table 3. 3) and pCMV-B-galactosidase plasmid as an internal control. 24-36h after transfection, cells were lysed with RGA lysis buffer (Potassium phosphate 100µM pH7.8, 1uM EDTA, 10% glycerol, 1% Triton X-100, 1µM DTT in MilliQ water). Cell lysates were assayed for luciferase and B-galactosidase activities. Fold induction represents the values of (luciferase activity/B-galactosidase activity) for each condition normalized to control condition. Data are presented as mean ± SD of quadruplicate assays.

8. Electromobility shift assay

Probes (Table 3. 7) were annealed (100mM Tris-HCl pH 7.5, 1 M NaCl, 10mM EDTA) and [γ^{32}P] ATP-labeled (PerkinElmer) with T4 polynucleotide kinase (New England Biolabs). Proteins were produced by coupled *in vitro* transcription and translation in rabbit reticulocyte lysates (TNT, Promega) (Table 3. 8). To ensure proper synthesis of the protein of interest, reticulocyte lysates were analyzed by Western blot. For electromobility shift assays, the indicated proteins were incubated with probe in 20µL binding reactions (15% Glycerol, 20mM Hepes pH 7.9, 5mM MgCl2, 50mM KCl, 0.01% Triton X-100, 10mM DTT, 5mM PMSF, 0.2µg/uL herring sperm DNA (Sigma-Aldrich-D7290) in MilliQ water) for 20min at RT. The mixtures were loaded onto 6% non-denaturing polyacrylamide gels in TBE running buffer (89mM Tris-base, 89mM Boric Acid and 2mM EDTA).

Table 3. 7 Primers used for EMSA probes

EMSA probe primer	Sequence
Hes5_FW	GCGGCCTGGGAAAAGGCAGCATATTGAGGCGCGGGGCTCTCAGCATCAGGCCCCGGGATGCTAATGAGGGCGAGCGCGTTCCCACAGCCC
Hes5_RV	GGGCTGTGGGAACGCGCTCGCCCTCATTAGCATCCCGGGGCCTGATGCTGAGAGCCCCGCGCCTCAATATGCTGCCTTTTCCCAGGCCGC
Hes1_WT_F	TGGCTGAAAGTTACTGTGGGAAAGAAAGTTTGGGAAGTTTCACACGAGCC
Hes1_WT_R	GGCTCGTGTGAAACTTCCCAAACTTTCTTTCCCACAGTAACTTTCAGCCA
Hes1_MyT1_BS1_mut_F	TGGCTGAACCCTACTGTGGGAAAGAAAGTTTGGGAAGTTTCACACGAGCC
Hes1_MyT1_BS1_mut_R	GGCTCGTGTGAAACTTCCCAAACTTTCTTTCCCACAGTAGGGTTCAGCCA
Hes1_MyT1_BS2_mut_F	TGGCTGAAAGTTACTGTGGGAAAGAACCATTGGGAAGTTTCACACGAGCC
Hes1_MyT1_BS2_mut_R	GGCTCGTGTGAAACTTCCCAATGGTTCTTTCCCACAGTAACTTTCAGCCA
Hes1_MyT1_BS3_mut_F	TGGCTGAAAGTTACTGTGGGAAAGAAAGTTTGGGAACCTTCACACGAGCC
Hes1_MyT1_BS3_mut_R	GGCTCGTGTGAAGGTTCCCAAACTTTCTTTCCCACAGTAACTTTCAGCCA
Hes1_MyT1_BS1+2+3_mut_F	TGGCTGAACCCTACTGTGGGAAAGAACCATTGGGAACCTTCACACGAGCC
Hes1_MyT1_BS1+2+3_mut_R	GGCTCGTGTGAAGGTTCCCAATGGTTCTTTCCCACAGTAGGGTTCAGCCA

Table 3. 8 Vectors and enzymes used for *in vitro* transcription and translation

Vector	Enzyme	Reference
pCAG-MyT1-IRES-GFP	T7	(Vasconcelos et al. Unpublished)
pSP73 RBPJ	SP6	Johnson, J. et al.

9. Protein lysates preparation

HEK293T cells were transiently transfected with expression constructs using PEI as described above. 24h post transfection cells were washed once with PBS and harvested by scraping in ice-cold lysis buffer (50mM Tris HCl pH 8.0, 150mM NaCl, 10% Glycerol, 0.1% NP-40, proteinase inhibitors (Roche)) and protein quantification was carried out using Bradford method.

10. Protein immunoprecipitation

An equal amount of each protein lysate (500-1000µg) was incubated with an antibody (Table 3. 9) in non-denaturing conditions (50mM Tris HCl pH 8.0, 150mM NaCl, 10% Glycerol, 0.1% NP-40) for 2h at 4ºC, followed by incubation with 25µl of pre-blocked Protein G Dynabeads (Invitrogen) for 2h. Negative controls without antibody or with purified rabbit IgG (MP Biomedicals) were run in parallel. Elution was performed by adding 1x Laemmli buffer to the beads. The immune complexes were analyzed by Western blot using the anti-tag antibodies.

Table 3. 9 Antibodies used in protein immunoprecipitation

Antigen (Species)	Volume used in Protein immunoprecipitation	Catalog number	Company / Reference
MyT1 (mouse)	8µL/50µL beads	WH0004661M2	Sigma-Aldrich
FLAG M2 (mouse)	1µL/50µL beads	F3165	Sigma-Aldrich
V5-tag (mouse)	2.5µL/50µL beads	R960-25	Life Technologies
Purified rabbit IgG	0.44µL/50µL beads	855944	MP Biomedicals

11. Western Blot

Crude cell lysates and immmunoprecipitated samples were diluted in 2x Laemmli buffer (Sigma-Aldrich) and denatured for 5min at 95ºC. Samples were separated in 10-12% SDS-PAGE gels and transferred to nitrocellulose membranes (GE Healthcare) using standard procedures. Blots were probed with the primary and HRP-conjugated secondary antibodies listed on
Table 3. 10 and Table 3. 11.

Table 3. 10 Primary antibodies used in Western blot

Antigen (Species)	Working dilution in WB	Catalog number	Company / Reference
FLAG M2 (mouse)	1:3000	F3165	Sigma-Aldrich
MyT1 (rabbit)	1:5000		(Wang S, Zhang J, Zhao A, Hipkens S, Magnuson MA, 2007)
V5-tag (mouse)	1:2000	R960-25	Life Technologies
α-tubulin (mouse)	1:10 000	T6074	Sigma-Aldrich

Table 3. 11 Secondary antibodies used in Western blot

Antigen / Species	Working dilution in WB	Company / Source
Goat Anti-Rabitt IgG (H+L) Poly-HRP	1:4000	Jackson ImmunoResearch
Donkey Anti-Mouse IgG (H+L) Poly-HRP	1:4000	Jackson ImmunoResearch

12. *In utero* electroporation

Electroporation was used to deliver expression vectors to the ventricular radial glial cells *in utero* as previously described (Saito, 2006). Briefly, uterine horns of E12.5 or E13.5 pregnant dams were exposed by midline laparotomy after anesthetization with Avertin (312mg/kg). 1mL of DNA plasmid corresponding to 3mg mixed with 0.03% fast-green dye in PBS was injected in the telencephalic vesicle using a pulled micropipette through the uterine wall and amniotic sac. 7mm platinum tweezer-style electrodes were placed outside the uterus over the telencephalon and four pulses of

42mV were applied at 400ms intervals by using a BTX square wave electroporator. The uterus was then replaced within the abdomen, the cavity was filled with warm sterile PBS, and the abdominal muscle and skin incisions were closed with silk sutures. The total amount of DNA was kept constant across conditions.

13. Fixation of mouse telencephalon and cryosections

E14.5 mouse heads were fixed at 4°C in 4% PFA PBS, washed once in PBS and dehydrated in 30% sucrose/PBS at 4°C overnight. The dehydrated tissue was then embedded in OCT, frozen and cut into cryosections. Sections were collected on SuperFrost microscope slides and stored at -20°C. Fixations periods with 4% PFA were the following: 60min for immunohistochemistry, ON for *in situ* hybridization and for double *in situ* hybridization/ immunohistochemistry.

14. *In situ* hybridization

Prior to hybridization, frozen sections were air-dried, washed once with PBS for 5min at RT and post-fixed with 4% PFA/PBS for 10min at RT. The sections were washed 3x5min in PBS at RT and incubated with 100mM triethanolamine pH 8.0 for 15min at RT on a rocking platform. During this incubation step, 0.25% acetic anhydride was added drop-wise. 3x5min washes in PBS at RT were performed and incubated for at least 60min at 70ºC in pre-warmed hybridization buffer. *In situ* hybridization was performed on sections with digoxigenin (DIG)-labelled riboprobes. Slides were incubated with RNA-antisense probe in washing buffer overnight at 70°C. Sections were washed 2x15min with buffer B1 at RT, 1x30min with buffer B2 at RT and incubated with anti-DIG coupled to alkaline phosphatase (Roche) (1:2000) in buffer B2 ON at 4ºC. Sections were washed 15min with buffer B1 at RT, 2x30min with buffer B3 at RT and overlaid with filtered NBT/BCIP-Tween 0.1% solution (Sigma) at RT in the dark. When the desired signal developed, the reaction was stopped by washing

3x15min with PBS and post-fixed with 4% PFA in PBS for 10min at RT. After washing in distilled water, slides were dried at RT and mounted in Aqua Poly/Mount (Polysciences).

20x SSC is composed of 3M NaCl, 0.3 M $C_6H_5Na_3O_7$ pH7. Hybridization buffer is composed of 5x SSC, 50% formamide, 250µg/ml yeast tRNA (Sigma-Aldrich), 5x Denhardt's solution, 500µg/ml herring DNA (Sigma-Aldrich). Washing buffer is composed of 2x SSC, 50% formamide and 0.1% Tween-20. Buffer B1 is composed of 100mM Tris-HCL pH 7.5, 150mM NaCl, 0.1% Tween 20. Buffer B2 is composed of 10% sheep inactivated serum in buffer B1. Buffer B2 is composed of 100mM Tris-HCL pH 9.5, 100mM NaCl, 50mM MgCl2, 0.1% Tween-20.

The MyT1 probe was produced from the plasmid pCRII-MyT1 (aka pmMyT1, Addgene # 22713, (Kim et al., 1997)).

The Hes1 probe was produced from the plasmid pBluescript II SK – Hes1.

15. Immunofluorescence

NS-5 cells were grown on glass coverslips coated with poly-L-Lysine (Sigma-Aldrich) and fixed with 4% formaldehyde for 10min. Immunofluorescence on fixed cells was performed using standard procedures. Cells were stained with the primary and secondary antibodies listed on Table 3. 12 and Table 3. 13. Cell nuclei were stained with DAPI (4',6-diamidino-2-phenylindole; Sigma-Aldrich) before mounting in Aqua Poly/Mount (Polysciences).

For immunohistochemistry, cryosection slides were rehydrated in PBS for 5min at RT and primary antibody incubation in blocking buffer (0.5% Triton X-100/10% NGS/PBS) was carried out overnight at 4ºC. The sections were washed 3x15min in PBT (0.1%Triton X-100 PBS) at RT and incubated with secondary antibody in blocking buffer for 2h at RT. The sections were washed 3x15min in PBT. Cell nuclei were stained with DAPI (1:10000) for 15min at RT. 1x15min wash in PBT and 3x15min

washes in PBS were performed before mounting the slides with Aqua Poly/Mount (Polysciences). The dilution of the antibodies used is listed on Table 3. 12 and Table 3. 13.

Table 3. 12 Primary antibodies used in Immunostaining

Antigen (Species)	Working dilution in immunostaining	Catalog number	Company / Reference
Ascl1 (guinea-pig)	1:10 000		Johnson et al.
FLAG M2 (mouse)	1:1000	F3165	Sigma-Aldrich
GFP (chicken)	1:1000	06-896	Millipore
HA-tag (rabbit)	1:1000	ab9110	Abcam
MyT1 (rabbit)	1:1000		(Wang et al., 2007)
Sox2 (rabbit)	1:500	ab5603	Millipore
Tubulin B III (mouse)	1:500	MAB1637	Millipore
Tuj1 (mouse)	1:500	MMS-435P	Covance
V5-tag (mouse)	1:200	R960-25	Life Technologies

Table 3. 13 Secondary antibodies used in Immunostaining

Antigen (Species	Working dilution in Immunostaining	Company / Source
Alexa Fluor 488 Goat Anti-Chicken IgG	1:1000	Life Technologies
Alexa Fluor 488 Goat Anti-mouse IgG	1:1000	Life Technologies
Alexa Fluor 568 Goat Anti-rabbit IgG	1:1000	Life Technologies
Alexa Fluor 568 Goat Anti-mouse IgG	1:1000	Life Technologies
Alexa Fluor 568 Goat Anti-guinea pig IgG	1:1000	Life Technologies

16. Double *in situ* hybridization/immunohistochemistry

For this technique, frozen sections were treated as described in the *in situ* hybridization protocol until the last post-fixation step with 4% PFA. After this step, the immunohistochemistry protocol for sections was performed.

Anti-MyT1 antibody dilution on Table 3. 12.

17. Microscopy

Bright field images or fluorescent images of fixed sections and coverslips were acquired using the microscope Leica DMRA2, equipped with a CoolSNAP HQ CCD (1.3MPx monochrome) digital camera. Confocal fluorescent images of fixed sections were acquired using the laser scanning confocal microscope Zeiss LSM 510 Meta.

18. Image analysis and fluorescence quantification

All images were treated using ImageJ. The number of DAPI, Sox2-, MyT1-HA-, MyT1-V5-, Ascl1-V5-positive cells was quantified using Threshold, Watershed and Analyze particles tools from ImageJ. The number of Act Notch-FLAG- and Tuj1-positive cells was quantified using the Cell Counter plugin from ImageJ. The number of cells counted per condition is mentioned in figures legend. Data is presented as mean ± SD.

19. Chromatin immunoprecipitation

19.1. Chromatin isolation from NS cell cultures

Cells were washed with PBS and fixed in PBS-Mg (1 mM $MgCl_2$ PBS) containing Di-succinimidyl-glutarate (DSG) (Sigma-Aldrich) for 45min at RT on a rocking platform. Cells were washed with PBS and fixed in PBS-Mg with 1% formaldehyde (Sigma-Aldrich) for 10min at RT on a rocking platform. Crosslinking was quenched by addition of glycine to a final concentration of 125mM for 5min at RT. Subsequently, cells were washed twice in PBS and harvested by scraping in 1mg/mL BSA PBS (with proteinase inhibitors (Roche)). After a low speed centrifugation, cell pellets were resuspended in SDS lysis buffer (1% SDS, 10mM EDTA, 50mM Tris pH 8.0, Proteinase inhibitors (Roche)) and incubated for, at least, 10min at +4ºC. 5-7.5µL of lysis buffer/µL of pellet were added. Chromatin was transferred to non-sticky eppendorfs (Ambion) and

sheared by sonication using a Bioruptor sonicator (Diagenode) at high power settings for 15min in 30s ON/OFF cycles at +4ºC. Centrifugation at 14 000rpm for 10min at +4ºC allowed the precipitation of cell debris and the soluble chromatin fraction on the supernatant was collected. DNA concentrations were typically 0.7-3µg/uL. Chromatins were snap-frozen in liquid nitrogen and stored at -80ºC. To verify the efficiency of the sonication, one aliquot of the chromatin was subjected to crosslinking reversal and Proteinase K (0.1mg/mL) (Roche) digestion followed by DNA purification by phenol-chloroform extraction. Fragment size was determined by agarose gel electrophoresis. Typical chromatin fragment size was 300-500bp.

The above described protocol for chromatin isolation was performed prior to all ChIPs except anti-Ascl1 ChIP which suffered the following modifications: cells were fixed only with 1% formaldehyde (Sigma-Aldrich) and sonication was performed for 12min.

19.2. Chromatin isolation from embryonic ventral telencephalon

Embryonic ventral telencephalon was dissected from E12.5 mice and chromatin isolation was performed as described above with the following modifications: chromatin was fixed with 1% formaldehyde (Sigma-Aldrich) for 15min, lysed and homogenized by pipetting in SDS lysis buffer. Sonication was performed for 40-45min.

19.3. Chromatin immunoprecipitation

Reactions were performed in non-sticky eppendorfs (Ambion) using 50-100µg of chromatin and 50µL of magnetic beads and the appropriate antibody in each ChIP reaction (Table 3. 14). As a negative control, an IP without antibody (no ab) was run in parallel. Beads were washed 5 times with washing buffers followed by one wash with TE (10mM Tris-HCl pH 8.0, 1mM EDTA) wash. Bound chromatin was eluted by

incubation of the beads with elution buffer (50mM Tris-HCl pH 8.0, 10mM EDTA, 1% SDS) for 12min at 65ºC. Proteins were digested by Proteinase K (0.1mg/mL) (Roche) for 2h at 42ºC and crosslinking was reverted overnight at 65ºC. The DNA was purified performing one phenol/chloroform extraction and one chloroform:isoamyl alcohol 25:24:1 extraction followed by isopropanol precipitation and centrifugation for 20min at 14 000rpm, +4ºC. Glycogen (40µg) (Sigma-Aldrich) was added on the isopropanol precipitation step to facilitate the visualization of the pellet after centrifugation.

For anti-Ascl1 ChIP, M-450 sheep anti-mouse IgG beads (Invitrogen), low salt IP buffer (20mM HEPES pH 8.0, 20mM NaCl, 2mM EDTA, 0.1% NaDOC, 1% Triton X-100, 1mg/mL BSA, Proteinase inhibitors (Roche)) were used and 5 washes with LiCl buffer (50mM HEPES pH 7.6, 1mM EDTA, 1% NP-40, 0.7% NaDOC, 512mM LiCl) were performed.

For all the other antibodies, Protein G Dynabeads (Invitrogen), high salt IP buffer (20mM HEPES pH 8.0, 200mM NaCl, 2mM EDTA, 0.1% NaDOC, 1% Triton X-100, 1mg/mL BSA, Proteinase inhibitors (Roche)) were used and 2 washes with NaCl buffer (50mM HEPES pH 7.6, 1mM EDTA, 1% NP-40, 0.7% NaDOC, 1 M NaCl) followed by 3 washes with LiCl buffer (50mM HEPES pH 7.6, 1mM EDTA, 1% NP-40, 0.7% NaDOC, 512mM LiCl) were performed.

Table 3. 14 Antibodies used in ChIP

Antigen (Species)	Volume used in ChIP	Catalog number	Company / Reference
Ascl1 (mouse)	3µL/50µL beads	556604	BD Pharmingen
MyT1 (mouse)	9.5µL/50µL beads	WH0004661M2	Sigma-Aldrich
RBPJ (rabbit)	7.5µL/50µL beads	5313	Cell signaling
HA-tag (rabbit)	3µL/50µL beads	ab9110	Abcam
Hes1 (rabbit)	1µL/50µL beads	ab71559	Abcam

19.4. ChIP-qPCR

The purified DNA retrieved from the ChIP was analyzed by qPCR (primers listed on Table 3. 15) using the standard mix protocol of PerfeCTa SYBR Green FastMix, ROX (Quanta Biosciences). Reaction was run under the following cycling conditions: 1 cycle (50ºC/ 2min; 95ºC/ 3min); 40 cycles (95ºC/ 15sec; 60ºC/ 1min); 1 cycle (95ºC/ 15sec; 60ºC/ 15sec; 95ºC/ 15sec) in ABI 7900HT (Applied Biosystems). Quantities of immmunoprecipitated DNA were calculated by comparison with a standard curve generated by serial dilutions of input DNA. Results are shown as mean ± SD of fraction of input chromatin or fold enrichment (Primer/ORF) for triplicate assays and Student's t test was applied for statistical significance. ORFs were used as negative control regions.

Table 3. 15 Primers used in ChIP-qPCR

Primers	Forward Primer	Reverse primer
Dll1 ORF (ORF1)	GTCTCAGGACCTTCACAGTAG	GAGCAACCTTCTCCGTAGTAG
Fbxw7 ORF (ORF2)	CTCGTCACATTGGAGAGTGG	CAGGAGCTTGGTTTCCTCAG
Ank2	CACAGCCTAGACAGGAAGCA	ACATGGTTCTGGGGAACATT
Aqp4	CCACGGTTTCCCTTGTCT	AAGAGATGGTGCCAAAGAGG
Btg2	CCAAACAAAAAGGTTGCTGA	CGGTCTCTCTTCCCAGAGG
Chd7	TTTTGGAAGCAGTTTTGCAC	TGCCACTGACTAAAGCCATC
Dtx4	TCACTTCTCCTTGTCCCAGA	ATTTTCACCTTCAGTGCCTTC
Egr1	CTCAACTTCTCCCTCCTTGC	ACCCTCCTCCTACCCATTCT
Hes1	GGGAAAGAAAGTTTGGGAAGT	GTTATCAGCACCAGCTCCAG
Hes5	GGGAAAAGGCAGCATATTGAGGCG	CACGCTAAATTGCCTGTGAATTGGCG
Id3	GAAAGGTTGCCTGGGACA	GTCTGCGCTGTTTTTGTTTC
Lfng	CTCCCCCACCACTAAGGAG	GGAGAGACACACAGGAAGCA
Lmcd1	ACAGGAAGGGCTGTTACCAT	CTGTTTGCTCTGTGTCTCTGG
MyT1	CTGGCAACACAATTCCAAAG	AGGGGTCATGCTGCTTCTAT
Notch1	CAGACCTGCTTAATTGGCTTC	GGAGACAGAGAAGGCTCCAG
Slc35b1	AAGTGCTCTGGGTGGTAAGG	CTTGGAGGATTGTGATCCAG

19.5. ChIP-Seq

For Sequencing, DNA purified from 4 (anti-HA ChIP-Seq in NS-5 MyT1-HA cells+DOX) or 10 (anti-MyT1, anti-RBPJ, anti-Hes1 ChIP-Seq in NS-5 cells) IPs was merged. Libraries were prepared from 10ng of input and immunoprecipitated DNA according to the standard Illumina ChIP-Seq protocol and sequenced with Illumina GAIIx.

Raw reads were mapped to the mouse genome (NCBI37/mm9) with Bowtie 0.12.7 (Langmead et al., 2009). Sequenced reads were processed after mapping with SAMTools for format conversion and removal of PCR duplicates (Li et al., 2009). Peaks for each sample were called against the input using 1.4.1 (Zhang et al., 2008).

The number of common peaks between two ChIP-Seq datasets was determined using Galaxy (Goecks et al., 2010) using the tools “Concatenate”, “Cluster, merge clusters into single intervals”, from the Operate in genomics intervals tab. Maximal distance between peaks, 1bp overlap. Minimum number of intervals per cluster, 2.

To retrieve the identity of the common peaks present in each dataset the same protocol was applied but the option “Cluster, find cluster intervals, output grouped by clusters” was used.

19.6. ChIP-Seq peak visualization

To visualize the ChIP-Seq peaks, the bigwig files from each ChIP-Seq dataset were loaded onto the UCSC genome browser (http://genome.ucsc.edu/).

19.7. Peak annotation

Annotation of ChIP-Seq peaks was done with GREAT (McLean et al., 2010) using single nearest TSS annotation. Maximal distance, 100 Kb. The percentage of peaks at a certain distance from the nearest TSS and the overlap with gene feature were plotted using PAVIS (Huang et al., 2013) with default settings.

19.8. Density plots

ChIP-seq normalized tag signals were calculated using a 10bp sliding window over the ± 2kb region around each peak summit to generate the occupancy profiles (in-house developed algorithm). These were plotted as heat maps of signal density using R/Bioconductor packages (http://www.Rproject.org/ and http://CRAN.R-project.org/package=gplots).

20. Gene expression analysis

NS-5 Ascl1-ERT2 cells were plated in 6-well plates (600 000 cells/ well). Differentiation was induced 24h after plating by reducing EGF concentration to 5ng/mL and by adding 4-hydroxy-tamoxifen (TAM) (Sigma-Aldrich) (50nm). Samples were collected 0, 4, 12, 24 and 48h post TAM.

NS-5 MyT1-V5 TetON cells were plated in 6-well plates (600 000 cells/ well). 24h after plating, MyT1-V5 expression was induced by adding doxycycline hylate (DOX) (Sigma-Aldrich) to the culture. Samples were collected 0 and 4h post DOX.

NS-5 MyT1-HA TetON cells were plated in 6-well plates (600 000 cells/ well). MyT1-HA expression was induced by adding doxycycline hylate (DOX) (Sigma-Aldrich) to the culture. Samples were collected 0, 2, 4, 6, 8 and 24h post DOX.

NS-5 wt cells were plated in 6-well plates (600 000 cells/ well). Notch signaling was inhibited by adding the gamma-secretase inhibitor LY411-575 (LY) (Lanz et al., 2004) to the culture. Samples were collected 0 and 4h post LY.

All samples were prepared in triplicate.

1.2. RNA extraction

Total RNA was isolated from cells by using Trizol reagent (Invitrogen) and alcohol precipitation. Extracted RNA was purified by DNAse I (Roche) treatment followed by

Rneasy column purification (RNA CleanUp protocol, Qiagen). EDTA inactivation of DNAse I step was omitted.

20.1. cDNA production and quantitative real-time PCR (RT-qPCR)

cDNA was synthetized using the High-Capacity RNA-to-cDNA kit (Applied Biosystems) according to the manufacturers' instruction. An equal amount (500-1000 ng) of total input RNA was used on each experiment.

Gene expression analysis by quantitative real-time PCR using PerfeCTa SYBR Green FastMix, ROX (Quanta Biosciences) was carried out according to the manufacturers' instructions on a ABI7900 HT machine (Applied Biosystems). The primers used are listed on Table 3. 16. Triplicates of each biological replicate were used in the RT-qPCR. Values are normalized to β-actin expression levels and to untreated sample. Results are shown as mean ± SD of triplicate assays and Student's t test was applied for statistical significance.

Table 3. 16 Primers used in expression-qPCR

Gene	Forward Primer	Reverse primer
β-actin	CTAAGGCCAACCGTGAAAAG	ACCAGAGGCATAGGGACA
Aqp4	GTTGGAGGATTGGGAGTCA	TCAGTTCGTTTGGAATCACAG
Btg2	TGGGTTTCCTCTCCAGTCTC	CCTTTGGATGGTTTTTCTGG
Dll1	GGGCTTCTCTGGCTTCAAC	TAAGAGTTGCCGAGGTCCAC
Dtx4	AACCAGTTCCGCCAAGAC	CTCCCATTCCCACACGAC
Egr1	TGAGCACCTGACCACAGAGT	AGTCGTTTGGCTGGGATAAC
GAPDH	GGGTTCCTATAAATACGGACTGC	CCATTTTGTCTACGGGACGA
Hes1	TGAAGGATTCCAAAATAAAATTCTCTGGG	CGCCTCTTCTCCTGATAGGCTTTGATGAC
Hes5	AAGTACCGTGGCGGTGGAGAT	CGCTGGAAGTGGTAAAGCAGC
Id3	TCATAGACTACATCCTCGACCTTC	CACAAGTTCCGGAGTGAGC
Lfng	CCACTCCCACCTAGAGAACCT	ACTGCGTTCCGCTTGTTC
Lmcd1	GATCCATCCAAAGAAGTGGAA	TGTCAGCGTAGACCACAGG
MyT1	GGCCATGCATGAAAATGTACT	GCAATGGGACATCCAGATAAA
Notch1	CTGGACCCCATGGACATC	GGATGACTGCACACATTGC
Tubb3	GCGCATCAGCGTATACTACAA	CATGGTTCCAGGTTCCAAGT

20.2. Gene expression microarrays

Samples used for microarray analysis were obtained from biological triplicates of NS-5 MyT1-V5 TetON cells 0 and 4h post DOX induction. Total RNA was extracted as described above. RNA concentration and purity were determined by spectrophotometry and integrity was confirmed using an Agilent 2100 Bioanalyzer with a RNA Nano Kit (Agilent Technologies). 100ng of RNA were processed by using the Ambion WT Expression Kit (Life Technologies) and hybridized to the Affymetrix Mouse Gene 1.0 ST Array, according to the manufacturers' protocol.

20.3. Gene expression microarrays analysis

Analysis of microarray CEL files was performed using Chispter software (v 3.1.0, (Kallio et al., 2011)). Quality control analysis of the chips was performed before normalization using relative expression values (RLE) and normalized unscaled standard error (NUSE) box plots. The RLE box plot allow the identification of deviant arrays. Assuming that most probesets on arrays do not change, most of the RLE values should be close 0. The deviant arrays can be identified by not being centered at 0, or being more spread out than the other arrays. The NUSE box plot allows the visualization of the standard errors from the probe-level model. The deviant arrays can be identified by not being centered at 0, or being more spread out than the other arrays. No deviant arrays were identified.

Calculation of expression estimates using the RMA normalization method and log2-transformation was performed using "Normalization / Affymetrix gene arrays" tool.

To determine the similarity between the chips, dendrogram and principle component analyses were run on normalized chips. Clustering of chips using Pearson correlation and average linkage method can be visualized with the dendrogram. Both dendrogram and principle component analysis of chips allows to visualize that biological replicates cluster, samples are distinct.

For significance analysis, empirical Bayes two-group test with Benjamini-Hochberg post-hoc p value correction was used. P value cutoff, 0.05. Linear fold change cutoff, |FC|>1.2. Annotation of probesets was performed using the Chipster tool "Annotation / Affymetrix, Illumina or Agilent gene list".

21. In silico TF motif identification

We have used CisFinder (Sharov and Ko, 2009) in order to identify motifs enriched in the vicinity of ChIP-Seq peak summits. Searches were run against a control dataset with the same number and the same length of the test dataset peaks located 2 Kb upstream. FDR<0.05%. The motifs shown are the result of "Identify motifs, Cluster of motifs" tool. Match threshold for clustering, 0.8 (MyT1 and Hes1) or 0.65 (RBPJ). FDR<0.05%.

Motif fold enrichment (test/control) and percentage of peaks with motif plots were made using the abundance tables obtained with the Cisfinder Search tool. Number of false positives per 10 Kb, 1. Control dataset with the same number of peaks and the same length of the test dataset but located 2 Kb upstream. MyT1 BS AAGTT, E-box, TC-box, N-box and C-site were searched as consensus motifs. X-box was searched as a PWM motif. ChIP-Seq datasets' cutoffs and fragment size are mentioned on the figures legend.

Frequency distributions were plotted using the frequency tables obtained with the Cisfinder Search tool upon search of the motifs in the 2000bp regions centered on the ChIP-Seq peak summit. Number of false positives per 10 Kb, 1. Interval for frequency distribution, 50 bp. Control dataset with the same number of peaks and the same length of the test dataset but located 2 Kb upstream. MyT1 BS AAGTT, E-box, TC-box, N-box and C-site were searched as consensus motifs. X-box was searched as a PWM motif. ChIP-Seq datasets' cutoffs are mentioned on the figures legend.

Hierarchical clustering of ChIP-Seq peaks based on the presence or absence of the represented motifs. MyT1 BS AAGTT, E-box, TC-box, N-box and C-site were searched as consensus motifs. X-box was searched as a PWM motif. Abundance tables obtained with the Cisfinder Search tool were converted to binary (1-presence, 0-absence). Only the peaks that have at least one of the motifs searched are represented. Hierarchical clustering was plotted as heat maps with R/Bioconductor "hclust", "heatmap" packages. ChIP-Seq datasets' cutoffs and fragment size are mentioned on the figures legend.

22. Gene ontology analysis

Gene ontology-based analysis was used for the identification of enriched gene functions.

The MyT1 repressed targets (bound by MyT1 and downregulated in MyT1 GoF microarrays) Gene Ontology Biological Process analysis with functional annotation clustering was carried out using DAVID v6.7 (Dennis et al., 2003). Control dataset, all the genes present on the gene expression microarray (MoGene 1.0 ST v1). Enrichment score (EASE) < 0.05. Similarity threshold for clustering, 0.8. P (MyT1 ChIP-Seq) < 10^{-5}. P (MyT1 GoF microarrays) < 0.05. Panther pathway analysis was carried out using DAVID v6.7 (Dennis et al., 2003). Control dataset, all the genes present on the gene expression microarray (MoGene 1.0 ST v1). Enrichment score (EASE) < 0.05. For the genes commonly bound by Hes1 and Ascl1, Gene Ontology Biological Process analysis was performed using GO Tool Box (http://genome.crg.es/GOToolBox/) with Hypergeometric test for statistical significance (P<0.01). P (Hes1 and Ascl1 ChIP-Seq) < 10^{-10}. Fragment size, whole peak width. Maximal distance for overlap between Hes1 and Ascl1 ChIP-Seq peaks, 1bp overlap.

23. Binding and expression data integration

Calculation of P values for the association between binding events and up- or down-regulated genes was performed by sampling the total number of genes represented in the microarray 1000 times and assuming a normal distribution. MyT1 ChIP-Seq peak overlap with expression data from MyT1 GoF microarrays calculated and plotted as heat maps with R/Bioconductor packages "genomeIntervals", "gplots", and in-house developed scripts.

24. Other datasets used

The ChIP-Seq, RNA-Seq and gene expression microarrays datasets used on this study but not directly generated for this study are listed on Table 3. 17.

Table 3. 17 Datasets used generated by other studies

Dataset	Reference	Accession numbers
ChIP-seq Ascl1-ERT2, t=30min	(Raposo et al., 2015)	E-MTAB-2384.
ChIP-seq Ascl1-ERT2, t=18h	(Wapinski et al., 2013)	PMID:24243019
ChIP-seq Ascl1-ERT2, input	(Wapinski et al., 2013)	PMID:24243019
ChIP-seq RBPJ in NS-5 cells	(Laranjeira, C; Castro, DS; unpublished)	
NS-5 HA-Ascl1-ERT2 microarrays (Ascl1 GoF)	(Raposo et al., 2015)	
Dataset	Reference	Description
Microarrays on Ascl1 LoF in telencephalon	(Parras, C. unpublished)	E 13.5 ventral telencephalon wt and Ascl1 $^{-/-}$ mice
Microarrays on Ascl1 GoF in telencephalon	(Gohlke et al., 2008)	*in utero* electroporated E10.5 mouse telencephalon with control or Ascl1 expressing vectors
Microarrays on Ascl1 LoF in NS cells	(Castro et al., 2011)	wild-type and bHLH domain of Ascl1 fused to EngR electroporated NS-5 cells
RNA-Seq on Notch inhibition in NS cells	(Laranjeira, C; Castro, DS; unpublished)	N5-5 0 and 4h post treatment with the g-secretase inhibitor LY-411575

25. Public *in situ* hybridization databases

In situ hybridization of sagittal sections of O.C.T. embedded and frozen mouse E14.5 and E13.5 embryos were collected from GenePaint (http://www.genepaint.org/) and

Allen Brain Atlas (http://developingmouse.brain-map.org/) public databases, respectively

Results

1. MyT1 transcriptional network in vertebrate neurogenesis

1.1. MyT1 expression pattern in mouse embryonic telencephalon is consistent with a role at the onset of neuronal differentiation

Several observations suggested the zinc finger TF MyT1 may be under the regulation of Ascl1, prompting our interest in understanding its function in vertebrate neurogenesis. Accordingly, MyT1 expression is increased or decreased in expression profiling studies using DNA arrays after Ascl1 GoF or LoF, respectively, both in cultured NS cells and in mouse embryonic telencephalon (Figure 3.S 1) (Castro et al. 2011; Gohlke et al. 2008; Raposo et al. 2015, Castro et al. unpublished). A previous characterization of MyT1 expression in the mouse embryo by *in situ* hybridization revealed expression of MyT1 during the neurogenic period in both PNS and CNS regions, starting in the earliest differentiated neurons within the neural epithelium and neural crest at E9.5 (Matsushita et al., 2002, 2013). At the peak of the neurogenic phase (E14.5) MyT1 transcript in the telencephalon is highest at SVZ (with some expression in scattered cells of the VZ), its expression decreasing in post mitotic neurons before being switch off as differentiation proceeds (Figure 3. 4A). We reinvestigated its expression by immunohistochemistry in the ventral telencephalon, a region where Ascl1 function as a regulator of neurogenesis has been well characterized. MyT1 expression domain is largely overlapping with that of the neuronal marker TuJ1 (Figure 3. 4B). At the cellular level, many but not all MyT1 expressing cells in the SVZ co-express TuJ1, suggesting MyT1 expression occurs in both INPs and differentiating neurons (Figure 3. 4D). Occasionally, MyT1 expressing cells can be seen interspersed in the VZ, showing also TuJ1 expression (Figure 3. 4D). While MyT1 and Ascl1 expression domains are mostly non-overlapping, some cells

co-expressing both factors can be found in the SVZ, as expected from Ascl1 expressing INPs (Figure 3. 4C-D). Overall, the observed expression pattern is consistent with MyT1 starting to be expressed at the transition from NSCs to differentiating neurons, either directly (VZ) or indirectly through the generation of INPs (SVZ). Thus, MyT1 expression is consistent with a function at the onset of neuronal differentiation. The persistent expression of MyT1 in differentiating neurons suggests also a function for MyT1 at later stages.

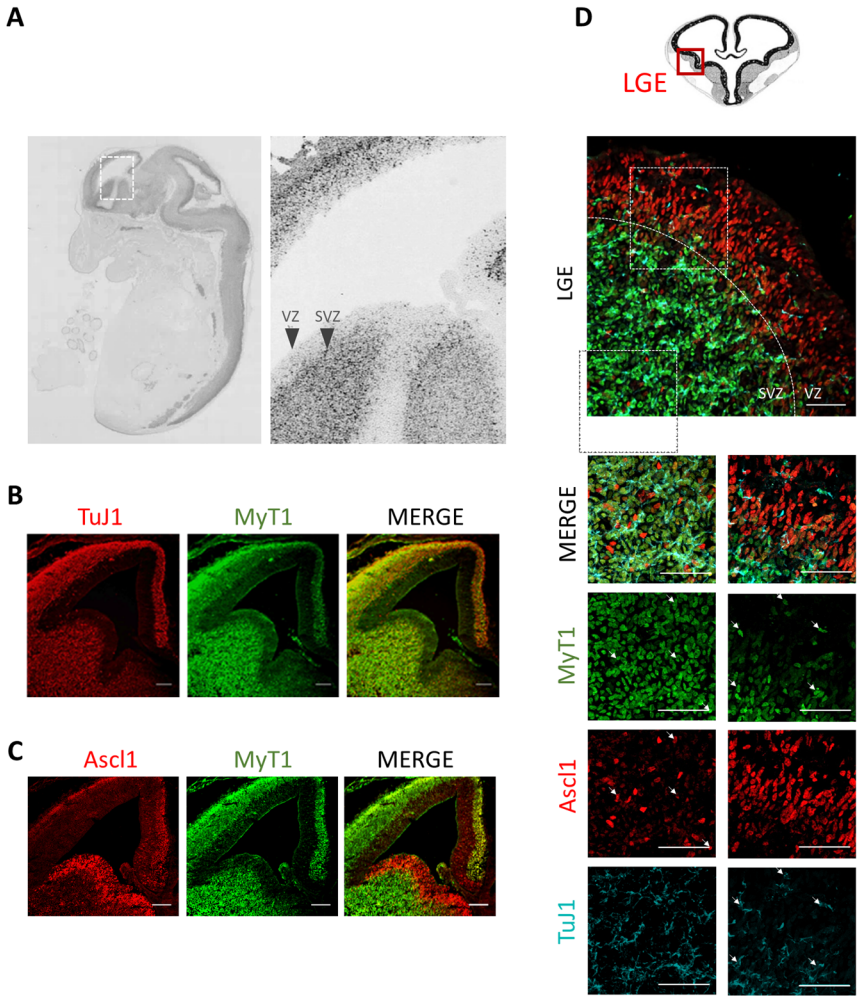

Figure 3. 4 MyT1 expression pattern is consistent with a function at the onset of neuronal differentiation.

(A) Expression pattern of MyT1 on sagittal sections of E14.5 mouse telencephalon (images from the public *in situ* hybridization database GenePaint). (Continued on the next page.)

Figure 3. 4 (continued) **(B)** MyT1 (green) and neuronal marker B-III-Tubulin (TuJ1, red) expression in frontal sections E14.5 mouse telencephalon detected by immunohistochemistry. Scale bar, 100µm. **(C)** MyT1 (green) and Ascl1 (red) expression in frontal sections E14.5 mouse telencephalon detected by immunohistochemistry. Scale bar, 100µm. **(D)** MyT1 (green), Ascl1 (red) and TuJ1 (cyan) expression in E14.5 mouse lateral ganglionic eminence (LGE) of the ventral telencephalon detected by immunohistochemistry. Scale bar, 100µm. Dashed squares highlight regions of the VZ and of SVZ. White arrows indicate co-localization of MyT1 and Ascl1 in the SVZ (left panel) or of MyT1 and TuJ1 in the VZ (right panel). VZ, ventricular zone; SVZ, subventricular zone.

1.2. MyT1 is a direct target of Ascl1

We next analyzed the temporal kinetics of MyT1 induction in a cellular model of neurogenesis driven by Ascl1 (NS-5 Ascl1-ERT2 cells, see Chapter 2) (Figure 3. 5A). Upon Ascl1-ERT2 activation, MyT1 protein levels increase (Figure 3. 5B). The induction of MyT1 occurs in the same cells in which TuJ1 is induced, suggesting that MyT1 is upregulated in differentiating neurons (Figure 3. 5C). The increase in MyT1 transcripts occurs after the increase in Dll1 transcript, an early Ascl1 target (Castro et al., 2006), and precedes the increase in B-III-Tubulin transcript (Figure 3. 5D), an early neuronal marker that is also directly activated by Ascl1 (Castro et al., 2011). This timing of MyT1 induction suggests MyT1 expression may be directly controlled by Ascl1. Effectively, visual inspection of the ChIP-Seq enrichment profile of Ascl1 in differentiating NS-5 Ascl1-ERT2 cells 18h post-TAM (Raposo et al., 2015) identifies several Ascl1 binding events during neuronal differentiation at MyT1 putative regulatory regions (Figure 3. 6A). We validated Ascl1 binding within the MyT1 locus by performing ChIP-qPCR in chromatin extracted from E12.5 mouse ventral telencephalon (Figure 3. 6B). Moreover, Ascl1 can transactivate a putative enhancer region of MyT1, in a reporter gene assay in transfected P19 cells (Figure 3. 6C). *In situ* hybridization of MyT1 in Ascl1 null embryos ($Ascl1^{-/-}$) reveals an overall decrease in MyT1 expression (Figure 3. 6D), consistent with an overall reduction of neurogenesis in the absence of Ascl1 (Casarosa et al., 1999). The fact that MyT1 expression in $Ascl1^{-/-}$ mice is not totally abolished suggests that, in addition to Ascl1, other

pathways must regulate MyT1 expression *in vivo*. Altogether, these results demonstrate that MyT1 is a direct target of Ascl1 in differentiating neuronal progenitors.

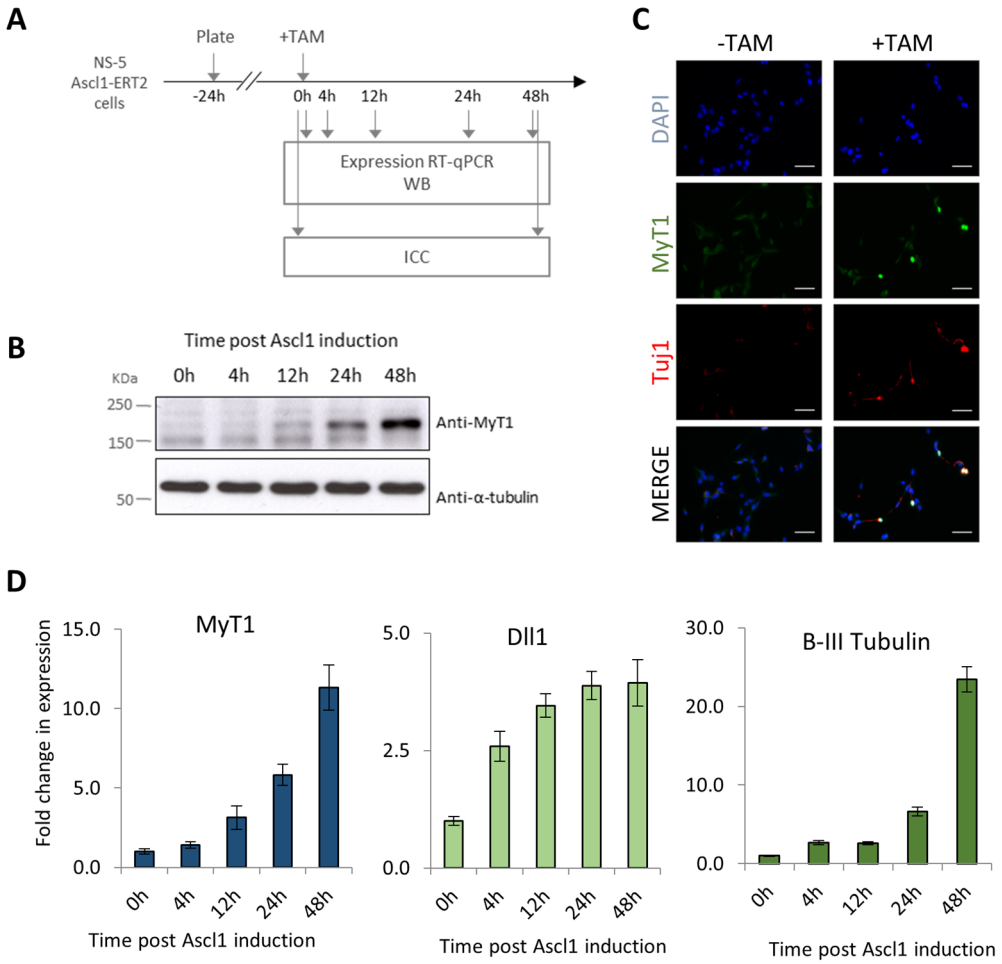

Figure 3. 5 MyT1 is induced during neuronal differentiation downstream Ascl1.

(A) Diagram depicting the experiment in which Ascl1-ERT2 was induced by addition of tamoxifen to NS-5 Ascl1-ERT2 cells. Subsequent expression Real-time PCR, Western blot and ICC analyses were performed at indicated time-points after induction. **(B)** Analysis of MyT1 protein levels performed by Western blot 0, 4, 12, 24, 48h upon induction. α-tubulin was used as loading control. **(C)** Immunocytochemical analysis of MyT1 (green) and Tuj1 (red). Cell nuclei are labeled with DAPI (blue). Scale bar, 40µm. **(D)** RNA expression analysis

of MyT1, Dll1 and B-III-Tubulin was performed by Real-time PCR at 0, 4, 12, 24, 48h post-TAM. Values are normalized to B-actin expression levels. Mean ± SD of triplicate assays are shown.

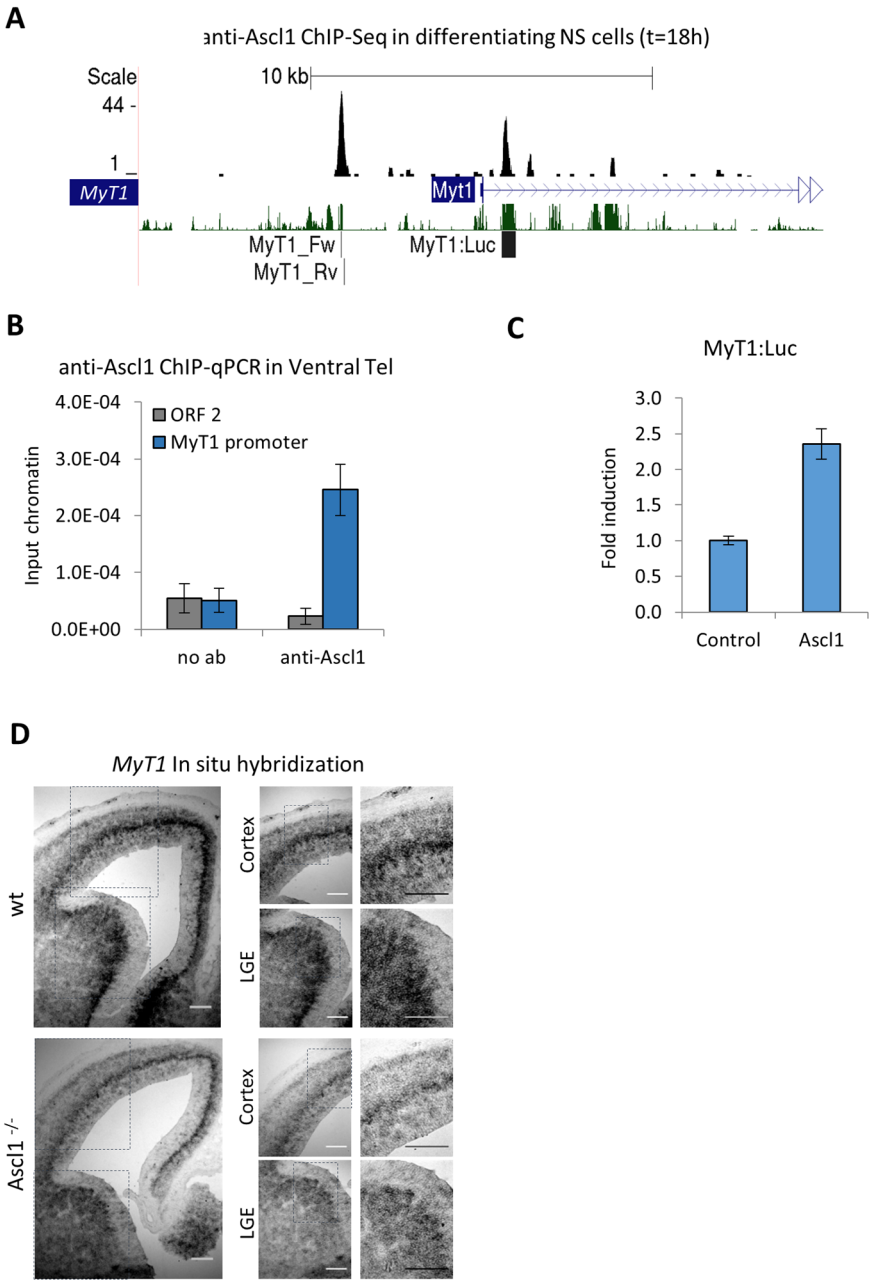

Figure 3. 6 MyT1 is a direct target of Ascl1 in neural stem cells.

(A) Visual representation of Ascl1 ChIP-Seq enrichment profiles at MyT1 locus in differentiating NS-5 Ascl1-ERT2 cells 18h post-TAM. Green track, Mammal conservation by PhastCons. MyT1_FW and MyT1_RV,

location on the genome of the primers used on ChIP-qPCR. MyT1:Luc, location on the genome of the MyT1 regulatory region present on the luciferase reporter (pMyT1:Luc). (Continued on the next page.)

Figure 3. 6 (continued) **(B)** Validation of Ascl1 binding to MyT1 regulatory region by ChIP-qPCR using chromatin extracted from E12.5 mouse ventral telencephalon. ORF2 refers to a negative control region. Mean ± SD of triplicate assays are shown. **(C)** Ascl1 induces MyT1 promoter activity. Reporter gene assay in P19 cells transfected with a control or Ascl1 expression vector in combination with a promoter-reporter construct expressing luciferase under the control of a MyT1 regulatory region (pMyT1:Luc). Mean ± SD of quadruplicate assays are shown. **(D)** *In situ* hybridization of MyT1 in the telencephalon of E14.5 wt or Ascl1 $^{-/-}$ mice. Scale bar, 140µm.

1.3. MyT1 enhances Ascl1 ability to promote neuronal differentiation of NS cells

We next asked if the cooperation between MyT1 and proneural genes during neuronal differentiation, previously demonstrated in Xenopus (Bellefroid et al., 1996; Quan et al., 2004; Schneider et al., 2001), also occurs in mammalian neurogenesis. To address this, we infected proliferating NS-5 cells with lentiviruses expressing Ascl1 and/or MyT1 and assayed neuronal differentiation by immunocytochemistry using an anti-Tuj1 antibody (Figure 3. 7A). In accordance with previous findings (Berninger et al., 2007; Farah et al., 2000; Nakada et al., 2004), Ascl1 expression induced neuronal differentiation of NS-5 cells, while MyT1 expression on its own did not. However, the combination of MyT1 with Ascl1 resulted in an increased number of neurons when compared to Ascl1 alone (Figure 3. 7B-C), indicating that MyT1 enhances the differentiation activity of Ascl1.

Following our observations in cultured NS cells, we next asked if MyT1 can promote neuronal differentiation in an *in vivo* model of neurogenesis. For that, we performed gain- and loss-of-function of MyT1 in the developing mouse telencephalon, using *in utero* electroporation. We chose to electroporate the lateral ganglionic eminence (LGE) at E12.5, an area of Ascl1-driven neurogenesis (Casarosa et al., 1999) where MyT1 is the only member of its family significantly expressed in the germinal layers (Matsushita et al., 2013). Two days after electroporation, a significantly higher number of cells co-electroporated with MyT1 and GFP migrated away from the VZ

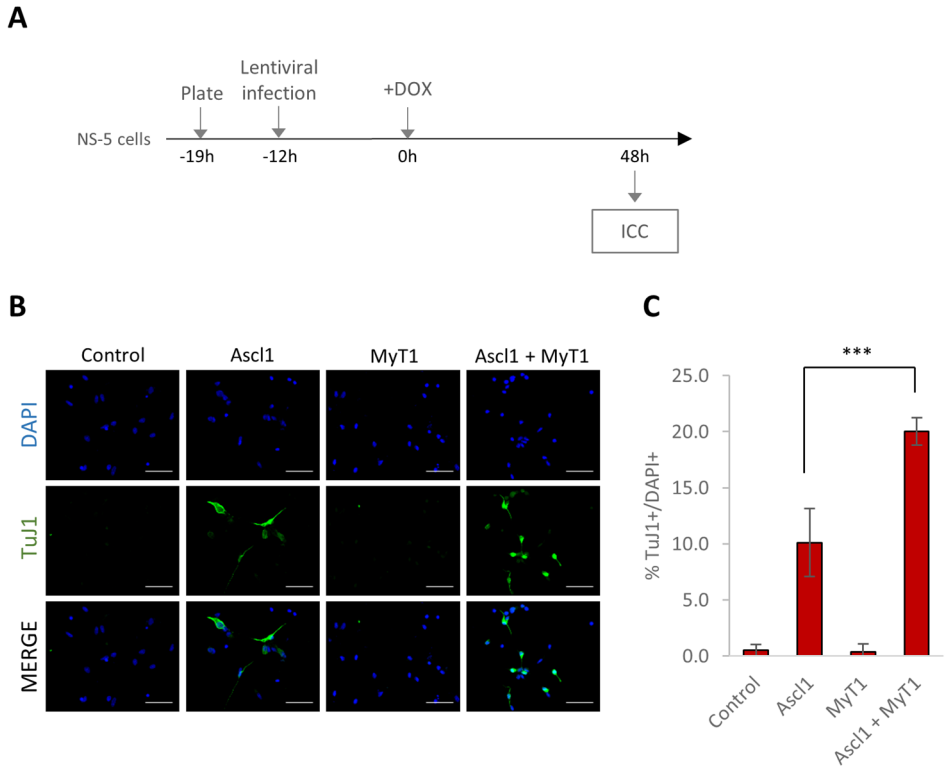

Figure 3. 7 MyT1 potentiates Ascl1-mediated neurogenesis in cultured NS cells.

(A) Diagram depicting the experiment in which NS-5 cells were infected with control, Ascl1 and/or MyT1 inducible lentiviruses and neuronal differentiation was assessed by the expression of the neuronal marker TuJ1. **(B)** Immunocytochemical analysis for the neuronal marker TuJ1 (green) upon infection with control, Ascl1- and/or MyT1-expressing lentiviruses. Nuclei were labeled with DAPI (blue). **(C)** Histogram represents the percentage of neurons ($TuJ1^+$/DAPI) on each condition. Data presented as the mean ± SD for at least 1500 cells on each condition. *** for $P<0.001$ according to Student's t-test.

with a concomitant increase in the number of neurons ($TuJ1^+$), when compared to a control electroporation (Figure 3. 8B-C). To perform MyT1 knock-down, we designed a MyT1 ShRNA that is able to suppress MyT1 expression from a MyT1 expressing vector in transfected cells (Figure 3. 8A). Contrary to MyT1 overexpression, electroporation of MyT1 ShRNA resulted in decreased migration from the VZ and decreased number of TuJ1-expressing neurons (Figure 3. 8B,D). Overall, our results are consistent with a role of MyT1 in promoting neurogenesis.

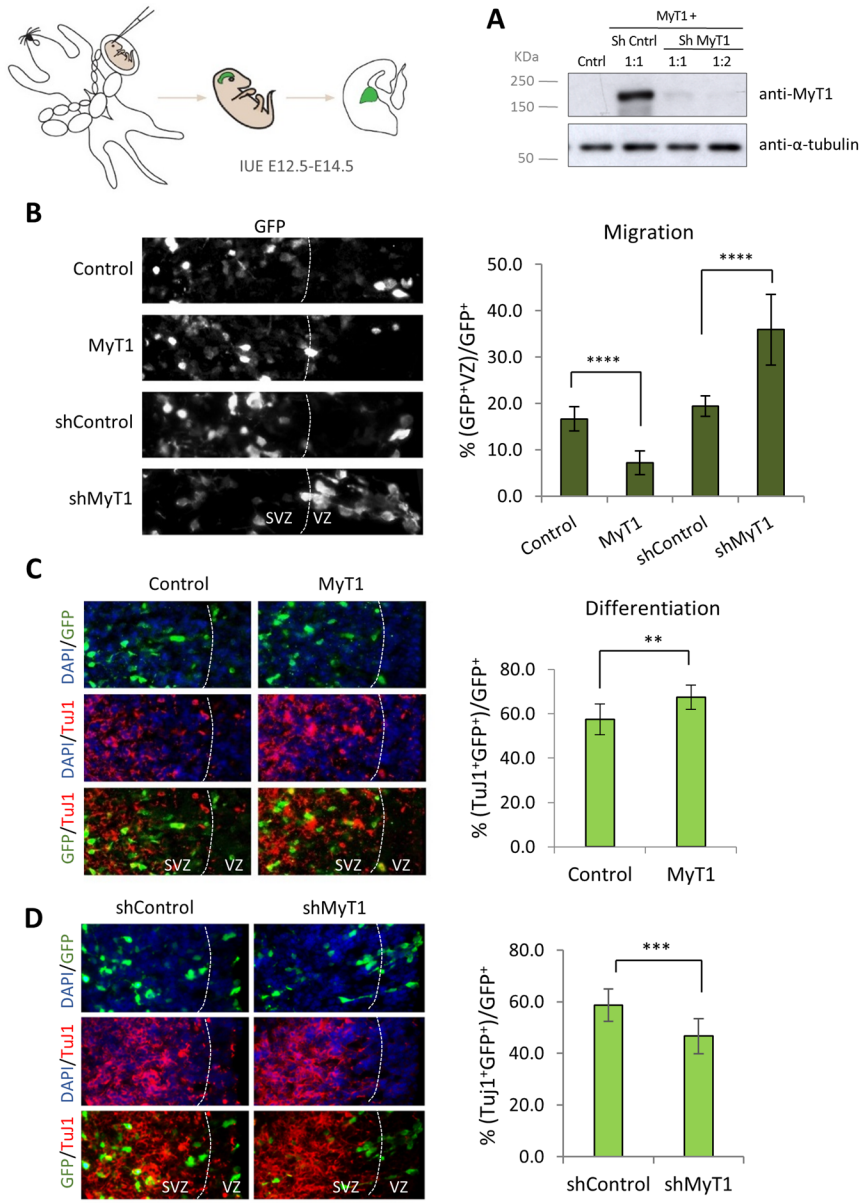

Figure 3. 8 MyT1 promotes neurogenesis in mouse ventral telencephalon.

(A) HEK293T cells were co-transfected with a MyT1 expression vector and scramble shRNA (shControl) or MyT1 ShRNA (shMyT1) on the proportion MyT1: ShRNA of 1:1 or 1:2. MyT1 protein levels were analyzed by Western blot. α-tubulin was used as loading control. **(B-D)** *In utero* electroporation (IUE) of control, MyT1, control ShRNA (shControl) or MyT1 ShRNA (shMyT1) expressing vectors in E12.5 mouse ventral telencephalon. Immunofluorescence analysis of coronal sections stained for GFP and TuJ1 performed 2 days after electroporation (E12.5-14.5). (Continued on the next page.)

Figure 3. 8 (continued) Cell nuclei are labeled with DAPI (blue). Dashed lines mark the basal margin of the ventricular zone. VZ, ventricular zone. SVZ, subventricular zone. **(B)** Quantification of cell migration based on fraction of GFP^+ cells that are retained in the VZ (GFP^+VZ/GFP^+). **(C-D)** Quantification of neuronal differentiation based on fraction of GFP^+ cells that express the neuronal marker TuJ1 (($TuJ1^+GFP^+$)/GFP^+). Data are presented as the mean ± SD, ** for P<0.01, *** for P<0.001, **** for P<0.0001 according to Student's t-test.

1.4. Genome-wide identification of MyT1 target genes

In order to investigate the molecular basis of MyT1 function in neurogenesis, we aimed at identifying its target genes in a neurogenic context. For that, we combined MyT1 location analysis by ChIP-Seq with gene expression profiling with DNA microarrays upon MyT1 GoF in neural stem cell cultures.

1.4.1. Generation of NS-5 MyT1 inducible cells

We generated NS-5 cells in which a tagged version of MyT1 (MyT1-HA or MyT1-V5) is induced by the addition of DOX to the culture (Figure 3. 9 and Figure 3.S 2). For that, we generated lentiviruses expressing MyT1-HA, MyT1-V5 or GFP under the control of a tetracycline responsive element (TRE). NS-5 cells were infected with MyT1-HA, GFP and reverse tetracycline-controlled transactivator (rTTA)-expressing lentiviruses (NS-5 MyT1-HA/GFP TetON cells, herein called NS-5 MyT1-HA inducible cells) (Figure 3.S 2). Alternatively, NS-5 cells were infected with MyT1-V5 and rTTA-expressing lentiviruses (NS-5 MyT1-V5 TetON cells, herein called NS-5 MyT1-V5 inducible cells) (Figure 3. 9). 24h post induction with DOX, approximately 30% or 25% of the cells overexpressed MyT1-V5 or MyT1-HA/GFP, respectively (Figure 3. 11B-C and Figure 3.S 2B-C).

1.4.2. Expression profiling upon MyT1 gain-of-function

In order to perform expression profiling upon MyT1 gain-of-function, we collected RNA samples in triplicates for subsequent microarray analysis before and 4h post-

DOX induction of NS-5 MyT1-V5 inducible cells. This time point was used in order to enrich for MyT1 direct targets amongst deregulated genes. MyT1 mRNA expression was induced 6-8 fold between the two conditions (Figure 3. 9D-E).

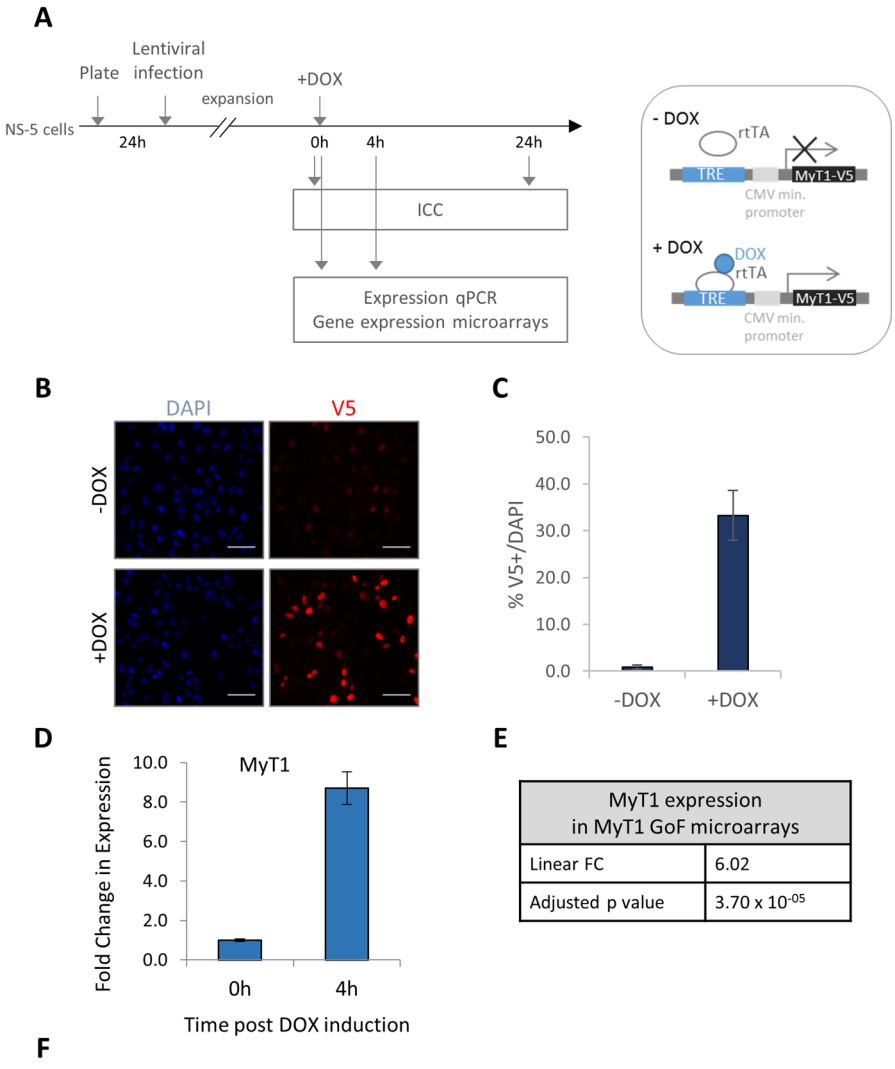

MyT1 expression in MyT1 GoF microarrays	
Linear FC	6.02
Adjusted p value	3.70×10^{-05}

F

MyT1 GoF Microarrays (FC >|1.2|)	# deregulated genes	# upregulated genes	# downregulated genes
P value < 0.05	1764	761	1003
P value < 0.01	100	37	63

Figure 3. 9 Expression profiling upon MyT1 gain-of-function in cultured NS cells.

(Continued on the next page.)

Figure 3. 9 (continued) **(A)** Scheme depicting experiment in which NS-5 MyT1-V5 TetON cells (NS-5 MyT1-V5 inducible cells) were induced by DOX and harvested for immunocytochemistry and gene expression analysis by Real-time PCR and by microarrays.**(B)** Immunocytochemistry using anti-V5 antibody before (-DOX) and 24h post DOX induction (+DOX). Nuclei were stained with DAPI (blue). Scale bar, 40µm. **(C)** Histogram represents the percentage of MyT1 induced cells upon DOX treatment ($V5^+$/DAPI). Data presented as the mean ± SD for at least 3000 cells on each condition. **(D)** Analysis of MyT1 expression by Real-time PCR. Values normalized to B-actin expression values. Mean ± SD of triplicate assays are shown. **(E)** Fold change of MyT1 expression between 0h and 4h in MyT1 GoF gene expression microarrays and associated p value. **(F)** Number of deregulated genes in MyT1 GoF gene expression microarrays for each p value cutoff. FC cutoff>|1.2|.

Normalized unscaled standard error (NUSE) and relative expression values (RLE) plots show that there are no deviant arrays in terms of standard error and expression levels of the probesets, respectively (Figure 3.S 3A-B). Dendrogram and principal component analysis plots demonstrate that technical replicates cluster and that samples are distinct (Figure 3.S 3C-D).

Calculation of fold change of gene expression before (0h) and after (4h) MyT1-V5 induction identified 1764 deregulated genes (|FC|>1.2, $p<0.05$), of which 57% are downregulated and 43% upregulated (Figure 3. 9F). As expected, the MyT1 transcript is the highest upregulated gene represented in the microarrays (Figure 3. 9E).

1.4.3. Location analysis of MyT1 by ChIP-Seq

In order to select direct targets of MyT1 from the deregulated genes in the MyT1 GoF microarrays, we performed a genome-wide mapping of MyT1 binding sites by ChIP-Seq, using two parallel approaches (Figure 3. 10C). First, we identified an anti-MyT1 antibody that is able to immunoprecipitate MyT1 protein in transfected P19 cells (Figure 3. 10B) and we used this antibody to perform ChIP-qPCR on chromatin prepared from NS-5 cells, which express low levels of MyT1 (Figure 3. 10A). Since no MyT1 targets had been previously identified in a neurogenic context, we selected candidate MyT1 target sites from genomic regions encompassing clusters of binding

sites of multiple transcription factors in neural stem cells, associated with at least one MyT1 consensus binding motif (AAGTT, herein called MyT1 motif) (Ben Martynoga, personal communication). From these regions, we selected several of those that are associated with genes expressed in the developing mouse telencephalon and tested them in ChIP-qPCR (data not shown). Regions associated with Ank2, Chd7 and Slc35b1 genes (each of which containing 6, 2 and 2 MyT1 motifs, respectively) were strongly enriched in MyT1 ChIPed material, as compared to negative control regions (Figure 3. 10D, upper plot) and were used as positive controls. To optimize ChIP efficiency, we tested several amounts of antibody and washing buffers (data not shown) and conditions that yielded the highest fold enrichment were used in the ChIP-Seq sample preparation.

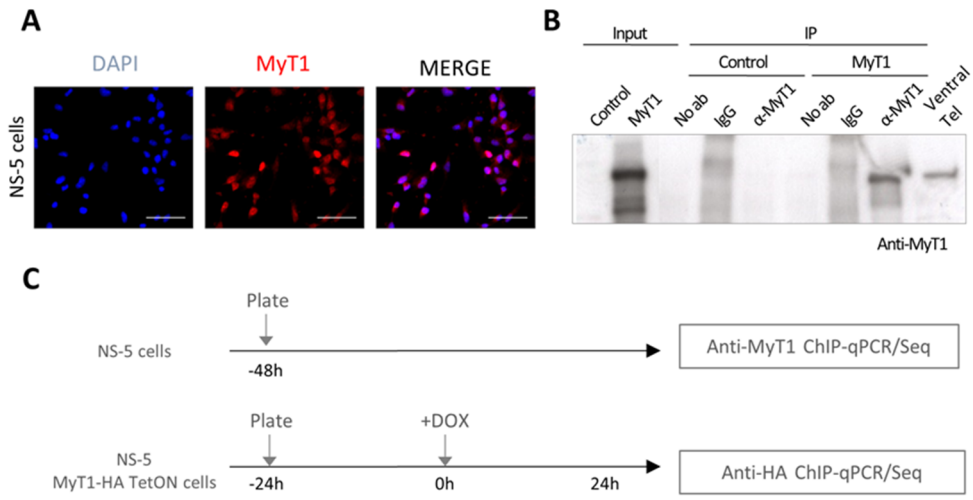

(Figure continued on the next page.)

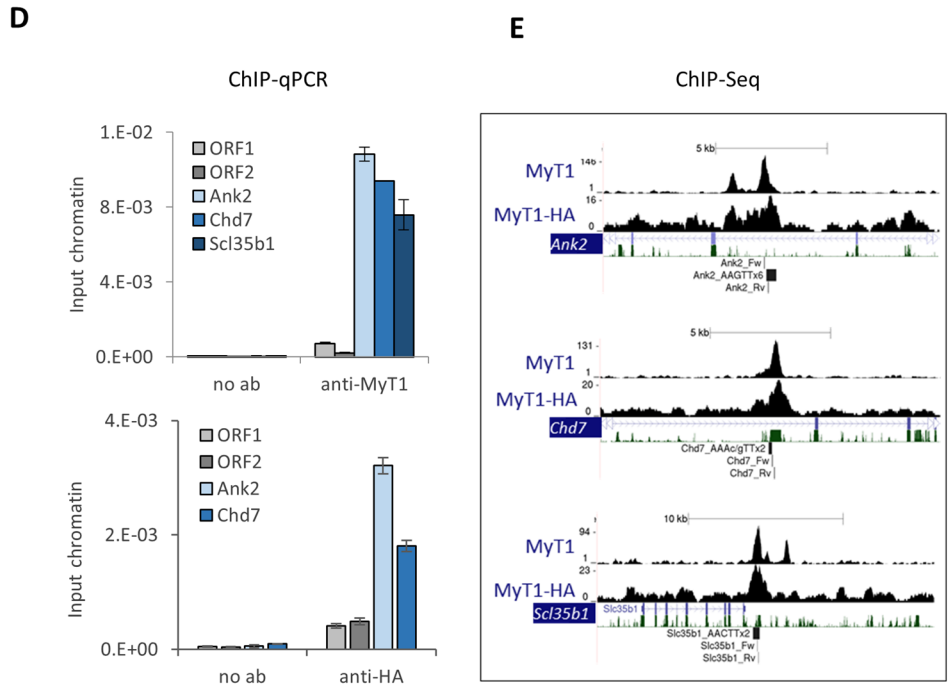

Figure 3. 10 Genome-wide identification of MyT1 BEs in neural stem cells.

(A) Expression of MyT1 (red) in NS-5 cells analyzed by immunocytochemistry. Nuclei were labeled with DAPI (blue). Scale bar, 40µm. **(B)** Validation of anti-MyT1 antibody used in ChIP assay. P19 cells were transfected with control or MyT1 expressing vectors. Immunoprecipitation was performed using anti-MyT1 antibody, IgG or no antibody (no ab). Crude protein lysates of E12.5 mouse ventral telencephalon, P19 transfected cells and immmunoprecipitated samples were analyzed by Western blot with rabbit anti-MyT1 antibody. **(C)** Scheme depicting the experiment in which genome-wide mapping of MyT1 binding was performed in undifferentiated NS-5 cells and in NS-5 MyT1-HA inducible cells 24h post-DOX using an antibody anti-MyT1 and anti-HA, respectively. **(D)** Binding of MyT1 (upper) and MyT1-HA (lower) to positive control regions by ChIP-qPCR in NS-5 cells and in NS-5 MyT1-HA inducible cells + DOX, respectively. ORF1 and ORF2 refer to two negative control regions. Mean ± SD of triplicate assays are shown. **(E)** Visual representation of ChIP-Seq enrichment profiles of MyT1 and MyT1-HA in positive control regions tested by ChIP-qPCR. Green track, Mammal conservation by PhastCons. Position on the genome of the ChIP-qPCR primers and location of AAGTT motifs are highlighted in figure.

The MyT1 ChIP-Seq on chromatin extracted from NS-5 cells identified 18 865 MyT1 binding events that associate with 7068 genes ($p<10^{-5}$) (Figure 3.S 4A). Most of the BEs are located within intergenic and intronic regions (42.7% and 45.3%, respectively)

and at long distances from the nearest identified transcription start site (TSS) (|distance to TSS|=50-500 Kb) (Figure 3.S 4B-D). As expected, well-defined MyT1 ChIP-Seq peaks at positive control regions are centered on the predicted MyT1 motifs (Figure 3. 10E).

In parallel, we used NS-5 MyT1-HA inducible cells to perform ChIP-Seq for overexpressed MyT1-HA 24h post induction, using an antibody against the HA-tag, and following a protocol previously established. In agreement with endogenous MyT1 ChIP, we could validate the binding of MyT1-HA to positive controls by ChIP-qPCR (Figure 3. 10D, lower plot). Accordingly, the enrichment plots of MyT1-HA ChIP-Seq at positive control regions reveal coincident binding of MyT1-HA and endogenous MyT1 (Figure 3. 10E). Overall, the ChIP-Seq data set for overexpressed MyT1-HA is, however, of lower quality than the ChIP-Seq data set for endogenous MyT1 as revealed by the lower peak height on positive control regions and reduced number of binding events identified (Figure 3. 10E, Figure 3.S 4A). Nevertheless, we found a strong enrichment of endogenous MyT1 sequencing reads at genomic regions centered at MyT1-HA peak summits (Figure 3. 11A), demonstrating that the peaks identified on the MyT1-HA ChIP-Seq data set are present on endogenous MyT1 ChIP-Seq data set. Moreover, both data sets exhibit a very similar distribution in terms of distance of BEs to nearest TSS and association with various genomic features (Figure 3.S 4B-C).

A *de novo* search for overrepresented DNA binding motifs within a close distance to the summits of the ChIP-Seq peaks common to both ChIP-Seq data sets identifies the previously described MyT1 motif (Gamsjaeger et al., 2008; Kim and Hudson, 1992) and an E-box motif (Figure 3. 11B). While the MyT1 motif is expected to mediate DNA binding, the presence of the E-box motif suggests a possible regulatory interaction with Ascl1 (see discussion).

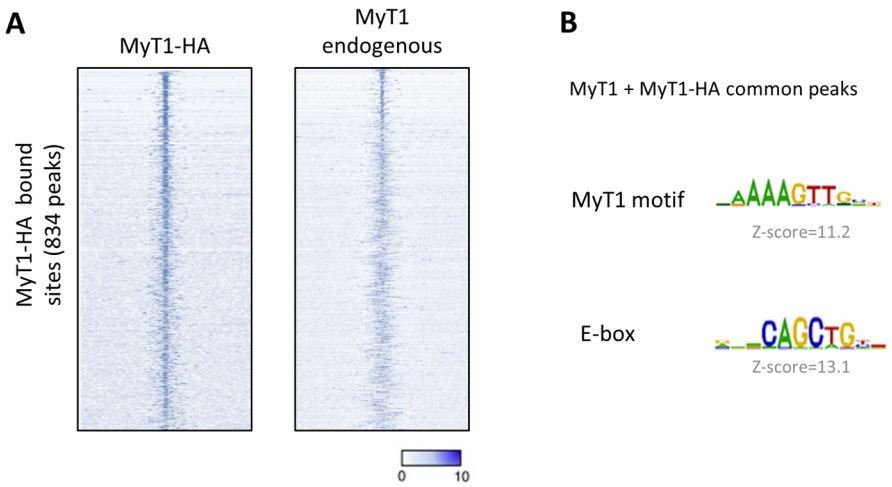

Figure 3. 11 MyT1 motif is enriched at MyT1 BEs.

(A) Density plot of MyT1-HA and MyT1 ChIP-Seq reads mapping to the genomic regions surrounding the summit of MyT1-HA BEs. The signal intensity represents the MyT1-HA (left) and MyT1 (right) ChIP-Seq normalized tag count in the 4kb region surrounding the summit of MyT1-HA peaks. P (MyT1-HA ChIP-Seq) $<10^{-5}$. **(B)** Motif logo of the top overrepresented motifs on a 100bp region centered on MyT1-HA peak summits that overlap with MyT1 peaks.

1.5. MyT1 acts as a repressor at the genome-wide level

Various lines of evidence implicate MyT1 in both transcriptional activation and repression (Bellefroid et al., 1996; Hu et al., 2013; Romm et al., 2005; Wang et al., 2008; Yokoyama et al., 2014). To gain an insight into the global transcriptional response mediated by MyT1 in our GoF model, we integrated MyT1-HA location analysis with the corresponding expression profiling analysis 4h upon MyT1 induction. Strikingly, we found a positive correlation between MyT1-HA peak height (which is proportional to the significance of binding defined by the p value) and its potential to downregulated gene expression. In contrast, the proportion of bound genes associated with upregulation is invariant with changes in peak size, suggesting no direct relation between MyT1-HA binding significance and upregulation of gene

expression (Figure 3. 12A). Moreover, we found the enrichment of MyT1 BEs in the vicinity of downregulated genes to be statistically significant ($p<2.8x10^{-15}$), as compared to the association of 1000 randomized data sets of equal size with downregulated genes, whereas such association with upregulated genes is not found ($p<0.09$) (Figure 3. 12B). In addition, we determined the fraction of up- and downregulated genes associated with MyT1-HA BEs (grouped in bins of increasing p value cutoff) and, therefore, considered to be targets of MyT1-HA (Figure 3. 12C, left). The statistical significance of the association was assessed by a similar comparison against 100 randomly generated control ChIP-Seq data sets of identical size (Figure 3. 12C, right). The resulting heat maps indicate that downregulated genes are highly enriched for MyT1 targets (bound by MyT1) as compared to genes upregulated upon MyT1 GoF (Figure 3. 12C, bottom left versus top left). Moreover, this enrichment is highly significant when compared to control set, whereas the fraction of upregulated genes that are considered MyT1 targets is very similar to that expected by chance (Figure 3. 12C, top left versus top right). Overall, our analyses demonstrate a genome-wide association between MyT1 binding and down-regulation of gene transcription, indicating this transcription factor functions globally as a transcriptional repressor. Importantly, the same strategy applied to endogenous MyT1 ChIP-Seq data set, reveals qualitatively identical results (Figure 3.S 5). Because of its higher genome coverage, the ChIP-Seq data set against endogenous MyT1 was used in the subsequent analysis, with final validation of results performed by ChIP-qPCR against HA-tag using chromatin extracted from NS-5 MyT1-HA inducible cells post-DOX.

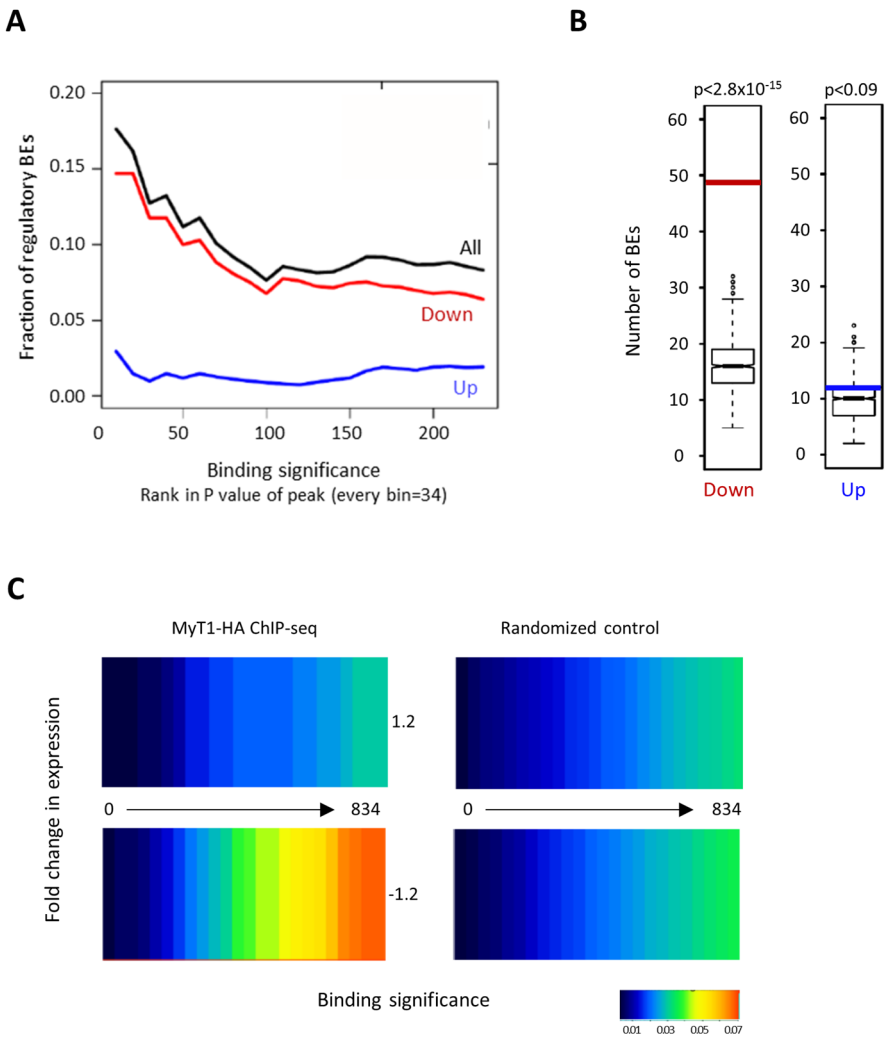

Figure 3. 12 MyT1 functions as a transcriptional repressor at a genome-wide level (analysis from MyT1 ChIP-Seq in NS-5 MyT1-HA inducible cells + DOX).

(A) Cumulative fraction of MyT1-HA BEs considered regulatory by association with up- or downregulated genes following a nearest gene annotation. P (MyT1-HA ChIP-Seq)<10^{-5}. P (MyT1 GoF microarrays)<0.05, FC>|1.2|. **(B)** Number of MyT1-HA BEs associated with up- (blue bar) or downregulated (red bar) genes in MyT1 GoF microarrays. Test data represented as box with median of test and first and third quartiles; whiskers, ±1.5 x interquartile range (IQR). P (MyT1-HA ChIP-Seq)<10^{-5}. P (MyT1 GoF microarrays)<0.05, FC>|1.2|. **(C)** Heat map displaying the cumulative fraction of deregulated genes in MyT1 GoF that are directly regulated by MyT1 (up, top left panel; down, bottom left panel). Number of transcripts with expression fold change >1.2 are plotted against MyT1 BEs with increasing p value (bin=35 BEs). Control: 100 sets of random BEs (right, mean value shown).

1.6. MyT1 directly represses genes involved in NS/PC maintenance and Notch signaling

We next investigated the expected function of MyT1 direct targets, by focusing on genes that are bound and repressed by MyT1. Gene ontology (GO) analysis showed that MyT1 targets are associated with GO terms that predict a function in the maintenance of a progenitor program (e.g., ‘‘negative regulation of neuron differentiation’’, ‘‘neuron fate commitment’’ and “positive regulation of cell proliferation”) and transcriptional regulation (‘‘regulation of transcription from RNA pol II” and ‘‘nucleosome assembly’’) (Figure 3. 13A, Table 3.S 1). Somehow consistent with this finding, the most statistical significant signaling pathway associated with MyT1 targets (determined using the Panther classification system) was the Notch pathway (Figure 3. 13B, Table 3.S 2), hence, we continue our study by focusing on this finding. Although MyT1 has been previously associated with Notch signaling (Bellefroid et al., 1996; Schneider et al., 2001), the molecular mechanism underlying such association has not been addressed.

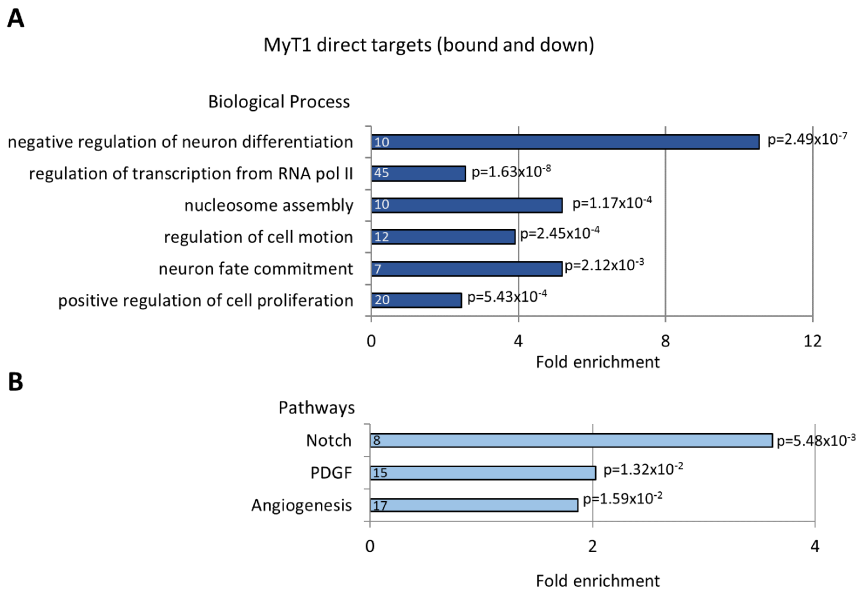

Figure 3. 13 MyT1 represses genes associated with NS/PC maintenance and Notch signaling.

(Continued on the next page.)

Figure 3. 13 (continued) **(A)** Enrichment of Biological Process terms (Gene Ontology) associated with MyT1 targets (genes bound and downregulated by MyT1). Numbers inside bars indicate number of genes. P value for each category is indicated in the outside end of each bar. **(B)** Enrichment of pathway terms (Panther classification) associated with MyT1 targets. Numbers inside bars indicate number of genes present in each category. P value for each category is indicated in the outside end of each bar.

1.7. MyT1 promotes neurogenesis by counteracting Notch signaling activity

To test if MyT1 could counteract Notch signaling inhibition of neurogenesis, as previously observed in the Xenopus model, we infected NS-5 cells with lentiviruses expressing inducible Ascl1, MyT1 and a dominant active version of the Notch1 receptor (herein referred to as "Act Notch") (Figure 3.S 6). Act Notch is membrane bound but is independent on the Notch receptor/ligand interaction for cleavage by g-secretase (Kageyama, R., personal communication). To assess neuronal differentiation, we analysed the expression of the progenitor marker Sox2 and of the neuronal differentiation marker TuJ1 (Figure 3. 14). As expected (Berninger et al., 2007; Farah et al., 2000; Nakada et al., 2004), Ascl1 overexpression induces the generation of $TuJ1^+$ neurons, with a concomitant decrease of Sox2 expression, and this effect is counteracted by the co-expression of Act Notch (Gaiano et al., 2000). Importantly, MyT1 can counteract the inhibition of Ascl1 by Act Notch, as observed by a rescue of the number of $TuJ1^+$ cells (and decrease of $Sox2^+$ cells) to levels similar to those obtained with Ascl1 alone (Figure 3. 14B-C).

We next asked if MyT1 could counteract Notch signaling activity *in vivo* by co-electroporating MyT1 and Act Notch in the dorsal telencephalon, a region where neuronal migration – the most striking effect of MyT1 GoF – is easier to quantify. In addition, we chose a stage at the peak of the neurogenic phase (E13.5), when an inhibition by Act Notch is expected to be more significant. Migration of electroporated cells (GFP^+) and neuronal differentiation ($Tuj1^+$) were examined 5 days after electroporation (Figure 3. 15).

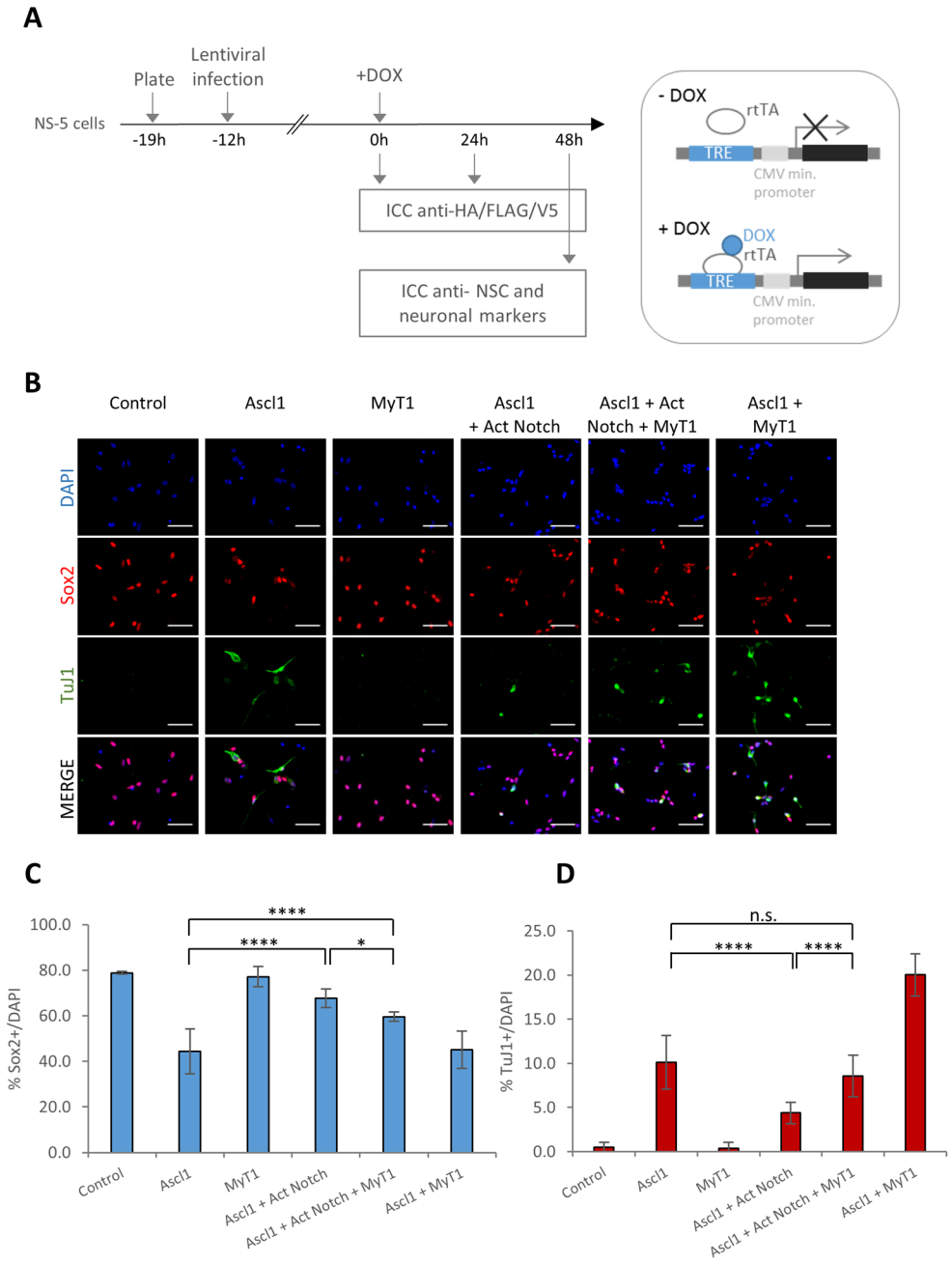

Figure 3. 14 MyT1 promotes neurogenesis by counteracting Notch signaling in cultured NS cells.

(A) Scheme depicting experiment in which NS-5 cells were infected with MyT1, Ascl1 and/or Act Notch inducible lentiviruses. Differentiation was assessed by the expression of the neuronal marker TuJ1 and by the loss of the neural progenitor marker Sox2. (Continued on the next page.)

Figure 3. 14 (continued) **(B)** Immunocytochemical analysis for the neural stem cell marker Sox2 (red) and the neuronal marker TuJ1 (green) upon infection with control, Ascl1-, Act Notch- and/or MyT1-expressing lentiviruses 48h post DOX treatment. Nuclei were labeled with DAPI (blue). Scale bar, 40µm.
Histogram represents the percentage of neural stem cells ($Sox2^+$/DAPI) **(C)** and neurons ($TuJ1^+$/DAPI) **(D)** on each condition. Data presented as the mean ± SD for at least 1500 cells on each condition. **** for P<0.0001, * for P<0.05, n.s. for P>0.05 according to one-way ANOVA with Bonferroni correction for multiple testing.

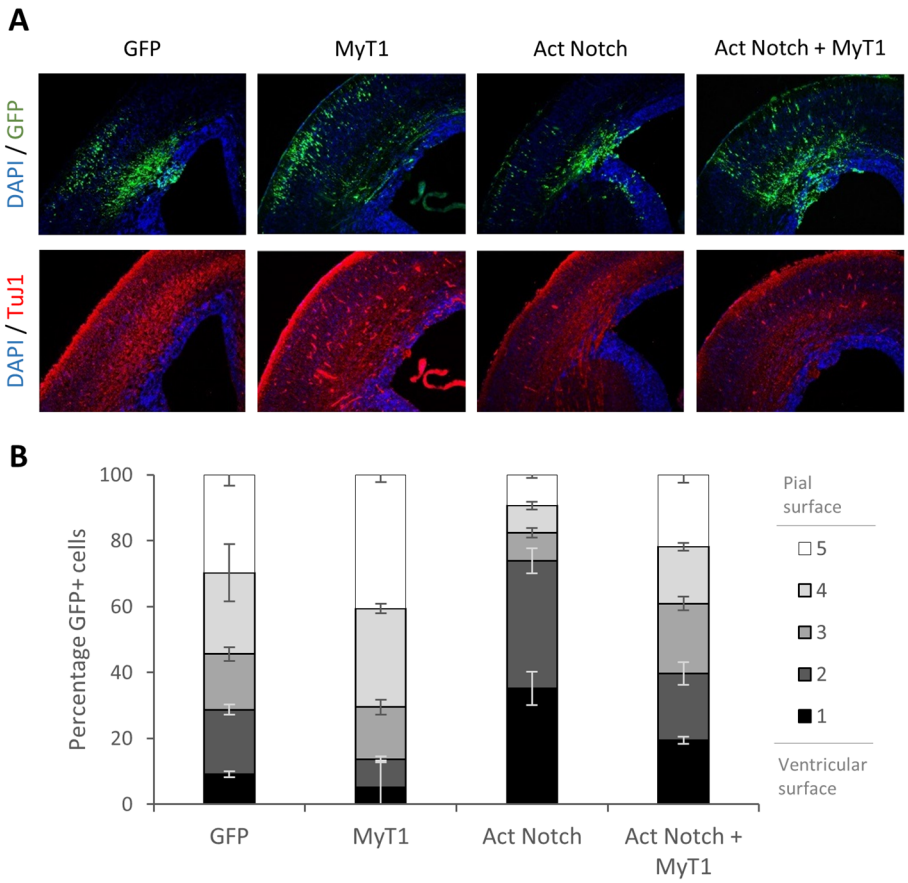

Figure 3. 15 MyT1 promotes neurogenesis by counteracting Notch signaling *in vivo*.

(A) *In utero* electroporation (IUE) of control, MyT1, Act Notch or Act Notch+MyT1 expression vectors in E13.5 mouse dorsal telencephalon. Immunofluorescence analysis of coronal sections stained for GFP (green) and TuJ1 (red) 5 days after electroporation (E13.5-18.5). Cell nuclei are labeled with DAPI (blue). **(B)** Histograms represent the percentage of electroporated cells present on 5 bins of equal length spanning the cortical thickness. Bins were numbered from 1 to 5 from ventricular to pial surface, respectively. Data are presented as the mean ± SD.

As expected, expression of Act Notch inhibits endogenous neurogenesis, resulting in the retention of electroporated cells in the ventricular zone, whereas MyT1 overexpression had the opposite effect. Notably, coexpression of Act Notch and MyT1 resulted in a significant rescue of Act Notch phenotype, with the pattern of migration of electroporated cells similar to that of control condition (GFP) (Figure 3. 15). Overall, our results indicate that MyT1 counteracts the inhibitory effect of the Notch pathway activity when promoting neurogenesis.

1.8. MyT1 represses genes activated by canonical Notch signaling

To address the molecular basis for the antagonism between MyT1 and Notch signaling pathways, we started by comparing the transcriptional changes observed in our MyT1 GoF model with those that take place upon inhibition of Notch signaling. To generate the latter expression profiling data set, we exposed NS-5 cells for 4h to a pharmacological inhibitor of g-secretase, (LY-411575 (LY)) previously shown to inhibit Notch signaling (Lanz et al., 2004) and assessed gene expression changes by RNA-Seq (data set produced by Cátia Laranjeira, unpublished) (Figure 3.S 7A,D). When considering a high confidence list of genes deregulated upon MyT1 induction (n=90), the vast majority (81%) is also deregulated upon LY treatment, with the expression of all but 17 genes changing in the same direction (1 deregulated in the opposite direction and 16 not detected as deregulated) (Figure 3. 16A). Notably, decreasing the stringency cutoff for deregulation by MyT1 ($P<0.05$) increased dramatically the number of MyT1 regulated genes that are also downstream Notch (although decreasing the percentage of overlap), with gene expression changes still occurring in the same direction in both experiments. In addition, decreasing the statistical significance of gene expression changes upon LY treatment ($q<0.05$) did not alter significantly the result (Figure 3. 16A). These results suggest that the gene

expression program downstream MyT1 is largely overlapping with that of the Notch signaling pathway.

Given the short time-points at which the expression profiling of NS-5 cells upon MyT1 GoF and LY treatment were performed (4h), it is likely that many direct targets of MyT1 may be canonical Notch targets, directly regulated by RBPJ. In order to identify such common targets, we focused on genes bound by MyT1 and RBPJ. By comparing the ChIP-Seq data sets of MyT1 and RBPJ in NS-5 cells (data set produced by Cátia Laranjeira, unpublished) (Figure 3.S 7A-C), we determined the overlap between MyT1 and RBPJ binding (Figure 3. 16B) and plotted the genome-wide occupancy of MyT1 around RBPJ peak summits. Interestingly, we found a strong enrichment of MyT1 sequencing reads at genomic regions centered at RBPJ peak summits, demonstrating that these TFs are recruited to a significant number of common genomic regions (Figure 3. 16C). Of those direct targets of MyT1 that are also bound by RBPJ, 64% are deregulated in the same direction by MyT1 and the Notch inhibitor, while only 2% are deregulated in the opposite direction (34% are not detected to be deregulated) (Figure 3. 16D).

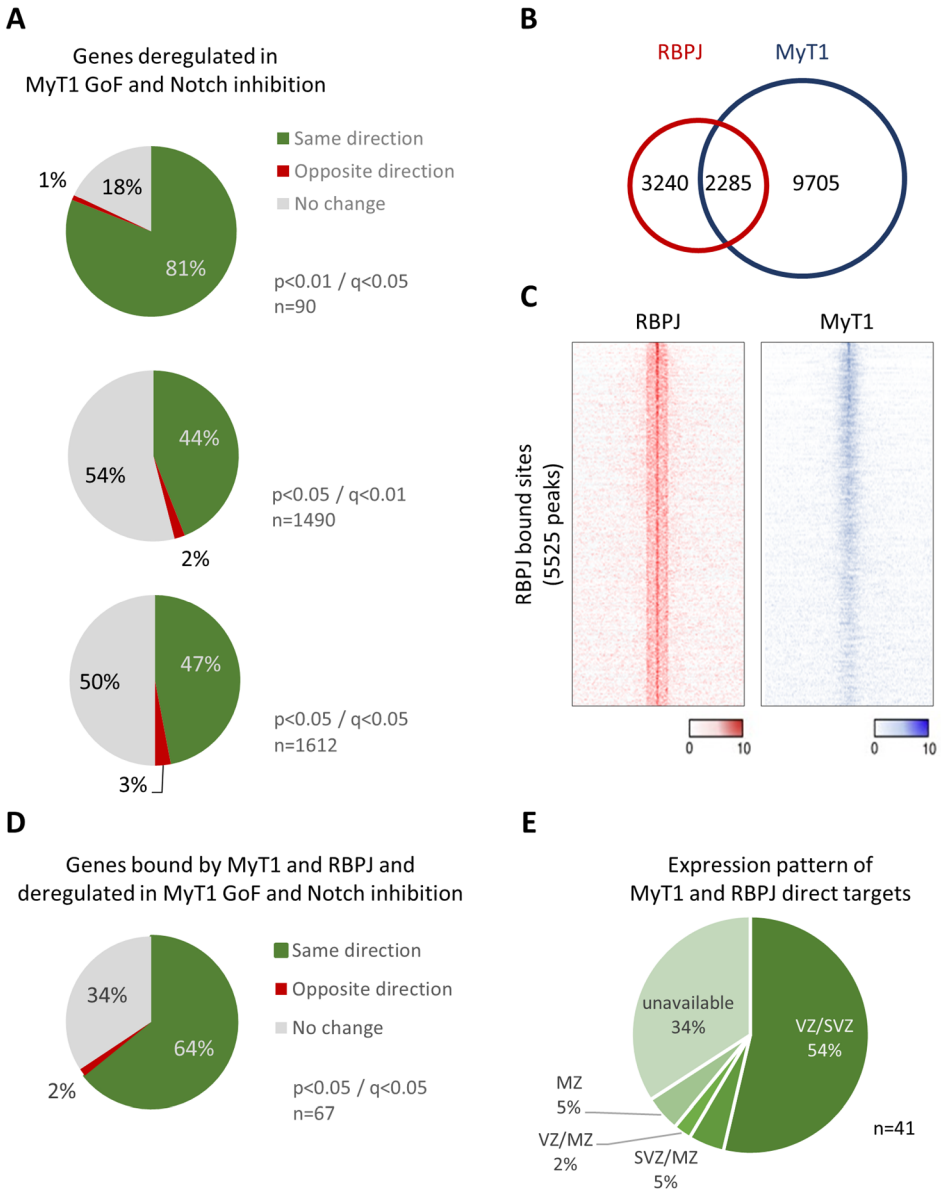

Figure 3. 16 MyT1 represses genes activated by Notch signaling in NS/PCs.

(A) Pie charts representing the percentage of genes deregulated in MyT1 GoF microarrays and deregulated in the same direction (green), opposite direction (red) or unchanged or data unavailable (gray) in Notch inhibitor RNA-Seq. n, total number of genes. P value cutoffs for MyT1 GoF microarrays and q value cutoffs for Notch inhibitor RNA-Seq are indicated in the figure. **(B)** (Continued on the next page.)

Figure 3. 16 (continued) Venn diagrams depicting the overlap between MyT1 and RBPJ ChIP-Seq data sets. P (MyT1 ChIP-Seq)<10^{-10}. P (RBPJ ChIP-Seq)<10^{-5}. Maximum distance between summits of overlapping peaks is 150bp. **(C)** Density plot of RBPJ and MyT1 ChIP-Seq reads mapping to the genomic regions surrounding the

summit of RBPJ BEs. The signal intensity represents the RBPJ (red) and MyT1 (blue) ChIP-Seq normalized tag count in the 4kb region surrounding the summit of RBPJ peaks. P (RBPJ ChIP-Seq)<10^{-5}. **(D)** Pie charts representing the percentage of genes bound by MyT1 and RBPJ, deregulated in MyT1 GoF and deregulated in the same direction (green), opposite direction (red) or unchanged or data unavailable (gray) in Notch inhibitor RNA-Seq. P (MyT1 and RBPJ ChIP-Seq)<10^{-10}. Maximum distance summits of overlapping peaks is 100bp. n, total number of genes. P value cutoffs for MyT1 GoF microarrays and q value cutoffs for Notch inhibitor RNA-Seq are indicated. **(E)** Pie chart representing the onset of expression of common MyT1/Notch target genes in mouse ventral telencephalon (n=41 genes). The expression patterns on sagittal sections of E14.5 and E13.5 mouse telencephalon are from the public *in situ* hybridization databases GenePaint and Allen Brain Atlas, respectively. VZ, ventricular zone. SVZ, subventricular zone. MZ, mantle zone. Unavailable, data unavailable on the databases.

Using publically available gene expression patterns (http://www.genepaint.org/, http://developingmouse.brain-map.org/), we found that most common MyT1/Notch direct targets are expressed exclusively on the VZ/SVZ of the mouse embryonic telencephalon (54%), while only 12% are either expressed in MZ or show a complex expression pattern (the expression pattern of the remaining 34% is not available) (Figure 3. 16E). Altogether, our analysis resulted in the identification of a significant set of target genes that are directly and oppositely regulated by MyT1 and Notch pathways in neural stem/progenitor cells.

1.9. Selection and validation of genes oppositely regulated by MyT1 and Notch/RBPJ

To further select MyT1/Notch common target genes, we focused on a subset of direct targets co-regulated by both pathways (genes downregulated by MyT1 and LY and bound by MyT1 and RBPJ), in a total of 41 genes. Of these, we selected genes expressed in the VZ/SVZ and/or genes with a described relevant function in NS/PCs (14 targets, 10 of which were tested) (Figure 3. 17A).

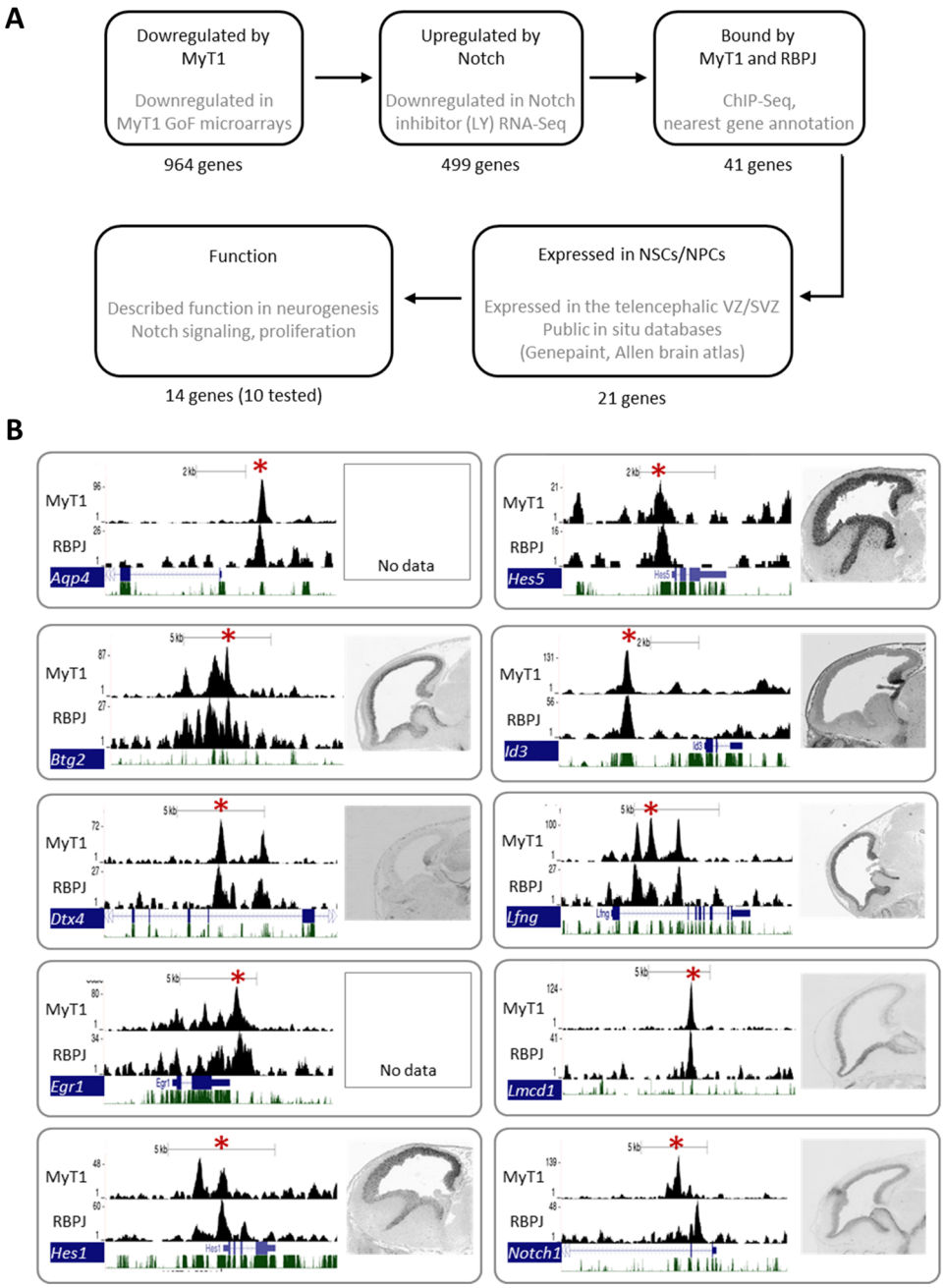

Figure 3. 17 Selection of target genes oppositely regulated by MyT1 and Notch signaling.

(Continued on the next page.)

Figure 3. 17 (continued) **(A)** Pipeline for the selection of candidate genes oppositely regulated by MyT1 and Notch signaling. Overlap between MyT1 and RBPJ ChIP-Seq data sets. P (MyT1 and RBPJ ChIP-Seq)<10^{-10}. Maximum distance between summits of overlapping peaks is, 100bp. **(B)** Visual representation of ChIP-Seq enrichment profile of MyT1 and RBPJ in the vicinity of the 10 selected genes. Asterisks indicate the position of the primers used for ChIP-qPCR validation. Green track, Mammal conservation by PhastCons. The expression patterns on sagittal sections of E14.5 and E13.5 mouse telencephalon (when available) are from the public *in situ* hybridization databases GenePaint and Allen Brain Atlas, respectively.

The identity of the targets and corresponding regulation data upon MyT1 GoF and Notch inhibition are listed on Table 3.S 3. Their expression patterns in embryonic telencephalon (when available) and associated MyT1 and RBPJ binding profiles are represented on Figure 3. 17B.

Validation of endogenous MyT1 and RBPJ binding to selected targets in NS-5 cells was performed by ChIP-qPCR. We could validate MyT1 binding to all tested targets (Figure 3. 18A), while RBPJ binding was validated in all but one cases (Egr1) (Figure 3. 18C). Moreover, all targets tested were also validated by ChIP-qPCR against MyT1-HA in NS-5 MyT1-HA inducible cells post-DOX induction (Figure 3.S 8). The result regarding binding to Notch1 is not represented due to technical problems (contamination in qPCR reaction). Non-normalized values for the ChIP-qPCRs from Figure 3. 18 and Figure 3.S 8 are presented on Figure 3.S 9. Validation of downregulation by MyT1 GoF and LY was performed by expression RT-qPCR (Figure 3. 18B,D) with all tested targets being validated on both conditions.

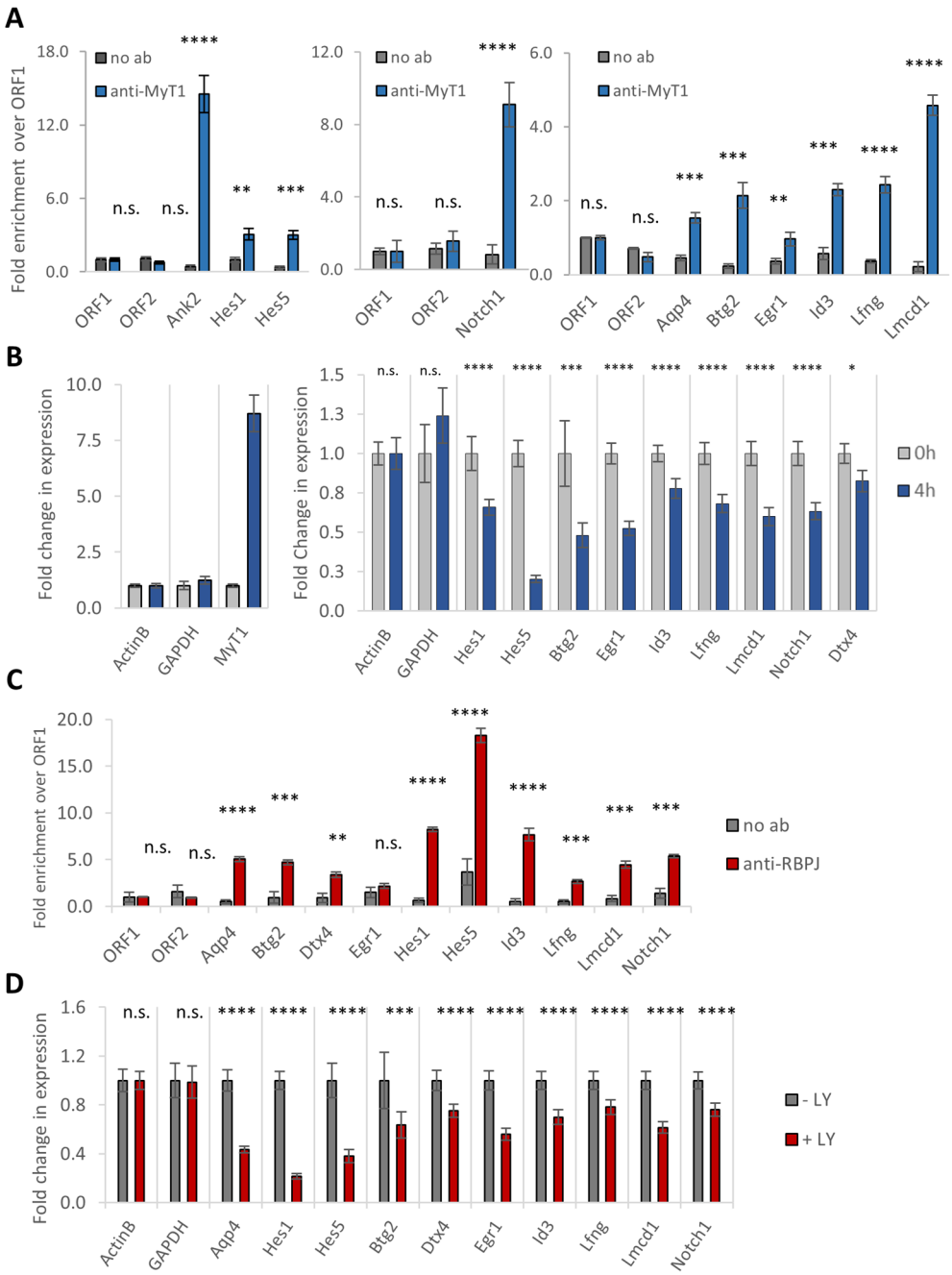

Figure 3. 18 Validation of MyT1 and Notch/RBPJ binding and regulation of selected target genes.

(A) Validation of MyT1 binding to selected genes by ChIP-qPCR in undifferentiated NS-5 cells. ORF1 and ORF2 refer to two negative control regions. Ank2 was used as positive control region. Mean ± SD of triplicate assays are shown. (Continued on the next page.)

Figure 3. 18 (continued) n.s. for P>0.05, * for P<0.05, ** for P<0.01, *** for P<0.001, **** for P<0.0001 according to Student's t-test. **(B)** Validation of gene expression changes of selected genes in NS-5 MyT1-V5 inducible cells before (0h) and 4h post-DOX by expression Real-time PCR. Mean ± SD of triplicate assays are shown. n.s. for P>0.05, * for P<0.05, ** for P<0.01, *** for P<0.001, **** for P<0.0001 according to Student's t-test. **(C)** Validation of RBPJ binding to selected genes by ChIP-qPCR in undifferentiated NS-5 cells. ORF1 and ORF2 refer to two negative control regions. Mean ± SD of triplicate assays are shown. n.s. for P>0.05, * for P<0.05, ** for P<0.01, *** for P<0.001, **** for P<0.0001 according to Student's t-test. **(D)** Validation of gene expression changes of selected genes in NS-5 cells before (-LY) or after (+LY) treatment with g-secretase inhibitor LY-411575 by expression real-time PCR. Mean ± SD of triplicate assays are shown. n.s. for P>0.05, * for P<0.05, ** for P<0.01, *** for P<0.001, **** for P<0.0001 according to Student's t-test.

Since Hes1 and Hes5 are the best characterized effectors of Notch signaling downstream of NICD/RBPJ (Artavanis-Tsakonas, S., Rand, M.D. & Lake, 1999; Kageyama et al., 2008), we thought to explore the mechanism of action of MyT1 on these two genes in more detail. Reassuringly, the expression patterns of Hes1 and Hes5 mRNA are complementary to that of MyT1 protein, as assessed by double *in situ*/immunohistochemical analysis of mouse embryonic telencephalon (Figure 3. 19).

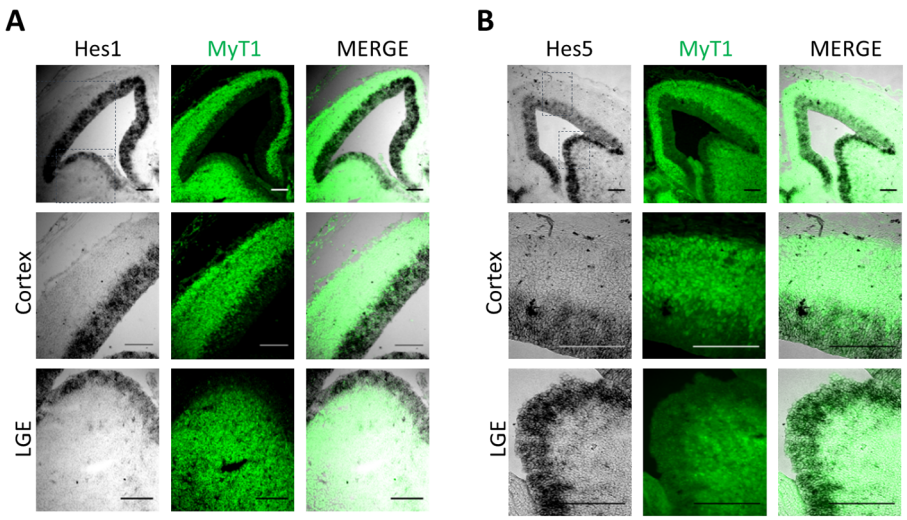

Figure 3. 19 MyT1 protein and Hes1 and Hes5 transcript expression patterns are mutually exclusive.
Anti-MyT1 immunofluorescence (green) and Hes1 **(A)** or Hes5 **(B)** *in situ* hybridization (gray) in sagittal sections of E14.5 mouse embryonic telencephalon. LGE, lateral ganglionic eminence. Scale bar, 140µm.

1.10. MyT1 counteracts Notch activation of Hes1 promoter through direct DNA binding

Previous studies have shown that canonical Notch activation of Hes1 expression is mediated by binding of RBPJ to 3 RBPJ DNA binding motifs (TC-box) within the proximal promoter region of the Hes1 gene (Arnett et al., 2010; Jarriault et al., 1995; Nam et al., 2007). The location of these motifs at the peak summits of RBPJ peaks confirms these mediate RBPJ binding in cultured NS cells (Figure 3. 20A). Strikingly, three evolutionarily conserved MyT1 motifs (AAGTT) are found in tandem and partially overlapping with those of RBPJ (Figure 3. 20A). To test the ability of MyT1 to bind to these 3 MyT1 consensus BSs, we performed an electromobility shift assay (EMSA) using *in vitro* transcribed and translated MyT1 protein and an oligonucleotide probe corresponding to the Hes1 proximal promoter region or mutated versions, in which MyT1 consensus BSs were disrupted individually or altogether (Figure 3. 20A-B). MyT1 is able to bind to the Hes1 promoter probe containing the 3 MyT1 consensus BSs, as shown by the formation of a large DNA/protein complex. However, MyT1 binding was strongly reduced or abolished when each of the MyT1 BS were disrupted separately or altogether, respectively (Figure 3. 20B). The fact that MyT1 binding to Hes1 requires the integrity of the 3 DNA binding motifs suggests cooperative binding of MyT1 to the Hes1 promoter.

The overlap between MyT1 and RBPJ sites on Hes1 promoter prompted us to test whether MyT1 could inhibit Act Notch activity on a previously characterized Hes1 proximal promoter reporter construct spanning all binding sites (pHes1:Luc). Reporter gene assays in transfected P19 cells show a strong activation of the Hes1 promoter by Act Notch and, notably, this effect was strongly inhibited by co-expression of MyT1 (Figure 3. 20C). To test if the inhibitory effect of MyT1 is dependent on DNA binding to the 3 MyT1 BSs, we performed mutagenesis on the MyT1 BSs on Hes1 promoter. Mutations were designed so as to minimize any effect

on Notch activation, resulting in promoter constructs that still respond, albeit less strongly, to Act Notch (Figure 3. 20D). We could observe that disruption of individual binding sites partially impaired the activity of MyT1 (Figure 3. 20E), while simultaneous disruption of the 3 BSs (BS1+2+3) had a stronger negative effect on MyT1 activity (Figure 3. 20E). This effect was clearer when lower ratios of MyT1 expression constructs were used (Figure 3. 20F). Altogether, we concluded that MyT1 counteracts Notch activity on Hes1 promoter via a mechanism that depends on binding to the 3 MyT1 motifs.

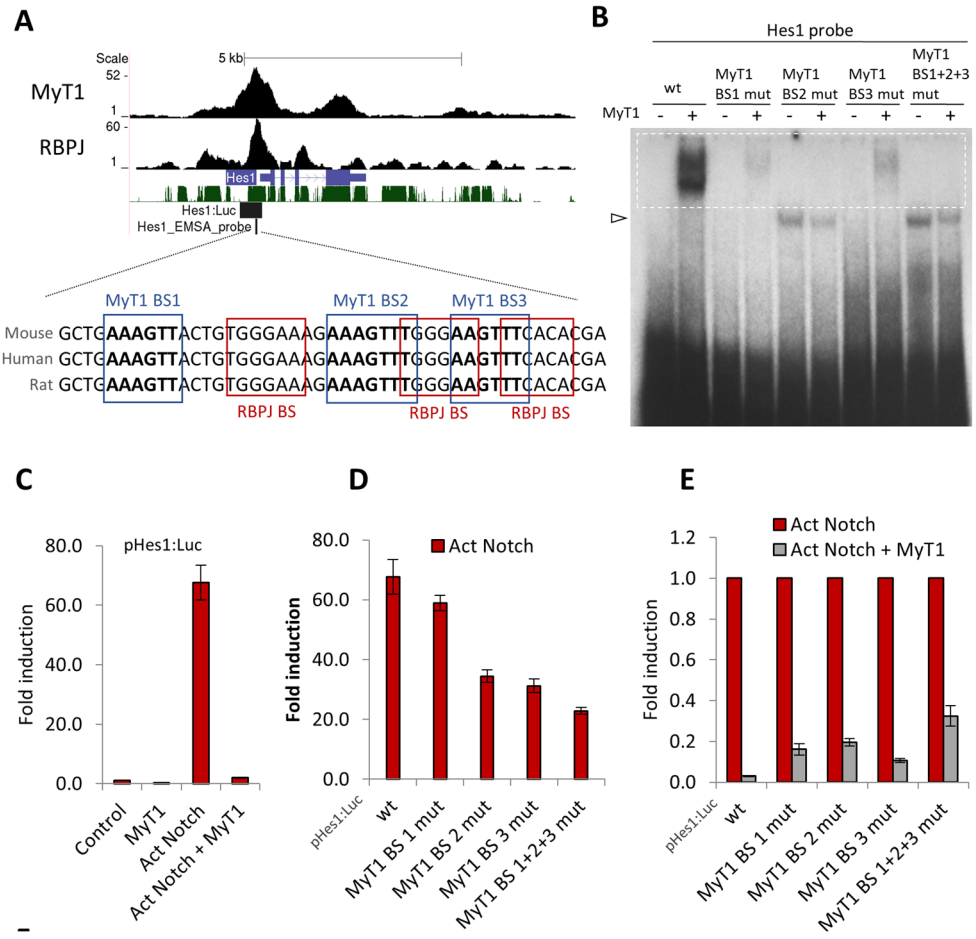

(Figure continued on the next page.)

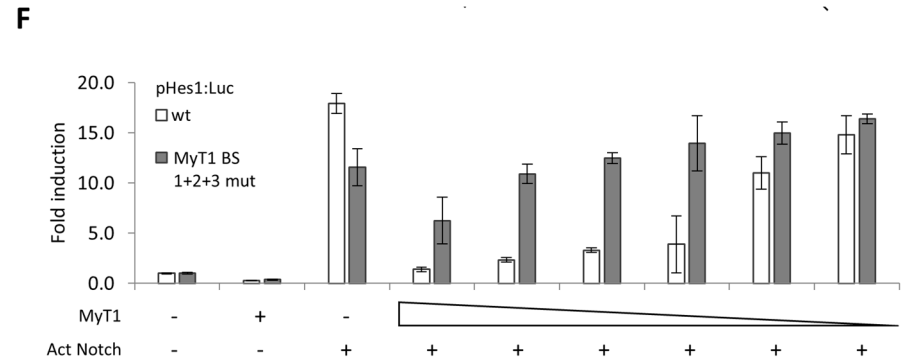

Figure 3. 20 MyT1 counteracts Notch activation of Hes1 promoter by direct binding to MyT1 motifs.

(A) Visual representation of ChIP-Seq enrichment profile of MyT1-HA and RBPJ in the vicinity of Hes1 gene. Hes1:Luc, localization on the genome of the Hes1 promoter region present on luciferase reporter construct (pHes1:Luc) Hes1 EMSA probe, localization on the genome of the evolutionary conserved sequence of Hes1 promoter used as probe in EMSA. RBPJ and MyT1 consensus binding motifs are marked with red and blue rectangles, respectively. Green track, Mammal conservation by PhastCons. **(B)** Electromobility shift assay showing MyT1 binding to the Hes1 promoter region (wt) or mutated version with MyT1 BSs individually or simultaneously disrupted (MyT1 BS1 mut, MyT1 BS2 mut, MyT1 BS3 mut or MyT1 BS1+2+3 mut). The dashed white rectangle highlights the position of MyT1:Hes1 probe complexes. The arrowhead indicates unspecific band. **(C-F)** Reporter gene assays in P19 cells co-transfected with control, MyT1 and/or Act Notch expression vectors and a reporter construct expressing luciferase under the control of Hes1 proximal promoter region (wt) or mutated version in which MyT1 binding sites were individually or simultaneously disrupted (MyT1 BS1 mut, MyT1 BS2 mut, MyT1 BS3 mut or MyT1 BS1+2+3 mut). Mean ± SD of quadruplicate assays are shown. Equal amounts of expression vectors were used, except in **(F)**, where different ratios of MyT1 and Act Notch expression vectors were used.

Importantly, this effect is specific of MyT1 since no other transcription factor tested was able to counteract Act Notch activity on Hes1 promoter (Figure 3.S 10A). Conversely, not all reporter constructs are affected by MyT1, as seen by its inability to interfere with LEF1-B-Catenin fusion protein (LEF1-B-Cat) activity on a synthetic LEF1-B-Catenin response element reporter (pTop-Flash:Luc) (Figure 3.S 10B).

1.11. MyT1 and RBPJ compete for DNA binding to Hes1 promoter

The cis-architecture of MyT1 and RBPJ binding sites on Hes1 proximal promoter (Figure 3. 20A) led us to hypothesize that MyT1 inhibits Notch activation of Hes1

promoter by directly competing with RBPJ for DNA binding, a possibility that we investigated by performing a competition assay between MyT1 and RBPJ for the Hes1 promoter (Figure 3. 21A). As expected, MyT1 and RBPJ alone form complexes with Hes1 promoter probe that migrate differently in the EMSA. When MyT1 and RBPJ were combined, no additional complexes were ever observed (Figure 3. 21A), suggesting that simultaneous binding of MyT1 and RBPJ to the Hes1 proximal promoter is not a likely event. Altogether, our data favors a model whereby MyT1 inhibition of Notch activity at the Hes1 promoter occurs via competition with RBPJ for binding to partially overlapping binding sites.

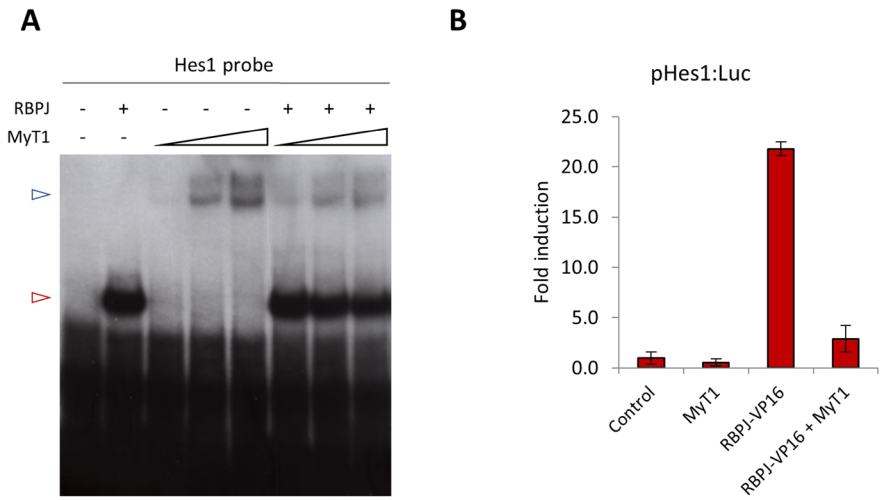

Figure 3. 21 MyT1 and RBPJ compete for DNA binding to Hes1 promoter.

(A) Electrophoretic mobility shift assay showing binding of MyT1 and RBPJ to Hes1 probe. Arrowheads indicates MyT1:Hes1 probe complex (blue) or RBPJ:Hes1 probe complex (red). **(B)** Reporter gene assay in P19 cells co-transfected with a control, MyT1 and/or RBPJ-VP16 expression vectors and Hes1 proximal promoter luciferase reporter construct (pHes1:Luc). Mean ± SD of quadruplicate assays are shown.

1.12. Distinct mechanisms account for MyT1-mediated inhibition of Hes1 and Hes5 genes

In addition to Hes1, Hes5 was also identified as a MyT1 target gene (Figure 3. 17). Moreover, MyT1 can specifically counteract Notch activation of a well characterized

Hes5 promoter construct in transfected P19 cells, although with less efficiency than it does on Hes1 promoter (Figure 3. 22C and Figure 3.S 11). However, contrary to Hes1 promoter, we could not identify any MyT1 motifs (AAGTT) on Hes5 promoter and we failed to detect direct binding of MyT1 to a probe spanning Hes5 proximal promoter region by EMSA (Figure 3. 22B). These results suggest that MyT1 regulates Hes5 promoter via a mechanism that does not involve direct binding to DNA. In line with that possibility, MyT1 can counteract RBPJ-VP16 on Hes1 promoter (Figure 3. 21B) but it is unable to do so on the Hes5 promoter (Figure 3. 22D), suggesting that an alternative mechanism, possibly involving an interaction with the coactivator complex, could be at place.

To investigate the importance of the RBPJ/NICD activator complex in MyT1 recruitment to Hes5 promoter, we treated NS-5 cells with the Notch inhibitor LY and performed ChIP-qPCR for MyT1 on chromatin extracted from treated (+LY) and untreated (wt) cells. While MyT1 recruitment to a site centered on MyT1 motifs (Ank2) remained unaltered across conditions, the recruitment of MyT1 to Hes5 promoter was decreased upon Notch inhibition (Figure 3. 22F). This result suggests that MyT1 inhibits Hes5 expression via a mechanism that does not rely on direct DNA binding but requires a functional interaction with the Notch/RBPJ activator complex.

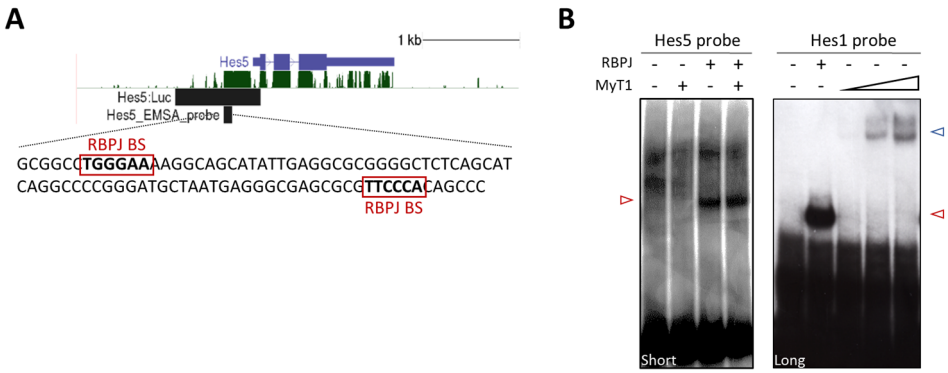

(Figure continued on the next page.)

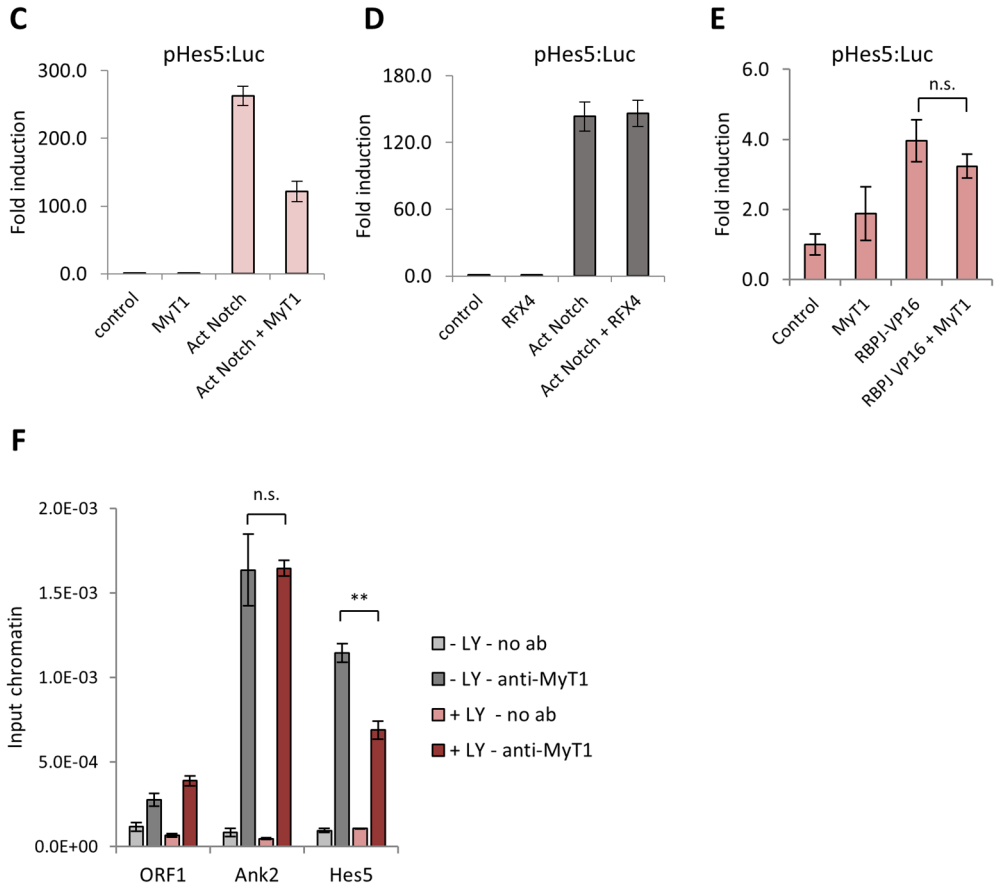

Figure 3. 22 MyT1 counteracts Notch activation of Hes5 promoter in the apparent absence of MyT1 consensus binding sites.

(A) Localization of the Hes5 proximal promoter present on the luciferase reporter construct (pHes5:Luc) and of the Hes5 EMSA probe relative to Hes5 gene. Sequence of Hes5 promoter used as probe in EMSA. Green track, Mammal conservation by PhastCons. **(B)** Electromobility shift assay testing MyT1 binding to Hes5 promoter. RBPJ binding to Hes5 promoter and MyT1 and RBPJ binding to Hes1 promoter were used as positive controls. The blue arrowhead indicates MyT1:Hes1 probe complex. The red arrowhead indicates RBPJ:Hes1 probe or RBPJ:Hes5 probe complexes. Pictures were obtained using different film exposure times (short and long). **(C-E)** Reporter gene assays in P19 cells co-transfected with a control, MyT1, RFX4 and/or Act Notch and/or RBPJ-VP16 expression vectors and Hes5 proximal promoter luciferase reporter construct (pHes5:Luc). Mean ± SD of quadruplicate assays are shown. n.s. for P>0.05 according to Student's t-test. **(F)** MyT1 binding in NS-5 cells before (-LY) and 4h post treatment with Notch inhibitor LY (+LY) was assayed by ChIP-qPCR. ORF1 refers to negative control region. Mean ± SD of triplicate assays are shown. ** for P<0.01, n.s. for P>0.05 according to Student's t-test.

2. Hes1 transcriptional program in NS cell cultures

Hes1 downregulation is a pivotal event at the onset of neuronal differentiation (Kageyama et al., 2008). Despite of that, little is known about the transcriptional program downstream this TF in this cellular context. Following our observation that MyT1 represses Hes1 expression in NS cell cultures, we wished to investigate the significance of such regulatory event by characterizing the Hes1 transcriptional program. With that aim, we performed a genome-wide map of Hes1 BEs in NS-5 cells by ChIP-Seq. We identified Hes1 binding to 6180 regions associated with 6179 genes (Figure 3.S 12A). Most of the BEs are located within intergenic and intronic regions (41.4% and 43.9%, respectively) and at long distances from the nearest identified transcription start site (TSS) (|distance to TSS|=50-500 Kb), consistent with binding mostly to distal enhancers (Figure 3.S 12B-C).

Hes1 is a transcriptional repressor that binds to N-boxes and C-sites (Lin and Lee, 2012; Nakao and Campos-Ortega, 1996; Oellers et al., 1994; Sasai et al., 1992). When we performed a *de novo* search for DNA binding motifs enriched at a 50bp region centered on Hes1 summits, we found the C-Site and the Ascl1-type E-box motifs to be overrepresented (Figure 3. 23A and Figure 3.S 13). In addition, we could detect a modest enrichment of N-box motif by calculating the fold enrichment at the peak summits and by plotting the frequency distribution (Figure 3.S 13) (however, this enrichment is below the stringency cutoffs used for the *de novo* search). The enrichment of Ascl1-type E-box in the vicinity of Hes1 peak summits prompted us to investigate the overlap between Hes1 and Ascl1 bound sites. We found an extensive overlap between Hes1 and Ascl1 binding events (70% of Hes1 peaks are overlapping to Ascl1 peaks) (Figure 3. 23B), suggesting that Hes1 and Ascl1 have a large cohort of common targets.

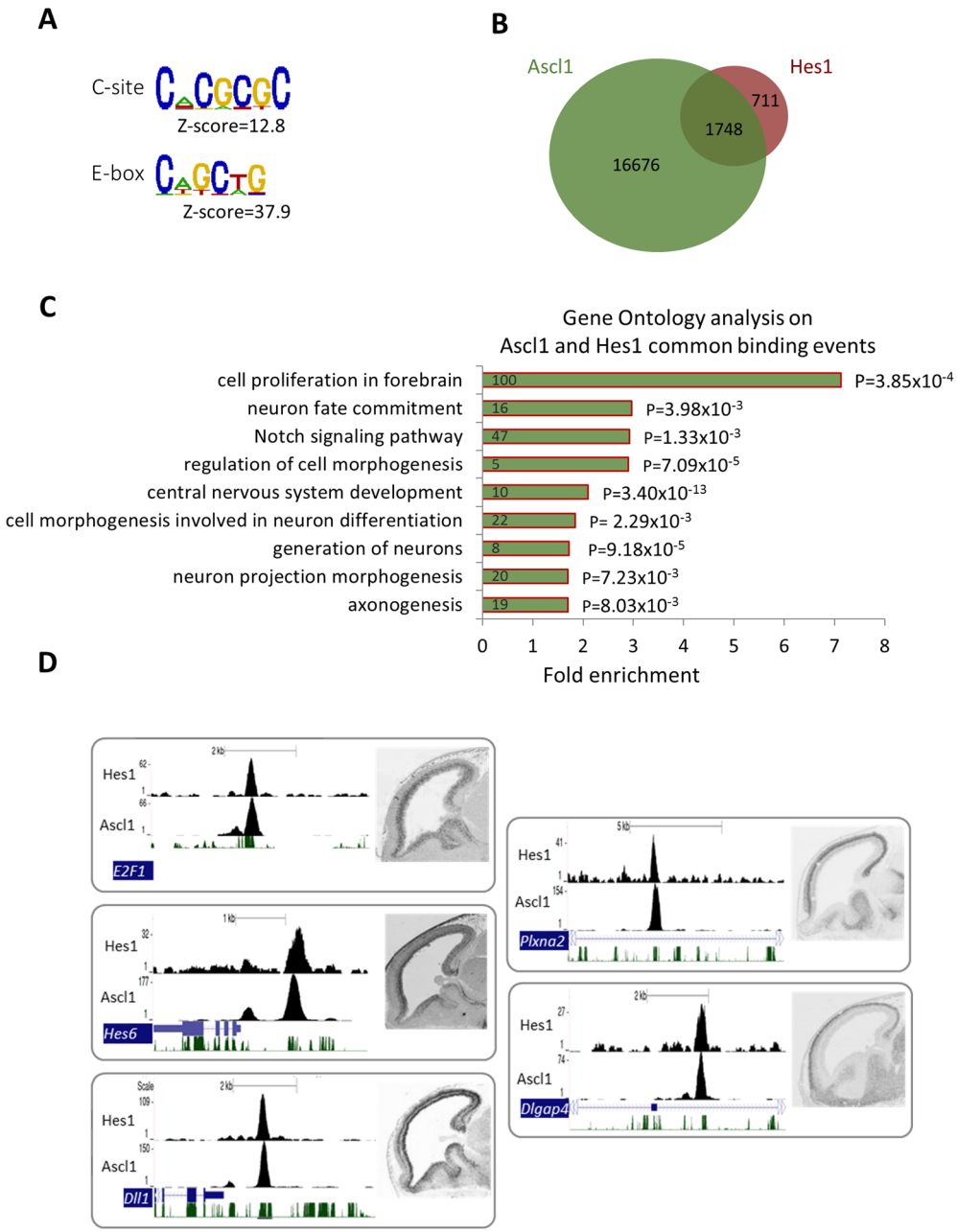

Figure 3. 23 An interplay between Hes1 and Ascl1 transcriptional networks.

(A) Motif logo of the two top overrepresented motifs within a 50bp region centered on Hes1 peak summits. P (Hes1 ChIP-Seq)<10^{-5}. **(B)** Venn diagrams depicting the overlap between Hes1 and Ascl1 ChIP-Seq peaks. P (Hes1 and Ascl1 ChIP-Seq)<10^{-10}. (Continued on the next page.)

Figure 3. 23 (continued) **(C)** Enrichment of Biological Process terms (Gene Ontology) associated with Hes1 and Ascl1 commonly bound genes. Numbers inside bars indicate number of genes. P value for each category is indicated in the outside end of each bar. P (Hes1 and Ascl1 ChIP-Seq)<10^{-10}. **(D)** Visual representation of ChIP-Seq enrichment profile of Hes1 and Ascl1 in the vicinity of 5 selected genes with a putative role in neuronal differentiation. Green track, Mammal conservation by PhastCons. The expression patterns on sagittal sections of E14.5 and E13.5 mouse telencephalon are from the public *in situ* hybridization databases GenePaint and Allen Brain Atlas, respectively.

Search for functional categories enriched on Hes1/Ascl1 commonly bound regions by Gene ontology analysis suggests that these are associated with genes involved in multiple steps of neurogenesis: from early steps of cell proliferation and neuron fate commitment, to late steps of neuron projection morphogenesis and axonogenesis (Figure 3. 23C). Accordingly, these common bound genes have distinct expression patterns in embryonic telencephalon: some are expressed in neural stem/progenitor cells in the VZ and SVZ, some are expressed in differentiating neurons in the MZ (Figure 3. 23D). Overall, these observations suggest that inhibition of neurogenesis by Hes1 goes beyond the regulation of Ascl1 expression, and takes place by counteracting the activation of Ascl1 target genes with functions at multiple stages of the differentiation program.

Discussion

The activation of a full program of neuronal differentiation by proneural TFs, such as Ascl1, requires the silencing of Notch signalling and the permanent downregulation of Hes1/5 genes in differentiating neural stem/progenitor cells (reviewed in (Kageyama et al. 2008; Imayoshi & Kageyama 2014)). However, the molecular mechanisms that control those events during the initial phases of neuronal differentiation, despite of incoming signalling from neighbouring cells, are still poorly understood.

In this study, we found that MyT1 is a direct target of Ascl1 and that it potentiates Ascl1-driven neuronal differentiation by counteracting the inhibitory effect of Notch signalling. In particular, we show that MyT1 directly controls the expression of Hes1, a key downstream effector of the Notch pathway during neurogenesis by a mechanism based on competition with RBPJ for DNA binding. A genome-wide search for additional MyT1 target genes indicates MyT1 functions globally as a repressor of gene expression, regulating many additional Notch target genes. Our work provides the first molecular basis for MyT1 function during neurogenesis, revealing a regulatory step whereby Ascl1 induction of MyT1 results in a cell-autonomous inhibition of Notch signalling at the onset of neuronal differentiation.

1. MyT1 enhances Ascl1-driven neurogenesis by conferring insensitivity to Notch signalling

In E12.5 ventral telencephalon, where endogenous Ascl1-driven neurogenesis is at place (Casarosa et al. 1999; Guillemot & Joyner 1993), MyT1 GoF results in increased migration from the VZ to SVZ/MZ and increased neuronal differentiation, while MyT1 LoF has the opposite effect (Figure 3. 8). Accordingly, we found that MyT1 synergizes with Ascl1 on the promotion of neurogenesis in NS cells in culture, as assessed by the

downregulation of the progenitor marker Sox2 and the induction of the neuronal marker TuJ1 (Figure 3. 7). However, when overexpressed on its own in NS cell cultures, MyT1 does not induce neuronal differentiation (Figure 3. 7), suggesting that, rather than playing an instructive role on the induction of neuronal differentiation, MyT1 functions in synergy with the proneural TF. Functional experiments both in NS cell cultures and in the telencephalon revealed that MyT1 enhances neuronal differentiation driven by proneural TFs by relieving inhibition by Notch signalling (Figure 3. 14, Figure 3. 15).

MyT1 has been shown to cooperate with proneural genes (X-NGNR-1, Xash3, Xash5 and Neurog3) to overcome Notch signalling inhibitory effect in primary and retinal neurogenesis in Xenopus and in endocrine cell differentiation in mouse pancreas (Bellefroid et al. 1996; Schneider et al. 2001; Ahnfelt-Rønne et al. 2007). We have shown for the first time that this genetic circuitry between proneural TFs, Notch signalling and MyT1 is also present during mammalian neurogenesis driven by Ascl1, suggesting it is conserved across phylogeny and ontogeny. Importantly, and considering that mouse models have so far failed to provide any support for a neurogenic function of MyT1 due to functional redundancy between MyT1 family members (Wang et al. 2007; Hudson et al. 2011), our results using electroporation in mouse telencephalon provide the first evidence for a role of MyT1 in mammalian neurogenesis *in vivo*. Further support from mouse models will likely require the analysis of embryos devoid of the three MyT1 family members. Recent technological developments in the field of genome engineering have greatly simplified genetic manipulation both in cultures and *in vivo*. Crispr/Cas9- and TALEN-based techniques have been shown to be particularly helpful to perform multiple manipulations at one step, allowing the possibility of targeting more than one gene at once (Yang et al. 2013; Vasileva et al. 2015). In the context of our work, these techniques would be

particularly helpful for the generation of MyT1:MyT1Like:MyT3 triple conditional knock-out mice.

2. How is MyT1 expression regulated during neurogenesis?

We found that MyT1 is a direct target of Ascl1 during neuronal differentiation (Figure 3. 6). MyT1 has been shown to function downstream proneural genes in other organisms and cell lineages. MyT1 is induced by X-NGNR1 during primary neurogenesis in Xenopus embryos and by Neurog3 during endocrine islet cell differentiation in the mouse pancreas (Wang et al. 2008; Bellefroid et al. 1996). However, none of these reports elucidated whether this regulation of MyT1 by proneural TFs was direct or indirect and did not implicate Ascl1 or any of its orthologues. Given the broad and pan-neuronal expression of MyT1 in the developing mouse CNS (Figure 3. 4) (Matsushita et al. 2013), it is possible that, in addition to Ascl1, other proneural TFs regulate MyT1 expression in progenitor domains of the CNS where Ascl1 is not expressed.

MyT1 expression is upregulated in INPs at the onset of neuronal differentiation (Mizutani et al. 2007; Kawaguchi et al. 2008). It remains to be determined why MyT1 displays a late onset of expression, when compared to other early Ascl1 targets that are already expressed in RG cells (Figure 2. 2). Below we describe two possible mechanisms that may contribute for the timing of MyT1 expression during neurogenesis.

It was recently demonstrated in Xenopus that the phosphorylation status of Ascl1 modulates its ability to induce neuronal differentiation. Although both forms are equally effective at inducing the expression of Dll1, the unphosphorylated form is much more potent at inducing MyT1 expression and neuronal differentiation when expressed in Xenopus embryos (Ali et al. 2014). Therefore, one possibility is that the

induction of MyT1 and consequent downregulation of Notch signalling depend on the pathways that control Ascl1 phosphorylation during neuronal differentiation.

As previously described on Chapter 2, Ascl1 binding to close chromatin regions occurs typically in the vicinity of Ascl1 target genes expressed *de novo* during neuronal differentiation (e.g. NeuroD4). Interestingly, a side-by-side comparison of Ascl1 ChIP-Seq and DNAse-Seq profiles at the MyT1 locus in proliferating and differentiating cells, reveals that Ascl1 binding precedes chromatin opening at few sites at the MyT1 proximal promoter region (Figure 2.S1, green arrows). Thus, another possibility is that chromatin accessibility at MyT1 regulatory region contributes to the kinetics (late onset) of MyT1 induction by Ascl1.

An important note is that, although the overall levels of MyT1 expression are reduced, MyT1 is still expressed in the developing nervous system of Ascl1 null embryos (Figure 3. 6D), indicating functional redundancy with other pathways.

3. MyT1 represses gene expression on a genome-wide level

MyT1 has been previously associated with both activation and repression of gene expression. Most of the experiments addressing the activator/repressor functions of MyT1 family members consist of reporter gene assays using artificial promoter constructs (Bellefroid et al. 1996; Jiang et al. 1996; Yee & Yu 1998; Hu et al. 2013) and functional assays using fusion proteins consisting of MyT1 truncations containing double ZFs fused to the activator (VP16) or repressor (EnR) domains (Wang et al. 2008; Bellefroid et al. 1996). Alternatively, direct repression of gene expression by full-length MyT1 protein has been clearly demonstrated in a neuroblastoma cell line, however, this evidence is relative to the regulation of one single gene (Pten) (Yokoyama et al. 2014). When characterizing the transcriptional program of MyT1 in a neurogenic context, we combined MyT1 location analysis with expression profiling upon MyT1 GoF in NS cell cultures. We found that MyT1 represses gene expression

at a genome-wide level (Figure 3. 12). It is possible that MyT1 activator or repressor functions are cell-context dependent which would justify the discrepancy between our and previous published results. On the other hand, the VP16 and EnR fusion constructs, that provide most of the evidence for MyT1 function as an activator (Wang et al. 2008; Bellefroid et al. 1996), contain truncated versions of MyT1 (ZF2-3) and lack the central domain previously demonstrated to be essential for its function (Bellefroid et al. 1996; Romm et al. 2005; Yokoyama et al. 2014). In addition, validation of these constructs on a transcriptional assay has never been performed, questioning the validity of such approaches.

The association of MyT1 with transcriptional repression stems mostly from the identification of co-factors shown to promote histone deacetylation and demethylation, such as HDAC1 or LSD1, respectively (Yokoyama et al. 2014; Romm et al. 2005). Following on our results, future work should address if MyT1 repressor function in neurogenesis involves the recruitment of this chromatin remodelling machinery.

4. Function of MyT1 target genes

MyT1 represses multiple genes associated with Notch signalling, a pathway of fundamental importance for the maintenance of the NSC state (Kageyama et al. 2008). Among those genes are Notch1 receptor, Notch targets Hesr1, Hesr2 (in addition to Hes1 and Hes5) and Notch signalling modulators, such as Lfng, Dtx4 and Nrarp (Pierfelice et al. 2011), suggesting that MyT1 regulates this pathway at multiple levels. MyT1 also directly represses Pax6 and Sox2, genes typically expressed in RG cells with a pivotal role on the maintenance of the NSC state (Gómez-López et al. 2011; Englund et al. 2005). Other MyT1 repressed genes are associated with cell cycle progression, such as Fgfr2, Btg2, Cdkn1a (p21) and Cdkn1b (p27) (GO term “positive regulation of cell proliferation”), suggesting it may have a direct role on the negative

regulation of cell proliferation during neuronal differentiation. Although we did not investigate in detail MyT1 direct effect on cell proliferation, a preliminary analysis of MyT1 LoF in ventral telencephalon 2 days after *in utero* electroporation of MyT1 ShRNA revealed a slight increase on the number of proliferating cells, as compared to control condition (data not shown).

MyT1 targets are also enriched for the GO category "regulation of transcription from RNA polymerase II promoter". In addition to the above mentioned TFs, examples of these genes are Id3, an inhibitor of bHLH activity that functions by sequestering E-proteins (Ruzinova & Benezra 2003), Olig1, a master regulator of oligodendrocyte differentiation (Ross et al. 2003) and NFIX, a TF that plays a major role on the induction of quiescence of NSCs (Martynoga et al. 2013). Overall, our data suggests that MyT1 promotes neuronal differentiation by repressing genes associated with NSC state and alternative cell fates.

5. MyT1 blocks Notch activation of Hes1 expression

Hes1 regulates its own expression in a delayed negative feedback loop, describing a self-sustained oscillatory mode of expression in NSCs (Shimojo et al. 2008). Given its place at the top of the hierarchy of the oscillatory TF expression in NSCs (Imayoshi et al. 2013), one may expect that shutting down Hes1 expression is a step of crucial importance for the progression of neuronal differentiation, highlighting the importance of our findings. At this stage it is difficult to evaluate how much of MyT1 function relates to its ability to repress Hes1. To assess the relevance of this regulatory event in the context of the whole MyT1 program, it will be important to perform a rescue experiment by co-expressing Hes1 in a GoF of MyT1.

A pair of ZFs has been shown to be the minimal functional unit for the recognition of a MyT1 motif (AAGTT) (Bellefroid et al. 1996; Gamsjaeger et al. 2013). MyT1 contains 3 pairs of ZFs (Figure 3. 3), suggesting that one MyT1 molecule can recognize

simultaneously 2 or 3 distinct MyT1 motifs *in vivo* (Gamsjaeger et al. 2013). We found that MyT1 represses Hes1 expression by binding to 3 MyT1 BSs on Hes1 promoter. Therefore, it is possible that one molecule of MyT1 binds simultaneously to the 3 MyT1 BSs on Hes1 promoter. Structural modelling of MyT1 binding to Hes1 promoter demonstrates that the distance between the two double ZFs ZF4-5 and ZF6-7 of MyT1 protein is compatible with binding of one molecule of MyT1 to a DNA fragment with the arrangement of the MyT1 BS2-3 on Hes1 promoter (data from Joel Mackay Lab, unpublished) (Figure 3.S 14). Although EMSA analysis showed that mutation of any one of the 3 MyT1 BSs on Hes1 promoter greatly affects binding of MyT1 (Figure 3. 20B), it did not allow to clearly dissect if one or more MyT1 molecules bind to the 3 MyT1 BSs on Hes1 promoter region.

It has been shown that MyT1 binds to AAGTT motifs with low affinity, questioning its function as a DNA binding TF or suggesting that multiple MyT1 BSs may be required for efficient binding to its target genes (Besold et al. 2014; Gamsjaeger et al. 2008). According with this idea, we could detect multiple AAGTT motifs not only on Hes1 promoter but also on MyT1 ChIP-qPCR positive controls (Ank2, Chd7 and Scl35b1) and on other validated MyT1 targets (such as Btg2, Dtx4, Egr1, Id3, Lfng and Lmcd1 which contain 3 or more AAGTT motifs) (data not shown). In case of the Hes1 promoter, we found that the 3 MyT1 BSs are partially overlapping with previously characterized RBPJ BSs (Figure 3. 20A). In all conditions tested, MyT1 and RBPJ form two alternative complexes (as opposed to a ternary complex) when binding to Hes1 probe on EMSA (Figure 3. 21A), suggesting that MyT1 and RBPJ binding to Hes1 promoter is mutually exclusive. It is tempting to speculate that this spatial arrangement of overlapping MyT1 and RBPJ BSs may provide a quick mechanism to shut down the activity of RBPJ at the Hes1 promoter, as compared to a mechanism that depends on the recruitment of chromatin remodelling complexes. Also, further

analysis is required to investigate if a similar competition mechanism takes place at other MyT1/Notch common target genes.

6. Do other MyT1 family members regulate Hes1?

MyT1 family members have high sequence homology within the ZF domains and all have been shown to recognize the AAGTT motif (Bellefroid et al. 1996; Yee & Yu 1998; Jiang et al. 1996). Thus, it is possible that they are all capable of regulating Hes1 expression. In fact, our preliminary data from a reporter gene assay demonstrates that MyT1Like and MyT3 can also counteract Notch activation of Hes1 promoter (Figure 3.S 16), suggesting these two TFs may regulate Hes1 by a mechanism similar to the one we identified for MyT1. This finding is in accordance with the proposed functional redundancy of MyT1 family members revealed in MyT1 null embryos (Wang et al. 2007).

Although downregulation of Notch signalling is required for the neurogenic transition to occur, several reports have highlighted a role for this same pathway on the regulation of dendritic growth and branching and migration of post-mitotic neurons (Redmond et al. 2000; Hashimoto-Torii et al. 2008; Sestan et al. 1999). It is tempting to speculate that the expression of MyT1 family members in post-mitotic cells may relate to the need to modulate Notch activity at later stages.

It was previously shown that MyT1Like cooperates with Ascl1 in the reprogramming of mouse embryonic fibroblasts (MEFs) into induced neurons (Vierbuchen et al. 2010). Although it is not clear what the levels of canonical Notch signalling may be in MEFs, Hes1 is expressed in MEFs as it is in NSCs, in an oscillatory manner (Yoshiura et al. 2007). One possibility suggested by our results is that MyT1Like functions in this reprogramming paradigm by repressing Hes1 expression. Of note, supporting this possibility, the regulatory region bound by MyT1 in the Hes1 promoter is in open

chromatin conformation in MEFs, as analysed by FAIRE-qPCR (Diogo Tomaz, unpublished), thus, accessible for TF binding.

7. MyT1 inhibition of Hes5 expression

In addition to repressing Hes1, MyT1 GoF results in a quick down-regulation of Hes5 expression (readily detected at 4h) and in a partial inhibition of its promoter in a transcriptional assay (Figure 3. 18B, Figure 3. 22C). Surprisingly, scanning of the Hes5 proximal promoter region bound by MyT1 in ChIP fails to identify the MyT1 motif (AAGTT) and EMSA analysis did not reveal any direct binding of MyT1 to this region (Figure 3. 22). These negative results suggest that MyT1 may regulate Hes5 through a mechanism independent of direct DNA binding. MyT1 recruitment to Hes5 promoter is decreased by treatment with the Notch inhibitor LY (Figure 3. 22F), which causes an overall reduction of NICD levels (Lanz et al. 2004), suggesting that MyT1 could be recruited to Hes5 promoter through protein-protein interactions with the Notch/RBPJ activator complex. To further explore this possibility, we attempted at determining if MyT1 protein physically interacts with the following members of the complex: RBPJ, NICD and Maml1. For that, we overexpressed MyT1 and each of these members of the Notch activator complex and performed immunoprecipitation against one of the putatively interacting proteins under non-denaturing conditions. We failed to co-immunoprecipitate MyT1 with any of the tested factors (Figure 3.S 15), suggesting no direct physical interaction between MyT1 and Maml1, NICD or RBPJ takes place. Therefore, the exact mechanism whereby MyT1 efficiently represses Hes5 expression remains to be elucidated.

8. Working model of MyT1 function in mammalian neurogenesis

Altogether our observations suggest a model in which the proneural factor Ascl1 induces neuronal differentiation and concomitantly inhibits Notch signalling in a cell-

autonomous manner through the induction of MyT1. MyT1 represses many canonical Notch target genes, including Hes1 and Hes5, resulting in lack of responsiveness to incoming Notch signalling from neighbouring cells and, therefore, facilitating neuronal differentiation. Importantly, MyT1 represses the expression of Hes1 through a mechanism that involves direct DNA binding and competition with RBPJ, a step of crucial importance for the onset of neuronal differentiation (Figure 3. 24).

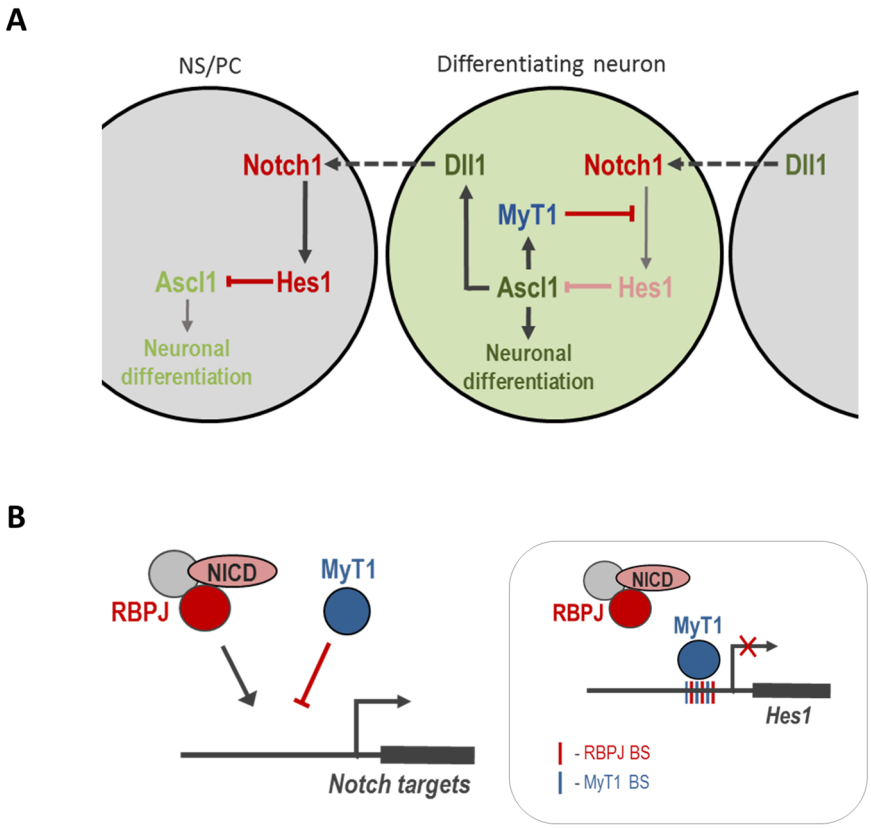

Figure 3. 24 Working model of MyT1 function in neurogenesis.

(A) Ascl1 promotes neuronal differentiation and coordinately inhibits Notch signaling cell-autonomously in differentiating neurons by inducing MyT1. **(B)** MyT1 interferes with the activation of canonical Notch targets. Particularly, MyT1 interferes with canonical Notch activation of Hes1 expression by direct DNA binding and competition with RBPJ.

9. An interplay between Hes1 and Ascl1 transcriptional networks

Data from mammalian cells and Drosophila show that overexpression of proneural TFs ectopically induces neurogenesis and that, surprisingly, co-expression of Hes1/E(spl) has a strong inhibitory effect over proneural function. If the only function of Hes1/E(spl) in neurogenesis was to repress proneural gene expression, co-expression of Hes1 would have negligible effects on a proneural GoF. However, these experiments suggest that Hes1 may have additional roles downstream of proneural factors (Hinz et al. 1994; Castella et al. 1999; Nakao & Campos-Ortega 1996). Interestingly, our genome-wide mapping of Hes1 binding shows that a large percentage of Hes1 BEs are common to Ascl1 in NS cell cultures (Figure 3. 23B). Gene ontology analysis reveals that genes associated with Hes1 and Ascl1 common binding events are involved in diverse steps of the neuronal differentiation program (Figure 3. 23C). Given that Ascl1 functions as a transcriptional activator and Hes1 as a transcriptional repressor, our results suggest that Ascl1 and Hes1 have opposite effects on neurogenesis by antagonistically regulating common target genes with distinct functions along the neurogenic program.

Our motif analysis on Hes1 bound regions (Figure 3. 23 and Figure 3.S 13, Figure 3.S 18) suggests that Hes1 recruitment to sites common to Ascl1 might not occur predominantly through binding to C-Site but reveals a differential enrichment of Ascl1-type E-boxes on those sites, raising two possibilities. The first possibility is that Hes1 is capable of binding to E-box motifs, competing with Ascl1 for binding to its sites. E(spl) TFs cannot bind to CAGCTG variant (Ascl1 E-box) (Oellers et al. 1994), but bind variants of E-box motifs CACGTG, CAGGTG with optimal and sub-optimal affinities, respectively (Jennings et al. 1999). Therefore, it was previously proposed but not demonstrated by others, that proneural and E(spl) TFs interact with common E-box motifs with different affinities (Jennings et al. 1999). Hes5 has been shown to

be unable to bind to E-box (CANNTG), while Hes1 has been shown to bind with low affinity to CACNTG E-box (Sasai et al. 1992; Akazawa et al. 1992). However, it was not yet formally demonstrated whether Hes1 can or cannot bind directly to Ascl1-type E-box (CAGCTG). A second possibility is that Hes1 establishes protein-protein interactions with Ascl1 when bound to E-boxes. Direct interactions between Hes/E(spl) proteins and bHLH factors have previously been reported. Hes1 has been shown to heterodimerize with E-proteins (Lin & Lee 2012) and Hes5 with Ascl1 (Akazawa et al. 1992). In addition, E(spl) interferes with the activity of Ac/Sc by physically interacting with them at the DNA (Giagtzoglou 2003). Further work will be needed to clearly understand the mechanisms of Hes1 interference with Ascl1 transcriptional activity during mammalian neurogenesis.

Supplemental data

MyT1 expression in Ascl1 GoF and LoF microarrays				
	NS cells		Telencephalon	
	FC	P value	FC	P value
Ascl1 LoF	0.20	8.17×10^{-3}	0.36	1.87×10^{-2}
Ascl1 GoF	4.23	9.95×10^{-4}	1.47	2.28×10^{-2}

Figure 3.S 1 MyT1 expression is deregulated upon Ascl1 GoF and LoF.

MyT1 expression data from Ascl1 GoF and LoF experiments in the E12.5 mouse telencephalon and in NSC cultures. FC, Fold Change. Ascl1 LoF in telencephalon, microarrays on E13.5 ventral telencephalon of wt and Ascl1 $^{-/-}$ mice (Parras, C. Unpublished). Ascl1 GoF in telencephalon, microarrays on *in utero* electroporated E10.5 mouse telencephalon with control or Ascl1 expressing vectors (Gohlke et al. 2008). Ascl1 LoF in NS cells, microarrays upon electroporation of control plasmid or the bHLH domain of Ascl1 fused to EnR domain in NS-5 cells (Castro et al. 2011). Ascl1 GoF in NS cells, microarrays on NS-5 Ascl1-ERT2 cells.

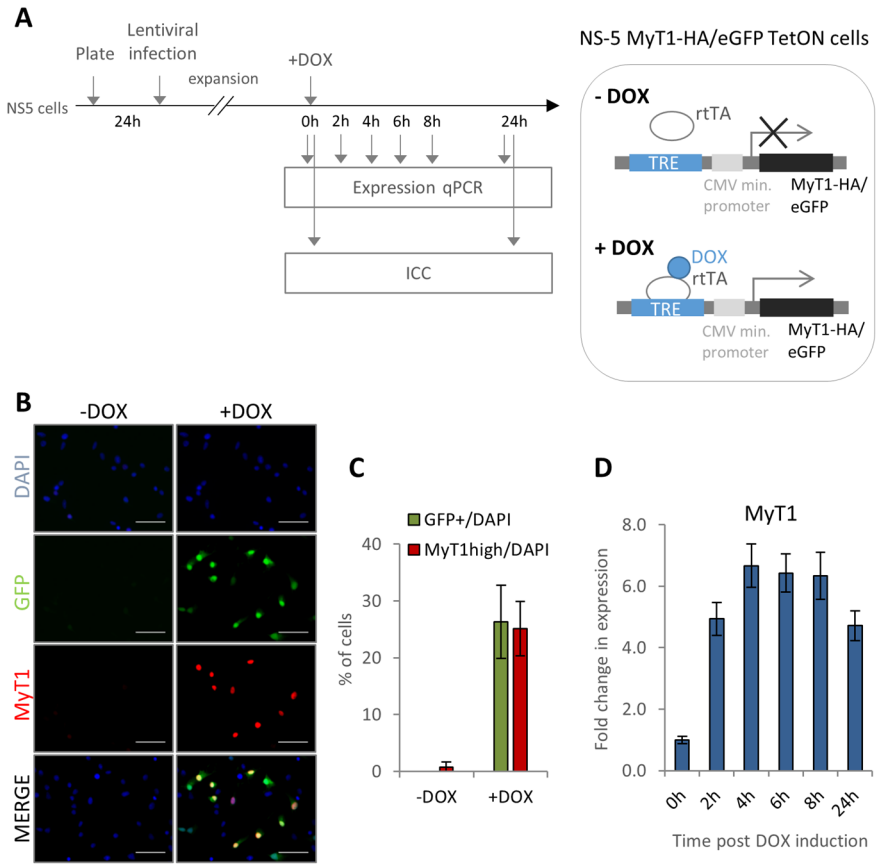

Figure 3.S 2 NS-5 MyT1-HA/GFP TetON cells (NS-5 MyT1-HA inducible cells).

(A) Scheme depicting the generation of NS-5 MyT1-HA/GFP TetON cells (NS-5 MyT1-HA inducible cells) and immunocytochemical analysis, gene expression analysis by Real-time PCR performed as indicated in figure. **(B)** Immunocytochemistry using anti-MyT1 and anti-GFP before (-DOX) and 24h post DOX induction (+DOX). Nuclei were stained with DAPI (blue). Scale bar, 40µm. **(C)** Histogram representing the percentage of GFP^+ cells (GFP^+/DAPI) and of MyT1 overexpressing cells ($MyT1^{high}$/DAPI) cells before (-DOX) and 24h post DOX induction (+DOX). Data presented as the mean ± SD for at least 1000 cells on each condition. **(D)** Analysis of MyT1 expression by expression Real-time PCR. Mean ± SD of triplicate assays are shown.

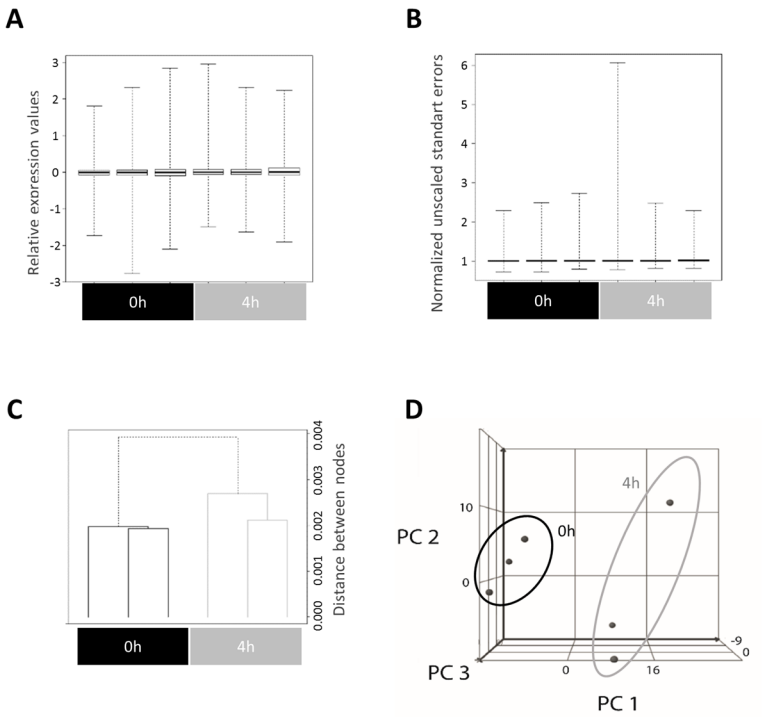

Figure 3.S 3 Quality control analysis of MyT1 gain-of-function DNA microarrays.

(A) Relative expression (RLE) values for the technical replicates of MyT1 GoF gene expression microarrays 0h and 4h post DOX. **(B)** Normalized unscaled standard errors (NUSE) for the technical replicates of MyT1 GoF gene expression microarrays 0h and 4h post DOX. **(C)** Dendrogram of technical replicates of MyT1 GoF gene expression microarrays 0h and 4h post DOX. **(D)** Principal component analysis (PCA) of the technical replicates of MyT1 GoF gene expression microarrays 0h and 4h post DOX.

A

MyT1 ChIP-Seq cutoff	# peaks	# of associated genes
P value < $1x10^{-5}$	18865	7068
P value < $1x10^{-10}$	11990	5135

MyT1-HA ChIP-Seq cutoff	# peaks	# of associated genes
P value < $1x10^{-5}$	834	573
P value < $1x10^{-10}$	493	336

B

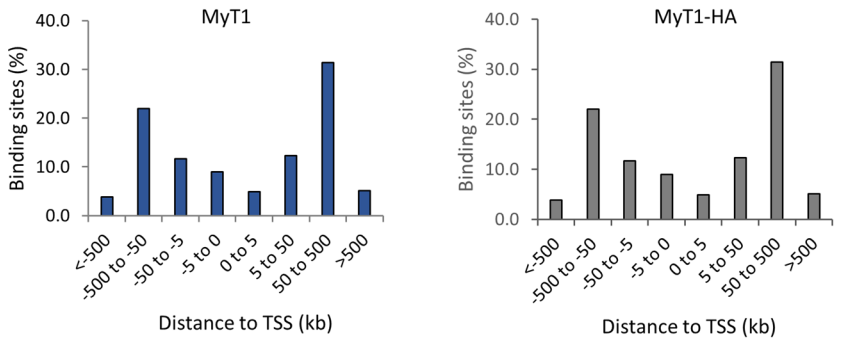

C

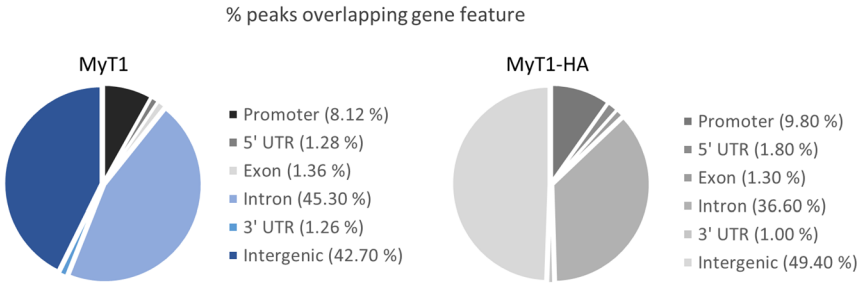

Figure 3.S 4 Location of MyT1 and MyT1-HA BEs in relation to genomic features.

(A) Number of peaks and associated genes (following a single nearest gene annotation) for two p value cutoffs for anti-MyT1 in NS-5 cells (left) and anti-HA in NS-5 MyT1-HA inducible cells + DOX (right) ChIP-Seq datasets. **(B)** Percentage of MyT1 (left) and MyT1-HA (right) ChIP-Seq peaks at indicated distances from the nearest TSS. $P<10^{-5}$. **(C)** Percentage of MyT1 (left) and MyT1-HA (right) ChIP-Seq peaks overlapping gene features. $P<10^{-5}$.

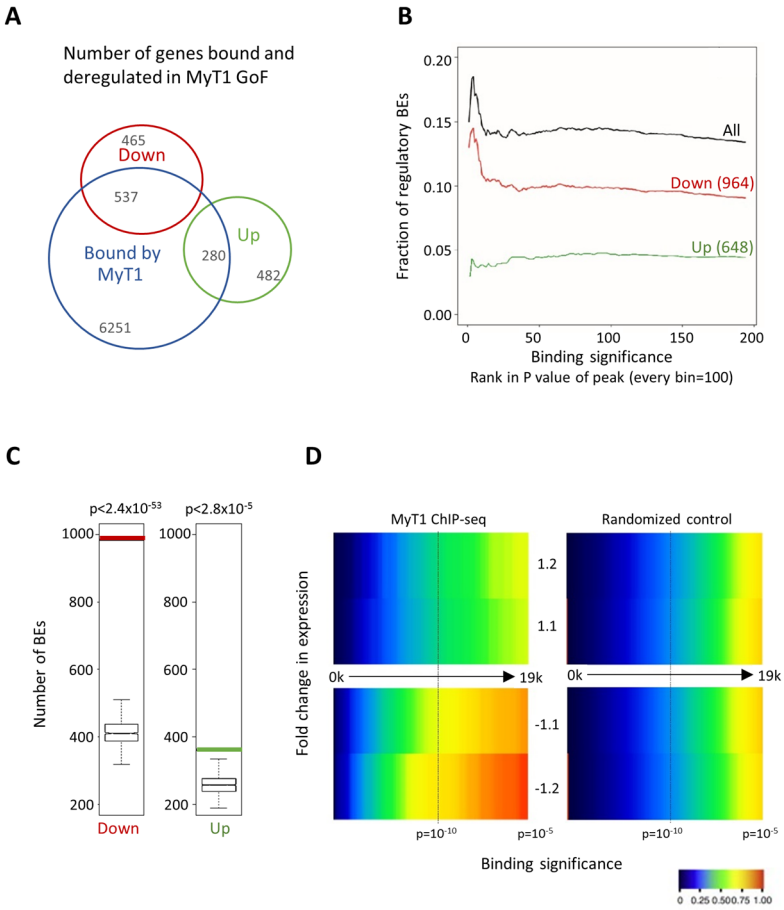

Figure 3.S 5 MyT1 functions as a transcriptional repressor at a genome-wide level (analysis from MyT1 ChIP-Seq in NS-5 cells).

(A) Venn diagram depicting the overlap between genes up- or downregulated in MyT1 GoF and genes bound by MyT1 following nearest gene annotation. P (MyT1 ChIP-Seq)<10^{-5}. P (MyT1 GoF microarrays)<0.05, FC>|1.2|. **(B)** Cumulative fraction of MyT1 BEs considered regulatory by association with up- or downregulated genes following a nearest gene annotation. Numbers in brackets represent the number of peaks associated with up- or downregulated genes. P (MyT1 ChIP-Seq)<10^{-5}. P (MyT1 GoF microarrays)<0.05, FC>|1.2|. **(C)** Number of MyT1 BEs associated with up- (green bar) or downregulated (red bar) genes in MyT1 GoF microarrays. Test data represented as box with median of test and first and third quartiles; whiskers, ±1.5 x interquartile range (IQR). P (MyT1 ChIP-Seq)<10^{-5}. P (MyT1 GoF microarrays)<0.05, FC>|1.2|. **(D)** Heat map displaying the cumulative fraction of deregulated genes in MyT1 GoF that are directly regulated by MyT1 (up, top left panel; down, bottom left panel). Transcripts are divided in equal bins of decreasing expression fold change and plotted against MyT1 BEs with increasing p value. Control: 100 sets of random BEs (right, mean value shown).

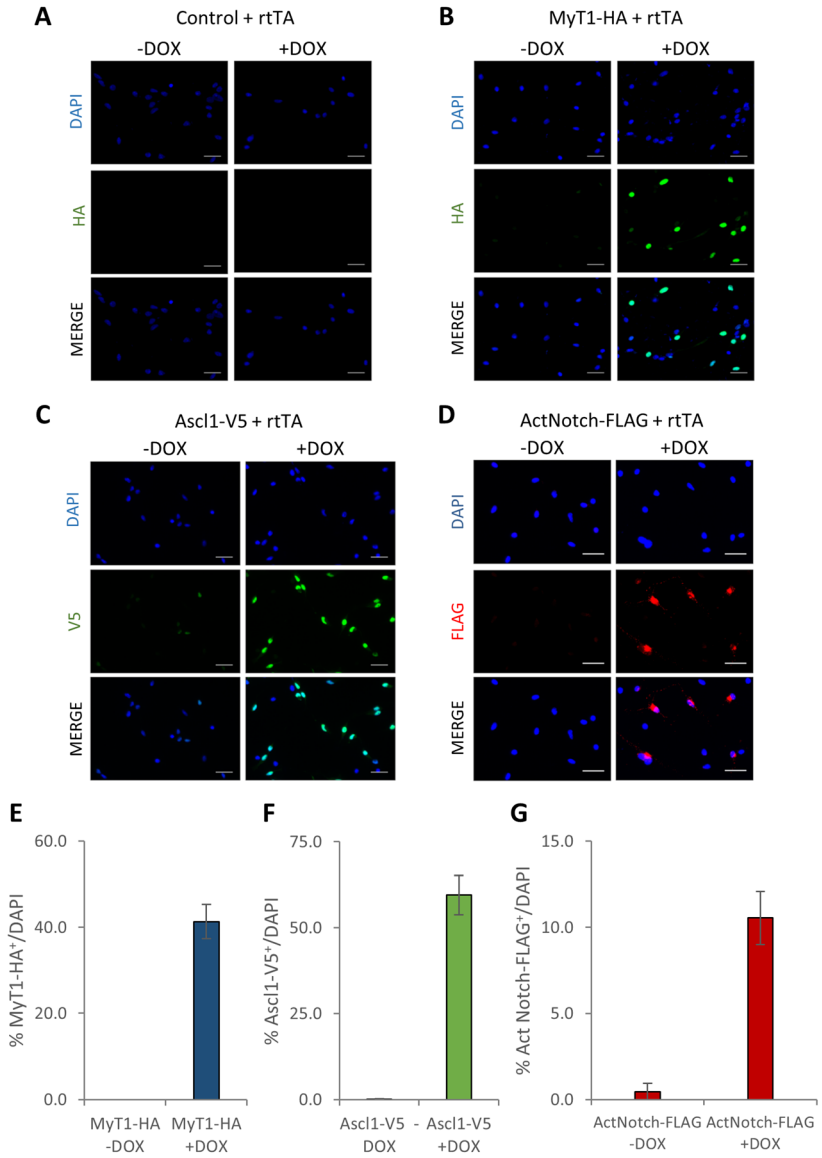

Figure 3.S 6 Controls for expression of TetON-FUW inducible lentiviruses.

Immunocytochemical analysis of control **(A)**, MyT1-HA **(B)**, Ascl1-V5 **(C)** or Act Notch-FLAG **(D)** TetON lentivirus-infected cells with anti-HA (green) **(A-B)**, anti-V5 (green) **(C)** and anti-FLAG (red) **(D)** antibodies before (-DOX) and 24h post DOX induction (+DOX). Nuclei were labeled with DAPI (blue). Scale bar, 140µm. Histograms represent the percentage of cells overexpressing MyT1-HA (HA^+/DAPI, **(E)**), Ascl1-V5 ($V5^+$/DAPI, **(F)**) and Act Notch-FLAG ($FLAG^+$/DAPI, **(G)**). Data presented as the mean ± SD for at least 1500 cells on each condition.

A

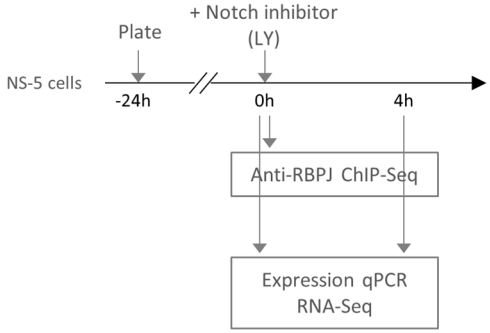

B

RBPJ ChIP-Seq cutoff	# peaks	# of associated genes
P value < $1x10^{-5}$	5526	3032
P value < $1x10^{-10}$	1254	793

C

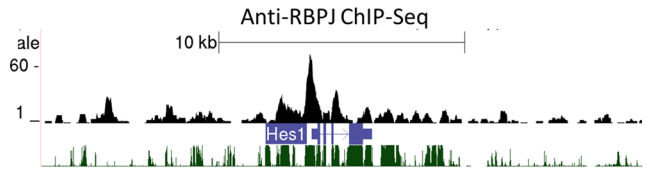

D

Notch inhibitor RNA-Seq (FC >|1.2|)	# deregulated genes	# upregulated genes	# downregulated genes
Q value < 0.05	4827	2469	2358
Q value < 0.01	4490	2308	2182

Figure 3.S 7 Genome-wide identification of RBPJ BEs and Notch regulated genes in NS-5 cells.

(A) Scheme depicting genome-wide mapping of RBPJ BEs in NS-5 cells and expression profiling of NS-5 cells before (-LY) or after a 4h exposure to g-secretase inhibitor LY-411575 (+LY) by RNA-Seq. **(B)** Visual representation of ChIP-Seq enrichment profile of RBPJ in the vicinity of the Hes1 gene. Green track, Mammal conservation by PhastCons. **(C)** Number of peaks and associated genes (following a nearest gene annotation) for two p value cutoffs of RBPJ ChIP-Seq data set. **(D)** Number of deregulated genes upon treatment with g-secretase inhibitor LY-411575 (LY) and associated q value cutoff. FC>|1.2|.

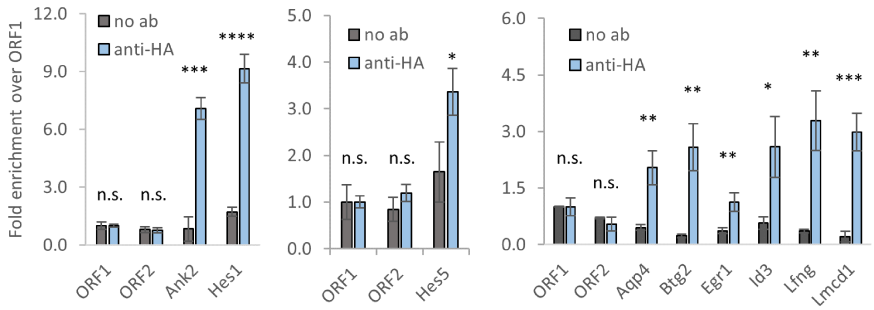

Figure 3.S 8 Validation of MyT1 binding in NS-5 MyT1-HA inducible cells.

Validation of MyT1 binding to selected genes by ChIP-qPCR with anti-HA antibody in NS-5 MyT1-HA inducible cells 24h post DOX induction. ORF1 and ORF2 refer to two negative control regions. Ank2 was used as a positive control region. Mean ± SD of triplicate assays are shown. n.s. for P>0.05, * for P<0.05, ** for P<0.01, *** for P<0.001, **** for P<0.0001 according to Student's t-test.

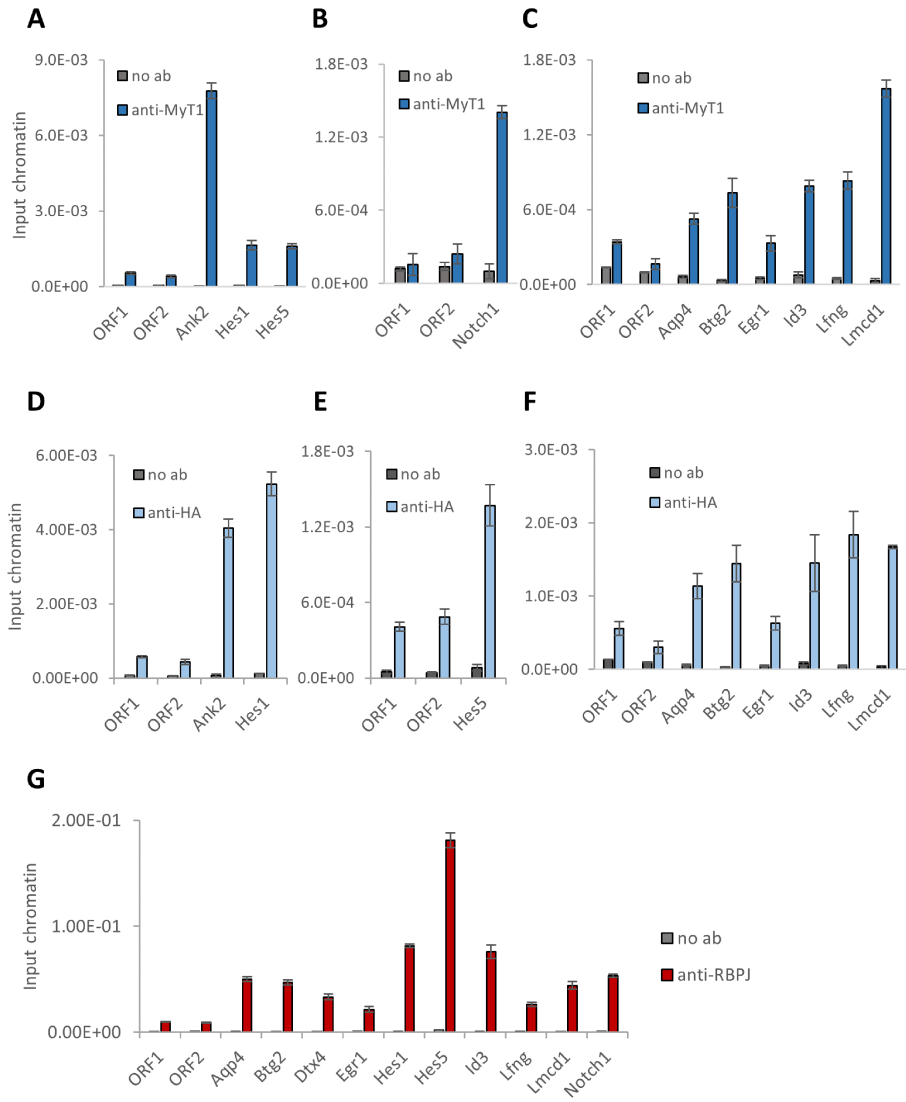

Figure 3.S 9 Validation of binding of MyT1, MyT1-HA and RBPJ to selected targets (non-normalized data). ChIP-qPCR using antibodies against MyT1 **(A-C)**, HA **(D-F)** and RBPJ **(G)** ChIP-qPCR using chromatin extracted from undifferentiated NS-5 cells **(A-C,G)** and NS-5 MyT1-HA inducible cells **(D-F)**. ORF1 and ORF2 refer to two negative control regions. Mean ± SD of triplicate assays are shown.

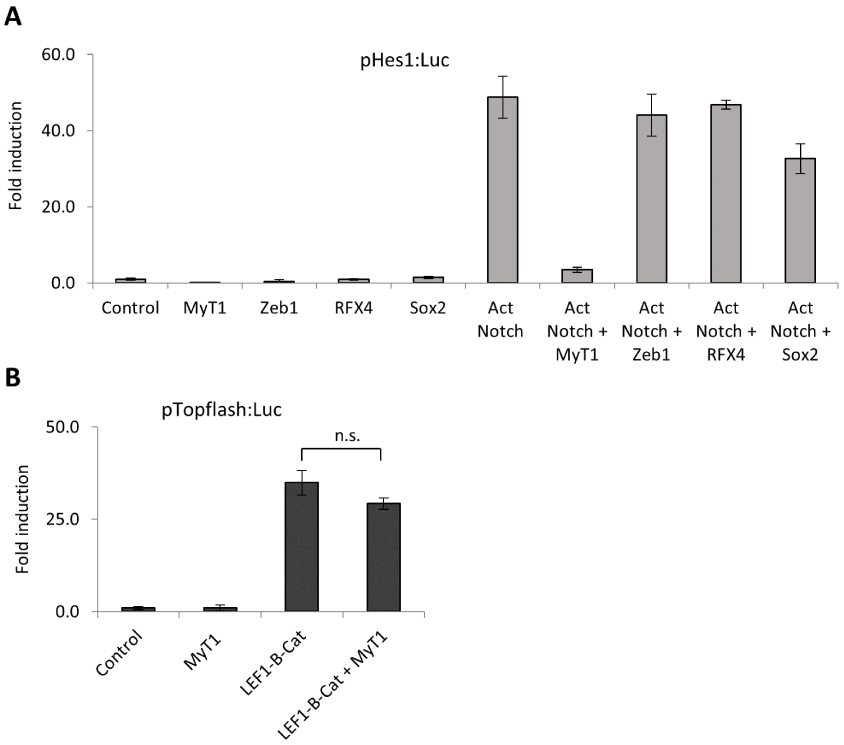

Figure 3.S 10 MyT1 interference with Notch activation of Hes1 promoter is specific.

(A) Reporter gene assay in P19 cells co-transfected with control vector, MyT1, Zeb1, RFX4, Sox2 and/or Act Notch expression vectors and Hes1 proximal promoter luciferase reporter construct (pHes1:Luc). Mean ± SD of quadruplicate assays are shown. **(B)** Reporter gene assay in P19 cells co-transfected with control, MyT1 and/or the fusion protein LEF1-B-Catenin (LEF1-B-Cat) expression vectors and a reporter construct expressing luciferase under the control of multimerized LEF1 BSs (pTopflash:Luc). Mean ± SD of quadruplicate assays are shown. n.s. for P>0.05 according to Student's t-test.

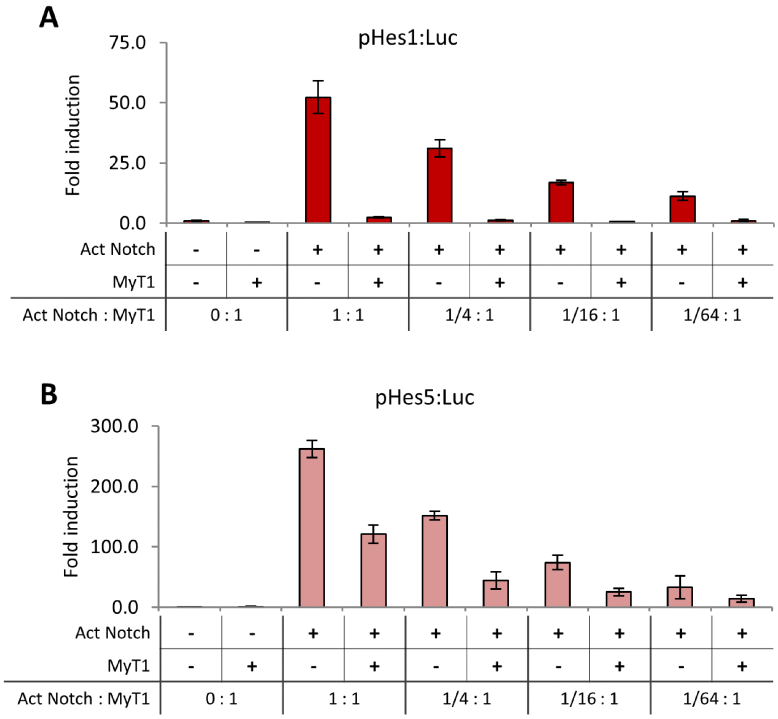

Figure 3.S 11 Comparison of MyT1 activity on Hes1 and Hes5 promoters.

(A-B) Reporter gene assays in P19 cells co-transfected with a control, MyT1, Act Notch and/or RBPJ-VP16 expression vectors and a reporter construct expressing luciferase under the control of Hes1 or Hes5 proximal promoters (pHes1:Luc or pHes5:Luc). Distinct ratios of expression vectors are used, as indicated in figure. Mean ± SD of quadruplicate assays are shown.

A

Hes1 ChIP-Seq cutoff	# peaks	# of associated genes
P value < $1x10^{-5}$	6180	6179
P value < $1x10^{-10}$	2459	2459

B

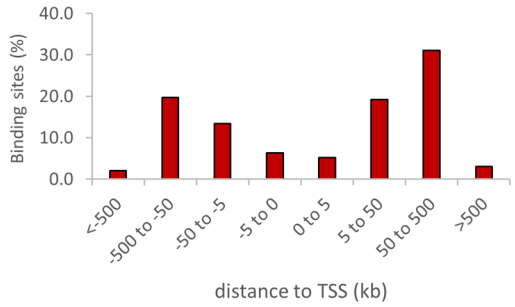

C

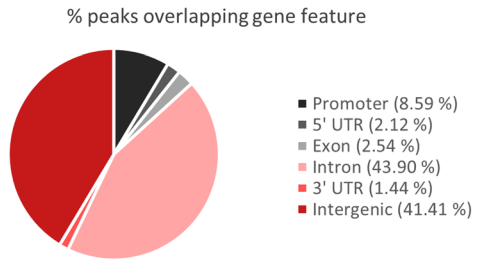

Figure 3.S 12 Location of Hes1 BEs in relation to various genomic features.

(A) Number of peaks and associated genes (following nearest gene annotation) for distinct p value cutoffs of Hes1 ChIP-Seq data set. **(B)** Percentage of Hes1 ChIP-Seq peaks at indicated distances from the nearest TSS. P (Hes1 ChIP-Seq)<10^{-5}. **(C)** Percentage of Hes1 ChIP-Seq peaks overlapping gene feature. P (Hes1 ChIP-Seq)<10^{-5}.

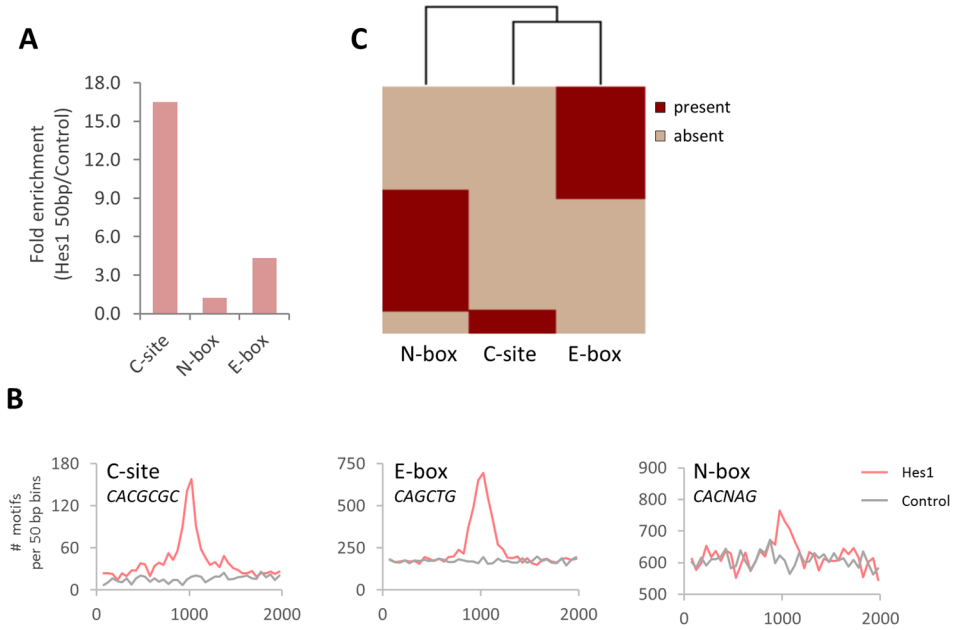

Figure 3.S 13 DNA binding motifs overrepresented on Hes1 ChIP-Seq.

(A) Fold enrichment of C-site, E-box and N-box motifs within a 50bp region centered at Hes1 peak summits as compared to control regions (of equal number and size located 2Kb upstream of Hes1 peaks). P (Hes1 ChIP-Seq)<10^{-5}. **(B)** Frequency distribution of C-site, E-box and N-box motifs within a 2000bp region centered at Hes1 peak summits (red) or 2Kb upstream (control, gray). Y axis represents the number of motifs present in bins of 50bp along the 2000bp region. P (Hes1 ChIP-Seq)<10^{-5}. **(C)** Hierarchical clustering of Hes1 peaks based on the presence (red) or absence (tan) of N-box, C-site or E-box. P (Hes1 ChIP-Seq)<10^{-5}.

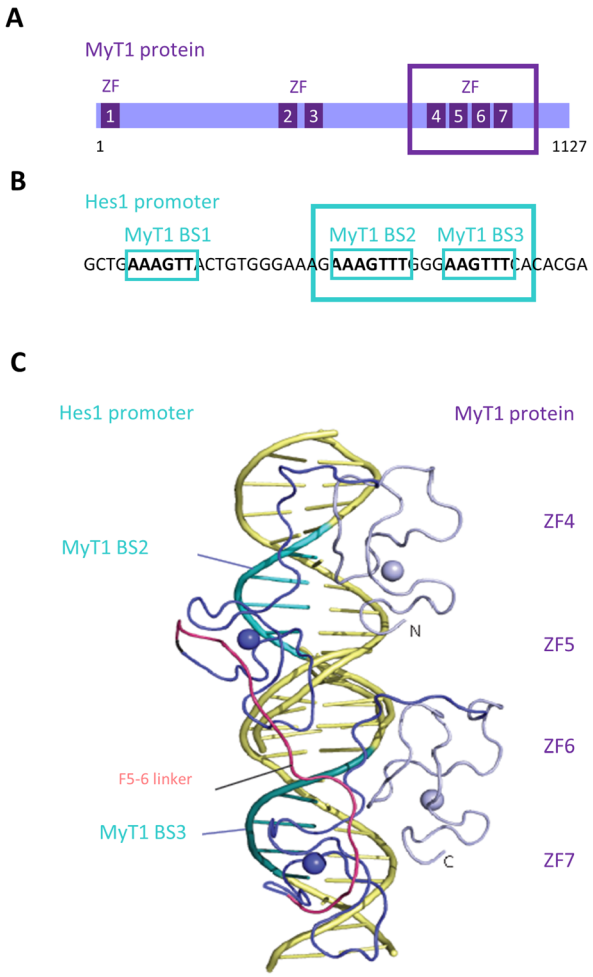

Figure 3.S 14 Structural modeling of MyT1:ZF4-ZF7 binding to Hes1 promoter.

(A) MyT1 protein sequence information. Zinc fingers (ZFs) 1–7 are indicated. ZF4-7 were used on the structural model. Numbers in black indicate the size of the protein in amino-acid residues. **(B)** Hes1 promoter sequence that contains the 3 MyT1 BSs. BS2 and BS3 were used on the structural model. **(C)** Structural model of two double zinc-fingers (ZF) of MyT1 protein binding to MyT1 BS2-3 on Hes1 promoter. The two double ZFs were linked by an artificial 19-residue sequence that is the same length as the real linker between F5 and F6.

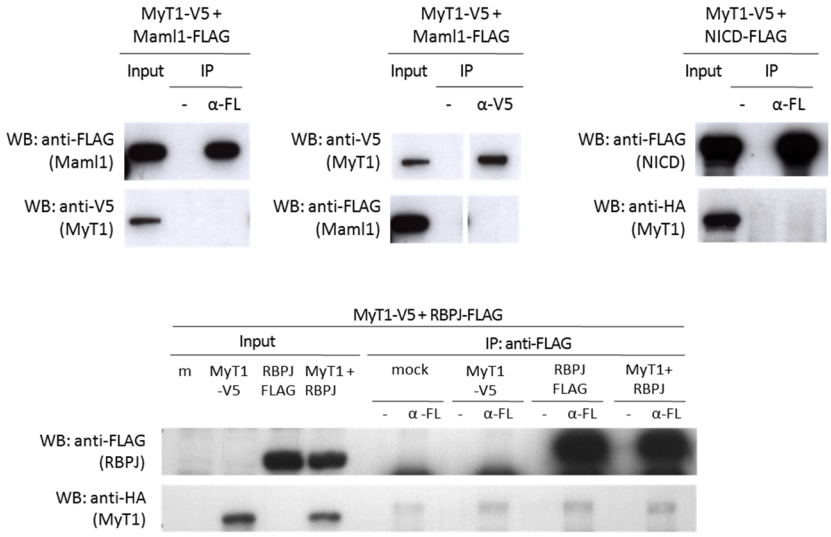

Figure 3.S 15 MyT1 co-immunoprecipitation experiments with members of the Notch transcriptional activator complex.

Co-immunoprecipitation experiments. HEK293T cells were transfected with expression vectors expressing tagged versions of MyT1, Maml1, NICD and/or RBPJ. Crude protein lysates were subjected to immunoprecipitation using an antibody against one of the tags (conditions with no antibody were used as controls). Crude protein lysates and immmunoprecipitated samples were analyzed by Western blot with an antibody against the second tag.

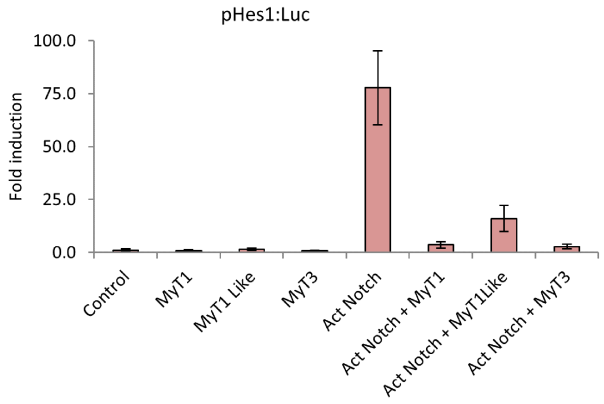

Figure 3.S 16 All MyT1 family members counteract Notch activity on Hes1 promoter.

Reporter gene assays in P19 cells co-transfected with control, MyT1, MyT1L, MyT3 and/or Act Notch expression vectors and a reporter construct expressing luciferase under the control of Hes1 proximal promoter region (wt). Mean ± SD.

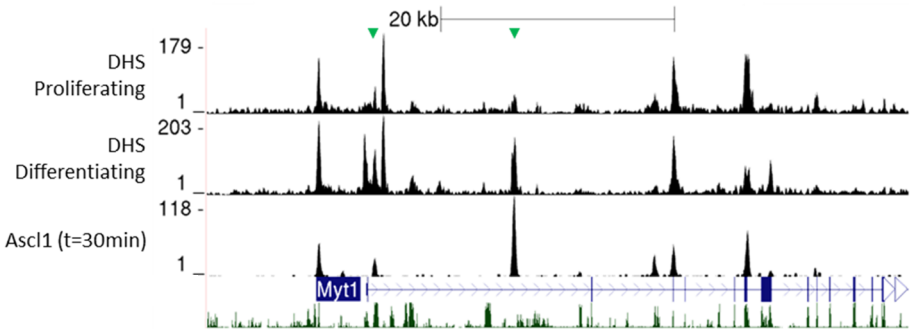

Figure 3.S 17 Ascl1 binding precedes chromatin opening on MyT1 proximal promoter.

Visual representation of ChIP-Seq and DNase-Seq enrichment profiles in the vicinity of MyT1 gene. Examples shown are of differentiation-induced DHSs localized at Ascl1 binding sites (green arrows). Green track, Mammal conservation by PhastCons.

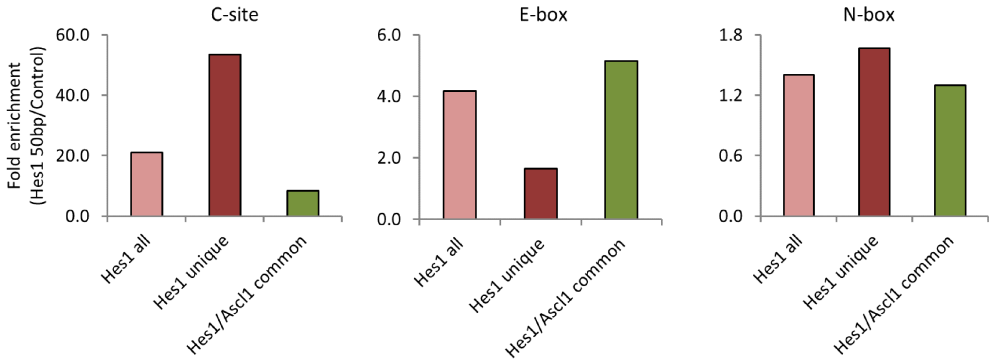

Figure 3.S 18 C-site is preferentially enriched at Hes1 unique and not at Hes1 and Ascl1 common BEs.

Fold enrichment of C-site, E-box and N-box motifs within a 50bp region centered at Hes1 peak summits as compared to control regions (regions of the same size located 2Kb upstream of Hes1 peak summits). Hes1 all, all Hes1 peaks. Hes1/Ascl1 common, Hes1 peaks overlapping with Ascl1 peaks. Hes1 unique, Hes1 peaks that are not overlapping with Ascl1 peaks. P (Hes1 and Ascl1 ChIP-Seq)<10^{-10}.

Table 3.S 1 MyT1 target genes associated with Gene ontology enriched terms.

Term	P Value	Fold Enr.	Genes
negative regulation of neuron differentiation	2.49E-07	10.54	HES1, HOXA2, NOTCH1, HES5, SOX2, PAX6, PBX1, DLL1, MEIS1, CD24A
regulation of transcription from RNA polymerase II promoter	1.63E-08	2.56	THRA, STAT5B, SOX2, TGFB3, PAX6, SOX4, NFIX, MXI1, TCF7L2, MEIS1, SOX8, FOS, HOXA1, HOXA2, MEIS2, HEY2, TRAK1, BCL6, RARA, SKIL, TOP2A, NR2F1, TXNIP, EGR1, ATF7IP, TRP53, KAT2B, JARID2, FOXJ1, RXRA, OTX1, RBL1, LMCD1, ARNTL, PKIA, GZF1, HES1, PKNOX2, NOTCH1, HES5, TGIF1, PBX1, HIVEP1, ID3, DNAJB5
nucleosome assembly	1.17E-04	5.19	TSPYL1, HIST4H4, HIST1H1E, HIST2H2BB, HIST1H1C, HIST1H1B, HIST1H1A, H2AFZ, HIST2H3C2, H2AFX, HIST1H4D, HIST2H4
regulation of cell motion	2.45E-04	3.90	ARHGAP5, CDKN1B, PDPN, GAB1, PAX6, MKKS, AMOT, RRAS, ABHD2, BCL6, NEXN, ADA
neuron fate commitment	2.12E-03	5.18	HES1, NOTCH1, HES5, SOX2, PAX6, DLL1, OLIG1
positive regulation of cell proliferation	5.43E-04	2.45	FGFR2, CRIP2, IL18, SOX2, STAT5B, PAX6, TLR4, CD24A, ADA, HES1, PRKCQ, NOTCH1, CDKN1A, ARHGAP5, CDKN1B, HEY2, TGIF1, BCL6, PBX1, RARA

Table 3.S 2 MyT1 target genes associated with Panther pathways categories.

Term	P Value	Fold Enr.	Genes
Notch signaling pathway	5.48E-03	3.62	HES1, NOTCH1, KAT2B, HEY1, HES5, HEY2, DLL1, LFNG
PDGF signaling pathway	1.32E-02	2.03	ERF, MRAS, STAT5B, MAPK10, FOS, PRKCQ, MAP3K4, ARHGAP5, GAB1, SRGAP3, RHOB, RRAS, RIT1, JAK2, PIK3R3
Angiogenesis	1.59E-02	1.87	WNT5A, FGFR2, FZD8, CRYAB, DLL1, MAPK10, FRZB, TCF7L2, FOS, EPHA4, PRKCQ, NOTCH1, RHOB, RRAS, PAK1, PIK3R3, WNT7A
TGF-β signaling pathway	9.76E-02	1.72	INHBB, FOS, FOXJ2, FOXJ1, MRAS, TGFB3, RRAS, RIT1, MAPK10, SKIL, FOXN3

Table 3.S 3 Regulation data referring to the 10 selected target genes oppositely regulated by MyT1 and Notch signaling, obtained from MyT1 GoF microarrays and RNA-Seq with Notch inhibitor.

Gene Symbol	Gene description	MyT1 GoF microarrays		Notch inhibitor RNASeq	
		Linear FC	P value	Linear FC	Q value
Aqp4	aquaporin 4	0.564	4.88E-03	0.267	3.01E-04
Btg2	B cell translocation gene 2, anti-proliferative	0.552	5.63E-03	0.176	1.76E-01
Hes1	hairy and enhancer of split 1 (Drosophila)	0.629	4.88E-03	0.523	5.23E-01
Hes5	hairy and enhancer of split 5 (Drosophila)	0.883	4.82E-02	0.031	3.07E-02
Egr1	early growth response 1	0.378	2.31E-04	0.680	6.80E-01
Id3	inhibitor of DNA binding 3	0.669	6.16E-03	0.595	5.95E-01
Lfng	LFNG O-fucosylpeptide 3-beta-N-acetylglucosaminyltransferase	0.677	5.63E-03	0.746	7.46E-01
Lmcd1	LIM and cysteine-rich domains 1	0.572	4.88E-03	0.402	4.02E-01
Notch1	notch 1	0.719	6.19E-03	0.350	3.50E-01
Dtx4	deltex 4 homolog (Drosophila)	0.790	1.36E-02	0.864	8.64E-01

References

Ahnfelt-Rønne, J., Hald, J., Bødker, A., Yassin, H., Serup, P., and Hecksher-Sørensen, J. (2007). Preservation of proliferating pancreatic progenitor cells by Delta-Notch signaling in the embryonic chicken pancreas. BMC Dev. Biol. *7*, 63.

Akazawa, C., Sasai, Y., Nakanishi, S., and Kageyama, R. (1992). Molecular characterization of a rat negative regulator with a basic helix-loop-helix structure predominantly expressed in the developing nervous system. J. Biol. Chem. *267*, 21879–21885.

Del Álamo, D., Rouault, H., and Schweisguth, F. (2011). Mechanism and significance of cis-inhibition in notch signalling. Curr. Biol. *21*, 40–47.

Ali, F.R., Cheng, K., Kirwan, P., Metcalfe, S., Livesey, F.J., Barker, R. a, and Philpott, A. (2014). The phosphorylation status of Ascl1 is a key determinant of neuronal differentiation and maturation *in vivo* and *in vitro*. Development *141*, 2216–2224.

Alifragis, P., Poortinga, G., Parkhurst, S.M., and Delidakis, C. (1997). A network of interacting transcriptional regulators involved in Drosophila neural fate specification revealed by the yeast two-hybrid system. Proc. Natl. Acad. Sci. U. S. A. *94*, 13099–13104.

Andersson, E.R., Sandberg, R., and Lendahl, U. (2011). Notch signaling: simplicity in design, versatility in function. Development *138*, 3593–3612.

Armstrong, R.C., Kim, J.G., and Hudson, L.D. (1995). Expression of myelin transcription factor I (MyTI), a "zinc-finger" DNA-binding protein, in developing oligodendrocytes. Glia *14*, 303–321.

Arnett, K.L., Hass, M., McArthur, D.G., Ilagan, M.X.G., Aster, J.C., Kopan, R., and Blacklow, S.C. (2010). Structural and mechanistic insights into cooperative assembly of dimeric Notch transcription complexes. Nat. Struct. Mol. Biol. *17*, 1312–1317.

Artavanis-Tsakonas, S., Rand, M.D. & Lake, R.J. (1999). Notch signaling: cell fate control and signal integration in development. Science (80-.). *284*, 770–776.

Bae, S., Bessho, Y., Hojo, M., and Kageyama, R. (2000). The bHLH gene Hes6, an inhibitor of Hes1, promotes neuronal differentiation. Development *127*, 2933–2943.

Bai, G., Sheng, N., Xie, Z., Bian, W., Yokota, Y., Benezra, R., Kageyama, R., Guillemot, F., and Jing, N. (2007). Id sustains Hes1 expression to inhibit precocious neurogenesis by releasing negative autoregulation of Hes1. Dev. Cell *13*, 283–297.

Basak, O., and Taylor, V. (2007). Identification of self-replicating multipotent progenitors in the embryonic nervous system by high Notch activity and Hes5 expression. Eur. J. Neurosci. *25*, 1006–1022.

Bellefroid, E.J., Bourguignon, C., Hollemann, T., Ma, Q., Anderson, D.J., Kintner, C., and Pieler, T. (1996). X-MyT1, a Xenopus C2HC-type zinc finger protein with a regulatory function in neuronal differentiation. Cell *87*, 1191–1202.

Berninger, B., Guillemot, F., and Götz, M. (2007). Directing neurotransmitter identity of neurones derived from expanded adult neural stem cells. Eur. J. Neurosci. *25*, 2581–2590.

Bertrand, N., Castro, D.S., and Guillemot, F. (2002). Proneural genes and the specification of neural cell types. Nat. Rev. Neurosci. *3*, 517–530.

Besold, A.N., Oluyadi, A. a., and Michel, S.L.J. (2013). Switching metal ion coordination and DNA recognition in a tandem CCHHC-type zinc finger peptide. Inorg. Chem. *52*, 4721–4728.

Besold, A.N., Amick, D.L., and Michel, S.L.J. (2014). A role for hydrogen bonding in DNA recognition by the non-classical CCHHC type zinc finger, NZF-1. Mol. Biosyst. *10*, 1753–1756.

Borggrefe, T., and Liefke, R. (2012). Fine-tuning of the intracellular canonical Notch signaling pathway © 2012 Landes Bioscience . Do not distribute . © 2012 Landes Bioscience . *11*, 264–276.

Borggrefe, T., and Oswald, F. (2009). The Notch signaling pathway: Transcriptional regulation at Notch target genes. Cell. Mol. Life Sci. *66*, 1631–1646.

Borromeo, M.D., Meredith, D.M., Castro, D.S., Chang, J.C., Tung, K.-C., Guillemot, F., and Johnson, J.E. (2014). A transcription factor network specifying inhibitory versus excitatory neurons in the dorsal spinal cord. Development 1–10.

Campos, L.S., Branco, T., and Henrique, D. (2001). Expression in the Developing Mouse Brain: Role in the Establishment of the Early Cortex. J. Neurosci. Res. *598*, 590–598.

Casarosa, S., Fode, C., Guillemot, F., Inserm, C., Louis, U., Cédex, I., and Strasbourg, C.U. De (1999). Mash1 regulates neurogenesis in the ventral telencephalon. *534*, 525–534.

Castella, P., Wagner, J. a, and Caudy, M. (1999). Regulation of hippocampal neuronal differentiation by the basic helix-loop-helix transcription factors HES-1 and MASH-1. J. Neurosci. Res. *56*, 229–240.

Castro, D.S., Skowronska-Krawczyk, D., Armant, O., Donaldson, I.J., Parras, C., Hunt, C., Critchley, J. a, Nguyen, L., Gossler, A., Göttgens, B., et al. (2006). Proneural bHLH and Brn proteins coregulate a neurogenic program through cooperative binding to a conserved DNA motif. Dev. Cell *11*, 831–844.

Castro, D.S., Martynoga, B., Parras, C., Ramesh, V., Pacary, E., Johnston, C., Drechsel, D., Lebel-Potter, M., Garcia, L.G., Hunt, C., et al. (2011). A novel function of the proneural factor Ascl1 in progenitor proliferation identified by genome-wide characterization of its targets. Genes Dev. *25*, 930–945.

Cave, J.W. (2011). Selective repression of Notch pathway target gene transcription. Dev. Biol. *360*, 123–131.

Cave, J.W., Loh, F., Surpris, J.W., Xia, L., and Caudy, M.A. (2005). A DNA Transcription Code for Cell-Specific Gene Activation by Notch Signaling. Curr. Biol. *15*, 94–104.

De Celis, J.F., and Bray, S. (1997). Feed-back mechanisms affecting Notch activation at the dorsoventral boundary in the Drosophila wing. Development *124*, 3241–3251.

Chi, Z., Zhang, J., Tokunaga, A., Harraz, M.M., Byrne, S.T., Dolinko, A., Xu, J., Blackshaw, S., Gaiano, N., Dawson, T.M., et al. (2012). Botch Promotes Neurogenesis by Antagonizing Notch. Dev. Cell *22*, 707–720.

Dai, Q., Andreu-agullo, C., Insolera, R., Wong, L.C., Shi, S., and Lai, E.C. (2013). BEND6 is a nuclear antagonist of Notch signaling during self- renewal of neural stem cells. *1902*, 1892–1902.

Englund, C., Fink, A., Lau, C., Pham, D., Daza, R. a M., Bulfone, A., Kowalczyk, T., and Hevner, R.F. (2005). Pax6, Tbr2, and Tbr1 are expressed sequentially by radial glia, intermediate progenitor cells, and postmitotic neurons in developing neocortex. J. Neurosci. *25*, 247–251.

Farah, M.H., Olson, J.M., Sucic, H.B., Hume, R.I., Tapscott, S.J., and Turner, D.L. (2000). Generation of neurons by transient expression of neural bHLH proteins in mammalian cells. Development *127*, 693–702.

Fior, R., and Henrique, D. (2009). "Notch-Off": A perspective on the termination of Notch signalling. Int. J. Dev. Biol. *53*, 1379–1384.

Fischer, A., and Gessler, M. (2007). Delta-Notch-and then? Protein interactions and proposed modes of repression by Hes and Hey bHLH factors. Nucleic Acids Res. *35*, 4583–4596.

Furriols, M., and Bray, S. (2001). A model Notch response element detects suppressor of hairless-dependent molecular switch. Curr. Biol. *11*, 60–64.

Gaiano, N., Nye, J.S., and Fishell, G. (2000). Radial glial identity is promoted by Notch1 signaling in the murine forebrain. Neuron *26*, 395–404.

Gamsjaeger, R., Swanton, M.K., Kobus, F.J., Lehtomaki, E., Lowry, J. a, Kwan, A.H., Matthews, J.M., and Mackay, J.P. (2008). Structural and biophysical analysis of the DNA binding properties of myelin transcription factor 1. J. Biol. Chem. *283*, 5158–5167.

Gamsjaeger, R., O'Connell, M.R., Cubeddu, L., Shepherd, N.E., Lowry, J. a, Kwan, A.H., Vandevenne, M., Swanton, M.K., Matthews, J.M., and Mackay, J.P. (2013). A structural analysis of DNA binding by myelin transcription factor 1 double zinc fingers. J. Biol. Chem. *288*, 35180–35191.

Gao, F., Zhang, Q., Zheng, M.-H., Liu, H.-L., Hu, Y.-Y., Zhang, P., Zhang, Z.-P., Qin, H.-Y., Feng, L., Wang, L., et al. (2009). Transcription factor RBP-J-mediated signaling represses the differentiation of neural stem cells into intermediate neural progenitors. Mol. Cell. Neurosci. *40*, 442–450.

Giagtzoglou, N. (2003). Two modes of recruitment of E(spl) repressors onto target genes. Development *130*, 259–270.

Giagtzoglou, N., Koumbanakis, K. a., Fullard, J., Zarifi, I., and Delidakis, C. (2005). Role of the Sc C terminus in transcriptional activation and E(spl) repressor recruitment. J. Biol. Chem. *280*, 1299–1305.

Gohlke, J.M., Armant, O., Parham, F.M., Smith, M. V, Zimmer, C., Castro, D.S., Nguyen, L., Parker, J.S., Gradwohl, G., Portier, C.J., et al. (2008). Characterization of the proneural gene regulatory network during mouse telencephalon development. BMC Biol. *6*, 15.

Gómez-López, S., Wiskow, O., Favaro, R., Nicolis, S.K., Price, D.J., Pollard, S.M., and Smith, A. (2011). Sox2 and Pax6 maintain the proliferative and developmental potential of gliogenic neural stem cells *in vitro*. Glia *59*, 1588–1599.

Gu, G., Wells, J.M., Dombkowski, D., Preffer, F., Aronow, B., and Melton, D. a (2004). Global expression analysis of gene regulatory pathways during endocrine pancreatic development. Development *131*, 165–179.

Guillemot, F., and Joyner, a L. (1993). Dynamic expression of the murine Achaete-Scute homologue Mash-1 in the developing nervous system. Mech. Dev. *42*, 171–185.

Hamada, Y., Kadokawa, Y., Okabe, M., Ikawa, M., Coleman, J.R., and Tsujimoto, Y. (1999). Mutation in ankyrin repeats of the mouse Notch2 gene induces early embryonic lethality. Development *126*, 3415–3424.

Hashimoto-Torii, K., Torii, M., Sarkisian, M.R., Bartley, C.M., Shen, J., Radtke, F., Gridley, T., Šestan, N., and Rakic, P. (2008). Interaction between Reelin and Notch Signaling Regulates Neuronal Migration in the Cerebral Cortex. Neuron *60*, 273–284.

Higuchi, M., Kiyama, H., Hayakawa, T., Hamada, Y., and Tsujimoto, Y. (1995). Differential expression of Notch1 and Notch2 in developing and adult mouse brain. Brain Res. Mol. Brain Res. *29*, 263–272.

Hinz, U., Giebel, B., and Campos-Ortega, J. a. (1994). The basic-helix-loop-helix domain of Drosophila lethal of scute protein is sufficient for proneural function and activates neurogenic genes. Cell *76*, 77–87.

Hoeck, J.D., Jandke, A., Blake, S.M., Nye, E., Spencer-Dene, B., Brandner, S., and Behrens, A. (2010). Fbw7 controls neural stem cell differentiation and progenitor apoptosis via Notch and c-Jun. Nat. Neurosci. *13*, 1365–1372.

Hori, K., Fostier, M., Ito, M., Fuwa, T.J., Go, M.J., Okano, H., Baron, M., and Matsuno, K. (2004). Drosophila deltex mediates suppressor of Hairless-independent and late-endosomal activation of Notch signaling. Development *131*, 5527–5537.

Hu, J., Ho, A.L., Yuan, L., Hu, B., Hua, S., Sarah, S., and Zhang, J. (2013). Neutralization of terminal differentiation in gliomagenesis.

Hudson, L.D., Romm, E., Berndt, J.A., and Nielsen, J. a (2011). A tool for examining the role of the zinc finger myelin transcription factor 1 (Myt1) in neural development: Myt1 knock-in mice. Transgenic Res. *20*, 951–961.

Imayoshi, I., and Kageyama, R. (2014a). bHLH Factors in Self-Renewal, Multipotency, and Fate Choice of Neural Progenitor Cells. Neuron *82*, 9–23.

Imayoshi, I., and Kageyama, R. (2014b). Oscillatory control of bHLH factors in neural progenitors. Trends Neurosci. 1–8.

Imayoshi, I., Isomura, A., Harima, Y., Kori, H., Miyachi, H., Fujiwara, T., Ishidate, F., and Kageyama, R. (2013). Oscillatory Control of Factors Determining Multipotency and Fate in Mouse Neural Progenitors.

Irvin, D.K., Zurcher, S.D., Nguyen, T., Weinmaster, G., and Kornblum, H.I. (2001). Expression patterns of Notch1, Notch2, and Notch3 suggest multiple functional roles for the Notch-DSL signaling system during brain development. J. Comp. Neurol. *436*, 167–181.

Ishibashi, M., Ang, S.L., Shiota, K., Nakanishi, S., Kageyama, R., and Guillemot, F. (1995). Targeted disruption of mammalian hairy and Enhancer of split homolog-1 (HES-1) leads to up-regulation of neural helix-loop-helix factors, premature neurogenesis, and severe neural tube defects. Genes Dev. *9*, 3136–3148.

Ishitani, T., Hirao, T., Suzuki, M., Isoda, M., Ishitani, S., Harigaya, K., Kitagawa, M., Matsumoto, K., and Itoh, M. (2010). Nemo-like kinase suppresses Notch signalling by interfering with formation of the Notch active transcriptional complex. Nat. Cell Biol. *12*, 278–285.

Jarriault, S., Brou, C., Logeat, F., Schroeter, E.H., Kopan, R., and Israel, A. (1995). Signalling downstream of activated mammalian Notch. Nature *377*, 355–358.

Jennings, B.H., Tyler, D.M., and Bray, S.J. (1999). Target specificities of Drosophila enhancer of split basic helix-loop-helix proteins. Mol. Cell. Biol. *19*, 4600–4610.

Jiang, Y., Yu, V.C., Buchholz, F., O'Connell, S., Rhodes, S.J., Candeloro, C., Xia, Y.R., Lusis, a J., and Rosenfeld, M.G. (1996). A novel family of Cys-Cys, His-Cys zinc finger transcription factors expressed in developing nervous system and pituitary gland. J. Biol. Chem. *271*, 10723–10730.

Kageyama, R., Ohtsuka, T., and Kobayashi, T. (2007). The Hes gene family: repressors and oscillators that orchestrate embryogenesis. Development *134*, 1243–1251.

Kageyama, R., Ohtsuka, T., Shimojo, H., and Imayoshi, I. (2008). Dynamic Notch signaling in neural progenitor cells and a revised view of lateral inhibition. Nat. Neurosci. *11*, 1247–1251.

Kageyama, R., Ohtsuka, T., Shimojo, H., and Imayoshi, I. (2009). Dynamic regulation of Notch signaling in neural progenitor cells. Curr. Opin. Cell Biol. *21*, 733–740.

Kaltezioti, V., Kouroupi, G., Oikonomaki, M., Mantouvalou, E., Stergiopoulos, A., Charonis, A., Rohrer, H., Matsas, R., and Politis, P.K. (2010). Prox1 regulates the Notch1-mediated inhibition of neurogenesis. PLoS Biol. *8*.

Kameyama, T., Matsushita, F., Kadokawa, Y., and Marunouchi, T. (2011). Myt/NZF family transcription factors regulate neuronal differentiation of P19 cells. Neurosci. Lett. *497*, 74–79.

Kawaguchi, A., Ikawa, T., Kasukawa, T., Ueda, H.R., Kurimoto, K., Saitou, M., and Matsuzaki, F. (2008). Single-cell gene profiling defines differential progenitor subclasses in mammalian neurogenesis. Development *135*, 3113–3124.

Kim, J.I.N.G., and Hudson, L.D. (1992). Novel Member of the Zinc Finger Superfamily : A C2-HC Finger That Recognizes a Glia-Specific Gene. *12*, 5632–5639.

Kim, J.G., Armstrong, R.C., v Agoston, D., Robinsky, a, Wiese, C., Nagle, J., and Hudson, L.D. (1997). Myelin transcription factor 1 (Myt1) of the oligodendrocyte lineage, along with a closely related CCHC zinc finger, is expressed in developing neurons in the mammalian central nervous system. J. Neurosci. Res. *50*, 272–290.

Kleinmann, E., Lay, A.G. Le, Kastner, P., Chan, S., Development, T., Kleinmann, E., Lay, A.G. Le, Sellars, M., Kastner, P., and Chan, S. (2008). Ikaros Represses the Transcriptional Response to Notch Signaling in T-Cell Development Ikaros Represses the Transcriptional Response to Notch Signaling in.

Kopan, R., and Ilagan, M.X.G. (2009). The Canonical Notch Signaling Pathway: Unfolding the Activation Mechanism. Cell *137*, 216–233.

Krebs, L.T., Xue, Y., Norton, C.R., Sundberg, J.P., Beatus, P., Lendahl, U., Joutel, A., and Gridley, T. (2003). Characterization of Notch3-Deficient Mice: Normal Embryonic Development and Absence of Genetic Interactions with a Notch1 Mutation. Genesis *37*, 139–143.

De la Pompa, J.L., Wakeham, a, Correia, K.M., Samper, E., Brown, S., Aguilera, R.J., Nakano, T., Honjo, T., Mak, T.W., Rossant, J., et al. (1997). Conservation of the Notch signalling pathway in mammalian neurogenesis. Development *124*, 1139–1148.

Lamar, E., Deblandre, G., Wettstein, D., Gawantka, V., Pollet, N., Niehrs, C., and Kintner, C. (2001). Nrarp is a novel intracellular component of the Notch signaling pathway. Genes Dev. *15*, 1885–1899.

Lanz, T.A., Hosley, J.D., Adams, W.J., and Merchant, K.M. (2004). Studies of A $^{N}_{L}$ Pharmacodynamics in the Brain , Cerebrospinal Fluid , and Plasma in Young (Plaque-Free) Tg2576 Mice Using dibenzo [b , d] azepin-7-yl] - L -alaninamide (LY-411575). *309*, 49–55.

Lin, C.H., and Lee, E.H.Y. (2012). JNK1 inhibits GluR1 expression and GluR1-mediated calcium influx through phosphorylation and stabilization of Hes-1. J. Neurosci. *32*, 1826–1846.

Louvi, A., and Artavanis-Tsakonas, S. (2006). Notch signalling in vertebrate neural development. Nat. Rev. Neurosci. *7*, 93–102.

Martynoga, B., Mateo, J.L., Zhou, B., Andersen, J., Achimastou, A., Urbán, N., van den Berg, D., Georgopoulou, D., Hadjur, S., Wittbrodt, J., et al. (2013). Epigenomic enhancer annotation reveals a key role for NFIX in neural stem cell quiescence. Genes Dev. *27*, 1769–1786.

Matsumoto, A., Onoyama, I., Sunabori, T., Kageyama, R., Okano, H., and Nakayama, K.I. (2011). Fbxw7-dependent degradation of notch is required for control of “Stemness” and neuronal-glial differentiation in neural stem cells. J. Biol. Chem. *286*, 13754–13764.

Matsuno, K., Diederich, R.J., Go, M.J., Blaumueller, C.M., and Artavanis-Tsakonas, S. (1995). Deltex acts as a positive regulator of Notch signaling through interactions with the Notch ankyrin repeats. Development *121*, 2633–2644.

Matsushita, F., Kameyama, T., and Marunouchi, T. (2002). NZF-2b is a novel predominant form of mouse NZF-2/MyT1, expressed in differentiated neurons especially at higher levels in newly generated ones. Mech. Dev. *118*, 209–213.

Matsushita, F., Kameyama, T., Kadokawac, Y., and Marunouchi, T. (2013). MatsushitaDevDyn2013_Myt family.

McGill, M. a., and McGlade, C.J. (2003). Mammalian Numb proteins promote Notch1 receptor ubiquitination and degradation of the Notch1 intracellular domain. J. Biol. Chem. *278*, 23196–23203.

McGill, M. a., Dho, S.E., Weinmaster, G., and McGlade, C.J. (2009). Numb regulates post-endocytic trafficking and degradation of notch1. J. Biol. Chem. *284*, 26427–26438.

Miller, A.C., Lyons, E.L., and Herman, T.G. (2009). cis-Inhibition of Notch by Endogenous Delta Biases the Outcome of Lateral Inhibition. Curr. Biol. *19*, 1378–1383.

Mizutani, K., Yoon, K., Dang, L., Tokunaga, A., and Gaiano, N. (2007). Differential Notch signalling distinguishes neural stem cells from intermediate progenitors. Nature *449*, 351–355.

Moloney, D.J., Panin, V.M., Johnston, S.H., Chen, J., Shao, L., Wilson, R., Wang, Y., Stanley, P., Irvine, K.D., Haltiwanger, R.S., et al. (2000). Fringe is a glycosyltransferase that modifies Notch. Nature *406*, 369–375.

Nakada, Y., Hunsaker, T.L., Henke, R.M., and Johnson, J.E. (2004). Distinct domains within Mash1 and Math1 are required for function in neuronal differentiation versus neuronal cell-type specification. Development *131*, 1319–1330.

Nakao, K., and Campos-Ortega, J. a. (1996). Persistent expression of genes of the enhancer of split complex suppresses neural development in Drosophila. Neuron *16*, 275–286.

Nam, Y., Sliz, P., Song, L., Aster, J.C., and Blacklow, S.C. (2006). Structural basis for cooperativity in recruitment of MAML coactivators to Notch transcription complexes. Cell *124*, 973–983.

Nam, Y., Sliz, P., Pear, W.S., Aster, J.C., and Blacklow, S.C. (2007). Cooperative assembly of higher-order Notch complexes functions as a switch to induce transcription. Proc. Natl. Acad. Sci. U. S. A. *104*, 2103–2108.

Nelson, B.R., Hodge, R.D., Bedogni, F., and Hevner, R.F. (2013). Dynamic Interactions between Intermediate Neurogenic Progenitors and Radial Glia in Embryonic Mouse Neocortex: Potential Role in Dll1-Notch Signaling. J. Neurosci. *33*, 9122–9139.

Neves, A., English, K., and Priess, J.R. (2007). Notch-GATA synergy promotes endoderm-specific expression of ref-1 in C. elegans. Development *134*, 4459–4468.

Nielsen, J. a, Berndt, J.A., Hudson, L.D., and Armstrong, R.C. (2004). Myelin transcription factor 1 (Myt1) modulates the proliferation and differentiation of oligodendrocyte lineage cells. Mol. Cell. Neurosci. *25*, 111–123.

Oellers, N., Dehio, M., and Knust, E. (1994). bHLH proteins encoded by the Enhancer of split complex of Drosophila negatively interfere with transcriptional activation mediated by proneural genes. MGG Mol. Gen. Genet. *244*, 465–473.

Pang, Z.P., Yang, N., Vierbuchen, T., Ostermeier, A., Fuentes, D.R., Yang, T.Q., Citri, A., Sebastiano, V., Marro, S., Südhof, T.C., et al. (2011). Induction of human neuronal cells by defined transcription factors. Nature *476*, 220–223.

Pfisterer, U., Kirkeby, A., Torper, O., Wood, J., Nelander, J., Dufour, A., Björklund, A., Lindvall, O., Jakobsson, J., and Parmar, M. (2011). Direct conversion of human fibroblasts to dopaminergic neurons. Proc. Natl. Acad. Sci. U. S. A. *108*, 10343–10348.

Pierfelice, T., Alberi, L., and Gaiano, N. (2011). Notch in the vertebrate nervous system: an old dog with new tricks. Neuron *69*, 840–855.

Piper, M., Barry, G., Hawkins, J., Mason, S., Lindwall, C., Little, E., Sarkar, A., Smith, A.G., Moldrich, R.X., Boyle, G.M., et al. (2010). NFIA controls telencephalic progenitor cell differentiation through repression of the Notch effector Hes1. J. Neurosci. *30*, 9127–9139.

Quan, X.-J., Denayer, T., Yan, J., Jafar-Nejad, H., Philippi, A., Lichtarge, O., Vleminckx, K., and Hassan, B. a (2004). Evolution of neural precursor selection: functional divergence of proneural proteins. Development *131*, 1679–1689.

Raposo, A.A.S.F., Vasconcelos, F.F., Drechsel, D., Marie, C., and Johnston, C. (2015). Ascl1 Coordinately Regulates Gene Expression and the Chromatin Landscape during Neurogenesis Article Ascl1 Coordinately Regulates Gene Expression and the Chromatin Landscape during Neurogenesis. Cell Rep. 1544–1556.

Redmond, L., Oh, S.R., Hicks, C., Weinmaster, G., and Ghosh, a (2000). Nuclear Notch1 signaling and the regulation of dendritic development. Nat. Neurosci. *3*, 30–40.

Romm, E., Nielsen, J. a, Kim, J.G., and Hudson, L.D. (2005). Myt1 family recruits histone deacetylase to regulate neural transcription. J. Neurochem. *93*, 1444–1453.

Ross, S.E., Greenberg, M.E., and Stiles, C.D. (2003). Basic helix-loop-helix factors in cortical development. Neuron *39*, 13–25.

Ruzinova, M.B., and Benezra, R. (2003). Id proteins in development, cell cycle and cancer. Trends Cell Biol. *13*, 410–418.

Sasai, Y., Kageyama, R., Tagawa, Y., Shigemoto, R., and Nakanishi, S. (1992). Two mammalian helix-loop-helix factors structurally related to Drosophila hairy and Enhancer of split. Genes Dev. *6*, 2620–2634.

Schneider, M.L., Turner, D.L., and Vetter, M.L. (2001). Notch signaling can inhibit Xath5 function in the neural plate and developing retina. Mol. Cell. Neurosci. *18*, 458–472.

Sestan, N., Artavanis-Tsakonas, S., and Rakic, P. (1999). Contact-dependent inhibition of cortical neurite growth mediated by notch signaling. Science *286*, 741–746.

Shimizu, T., Nakazawa, M., Kani, S., Bae, Y.-K., Shimizu, T., Kageyama, R., and Hibi, M. (2010). Zinc finger genes Fezf1 and Fezf2 control neuronal differentiation by repressing Hes5 expression in the forebrain. Development *137*, 1875–1885.

Shimojo, H., Ohtsuka, T., and Kageyama, R. (2008). Oscillations in notch signaling regulate maintenance of neural progenitors. Neuron *58*, 52–64.

Sim, F.J., Zhao, C., Penderis, J., and Franklin, R.J.M. (2002). The age-related decrease in CNS remyelination efficiency is attributable to an impairment of both oligodendrocyte progenitor recruitment and differentiation. J. Neurosci. *22*, 2451–2459.

Sprinzak, D., Lakhanpal, A., Lebon, L., Santat, L. a, Fontes, M.E., Anderson, G. a, Garcia-Ojalvo, J., and Elowitz, M.B. (2010). Cis-interactions between Notch and Delta generate mutually exclusive signalling states. Nature *465*, 86–90.

Tiberi, L., van den Ameele, J., Dimidschstein, J., Piccirilli, J., Gall, D., Herpoel, A., Bilheu, A., Bonnefont, J., Iacovino, M., Kyba, M., et al. (2012). BCL6 controls neurogenesis through Sirt1-dependent epigenetic repression of selective Notch targets. Nat. Neurosci. *15*, 1627–1635.

Vasileva, E. a, Shuvalov, O.U., Garabadgiu, a V, Melino, G., and Barlev, N. a (2015). Genome-editing tools for stem cell biology. Cell Death Dis. *6*, e1831.

Vierbuchen, T., Ostermeier, A., Pang, Z.P., Kokubu, Y., Südhof, T.C., and Wernig, M. (2010). Direct conversion of fibroblasts to functional neurons by defined factors. Nature *463*, 1035–1041.

Wang, S., Zhang, J., Zhao, A., Hipkens, S., Magnuson, M. a., and Gu, G. (2007). Loss of Myt1 function partially compromises endocrine islet cell differentiation and pancreatic physiological function in the mouse. Mech. Dev. *124*, 898–910.

Wang, S., Hecksher-Sorensen, J., Xu, Y., Zhao, A., Dor, Y., Rosenberg, L., Serup, P., and Gu, G. (2008). Myt1 and Ngn3 form a feed-forward expression loop to promote endocrine islet cell differentiation. Dev. Biol. *317*, 531–540.

Webb, A., Pollina, E., Vierbuchen, T., Urbán, N., Ucar, D., Leeman, D., Martynoga, B., Sewak, M., Rando, T., Guillemot, F., et al. (2013). FOXO3 shares common targets with ASCL1 genome-wide and inhibits ASCL1-dependent neurogenesis. Cell Rep. *4*, 477–491.

Wrathall, J.R., Li, W., and Hudson, L.D. (1998). Myelin gene expression after experimental contusive spinal cord injury. J. Neurosci. *18*, 8780–8793.

Yang, H., Wang, H., Shivalila, C.S., Cheng, A.W., Shi, L., and Jaenisch, R. (2013). One-step generation of mice carrying reporter and conditional alleles by CRISPR/cas-mediated genome engineering. Cell *154*, 1370–1379.

Yee, K.S., and Yu, V.C. (1998). Isolation and characterization of a novel member of the neural zinc finger factor/myelin transcription factor family with transcriptional repression activity. J. Biol. Chem. *273*, 5366–5374.

Yokoyama, A., Igarashi, K., Sato, T., Takagi, K., Otsuka I, M., Shishido, Y., Baba, T., Ito, R., Kanno, J., Ohkawa, Y., et al. (2014). Identification of myelin transcription factor 1 (MyT1) as a subunit of the neural cell type-specific lysine-specific demethylase 1 (LSD1) complex. J. Biol. Chem. *289*, 18152–18162.

Yoo, A.S., Sun, A.X., Li, L., Shcheglovitov, A., Portmann, T., Li, Y., Lee-Messer, C., Dolmetsch, R.E., Tsien, R.W., and Crabtree, G.R. (2011). MicroRNA-mediated conversion of human fibroblasts to neurons. Nature *476*, 228–231.

Yoon, K.J., Koo, B.K., Im, S.K., Jeong, H.W., Ghim, J., Kwon, M.C., Moon, J.S., Miyata, T., and Kong, Y.Y. (2008). Mind Bomb 1-Expressing Intermediate Progenitors Generate Notch Signaling to Maintain Radial Glial Cells. Neuron *58*, 519–531.

Yoshiura, S., Ohtsuka, T., Takenaka, Y., Nagahara, H., Yoshikawa, K., and Kageyama, R. (2007). Ultradian oscillations of Stat, Smad, and Hes1 expression in response to serum. Proc. Natl. Acad. Sci. U. S. A. *104*, 11292–11297.

Acknowledgements

I would like to acknowledge François Guillemot for receiving me for the initial four months of my PhD at his laboratory at the National Institute for Medical Research (London, UK) and Daniela Drechsel, Ben Martynoga and Vydia Ramesh for teaching me while I was there.

I would like to thank Vera Teixeira for strong technical support on molecular biology and for performing the *in situ* hybridization and Immunohistochemical analyses on mouse embryonic telencephalon (Figure 3. 4B-C, Figure 3. 6E). I would like to thank Alexandre Raposo for ChIP-Seq datasets pre-processing (alignment with the genome, peak calling) and subsequent analyses (Figure 3. 11A, Figure 3. 12, Figure 3. 16C, Figure 3.S 5B-D). I would like to thank Cátia Laranjeira for providing Notch inhibitor RNA-Seq and anti-RBPJ ChIP-Seq datasets (Figure 3.S 7) and Pedro Rosmaninho for providing pCAG-Zeb1-IRES-GFP and for technical advice on Chipster, DAVID and virus production.

I would like to thank Alessandro Sessa and Vania Broccoli for performing the *in utero* electroporation experiments (Figure 3. 8, Figure 3. 15).

I would like to thank Joel Mackay for the structural modeling (Figure 3.S 14).

I would like to thank Jane Johnson for providing pSP73 RBPJ plasmid and guinea pig anti-Ascl1 antibody, Guoqiang Gu for the rabbit anti-MyT1 antibody, Lynn Hudson for pMycMyT1-7ZF-IRES/Red and pCRII-MyT1 plasmids, Ryoichiro Kageyama for pME-FNIC Act Notch, pHes1:Luc and pHes5:Luc plasmids, Jonas Muhr for pCAG-Sox2-IRES-GFP plasmid, Hua Han for pCMX-VP16-RBPJ, pFLAG-CMV2-RBPJ plasmids and Lizi Wu for pFLAG-CMV2-Maml1 plasmid and Debbie Van der Berg for Ascl1-V5 TetON FUW, pPyCAG-MCS-V5 and pPyCAG-MCS-FLAG plasmids and for technical advice on immunoprecipitation.

I would like to thank Carlos Parras for providing access to microarrays datasets on telencephalon of Ascl1 knock-out and wild-type mice, Domingos Henrique, Evgenia Bekman and Elsa Abranches for Hes1 and Hes5 plasmids for *in situ* probe production, EGF, bFGF and LY-411575 aliquots.

I would like to thank Pedro Prudêncio for purified rabbit IgGs and technical advice on immunoprecipitation and Western blot, Gaston Guilgur for technical advice on RNA extraction, expression RT-qPCR and subcloning, João Mata for technical advice on site-directed mutagenesis and immunofluorescence, Ana Casaca for technical advice on EMSA, Sónia Rosa for competent DH5α bacteria production and standard lab solutions preparation.

I would like to thank Abdul Sesay and the NIMR high-throughput sequencing facility for ChIP-Seq library preparation and sequencing and João Sobral and the IGC gene expression sequencing facility for microarray RNA processing and microarray hybridization.

I was supported by a doctoral fellowship (SFRH/BD/51178/2010) from Fundação para a Ciência e a Tecnologia (FCT) and by Instituto Gulbenkian de Ciência.

Chapter 4 – **General Discussion**

During embryonic development, the fertilized egg divides and progressively differentiates into hundreds of specialized cell types that compose a multicellular organism. Understanding how progenitor cells, despite of having the same genome, differentiate into different cell types is one of the major challenges in developmental biology. Cell differentiation programs have been associated with extensive and precise changes in gene expression that are, ultimately, controlled by the activity of lineage-specific transcription factors. Therefore, studying the role and the molecular mechanisms underlying the activity of these TFs is a crucial step towards the understanding of how changes in cell identity are established during embryonic development.

Contribution

This thesis aimed at gaining new insights into the molecular mechanisms of TFs activity and the interplay between their transcriptional networks during vertebrate neurogenesis. We used adherent cultures of NS cells and a cellular model of neurogenesis as major "substrates" for TF binding, chromatin accessibility and gene expression genome-wide analyses. At instances, we validated our findings with *in vivo* observations produced from the telencephalon of mouse embryos.

The first part of the work describes the mutual interactions between the transcription factor Ascl1, a master regulator of neurogenesis in vertebrates, and the evolving chromatin landscape in a cellular model of neurogenesis. This study identified a novel function of Ascl1 in promoting chromatin accessibility and provides a mechanism that will contribute to the temporal specificity of expression of its target genes.

The second part of the work investigates the function of one Ascl1 target gene, the zinc-finger transcription factor MyT1. We found that MyT1 promotes neurogenesis by relieving the inhibitory activity of Notch signaling, namely by blocking Hes1 gene

expression, a key regulatory event at the onset of neuronal differentiation. Importantly, the activation of MyT1 by Ascl1 defines an important regulatory step whereby Ascl1 efficiently counteracts Notch signaling in a cell-autonomous manner. Overall, the studies presented in this thesis contribute to a better understanding of the molecular mechanisms that control the initial stages of the neurogenic process.

Perspectives

Embryonic brain tissue is very complex, being composed of a multitude of cell types at distinct developmental stages and, therefore, represents a very heterogeneous source of material unsuitable for genome-wide studies. For that reason, we used NS cell cultures that are clonal populations and are homogeneous in their composition in the sense they are composed of only one cell type at a specific developmental stage. However, despite of this apparent homogeneity, even clonal cell populations exhibit significant variability in gene expression once individual cells are considered (Chang et al. 2008; Huang 2009). Importantly, this transcriptional heterogeneity has been shown to have a functional role in stem cells during cell fate decisions and has been particularly well studied in hematopoietic and embryonic stem cells. In these lineages the transcriptional heterogeneity is derived from two major sources. In one hand, gene expression is itself an inherently noisy process. This process is made up of a network of stochastic and largely promiscuous individual interactions, at all levels from TFs to enhancers. Therefore, the accumulation of variations at each step may result in remarkable differences between individual cells within a population at a given time-point (Pina et al. 2012). On the other hand, individual stem cells exhibit highly dynamic expression of multiple lineage-specific TFs and associated transcriptional networks (Chang et al. 2008). Therefore, within a stem cell population there are a multitude of interconvertible transcriptional states. These multitude of

transcriptional states have been shown to have significant biological functionality in the reversible stochastic priming of multi/pluripotent cells during cell fate commitment (Enver et al. 2009; Chang et al. 2008). Thus, the multi- or pluripotent state has been conceptualized as an ensemble of transcriptional states that converge overtime to a metastable attractor state, and cell differentiation as the transition between two attractor states. Transcriptional heterogeneity enhances the probability of this transition and, therefore, the expression of lineage-specific TFs is regarded as a probabilistic rather than a deterministic event during cell fate decisions (Enver et al. 2009; Eldar & Elowitz 2010). Analysis of large pools of cells provides a population average that can mask minor yet important trends in gene expression by groups of cells, for instance, bimodality of gene expression (i.e., the existence of subpopulations) and heterogeneity in gene expression levels. Understanding the temporal dynamics of gene expression and TF activity at the single-cell level is, therefore, important for the comprehension of how cell fate decisions are molecularly established. FACS analysis coupled with whole-transcript single-cell RNA-Seq allowed for an unprecedented characterization of the transcriptional heterogeneity in stem cell populations (Chang et al. 2008). Although recent improvements in the ChIP protocols allow to scale down these experiments to hundreds of cells, technological improvement is still required to map TF binding genome-wide at the single cell level. In neural stem cells, one of the most paradigmatic examples of dynamic co-expression of lineage-specific TFs is the oscillatory expression of Hes1, Ascl1 and Olig2 (Figure 4. 1). These oscillations have been shown to be asynchronous between cells and, thus, at a given time-point, the expression of these TFs and of, possibly, their associated transcriptional networks, will be different across individual cells. This heterogeneity can be appreciated by the salt-and-pepper patterns of expression of these TFs both in cultured cells and in the germinal layers of the developing embryo (Imayoshi et al. 2013; Imayoshi &

Kageyama 2014). In particular, MyT1 expression is low but heterogeneous within the NS cell cultures (Figure 3. 10A), suggesting that MyT1 expression may also be dynamic within these cells. Understanding how MyT1 levels change, the relationship between MyT1, Ascl1, and Hes1 expression dynamics in NSCs and how they affect the metastable stem cell state and the likelihood of neuronal differentiation, will be important for a better understanding of the NSC behavior and the requirements for neuronal differentiation.

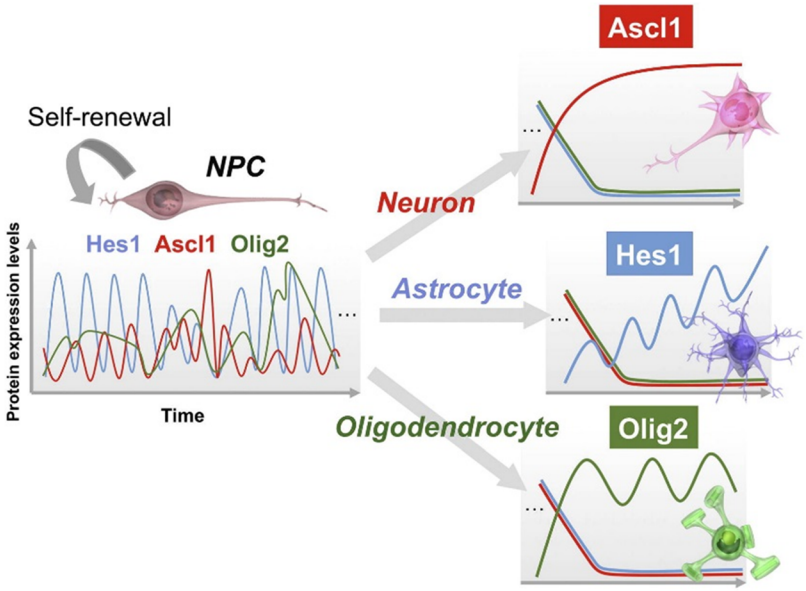

Figure 4. 1 Expression dynamics of bHLH factors in NSC multipotency and cell fate choice.

The lineage-specific transcription factors Ascl1, Hes1 and Olig2 are dynamically co-expressed in multipotent NSCs where they exhibit an oscillatory mode of expression. During differentiation, the expression of one of this TFs becomes sustained while the other two are downregulated. Ascl1, Hes1 or Olig2 sustained expression results in the differentiation of NSCs into neurons, astrocytes or oligodendrocytes, respectively. Figure from (Imayoshi & Kageyama 2014).

Current functional genomics studies of neurogenesis mainly focus on evolutionary conservation, mapping of TF binding sites and histone modifications by ChIP-Seq, or mapping of regulatory potential by, for example, DNAse I profiling. These approaches produce linear maps of genomic information and ignore the tridimensional structure

of the DNA. Specifically, in these studies it is difficult to ascertain which gene or genes are regulated by a given enhancer and nearest gene annotation is not always a very accurate association. Chromosome conformation capture-based (3C) methods (3C, 4C, 5C, Hi-C) identify chromosomal loops mediated by multiple long range protein-protein interactions and reveal interactions between enhancers and promoters (de Wit & de Laat 2012). Therefore, the integration of these approaches with high-resolution 3C-based genomic methods might facilitate the understanding of the wiring of the genes with regulatory sequences in the genome. It is important to note, however, that 3C-based methods fail to detect cell-to-cell variation and cannot assess the dynamics in the system. Recent development of single molecule live-cell imaging may allow for the study of the dynamics of TF binding to specific regulatory loci in live cells at a single-cell level. This method allows tracking of the movements and behaviors of individual TFs as they search for cognate binding sites within the nucleus of individual living cells (Levine et al. 2014). Thus, the use of these techniques will contribute for a better understanding of the dynamics underlying enhancer-promoter interactions and the cell-to-cell variation of these interactions.

Another general difficulty from genome-wide studies is the extraction of relevant information or general principles from the integration of different datasets in an unbiased way. One approach that holds great promise is the use of computational algorithms that integrate various data elements into descriptive and predictive models, as it was successfully applied, for example, in the field of ESCs (Sasai et al. 2013; Walker et al. 2007). One benefit of these approaches is to process a collection of correlations into cause-effect relationships. The predictive nature of these models may also be extremely useful to identify new regulatory nodes in the transcription network.

References

Chang, H.H. et al., 2008. Transcriptome-wide noise controls lineage choice in mammalian progenitor cells. *Nature*, 453(7194), pp.544–7. Available at: http://www.ncbi.nlm.nih.gov/pubmed/18497826 [Accessed February 27, 2013].

Eldar, A. & Elowitz, M.B., 2010. Functional roles for noise in genetic circuits. *Nature*, 467(7312), pp.167–173. Available at: http://dx.doi.org/10.1038/nature09326.

Enver, T. et al., 2009. Stem cell states, fates, and the rules of attraction. *Cell stem cell*, 4(5), pp.387–97. Available at: http://www.ncbi.nlm.nih.gov/pubmed/19427289 [Accessed February 27, 2013].

Huang, S., 2009. Non-genetic heterogeneity of cells in development: more than just noise. *Development (Cambridge, England)*, 136(23), pp.3853–3862.

Imayoshi, I. et al., 2013. Oscillatory Control of Factors Determining Multipotency and Fate in Mouse Neural Progenitors. , (October).

Imayoshi, I. & Kageyama, R., 2014. Review bHLH Factors in Self-Renewal , Multipotency , and Fate Choice of Neural Progenitor Cells. *Neuron*, 82(1), pp.9–23. Available at: http://dx.doi.org/10.1016/j.neuron.2014.03.018.

Levine, M., Cattoglio, C. & Tjian, R., 2014. Looping back to leap forward: Transcription enters a new era. *Cell*, 157(1), pp.13–25. Available at: http://dx.doi.org/10.1016/j.cell.2014.02.009.

Pina, C. et al., 2012. Inferring rules of lineage commitment in haematopoiesis. *Nature Publishing Group*, 14(3), pp.287–294. Available at: http://discovery.ucl.ac.uk/1340480/.

Sasai, M. et al., 2013. Time scales in epigenetic dynamics and phenotypic heterogeneity of embryonic stem cells. *PLoS computational biology*, 9(12), p.e1003380. Available at: http://www.pubmedcentral.nih.gov/articlerender.fcgi?artid=3861442&tool=pmcentrez&rendertype=abstract [Accessed March 24, 2014].

Walker, E. et al., 2007. Prediction and Testing of Novel Transcriptional Networks Regulating Embryonic Stem Cell Self-Renewal and Commitment. *Cell Stem Cell*, 1(1), pp.71–86.

De Wit, E. & de Laat, W., 2012. A decade of 3C technologies: Insights into nuclear organization. *Genes and Development*, 26(1), pp.11–24.

Appendix 1 – **Transcriptional control of vertebrate neurogenesis by the proneural factor Ascl1**

frontiers in
CELLULAR NEUROSCIENCE

MINI REVIEW ARTICLE
published: 02 December 2014
doi: 10.3389/fncel.2014.00412

Transcriptional control of vertebrate neurogenesis by the proneural factor Ascl1

Francisca F. Vasconcelos and Diogo S. Castro*

Molecular Neurobiology, Instituto Gulbenkian de Ciência, Oeiras, Portugal

Edited by:
Marcos R. Costa, Federal University of Rio Grande do Norte, Brazil

Reviewed by:
Joao R. L. Menezes, Universidade Federal do Rio de Janeiro, Brazil
Carol Schuurmans, University of Calgary, Canada

***Correspondence:**
Diogo S. Castro, Molecular Neurobiology, Instituto Gulbenkian de Ciência, Rua da Quinta Grande 6, P-2780-156 Oeiras, Portugal
e-mail: dscastro@igc.gulbenkian.pt

Proneural transcription factors (TFs) such as Ascl1 function as master regulators of neurogenesis in vertebrates, being both necessary and sufficient for the activation of a full program of neuronal differentiation. Novel insights into the dynamics of Ascl1 expression at the cellular level, combined with the progressive characterization of its transcriptional program, have expanded the classical view of Ascl1 as a differentiation factor in neurogenesis. These advances resulted in a new model, whereby Ascl1 promotes sequentially the proliferation and differentiation of neural/stem progenitor cells. The multiple activities of Ascl1 are associated with the activation of distinct direct targets at progressive stages along the neuronal lineage. How this temporal pattern is established is poorly understood. Two modes of Ascl1 expression recently described (oscillatory *vs.* sustained) are likely to be of importance, together with additional mechanistic determinants such as the chromatin landscape and other transcriptional pathways. Here we revise these latest findings, and discuss their implications to the gene regulatory functions of Ascl1 during neurogenesis.

Keywords: Ascl1/Mash1, neurogenesis, proneural gene, transcription, Notch signaling

INTRODUCTION

Neurogenesis in the developing mammalian brain is a highly complex process that requires neural progenitor cells to progress through a succession of distinct cellular states. These developmental steps have been particularly well defined in the embryonic telencephalon, where distinct types of progenitors have been identified during the neurogenesis period (Kriegstein and Alvarez-Buylla, 2009). Radial glial (RG) cells in the ventricular zone (VZ) have characteristic features of neural stem/progenitor cells, as they self-renew by asymmetric division and have the potential to differentiate into both neurons and glial cells (Götz and Huttner, 2005). Upon cell division, RG cells give rise to another RG cell and either a post-mitotic neuron, or an intermediate progenitor that can divide further to amplify the lineage (Haubensak et al., 2004; Miyata et al., 2004; Noctor et al., 2004; Pilz et al., 2013). These various progenitor types are differentially segregated between two germinal layers. Most RG cells divide at the apical surface of the VZ, while most intermediate progenitors divide more basally in the sub-ventricular zone (SVZ).

Proneural transcription factors (TFs) of the bHLH family including Ascl1 (also called Mash1) and members of the Neurogenin family are the main regulators of vertebrate neurogenesis. Both gain and loss-of-function analyses have shown they are both required and sufficient to induce a complete program of neuronal differentiation (Bertrand et al., 2002; Wilkinson et al., 2013). While genetic ablation of Ascl1 in mice results in neural developmental defects associated with reduced generation of neurons (Casarosa et al., 1999; Horton et al., 1999; Marin et al., 2000), overexpression of this TF in neural progenitors induces cell-cycle exit and full neuronal differentiation and specification (Nakada et al., 2004; Castro et al., 2006; Berninger et al., 2007b; Geoffroy et al., 2009). In line with its master regulatory role in the neuronal lineage, recent studies have revealed the ability of Ascl1 to convert various non-neural somatic cells (e.g., fibroblasts) into induced neurons (Berninger et al., 2007a; Vierbuchen et al., 2010; Karow et al., 2012), renewing interest in understanding how this important TF works at the molecular level.

PRONEURAL FACTORS AND THE NOTCH SIGNALING PATHWAY

While driving neuronal differentiation, proneural factors also activate the Notch signaling pathway in neighboring progenitors, a process that is highly reminiscent of the lateral inhibition model proposed for *Drosophila* neurogenesis (Louvi and Artavanis-Tsakonas, 2006). Proneural factors directly activate the transcription of Notch ligands such as Dll1 (Castro et al., 2006; Henke et al., 2009), which interact with a transmembrane Notch receptor in neighboring cells. This event results in the cleavage and release of the Notch intracellular domain (NICD) from the cell membrane into the nucleus, where it forms a complex with the DNA-binding TF Rbpj and additional coactivators. Direct targets of this complex include the bHLH transcriptional repressors Hes1 and Hes5, which in turn bind to the promoters of proneural genes, repressing their expression and thereby inhibiting neuronal differentiation (Kageyama et al., 2005). Thus, proneural genes are both regulators and regulated by the Notch

signaling pathway, a network that functions in parallel to the differentiation program to keep—even if only transiently—adjacent cells undifferentiated. Such lateral inhibition results in proneural factors being expressed in a "salt-and-pepper" pattern and prevents simultaneous differentiation of all progenitors, ensuring that an appropriate number is maintained during embryonic development.

A REVISED VIEW OF LATERAL INHIBITION IN VERTEBRATES

It is known that in a variety of cell types (e.g., fibroblasts), Hes1 expression levels regularly alternate over time due to its ability to behave as an intrinsic oscillator (Hirata et al., 2002; Masamizu et al., 2006; Kobayashi et al., 2009). Hes1 represses its own promoter in a feedback mechanism, which associated with short-lived Hes1 transcript and protein, results in autonomous oscillations of its expression with a 2–3 h period. It was recently shown that Hes1 also oscillates in neural progenitors (Shimojo et al., 2008). Because Hes1 and proneural factors display complementary patterns of expression, one possibility is that oscillation of Hes1 results in the oscillation of proneural genes. This is indeed the case for both Neurog2 and Ascl1, as shown by a variety of approaches (Shimojo et al., 2008; Imayoshi et al., 2013). Most notably was the generation of transgenic mice bearing a bacterial artificial chromosome (BAC) containing the Ascl1 regulatory regions driving the expression of Ascl1 fused to either luciferase or green fluorescent protein (GFP), where the activity of the reporter monitors faithfully the expression of the endogenous Ascl1 protein (Imayoshi et al., 2013). Proneural proteins are direct activators of Dll1, resulting in its oscillation and mutual activation of Notch signaling in neighboring progenitors (Castro et al., 2006; Shimojo et al., 2008). There is evidence that Hes1 activity both promotes and inhibits the cell cycle and therefore its oscillation may be required for cell proliferation (Castella et al., 2000; Hartman et al., 2004; Sang et al., 2008). Oscillatory expression of TFs with lineage specification functions has also been observed in other systems, and the function of such oscillations is still a matter of debate. As opposed to steady-state mode, oscillatory expression may generate heterogeneity of response of an apparently homogeneous progenitor cell population to a given input signal. In addition, different inputs may affect different parameters of the oscillation (e.g., period, amplitude) and, hence, trigger different functional outcomes (Mengel et al., 2010; Pina et al., 2012; Sequerra et al., 2013).

In light of these recent findings, the "salt-and-pepper" expression pattern of proneural factors is perceived as a snapshot of a dynamic mode of expression. Proneural factors are therefore expressed in neural progenitors at different stages of differentiation, and not only in committed progenitors that will soon become post-mitotic, as was previously thought (**Figure 1**).

OSCILLATORY VS. SUSTAINED MODE OF EXPRESSION

Time-lapse imaging of individual neural progenitors in culture revealed that during neuronal induction, Ascl1 and Neurog2 switch from an oscillatory to a sustained mode of expression after the last cell division, followed by the expression of the neuronal marker doublecortin 6–8 h later (Shimojo et al., 2008; Imayoshi et al., 2013). This suggested the ability of proneural factors to trigger differentiation may require their expression to be sustained. Such a causal link was established upon the use of an optogenetic approach where Ascl1 expression is regulated by a light-switchable transactivator (Imayoshi et al., 2013). This system was introduced in an Ascl1 null background to investigate the consequence of different dynamics of Ascl1 expression induced by different pulses of light. An oscillatory mode with a 3 h periodicity increased proliferation, compensating the lower proliferation rate observed in Ascl1 null progenitors in culture. By contrast, sustained expression of Ascl1 for 6 h resulted in cell-cycle exit and neuronal differentiation. The same approach used in slice cultures of the dorsal telencephalon where Ascl1 is usually expressed at very low levels reached similar conclusions. What determines the transition to a sustained mode of Ascl1 expression remains an open question, but it was suggested that varying levels of NICD may play a role in this step (Imayoshi et al., 2013).

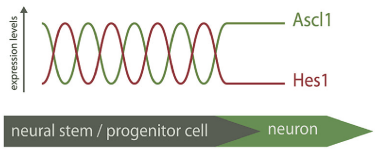

FIGURE 1 | Distinct modes of expression of Ascl1 in neural stem/progenitor cells. Hes1 and Ascl1 oscillate in neural progenitors with a 2–3 h period. The inverse correlation of expression of Hes1 and Ascl1 proteins suggest these TFs oscillate out-of-phase. At the onset of differentiation, Hes1 expression is extinguished and Ascl1 expression becomes sustained. The "salt-and-pepper" expression of Ascl1 in the neural tube is therefore the result of a dynamic pattern of expression, and Ascl1 expression is not necessarily an indicative of differentiation.

Overall, these findings explain why most evidence based on Ascl1 gain-of-function (sustained expression) points to a role in promoting differentiation (with concomitant cell cycle-exit) of progenitors (Nakada et al., 2004; Castro et al., 2006; Geoffroy et al., 2009). By contrast, knock-down of Ascl1 levels upon expression of sequence-specific shRNA decreased proliferation of neural progenitors in culture (Castro et al., 2011), while acute knock-out of Ascl1 in the ventral telencephalon caused premature cell-cycle withdrawal of both VZ and SVZ progenitors (Castro et al., 2011; Pilz et al., 2013), suggesting a role in maintaining proliferation in both RG cells and intermediate progenitors.

CHARACTERIZATION OF Ascl1 TARGET GENES

Proneural factors function primarily as transcriptional activators, binding in heterodimeric complexes with bHLH E-proteins to the regulatory regions of their target genes (Bertrand et al., 2002). A major leap forward in our understanding of the molecular mechanisms underlying Ascl1 function has been the progressive characterization of its transcriptional program. The advent of genomic approaches based on chromatin immunoprecipitation allowed the characterization of a large number of genes directly controlled by Ascl1 in a neurogenesis context. Two studies have

used chromatin immunoprecipitation followed by hybridization to DNA arrays (ChIP-chip), or massive parallel sequencing (ChIP-seq), to characterize the Ascl1 transcriptional program in ventral telencephalon and dorsal spinal cord of the developing mouse embryo, respectively (Castro et al., 2011; Borromeo et al., 2014). A common theme of both studies was the diversity of biological functions of Ascl1 target genes, indicating Ascl1 directly controls various stages of neurogenesis, including neuronal differentiation, migration, axon guidance and synapse formation. In the ventral telencephalon, the region of the murine brain with the largest SVZ during the neurogenic period, the pro-proliferation activity of Ascl1 extends beyond the maintenance of Notch/Hes1 oscillations through activation of Dll1, and includes the activation of genes required for cell-cycle progression such as E2F1 and Foxm1 (Castro et al., 2011).

The Ascl1 targets are associated with progressive functions along neurogenesis and have distinct onsets of expression along the neuronal lineage in this brain region, as indicated by their expression patterns. The expression of the largest group mirrors that of Ascl1 itself in both germinal layers and includes genes expected to promote cell proliferation (e.g., E2F1), whereas that of a smaller but significant group of targets is restricted to the mantle zone (e.g., MAP2) (**Figure 2**).

All the above observations resulted in a model whereby Ascl1 sequentially promotes proliferation and differentiation of progenitors along the neuronal lineage, with the concomitant activation of partially distinct transcriptional programs. This reconciles the classical view of Ascl1 as a differentiation factor with the fact that this proneural factor is expressed mostly in cycling cells. The different kinetics of Ascl1 targets may result from the integration of various mechanistic determinants, including its two modes of expression as briefly discussed below.

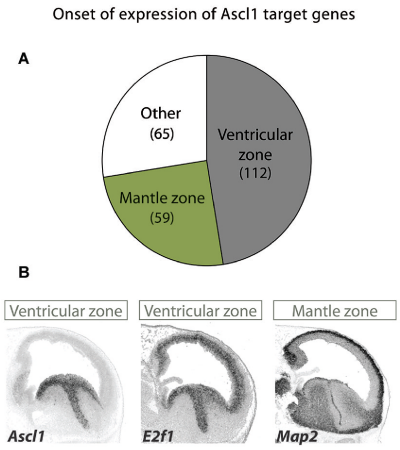

FIGURE 2 | Different patterns of expression of Ascl1 target suggest distinct kinetics of gene activation. (A) A large screening of expression patterns of Ascl1 direct targets in embryonic mouse ventral telencephalon revealed distinct patterns of expression (Castro et al., 2011). Three distinct groups can be identified. Genes in the largest set display an onset of expression at the VZ (which includes mostly neural stem cells), while in another the onset occurs at the mantle zone (here defined as including SVZ and all other outer layers, comprising intermediate progenitors and post-mitotic neurons). A third group includes genes with a uniform or more complex pattern of expression. Number of genes in each set is indicated in between brackets. **(B)** Examples of two Ascl1 direct targets with distinct patterns of expression revealed by *in situ* hybridization on sagittal sections of mouse telencephalon at E13.5 stage of embryonic development. Expression of the proliferation gene E2f1 in VZ/SVZ mirrors that of Ascl1. By contrast, the neuronal differentiation gene MAP2 is expressed in post-mitotic neurons. Images are from Allen Developing Mouse Brain Atlas.[1]

REGULATION OF Ascl1 PROTEIN LEVELS AND TRANSCRIPTIONAL ACTIVITY

One simple possibility is that increasing levels of Ascl1 activity, resulting from changes in the Ascl1 mode of expression (oscillatory *vs.* sustained), protein levels and/or its transcriptional function, will result in the sequential activation of promoters with an increasing threshold of response. Although not formally demonstrated, it is likely that some Ascl1 targets respond differently to the oscillatory or sustained expression of Ascl1. One possible model invokes the function of a feed-forward-loop (FFL), a motif highly enriched in transcriptional networks. A variant of such motif called coherent FFL (whereby one TF activates another TF, and both co-activate target genes) has been shown to allow for a discriminated response of the target gene triggered by transient or sustained input signals from the first TF (Shen-Orr et al., 2002; Mangan and Alon, 2003). Considering the large number of TFs found amongst Ascl1 targets, it would be of interest to investigate if any may establish with this proneural factor such a network motif, providing a mechanistic basis for differential activation of Ascl1 targets upon its two modes of expression.

Some observations suggest Ascl1 protein levels may also play a role at the onset of neuronal differentiation. Time-lapse imaging of Ascl1/luciferase expressing neural progenitors in culture revealed an increase in Ascl1 levels in 90% of the cells that undergo asymmetrical (neurogenic) cell division, against 30% of the cells that undergo a proliferative symmetric division (Imayoshi et al., 2013). Thus, although not being strictly required or sufficient, an increase in Ascl1 protein levels before cell division does bias cells towards the neuronal fate.

A few signaling pathways have been implicated in the regulation of Ascl1 protein levels in different cellular contexts (Sriuranpong et al., 2002; Viñals et al., 2004; Oishi et al., 2009). In the most striking example, varying Ascl1 protein levels regulated by retinoic acid, result in the generation of different types of neurons at the p3 domain of hindbrain and spinal cord (Jacob et al., 2013). In all cases studied however, it is unclear if and how Ascl1 levels affect the activation of its target genes. Thus, while all these results indicate that various pathways converge to control Ascl1 protein levels, their relevance to the differential regulation of subsets of Ascl1 targets remains to be explored.

[1]Available at: http://developingmouse.brain-map.org

Two recent studies provided evidence that Ascl1 function can be modulated by phosphorylation at multiple serine-proline sites. During cortical development, manipulating RAS/ERK signaling to abnormal high level induces a Neurog2 to Ascl1 switch of expression and modifies Ascl1 activity by direct phosphorylation. As a result, Ascl1 drives a glioblast-like differentiation program reminiscent of its function in oligodendrogenesis. Another work showed that Ascl1 phosphorylation is sensitive to levels of Cdk/Cdk inhibitors, and diminishes its ability to drive primary neurogenesis in *Xenopus* embryos, providing a direct link between the cell-cycle machinery and regulation of neurogenesis (Ali et al., 2014). It is currently not known how phosphorylation impacts the neurogenic activity of Ascl1. Possible mechanisms include differential binding to DNA (as shown with Neurog2 phosphorylation) (Ali et al., 2011), or co-factor recruitment. Strikingly, phosphorylation affects the ability of Ascl1 to up-regulate the late/differentiation targets Myt1 and neural β-tubulin, while having little effect on *Dll1* induction (Ali et al., 2014). Moreover, a differential effect is also observed on the ability of Ascl1 to transactivate the promoters of various target genes (Li et al., 2014). Differential sensitivity of promoters to Ascl1 phosphorylation may thus be one important mechanism determining which targets Ascl1 regulates in proliferating vs. differentiating progenitors.

IMPORTANCE OF CHROMATIN LANDSCAPE AND Ascl1 BINDING SITES

Distinct thresholds of response to Ascl1 may result from differences in requirements for chromatin remodeling across its target genes. Very little is known however, on the impact that Ascl1 and proneural factors in general may have on the chromatin landscape when regulating gene transcription. Expression of a dominant negative form of Brg1, a catalytic component of SWI/SNF chromatin remodeling complex, blocks neuronal differentiation of P19 cells mediated by Neurog3 (Seo et al., 2005). In addition, it inhibits Neurog3 activation of the promoter of *NeuroD2*, the paradigm of a late/differentiation target of Neurogenins. In spite of this suggestive example, the importance of chromatin remodeling to the overall temporal patterning of the transcriptional program downstream of proneural factors remains to be investigated.

The chromatin landscape can contribute to restrict the accessibility of a TF to its target sites. A study of Ascl1 mediated neuronal reprogramming has recently shown that Ascl1 binds to its *bona fide* target sites when ectopically expressed in fibroblasts, even to those located within closed chromatin context, as defined by FAIRE-seq (Wapinski et al., 2013). The term "on target" pioneer factor was coined to indicate the ability of Ascl1 to recognize its cognate binding sites when ectopically expressed, as opposed to other TFs in iPS reprogramming (Soufi et al., 2012). Although the ability to bind nucleosomal DNA may argue against a dominant role of the chromatin structure in controlling Ascl1 function, it remains possible that Ascl1 accessibility to its target sites may be different in proliferating vs. differentiating progenitors.

The affinity of a TF binding site, determined by the DNA sequence, can dictate the kinetics of response of its direct targets. A striking example of how such mechanism can establish the temporal pattern of a developmental program is the activation of pharyngeal genes by the forkhead factor PHA4 at different developmental stages in *Caenorhabditis elegans* (Gaudet and Mango, 2002). Binding site mutations result in abnormalities in the timing of target gene expression *in vivo*, according to the resulting affinity to PHA4 binding. Concerning bHLH TFs, and in addition to the two central bases of the E-box, which provide specificity to distinct factors, residues flanking the hexamer sequence contribute to modulate binding affinity (Blackwell and Weintraub, 1990; Fisher et al., 1993). A study investigating the regulation of the Dll1 gene by Ascl1 has shown that residues at each side and immediately adjacent to the CAGSTG E-box determine binding affinity of Ascl1 *in vitro*, and strength of response in transcriptional assays (Castro et al., 2006). Although a possibility, the contribution of varying affinities for its binding sites to the kinetics of Ascl1 targets remains to be investigated.

FUNCTIONAL INTERACTIONS WITH OTHER TRANSCRIPTIONAL NETWORKS

Transcriptional programs are at the intersection of multiple transcriptional networks. Thus, a comprehensive view of the dynamics of the Ascl1 program will require its integration within other transcriptional pathways operating in neural progenitors. Very few studies have so far identified functional interactions between Ascl1 and other TFs. The forkhead factor FOXO3 regulates neural stem cell maintenance and is required to preserve the neural stem cell pool in adult mice (Renault et al., 2009). Recently, it has been shown that FOXO3 inhibits Ascl1-induced neuronal differentiation in cultured neural progenitors and direct neuronal conversion in fibroblasts (Webb et al., 2013). Although the molecular basis for this antagonism is not yet clear, it is likely to make use of the large number of regulatory regions co-bound by both TFs, many of which regulate Notch pathway related genes. Also SOX1B factors (Sox1/2/3) have been previously shown to counteract proneural proteins in gain-of-function experiments in the chick neural tube (Bylund et al., 2003). Thus, the intertwining of transcriptional networks regulating neural progenitor maintenance and differentiation may be a recurrent feature to be explored in future studies.

One immediate example is the Notch pathway. Within the large number of Ascl1 targets identified in ventral telencephalon, the Rbpj consensus binding sequence is enriched at the vicinity of Ascl1 binding sites, specifically in targets that promote proliferation (Castro et al., 2011). Previous studies of neurogenesis in *Drosophila* provide important clues on how the two factors may interact at the molecular level (Nellesen et al., 1999; Cave et al., 2005). In co-bound regulatory regions with a specific cis-architecture, efficient transactivation is only achieved upon the simultaneous activation of both proneural and Notch pathways. A similar synergy between Ascl1 and Rbpj can be observed in transcriptional assays in murine cells (Cave et al., 2005), although it remains to be shown whether such interaction does take place in gene regulatory regions. RG cells can be distinguished from intermediate progenitors in ventral telencephalon based on their high levels of canonical Notch signaling

(Mizutani et al., 2007), thus in principle such a mechanism could be used to differentially activate Ascl1 targets in the two types of progenitors.

PERSPECTIVE

Proneural TFs such as Ascl1 have been seen as master regulators of the neuronal lineage that play an important regulatory role at the onset of differentiation. Recent findings have uncovered a far more complex picture in which Ascl1 plays sequential functions in proliferating and differentiating neural stem/progenitor cells, with the concomitant regulation of distinct target genes. How sub-sets of the Ascl1 transcriptional program are differentially activated along the neuronal lineage is poorly understood, and will certainly result from the combination of distinct mechanistic determinants. This important question will surely remain a subject of intense research for the foreseeable future.

ACKNOWLEDGMENTS

We thank A. Raposo for critically reading this manuscript. Our work is supported by grants PTDC/SAU-BID/117418/2010 and PTDC/NEU-NMC/0315/2012 from FCT and a Marie Curie CIG to DSC. FFV and DSC are recipients of SFRH/BD/51178/2010 and IF/00413/2012 from FCT.

REFERENCES

Ali, F. R., Cheng, K., Kirwan, P., Metcalfe, S., Livesey, F. J., Barker, R. A., et al. (2014). The phosphorylation status of Ascl1 is a key determinant of neuronal differentiation and maturation in vivo and in vitro. *Development* 141, 2216–2224. doi: 10.1242/dev.106377

Ali, F., Hindley, C., McDowell, G., Deibler, R., Jones, A., Kirschner, M., et al. (2011). Cell cycle-regulated multi-site phosphorylation of neurogenin 2 coordinates cell cycling with differentiation during neurogenesis. *Development* 138, 4267–4277. doi: 10.1242/dev.067900

Berninger, B., Costa, M. R., Koch, U., Schroeder, T., Sutor, B., Grothe, B., et al. (2007a). Functional properties of neurons derived from in vitro reprogrammed postnatal astroglia. *J. Neurosci.* 27, 8654–8664. doi: 10.1523/jneurosci.1615-07.2007

Berninger, B., Guillemot, F., and Götz, M. (2007b). Directing neurotransmitter identity of neurones derived from expanded adult neural stem cells. *Eur. J. Neurosci.* 25, 2581–2590. doi: 10.1111/j.1460-9568.2007.05509.x

Bertrand, N., Castro, D. S., and Guillemot, F. (2002). Proneural genes and the specification of neural cell types. *Nat. Rev. Neurosci.* 3, 517–530. doi: 10.1038/nrn874

Blackwell, T. K., and Weintraub, H. (1990). Preferences of MyoD and E2A protein complexes revealed by binding site selection. *Science* 250, 1104–1110. doi: 10.1126/science.2174572

Borromeo, M. D., Meredith, D. M., Castro, D. S., Chang, J. C., Tung, K.-C., Guillemot, F., et al. (2014). A transcription factor network specifying inhibitory versus excitatory neurons in the dorsal spinal cord. *Development* 141, 2803–2812. doi: 10.1242/dev.105866

Bylund, M., Andersson, E., Novitch, B. G., and Muhr, J. (2003). Vertebrate neurogenesis is counteracted by Sox1–3 activity. *Nat. Neurosci.* 6, 1162–1168. doi: 10.1038/nn1131

Casarosa, S., Fode, C., and Guillemot, F. (1999). Mash1 regulates neurogenesis in the ventral telencephalon. *Development* 126, 525–534.

Castella, P., Sawai, S., Nakao, K., Wagner, J. A., and Caudy, M. (2000). HES-1 repression of differentiation and proliferation in PC12 cells: role for the helix 3-helix 4 domain in transcription repression. *Mol. Cell. Biol.* 20, 6170–6183. doi: 10.1128/mcb.20.16.6170-6183.2000

Castro, D. S., Martynoga, B., Parras, C., Ramesh, V., Pacary, E., Johnston, C., et al. (2011). A novel function of the proneural factor Ascl1 in progenitor proliferation identified by genome-wide characterization of its targets. *Genes Dev.* 25, 930–945. doi: 10.1101/gad.627811

Castro, D. S., Skowronska-Krawczyk, D., Armant, O., Donaldson, I. J., Parras, C., Hunt, C., et al. (2006). Proneural bHLH and Brn proteins coregulate a neurogenic program through cooperative binding to a conserved DNA motif. *Dev. Cell* 11, 831–844. doi: 10.1016/j.devcel.2006.10.006

Cave, J. W., Loh, F., Surpris, J. W., Xia, L., and Caudy, M. A. (2005). A DNA transcription code for cell-specific gene activation by notch signaling. *Curr. Biol.* 15, 94–104. doi: 10.1016/j.cub.2004.12.070

Fisher, F., Crouch, D. H., Jayaraman, P. S., Clark, W., Gillespie, D. A., and Goding, C. R. (1993). Transcription activation by Myc and Max: flanking sequences target activation to a subset of CACGTG motifs in vivo. *EMBO J.* 12, 5075–5082.

Gaudet, J., and Mango, S. E. (2002). Regulation of organogenesis by the Caenorhabditis elegans FoxA protein PHA-4. *Science* 295, 821–825. doi: 10.1126/science.1065175

Geoffroy, C. G., Critchley, J. A., Castro, D. S., Ramelli, S., Barraclough, C., Descombes, P., et al. (2009). Engineering of dominant active basic helix-loop-helix proteins that are resistant to negative regulation by postnatal central nervous system antineurogenic cues. *Stem Cells* 27, 847–856. doi: 10.1002/stem.17

Götz, M., and Huttner, W. B. (2005). The cell biology of neurogenesis. *Nat. Rev. Mol. Cell Biol.* 6, 777–788. doi: 10.1038/nrm1739

Hartman, J., Müller, P., Foster, J. S., Wimalasena, J., Gustafsson, J.-A., and Ström, A. (2004). HES-1 inhibits 17beta-estradiol and heregulin-beta1-mediated upregulation of E2F-1. *Oncogene* 23, 8826–8833. doi: 10.1038/sj.onc.1208139

Haubensak, W., Attardo, A., Denk, W., and Huttner, W. B. (2004). Neurons arise in the basal neuroepithelium of the early mammalian telencephalon: a major site of neurogenesis. *Proc. Natl. Acad. Sci. U S A* 101, 3196–3201. doi: 10.1073/pnas.0308600100

Henke, R. M., Meredith, D. M., Borromeo, M. D., Savage, T. K., and Johnson, J. E. (2009). Ascl1 and Neurog2 form novel complexes and regulate Delta-like3 (Dll3) expression in the neural tube. *Dev. Biol.* 328, 529–540. doi: 10.1016/j.ydbio.2009.01.007

Hirata, H., Yoshiura, S., Ohtsuka, T., Bessho, Y., Harada, T., Yoshikawa, K., et al. (2002). Oscillatory expression of the bHLH factor Hes1 regulated by a negative feedback loop. *Science* 298, 840–843. doi: 10.1126/science.1074560

Horton, S., Meredith, A., Richardson, J. A., and Johnson, J. E. (1999). Correct coordination of neuronal differentiation events in ventral forebrain requires the bHLH factor MASH1. *Mol. Cell. Neurosci.* 14, 355–369. doi: 10.1006/mcne.1999.0791

Imayoshi, I., Isomura, A., Harima, Y., Kawaguchi, K., Kori, H., Miyachi, H., et al. (2013). Oscillatory control of factors determining multipotency and fate in mouse neural progenitors. *Science* 342, 1203–1208. doi: 10.1126/science.1242366

Jacob, J., Kong, J., Moore, S., Milton, C., Sasai, N., Gonzalez-Quevedo, R., et al. (2013). Retinoid acid specifies neuronal identity through graded expression of Ascl1. *Curr. Biol.* 23, 412–418. doi: 10.1016/j.cub.2013.01.046

Kageyama, R., Ohtsuka, T., Hatakeyama, J., and Ohsawa, R. (2005). Roles of bHLH genes in neural stem cell differentiation. *Exp. Cell Res.* 306, 343–348. doi: 10.1016/j.yexcr.2005.03.015

Karow, M., Sánchez, R., Schichor, C., Masserdotti, G., Ortega, F., Heinrich, C., et al. (2012). Reprogramming of pericyte-derived cells of the adult human brain into induced neuronal cells. *Cell Stem Cell* 11, 471–476. doi: 10.1016/j.stem.2012.07.007

Kobayashi, T., Mizuno, H., Imayoshi, I., Furusawa, C., Shirahige, K., and Kageyama, R. (2009). The cyclic gene Hes1 contributes to diverse differentiation responses of embryonic stem cells. *Genes Dev.* 23, 1870–1875. doi: 10.1101/gad.1823109

Kriegstein, A., and Alvarez-Buylla, A. (2009). The glial nature of embryonic and adult neural stem cells. *Annu. Rev. Neurosci.* 32, 149–184. doi: 10.1146/annurev.neuro.051508.135600

Li, S., Mattar, P., Dixit, R., Lawn, S. O., Wilkinson, G., Kinch, C., et al. (2014). RAS/ERK signaling controls proneural genetic programs in cortical development and gliomagenesis. *J. Neurosci.* 34, 2169–2190. doi: 10.1523/jneurosci.4077-13.2014

Louvi, A., and Artavanis-Tsakonas, S. (2006). Notch signalling in vertebrate neural development. *Nat. Rev. Neurosci.* 7, 93–102. doi: 10.1038/nrn1847

Mangan, S., and Alon, U. (2003). Structure and function of the feed-forward loop network motif. *Proc. Natl. Acad. Sci. U S A* 100, 11980–11985. doi: 10.1073/pnas.2133841100

Marin, O., Anderson, S. A., and Rubenstein, J. L. (2000). Origin and molecular specification of striatal interneurons. *J. Neurosci.* 20, 6063–6076.

Masamizu, Y., Ohtsuka, T., Takashima, Y., Nagahara, H., Takenaka, Y., Yoshikawa, K., et al. (2006). Real-time imaging of the somite segmentation clock: revelation of unstable oscillators in the individual presomitic mesoderm cells. *Proc. Natl. Acad. Sci. U S A* 103, 1313–1318. doi: 10.1073/pnas.0508658103

Mengel, B., Hunziker, A., Pedersen, L., Trusina, A., Jensen, M. H., and Krishna, S. (2010). Modeling oscillatory control in NF-κB, p53 and Wnt signaling. *Curr. Opin. Genet. Dev.* 20, 656–664. doi: 10.1016/j.gde.2010.08.008

Miyata, T., Kawaguchi, A., Saito, K., Kawano, M., Muto, T., and Ogawa, M. (2004). Asymmetric production of surface-dividing and non-surface-dividing cortical progenitor cells. *Development* 131, 3133–3145. doi: 10.1242/dev.01173

Mizutani, K., Yoon, K., Dang, L., Tokunaga, A., and Gaiano, N. (2007). Differential notch signalling distinguishes neural stem cells from intermediate progenitors. *Nature* 449, 351–355. doi: 10.1038/nature06090

Nakada, Y., Hunsaker, T. L., Henke, R. M., and Johnson, J. E. (2004). Distinct domains within Mash1 and Math1 are required for function in neuronal differentiation versus neuronal cell-type specification. *Development* 131, 1319–1330. doi: 10.1242/dev.01008

Nellesen, D. T., Lai, E. C., and Posakony, J. W. (1999). Responsiveness of enhancer of split complex genes to common transcriptional activators. *Dev. Biol.* 53, 33–53.

Noctor, S. C., Martínez-Cerdeño, V., Ivic, L., and Kriegstein, A. R. (2004). Cortical neurons arise in symmetric and asymmetric division zones and migrate through specific phases. *Nat. Neurosci.* 7, 136–144. doi: 10.1038/nn1172

Oishi, K., Watatani, K., Itoh, Y., Okano, H., Guillemot, F., Nakajima, K., et al. (2009). Selective induction of neocortical GABAergic neurons by the PDK1-Akt pathway through activation of Mash1. *Proc. Natl. Acad. Sci. U S A* 106, 13064–13069. doi: 10.1073/pnas.0808400106

Pilz, G.-A., Shitamukai, A., Reillo, I., Pacary, E., Schwausch, J., Stahl, R., et al. (2013). Amplification of progenitors in the mammalian telencephalon includes a new radial glial cell type. *Nat. Commun.* 4:2125. doi: 10.1038/ncomms3125

Pina, C., Fugazza, C., Tipping, A. J., Brown, J., Soneji, S., Teles, J., et al. (2012). Inferring rules of lineage commitment in haematopoiesis. *Nat. Cell. Biol.* 14, 287–294. doi: 10.1038/ncb2442

Renault, V. M., Rafalski, V. A., Morgan, A. A., Salih, D. A. M., Brett, J. O., Webb, A. E., et al. (2009). FoxO3 regulates neural stem cell homeostasis. *Cell Stem Cell* 5, 527–539. doi: 10.1016/j.stem.2009.09.014

Sang, L., Coller, H. A., and Roberts, J. M. (2008). Control of the reversibility of cellular quiescence by the transcriptional repressor HES1. *Science* 321, 1095–1100. doi: 10.1126/science.1155998

Seo, S., Richardson, G. A., and Kroll, K. L. (2005). The SWI/SNF chromatin remodeling protein Brg1 is required for vertebrate neurogenesis and mediates transactivation of Ngn and NeuroD. *Development* 132, 105–115. doi: 10.1242/dev.01548

Sequerra, E. B., Costa, M. R., Menezes, J. R. L., and Hedin-Pereira, C. (2013). Adult neural stem cells: plastic or restricted neuronal fates?. *Development* 140, 3303–3309. doi: 10.1242/dev.093096

Shen-Orr, S. S., Milo, R., Mangan, S., and Alon, U. (2002). Network motifs in the transcriptional regulation network of Escherichia coli. *Nat. Genet.* 31, 64–68. doi: 10.1038/ng881

Shimojo, H., Ohtsuka, T., and Kageyama, R. (2008). Oscillations in notch signaling regulate maintenance of neural progenitors. *Neuron* 58, 52–64. doi: 10.1016/j.neuron.2008.02.014

Soufi, A., Donahue, G., and Zaret, K. S. (2012). Facilitators and impediments of the pluripotency reprogramming factors' initial engagement with the genome. *Cell* 151, 994–1004. doi: 10.1016/j.cell.2012.09.045

Sriuranpong, V., Borges, M. W., Christopher, L., Nakakura, E. K., Watkins, D. N., Christine, M., et al. (2002). Notch signaling induces rapid degradation of achaete-scute homolog 1 notch signaling induces rapid degradation of achaete-scute homolog 1. *Mol. Cell. Biol.* 22, 3129–3139. doi: 10.1128/mcb.22.9.3129-3139.2002

Vierbuchen, T., Ostermeier, A., Pang, Z. P., Kokubu, Y., Südhof, T. C., and Wernig, M. (2010). Direct conversion of fibroblasts to functional neurons by defined factors. *Nature* 463, 1035–1041. doi: 10.1038/nature08797

Viñals, F., Reiriz, J., Ambrosio, S., Bartrons, R., Rosa, J. L., and Ventura, F. (2004). BMP-2 decreases Mash1 stability by increasing Id1 expression. *EMBO J.* 23, 3527–3537. doi: 10.1038/sj.emboj.7600360

Wapinski, O. L., Vierbuchen, T., Qu, K., Lee, Q. Y., Chanda, S., Fuentes, D. R., et al. (2013). Hierarchical mechanisms for direct reprogramming of fibroblasts to neurons. *Cell* 155, 621–635. doi: 10.1016/j.cell.2013.09.028

Webb, A. E., Pollina, E. A., Vierbuchen, T., Urbán, N., Ucar, D., Leeman, D. S., et al. (2013). FOXO3 shares common targets with ASCL1 genome-wide and inhibits ASCL1-dependent neurogenesis. *Cell Rep.* 4, 477–491. doi: 10.1016/j.celrep.2013.06.035

Wilkinson, G., Dennis, D., and Schuurmans, C. (2013). Proneural genes in neocortical development. *Neuroscience* 253, 256–273. doi: 10.1016/j.neuroscience.2013.08.029

Conflict of Interest Statement: The authors declare that the research was conducted in the absence of any commercial or financial relationships that could be construed as a potential conflict of interest.

Received: 30 August 2014; accepted: 12 November 2014; published online: 02 December 2014.

*Citation: Vasconcelos FF and Castro DS (2014) Transcriptional control of vertebrate neurogenesis by the proneural factor Ascl1. Front. Cell. Neurosci. **8**:412. doi: 10.3389/fncel.2014.00412*

This article was submitted to the journal Frontiers in Cellular Neuroscience.

Copyright © 2014 Vasconcelos and Castro. This is an open-access article distributed under the terms of the Creative Commons Attribution License (CC BY). The use, distribution and reproduction in other forums is permitted, provided the original author(s) or licensor are credited and that the original publication in this journal is cited, in accordance with accepted academic practice. No use, distribution or reproduction is permitted which does not comply with these terms.

Appendix 2 – **Ascl1 coordinately regulates gene expression and the chromatin landscape during neurogenesis**

Article

Cell Reports

Ascl1 Coordinately Regulates Gene Expression and the Chromatin Landscape during Neurogenesis

Graphical Abstract

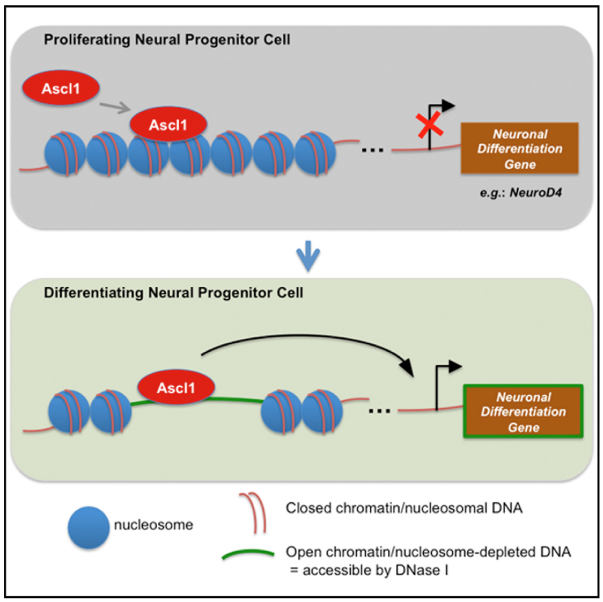

Highlights

- Genome-wide binding of Ascl1 correlates with transcription activation
- Ascl1 can bind to both open and closed chromatin in proliferating cells
- Ascl1 promotes local chromatin accessibility at its target sites
- Chromatin dynamics at Ascl1 sites regulates temporal progression of its program

Authors

Alexandre A.S.F. Raposo, Francisca F. Vasconcelos, ..., François Guillemot, Diogo S. Castro

Correspondence

dscastro@igc.gulbenkian.pt

In Brief

The proneural transcription factor Ascl1 sequentially activates target genes in proliferating and differentiating progenitors during neurogenesis. Here Raposo et al. show that Ascl1 binds closed and open chromatin in proliferating cells. Binding to closed chromatin promotes accessibility and activation of differentiation specific genes. Thus, dynamics of chromatin landscape at Ascl1 target regions regulate the temporal onset of Ascl1 targets.

Raposo et al., 2015, Cell Reports *10*, 1544–1556
March 10, 2015 ©2015 The Authors
http://dx.doi.org/10.1016/j.celrep.2015.02.025

OPEN ACCESS CellPress

Cell Reports
Article

Ascl1 Coordinately Regulates Gene Expression and the Chromatin Landscape during Neurogenesis

Alexandre A.S.F. Raposo,[1,13] Francisca F. Vasconcelos,[1,13] Daniela Drechsel,[2,13] Corentine Marie,[3] Caroline Johnston,[4] Dirk Dolle,[5,6] Angela Bithell,[7] Sébastien Gillotin,[2] Debbie L.C. van den Berg,[2] Laurence Ettwiller,[8] Paul Flicek,[5,6] Gregory E. Crawford,[9] Carlos M. Parras,[3] Benedikt Berninger,[10,11] Noel J. Buckley,[12] François Guillemot,[2] and Diogo S. Castro[1,*]

[1]Instituto Gulbenkian de Ciência, 2780-156 Oeiras, Portugal
[2]MRC National Institute for Medical Research, London NW7 1AA, UK
[3]Inserm U1127, CNRS UMR 7225, Sorbonne Universités, UPMC University Paris 06, UMR-S 1127, Institut du Cerveau et de la Moelle Épinière, ICM, 75013 Paris, France
[4]Centre for the Cellular Basis of Behavior, Institute of Psychiatry, King's College London, London SE5 9NU, UK
[5]European Molecular Biology Laboratory, European Bioinformatics Institute, Wellcome Trust Genome Campus, Hinxton, Cambridge CB10 1SD, UK
[6]Wellcome Trust Sanger Institute, Wellcome Trust Genome Campus, Cambridge CB10 1SA, UK
[7]University of Reading, School of Pharmacy, Hopkins Life Sciences Building, Reading RG6 6AP, UK
[8]Centre for Organismal Studies (COS), Ruprecht-Karls-University, 69120 Heidelberg, Germany
[9]Institute of Genome Sciences & Policy, Duke University, Durham, NC 27708, USA
[10]Institute of Physiological Chemistry, University Medical Center Johannes Gutenberg University Mainz, 55128 Mainz, Germany
[11]Department of Physiological Genomics, Institute of Physiology, Ludwig-Maximilians University Munich, 80336 Munich, Germany
[12]Department of Psychiatry, University of Oxford, Oxford OX3 7JX, UK
[13]Co-first author
*Correspondence: dscastro@igc.gulbenkian.pt
http://dx.doi.org/10.1016/j.celrep.2015.02.025
This is an open access article under the CC BY-NC-ND license (http://creativecommons.org/licenses/by-nc-nd/3.0/).

SUMMARY

The proneural transcription factor Ascl1 coordinates gene expression in both proliferating and differentiating progenitors along the neuronal lineage. Here, we used a cellular model of neurogenesis to investigate how Ascl1 interacts with the chromatin landscape to regulate gene expression when promoting neuronal differentiation. We find that Ascl1 binding occurs mostly at distal enhancers and is associated with activation of gene transcription. Surprisingly, the accessibility of Ascl1 to its binding sites in neural stem/progenitor cells remains largely unchanged throughout their differentiation, as Ascl1 targets regions of both readily accessible and closed chromatin in proliferating cells. Moreover, binding of Ascl1 often precedes an increase in chromatin accessibility and the appearance of new regions of open chromatin, associated with de novo gene expression during differentiation. Our results reveal a function of Ascl1 in promoting chromatin accessibility during neurogenesis, linking the chromatin landscape at Ascl1 target regions with the temporal progression of its transcriptional program.

INTRODUCTION

The generation of neurons in the developing central nervous system requires a number of precisely orchestrated steps, whereby proliferating neural progenitors become committed to the neuronal fate, exit cell cycle, and undergo a long and complex program of migration and differentiation (Kriegstein and Alvarez-Buylla, 2009). Proneural transcription factors (TFs) of the bHLH family, such as Ascl1/Mash1, are the main regulators of neurogenesis in the mammalian brain, and gain and loss-of-function analyses have shown that they are both required and sufficient to promote neurogenesis (Bertrand et al., 2002; Wilkinson et al., 2013). Accordingly, while genetic ablation of proneural genes in mice results in neural developmental defects associated with reduced neurogenesis, overexpression of proneural factors in neural progenitors induces a full neuronal differentiation program (Berninger et al., 2007b; Casarosa et al., 1999; Geoffroy et al., 2009). In addition to its pivotal role in development, Ascl1 has been extensively used in protocols to reprogram somatic cells, including fibroblasts, astrocytes, and pericytes, into induced neurons (Berninger et al., 2007a; Karow et al., 2012; Vierbuchen et al., 2010), renewing interest in understanding the neurogenic activity of this proneural factor.

Previously, we characterized the transcriptional program of Ascl1 in the ventral telencephalic region of the embryonic mouse brain by combining gene expression profiling with chromatin immunoprecipitation (ChIP), followed by hybridization to promoter oligonucleotide arrays (ChIP-chip). This work resulted in the identification of a set of Ascl1 target genes with various biological roles at distinct stages of the differentiation program, raising intriguing questions concerning the molecular basis for such temporal pattern (Castro et al., 2011; Vasconcelos and Castro, 2014). In addition, it led to the identification of a novel function for Ascl1 in maintaining cell proliferation, mediated by the direct activation of genes that promote cell cycle

OPEN ACCESS
CellPress

progression. This resulted in a model whereby this proneural factor sequentially promotes the proliferation and differentiation of progenitor cells along the neuronal lineage, reconciling the classical view of this proneural protein as a differentiation factor with the fact that it is mostly expressed in cycling progenitors. Moreover, a recent study has shown that these two opposing activities are associated with distinct modes of Ascl1 expression, with oscillating or sustained Ascl1 promoting proliferation or differentiation, respectively (Imayoshi et al., 2013).

In spite of the significant progress made on the characterization of its transcriptional targets, little is still known about how Ascl1 regulates gene expression. In particular, the relationship between Ascl1 binding, regulation of the chromatin landscape, and gene transcription is poorly understood. It was recently shown that during neuronal reprogramming, Ascl1 can access its cognate sites in nucleosomal-DNA when ectopically expressed in fibroblasts, defining it as a pioneer TF (Wapinski et al., 2013). However, it remains to be seen whether Ascl1 works as a pioneer factor in a neurogenic context and whether binding of Ascl1 results in alterations to the chromatin landscape at its target regions, as it has been shown for some, but not all, other pioneer TFs (Zaret and Carroll, 2011).

Mammalian neurogenesis is not a synchronized process at a cell population level and studies to investigate the mechanistic basis of Ascl1 function at a genome-wide scale are difficult to perform in the developing embryo or in the adult brain. An alternative is the use of adherent cultures of neural stem (NS) cell lines derived from embryonic stem cells or embryonic neural precursors (Conti et al., 2005; Pollard et al., 2006). These cultures provide us with reliable models to study neurogenesis in culture, without the confounding effects of cellular heterogeneity, characteristic of other cellular models such as neurospheres. In proliferating culture conditions, endogenous Ascl1 regulates a progenitor program that functions to maintain cell proliferation (Castro et al., 2011), whereas overexpression of Ascl1 leads to efficient cell cycle exit and neuronal differentiation.

Here we investigate how Ascl1 activity is restricted by and impacts the chromatin landscape, when driving neuronal differentiation. We combined expression profiling with genome-wide mapping of Ascl1 binding sites (ChIP-seq) (Park, 2009), and DNase I hypersensitivity sites (DNase-seq) (Song and Crawford, 2010), in a cellular model of neurogenesis driven by overexpressed Ascl1. We identify a large number of genes directly regulated by Ascl1 and characterize widespread changes in chromatin accessibility during differentiation. Ascl1 binding correlates with activation of gene transcription, targeting not only regions of accessible but also of closed chromatin. In addition, binding of Ascl1 to DNA precedes a local increase in chromatin accessibility at the regulatory regions of its target genes, providing the first direct link between Ascl1 regulation of gene expression and local changes in chromatin landscape.

RESULTS

A Cellular Model of Ascl1-Driven Neurogenesis

Overexpression of Ascl1 promotes cell cycle exit and neuronal differentiation of neural progenitor cells (Castro et al., 2006). To study this process in controlled conditions, we established a cellular model of Ascl1-driven neurogenesis by expressing an inducible version of Ascl1 in NS cells in culture (NS5 cell line) (Pollard et al., 2006). Fusion of full-length Ascl1 to the modified ligand binding domain of the estrogen receptor (ERT2) renders Ascl1 activity dependent on the presence of 4-hydroxytamoxifen (herein referred to as tamoxifen) (Bergstrom et al., 2002; Burk and Klempnauer, 1991; Littlewood et al., 1995). In a transcriptional assay in transfected NS cells, Ascl1-ERT2 induces the transcriptional activation of an enhancer of the Ascl1 target gene *Dll1* (Castro et al., 2006) in an inducible manner to levels that are similar to its WT counterpart (Figure S1A). In order to test for the ability of the inducible Ascl1 protein to promote neuronal differentiation, we transduced NS cells in culture with a retrovirus vector co-expressing Ascl1-ERT2 and green fluorescent protein (GFP). In the vast majority of transduced cells, drastic morphological changes characterized by the extension of long processes and associated with the expression of the neuronal marker Tuj1 were observed only upon the addition of tamoxifen, confirming the ability of Ascl1-ERT2 to activate the neurogenic differentiation program in an inducible manner (Figure S1B). Although activation is associated with the nuclear translocation of a small fraction of Ascl1-ERT2, most of the protein is already nuclear prior to addition of tamoxifen (as previously reported with other cases of TFs fused to ERT2) (Burk and Klempnauer, 1991; Roemer and Friedmann, 1993), and additional mechanisms must therefore contribute to the inducibility of Ascl1-ERT2 (Figure 1A).

To obtain large numbers of synchronized differentiating neural progenitors, we used antibiotic selection following the retroviral delivery of the Ascl1-ERT2 transgene. Quantification of immunofluorescence levels upon immunohistochemistry estimated the total Ascl1 protein level in transduced cells to be 8- to 9-fold higher when compared with endogenous Ascl1 expressed in embryonic ventral telencephalic progenitors (Figure 1B). NS cells expressing Ascl1-ERT2 plated at low density differentiate with great efficiency upon addition of tamoxifen (Figure 1C). Four days after induction, immunocytochemical analysis shows expression of the rate limiting enzyme for GABA synthesis glutamic acid decarboxylase GAD65/67 (15.1% ± 0.3%) (Figure 1D). Whole-cell patch-clamp recordings of retrovirus-transduced cells 14 days after onset of tamoxifen treatment show that these cells consistently exhibit electrophysiological properties of neurons (Figure 1E). Moreover, their action potential discharges pattern in response to step current injections is highly reminiscent of low-threshold burst spiking interneurons and very similar to those generated from medial ganglionic eminence progenitors of the ventral telencephalon (Figure 1D) (Martínez-Cerdeño et al., 2010). To characterize the transcriptome changes in our model, we performed expression profiling at various time points −4, 12, 24, and 50 hr after the onset of differentiation. A large number of genes (1,508) are differentially regulated at least at one time point (fold change >1.5, $p < 10^{-3}$; see Figure 1F for a breakdown of numbers), as expected upon induction of a cellular differentiation program (Table S1). Functional annotation of differentially expressed genes by Gene Ontology shows considerable enrichment in terms associated with distinct phases of neurogenesis, describing both early events (e.g., "Notch signaling," "cell division") and later steps of the differentiation program (e.g., "cell

OPEN ACCESS
CellPress

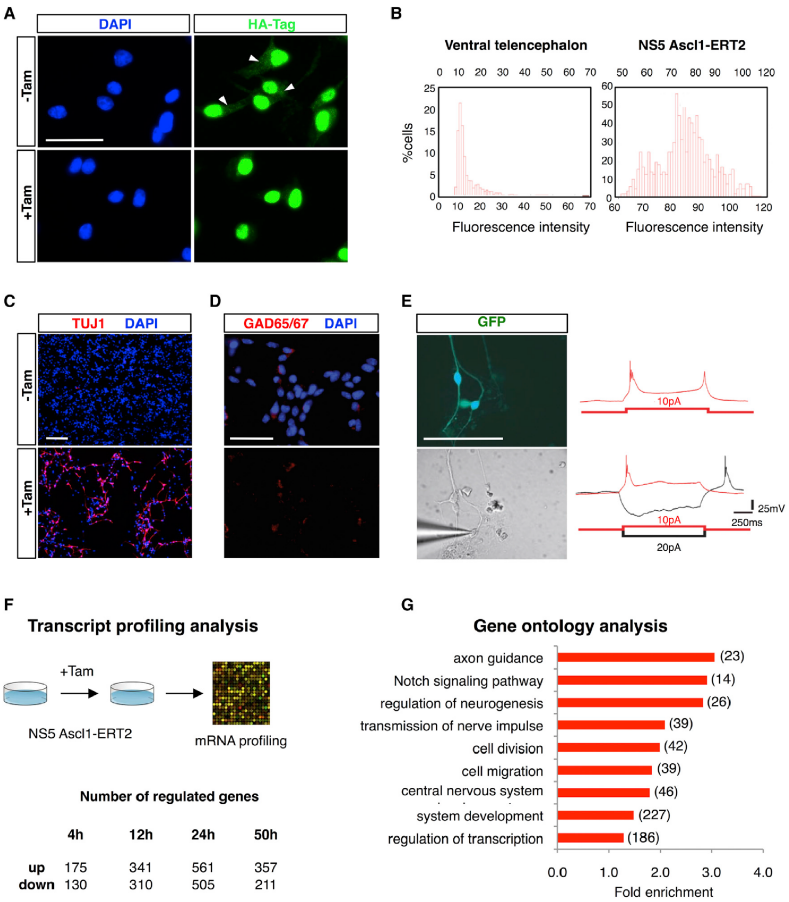

Figure 1. A Cellular Model of Neurogenesis Driven by Ascl1

(A) Cellular localization of Ascl1-ERT2 in NS5 cells before and 30 min after the addition of tamoxifen, as assessed by immunostaining against HA-tag (green). White arrowheads mark cytoplasmic expression in the absence of tamoxifen. Cell nuclei are labeled with DAPI (blue). Scale bar represents 30 μm.

(B) Quantification of total Ascl1 protein levels in E14.4 ventral telencephalic progenitors (left) or NS5 Ascl1-ERT2 cells (right). Histograms show absolute fluorescence intensity after normalization (see Experimental Procedures for details).

(C) State of differentiation of NS5 Ascl1-ERT2 cells in the presence or absence of tamoxifen 3 days after induction of differentiation, as assessed by the expression of the neuronal marker TUJ1 (red). Cell nuclei are labeled with DAPI (blue). Scale bar represents 200 μm.

(D) Expression of Gad65/67 (red) in NS5 Ascl1-ERT2 cells 4 days after induction of differentiation. Cell nuclei are labeled with DAPI (blue). Scale bar represents 200 μm.

(E) Electrophysiological properties of GFP-labeled neurons generated from NS5 Ascl1-ERT2 cells 14 days upon induction of differentiation. Representative responses of two neurons to step-current injection at a holding potential of −70mV in current-clamp mode. Note the brief burst of action potentials on top of a prolonged calcium spike following depolarization (red traces) and the rebound burst following release from hyperpolarization (black trace). Scale bar represents 200 μm.

(legend continued on next page)

OPEN ACCESS
CellPress

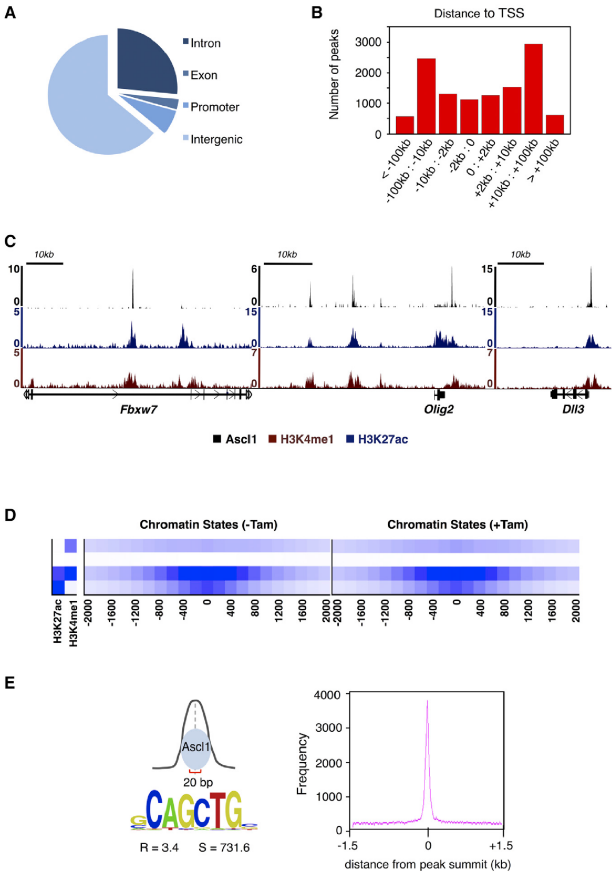

Figure 2. Genome-wide Mapping of Ascl1 Binding Sites in Differentiating NS Cells

(A) Location of Ascl1 BEs respective to various genomic features.

(B) Location of Ascl1 BEs in relation to the closest annotated TSS.

(C) Chromatin state in differentiating NS cells, at Ascl1 bound regions in the vicinity of *Fbxw7*, *Olig2*, and *Dll3* genes.

(D) Heat maps of chromatin states for H3K27ac and H3K4me1 within ±2 kb of Ascl1-ERT2 peak summits in proliferating or differentiating NS cells (before and 24 hr after the addition of tamoxifen, respectively).

(E) DNA motif enrichment for Ascl1 E-box within a 20-bp region centered at Ascl1 peak summits (R, enrichment over local genomic background; S, motif score).

See also Figure S2.

migration,'' ''axon guidance'') (Figure 1G). Overall, these results show Ascl1 drives an extended program of neuronal differentiation in our model.

Genome-wide Location Analysis of Ascl1 in Differentiating NS Cells

To understand how the observed changes in gene expression relate to Ascl1 function, we mapped Ascl1 binding sites genome-wide by ChIP followed by massive parallel sequencing (ChIP-seq) (Wapinski et al., 2013), using an antibody against the HA tag of Ascl1-ERT2. This was performed 18 hr after the onset of differentiation, at a time point when NS cells have already undergone large transcriptional changes. Using input chromatin as control, we defined an extended list comprising 21,582 Ascl1 binding sites, with FDR <0.5% and $p < 10^{-10}$ (Table S2).

In order to validate binding events (BEs) mediated by the Ascl1-ERT2 protein, we used ChIP-PCR against WT Ascl1, with chromatin extracted from embryonic E14.5 ventral telencephalic progenitors, or WT NS5 cells (Figure S2A). We reasoned that most BEs in differentiating NS cells should be identified in at least one of the chromatin samples. Indeed, this is the case for all ChIP-seq peaks associated with $p < 10^{-18}$ (with the majority of BEs validated in both chromatins), indicating a good match between Ascl1-ERT2 and WT Ascl1. Most of the 11,782 Ascl1 BEs defined by this high-confidence list ($p < 10^{-18}$) are located within intergenic regions (63%) and at long distances from the nearest identified transcription start site (TSS). Less than one third of Ascl1 binding occurs inside genes (30%) or their promoter regions (7%) (Figures 2A and 2B), suggesting that Ascl1 binds predominantly to distal enhancer regions. We next used a Hidden-Markov model to

(F) Experiment design for the transcriptome analysis and the resulting number of deregulated genes determined at different time points after induction of differentiation (fold change > 1.2, $p < 10^{-3}$).

(G) Enrichment of Gene Ontology biological process terms among genes deregulated during neuronal differentiation. Total number of genes associated with each term is in brackets.

See also Figure S1.

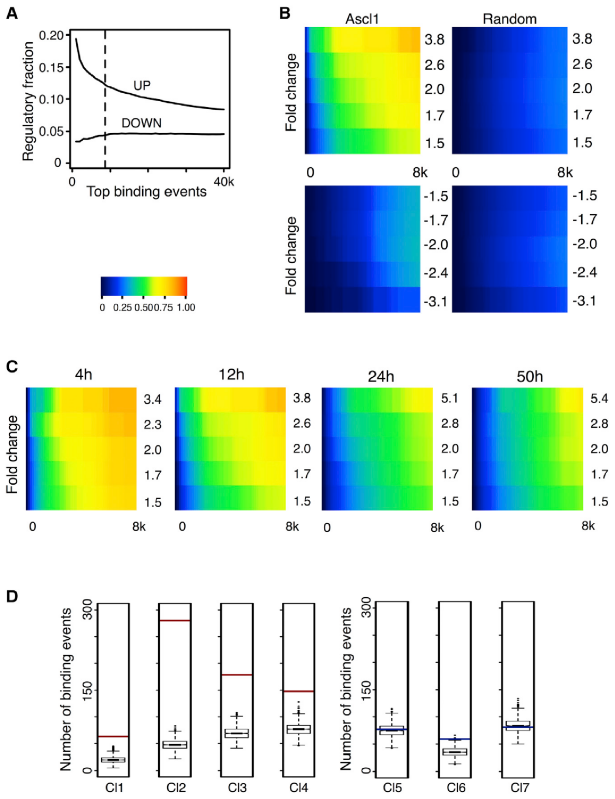

Figure 3. Ascl1 Functions as a Transcriptional Activator at a Genome-wide Level

(A) Cumulative fraction of Ascl1 BEs considered regulatory by association with upregulated or downregulated genes following a nearest gene annotation. The dashed line marks the most stringent cutoff ($p < 10^{-25}$) for peak enrichment and defines a list of BEs with the highest regulatory potential (n = 8,624, 2.5 times over control).

(B) Heat map displaying the cumulative fraction of deregulated genes 12 hr after induction of differentiation that is directly regulated by Ascl1 (up, top left panel; down, bottom left panel). Transcripts are divided in equal bins of decreasing expression fold change and plotted against Ascl1 BEs (bin = 166) with increasing p value. Control: 100 sets of random BEs (right, mean value shown).

(C) Heat maps displaying the cumulative fraction of upregulated genes at 4, 12, 24, and 50 hr after induction of differentiation, defined as in (B).

(D) Association of Ascl1 BEs to each gene cluster. The red (activation) or blue (repression) bar represents the number of high-confidence Ascl1 BEs ($p < 10^{-25}$) annotated to genes belonging to each cluster and is juxtaposed to the distribution of Ascl1 binding annotations, which can be found in 1,000 different random clusters of genes. Test data represented as box with median of test and first and third quartiles; whiskers, ±1.5 × interquartile range (IQR).

See also Figures S3–S5.

characterize the chromatin states at Ascl1-bound regions, using genome-wide profiles of histone modifications generated from proliferating and differentiating NS cells (before or 24 hr after addition of tamoxifen, respectively) (Ernst and Kellis, 2012). Ascl1 BEs fall mostly within regions of chromatin highly co-enriched for H3K4me1 and H3K27ac, characteristic of active enhancers (same result for $p < 10^{-10}$; data not shown). Moreover, the same association with this chromatin state is found in proliferating NS cells, indicating that during differentiation Ascl1 binds predominantly to regions that are already marked as active enhancers in proliferating NS cells (Figures 2C, 2D, and S2B).

To determine the DNA sequence mediating Ascl1 binding, we searched for motifs enriched within the 20 nucleotides region centered under the Ascl1 peak summits. A strong preference is found for the hexamer sequence CAGCTG, corresponding to the E-box type sequence previously associated with Ascl1 binding (Castro et al., 2011) and in agreement with its role in mediating direct DNA binding (Figure 2E).

Ascl1 Functions Globally as a Transcriptional Activator

Although it is generally believed that proneural factors function by activating gene transcription, some reports have challenged this view (Alvarez-Rodríguez and Pons, 2009; Rheinbay et al., 2013). In order to investigate this issue, we started by performing an in depth cross-comparison between the location analysis and expression profiling results, annotating each Ascl1 BE to its nearest TSS. Direct comparison with the set of deregulated genes previously described shows that only a small fraction of BEs are considered to be regulatory using nearest gene annotation (Figure 3A). Nonetheless, we find a positive correlation between peak height (which is proportional to significance of binding, or p value) and its potential to upregulate gene expression (top peaks ~20%). In contrast, the fraction of regulatory peaks that can be associated to repressed genes is invariant with changes in peak size, suggesting no direct relation between Ascl1 binding significance and downregulation of gene expression. Therefore, mere binding of Ascl1 to chromatin does not predict a regulatory event; however, the size of an Ascl1 peak may be correlated with its potential to activate gene transcription.

OPEN ACCESS
CellPress

To have a global view of the association between the data sets of genes bound by Ascl1 and regulated during differentiation, we determined the frequency at which deregulated genes (grouped in bins of increasing thresholds of fold change of expression) are associated with Ascl1 BEs (grouped in bins of increasing p value cutoff) and therefore considered to be directly regulated by Ascl1 (Figure 3B, left). The statistical significance of the overlaps was assessed by a similar comparison against 100 randomly generated control ChIP-seq data sets of identical size (Figure 3B, right). The resulting heat maps indicate a strong association between Ascl1-bound genes and those upregulated during differentiation and a much less pronounced association with downregulated genes (Figure 3B, top left versus bottom left). Moreover, the fraction of downregulated genes that are considered Ascl1 targets is very similar to that expected by chance (Figure 3B, left versus right). Altogether, the above analysis indicates that Ascl1 functions globally as a transcriptional activator. In addition, this function is independent of the progress of differentiation during the first 50 hr, as shown with similar analyses for the different time points considered in the transcription profiling (Figures 3C and S3). Importantly, restricting the analysis to the Ascl1 BEs located within ±5 kb of a TSS, producing a more stringent gene annotation, results in a similar conclusion (Figure S4).

To integrate the transcriptional profiling data sets collected at distinct time points, we applied a fuzzy c-means clustering algorithm, resulting in the identification of seven distinct temporal clusters (clusters 1–4 comprised of upregulated genes, clusters 5–7 of downregulated genes) (Figure S5; Table S3). Clusters of genes that are upregulated during differentiation are all strongly associated with Ascl1 BEs ($p \leq 1.3 \times 10^{-11}$, 8.0×10^{-126}, 1.1×10^{-22}, and 7.9×10^{-10} for clusters 1, 2, 3, and 4, respectively), whereas clusters of downregulated genes show no such association (Figure 3D), further indicating that Ascl1 binding correlates with transcriptional activation.

Characterization of Ascl1 Transcriptional Program

The relative size of each cluster (Figure S5B) and their enrichment for BEs indicate that most Ascl1 target genes fall within a cluster characterized by an early activation profile (cluster 2), while a smaller but significant number is upregulated at mid or late time points (clusters 3 and 4, respectively). We then compiled a high-confidence list of 272 Ascl1 direct targets comprising genes from clusters 2, 3, and 4 that are associated with at least one Ascl1 BE with high regulatory potential ($p < 10^{-25}$) (Table S4). A search for terms describing "Biological Process," "Molecular Function," and "Pathways" (Panther Classification System) revealed the segregation in each temporal cluster of Ascl1 target genes encoding proteins of distinct classes and functions, suggesting the control of various subprograms at distinct developmental stages (Figure S5C). Genes with the earliest onset of activation (belonging to cluster 2) are associated with signal transduction and cell communication, while targets with a mid-onset of activation (cluster 3) encode mostly proteins with a function related to transcription or Notch signaling. Genes with latest onset (cluster 4) are enriched for generic terms associated with neural development and relate to late events in the differentiation program, from cell migration to axonal growth and guidance (Figure S5C). In summary and in agreement with our previous study performed on a smaller scale, the identification of Ascl1 target genes in our neurogenesis model demonstrates the direct control of distinct components of the neurogenic differentiation program by Ascl1.

Ascl1 Access to Its Target Sites Does Not Depend on the Differentiation Stage of NS Cells

It was previously shown that Ascl1 target genes display different onsets of expression at distinct stages of the neuronal lineage (Borromeo et al., 2014; Castro et al., 2011). Such temporal patterning could be associated with distinct accessibilities of Ascl1 to its binding sites (e.g., due to differences in the chromatin landscape). To investigate this, we compared the binding profile of overexpressed Ascl1 at two distinct stages by extending the previous ChIP-seq analysis to a time point at the onset of differentiation (30 min upon addition of tamoxifen) (Table S9). Surprisingly, visual inspection of the genomic distribution of Ascl1 peaks finds a remarkable similarity between Ascl1 BEs at t = 30 min and t = 18 hr (Figure 4A). Comparison of the two Ascl1 binding profiles in a bin-by-bin approach within the confidence limits defined by the previous ChIP-PCR validation (Figure 4B, dashed line) shows an overlap of 86% between the two stages (Figure 4B). Furthermore, the presence of normalized sequencing signal across both samples in genomic regions centered at putative sample-specific BEs suggests that the overlap of occupancies may have been underestimated by peak calling conditions (Figure 4C). Overall, our results indicate that the accessibility of Ascl1 to the full complement of its binding sites remains largely identical throughout differentiation.

Characterization of Chromatin Landscape Changes during Differentiation

We next asked what impact Ascl1 may have on the chromatin landscape when it promotes neuronal differentiation of NS cells. We started by characterizing the chromatin landscape of proliferating NS cells and of NS cells undergoing differentiation by Ascl1, using a DNase I hypersensitivity assay coupled to massive parallel sequencing (DNase-seq). This technique identifies regions of decreased nucleosome occupancy (herein referred as "open chromatin") on a genome-wide scale, which correspond mostly to active regulatory elements such as promoters, enhancers, insulators, and silencers (Boyle et al., 2008; Natarajan et al., 2012; Thurman et al., 2012). The density of mapped reads for each genome position was computed to generate a comprehensive list of DNase I hypersensitivity sites (DHSs). Using a constant threshold of $p < 10^{-5}$, we identified ~87,000 and ~94,000 DHSs in proliferating and differentiating NS cells, respectively (Tables S5 and S6), numbers with a magnitude consistent with those obtained in other cell types (Song et al., 2011). Although the majority of these sites is shared by both experimental conditions, each cell state exhibits a specific set of ~20,000 DHSs (Figure 5A).

Since Ascl1 functions as a transcriptional activator, we focused on the DHSs induced during differentiation (Table S7), as these are more likely to provide new insights into Ascl1

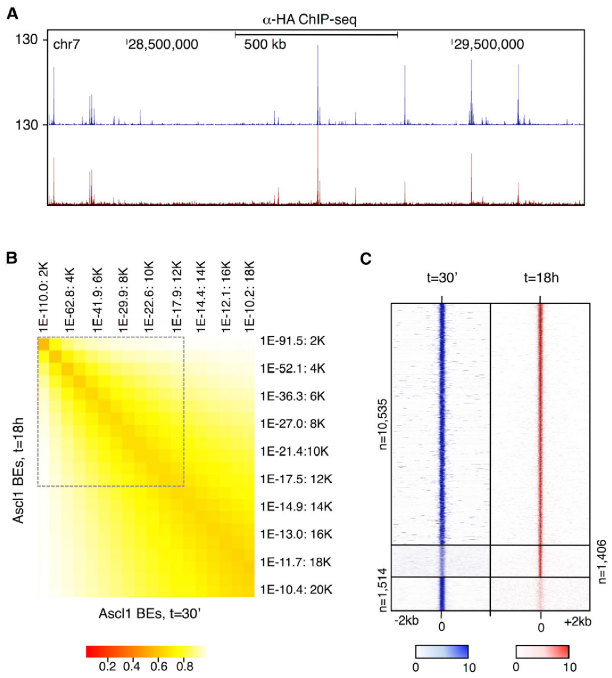

Figure 4. Ascl1 Accessibility to Its Target Sites Remains Similar throughout Differentiation

(A) Visual representation of ChIP-seq profiles at t = 30 min (blue) and t = 18 hr (red) in a large genomic region centered on *Dll3* gene.

(B) Comparison of Ascl1 BEs at t = 30 min and t = 18 hr ($p < 10^{-10}$) by cumulative bins of increasing p value (bin = 1,007). The proportion of sites bound by Ascl1 in both conditions (overlapping peaks) is calculated in relation to the condition with the lowest number of BEs. Dashed lines represent higher confidence lists defined by $p < 10^{-18}$, analyzed in (C).

(C) Density plot of Ascl1 ChIP-seq reads mapping to the genomic regions surrounding the summit of Ascl1 BEs. The signal intensity represents the Ascl1 ChIP-seq normalized tag count in the 4kb region surrounding the summit of each overlapping (top) and nonoverlapping peak at t = 30 min (blue) and t = 18 hr (red).

function. To validate these DHSs, we used formaldehyde-assisted isolation of regulatory elements (FAIRE), an alternative method to identify regions of open chromatin. Although distinct preferences have been described for each technique in the identification of distal or proximal regulatory regions, the two techniques have been shown to yield largely overlapping results on a genome-wide basis (Song et al., 2011). Indeed, 9 of 13 tested regions presented more than 2-fold enrichment by FAIRE-PCR across samples collected before and 24 hr after addition of tamoxifen, as opposed to control regions (Figure 5B).

Induced DHSs Are Associated with Genes Expressed De Novo during Differentiation

Next, we investigated how regions of chromatin newly opened during differentiation may be associated with the observed changes in gene expression. We find a statistically significant enrichment of differentiation-induced DHSs in the vicinity of upregulated genes (the sum of clusters 1–4; $p < 1.3 \times 10^{-29}$), in sharp contrast with downregulated genes (clusters 5–7) (Figure 5C). Moreover, a large fraction of all upregulated genes (413 of 760) is associated with at least one differentiation-induced DHS, suggesting the importance of these putative regulatory regions in activating gene expression during neurogenesis. Notably, upregulated genes associated with differentiation-induced DHSs are either not expressed in proliferating NS cells or expressed at a low level when compared with upregulated genes near constant DHSs (Figure 5D). This is well exemplified by the induction of NeuroD4, a pro-differentiation TF only expressed in post-mitotic precursors (Ohsawa et al., 2005), and which is associated with newly open DHSs (Figure 6B). Overall, our results indicate that activation of differentiation genes is strongly associated with the appearance of new DHSs.

Ascl1 Promotes Chromatin Accessibility

In order to investigate which DNA-binding TFs may be associated with the appearance of newly open chromatin regions, we took advantage of the high resolution potential of Digital Genomic Footprinting (DGF) applied to DNase-seq data to determine the position of sites occupied by TFs within differentiation-induced DHSs (Figure 5E) (Piper et al., 2013). DGF identified almost 17,000 genomic sites (Table S8) with significant occupancy levels ($p < 10^{-10}$), and the corresponding sequences were then subject to a search for frequency of motif occurrence. The most abundant motif found corresponds to the consensus sequence of CTCF and is likely to reflect its frequent binding to insulator regions identified by DNase-seq (Figure 5E) (Thurman et al., 2012). Three additional motifs reveal binding by TFs of the bHLH or NFI families, with the most frequent one corresponding to the E-box consensus sequence, which mediates Ascl1 binding. This observation establishes Ascl1 as a prime candidate to promote the opening of chromatin structure and induce new DHSs during differentiation.

OPEN ACCESS
CellPress

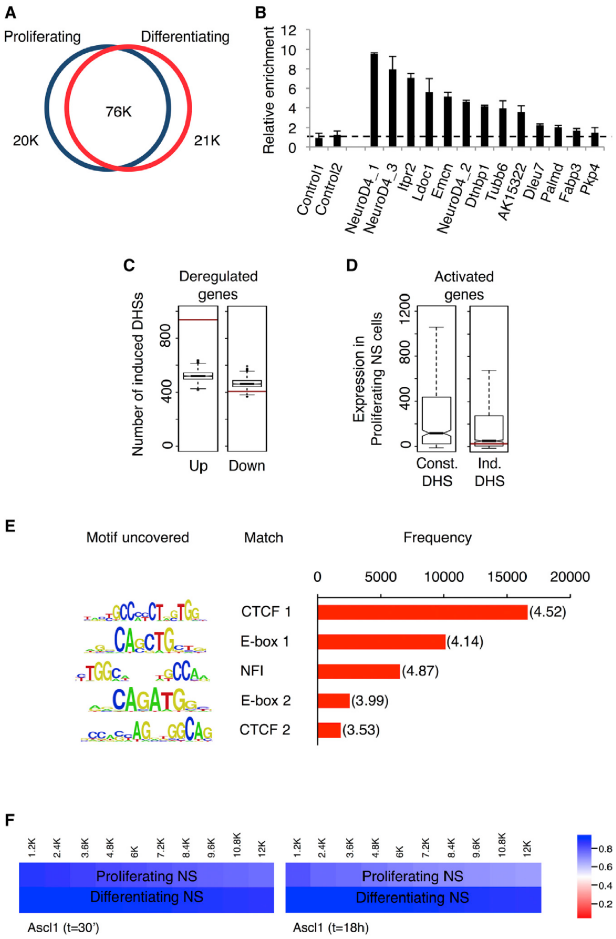

Figure 5. Characterization of Changes in Chromatin Accessibility during Differentiation of NS Cells

(A) Number of DHSs in proliferating NS cells and 24 hr upon Ascl1-mediated differentiation.

(B) FAIRE-PCR validation of differentiation-induced DHSs. Bars show fold enrichment of genomic DNA obtained from NS cells 24 hr after induction over cells prior to addition of tamoxifen. Data are represented as mean ± SD.

(C) Differentiation-induced DHSs are significantly associated with clusters of activated genes (left) and not with clusters of repressed genes (right). Red bars, total number of DHSs annotated to each set of genes; boxplots, distribution of DHSs associations with 1,000 random sets of genes. Test data are represented as box with median of test and first and third quartiles; whiskers, ±1.5 × IQR.

(D) Activated genes associated with differentiation-induced DHSs have low or no expression in proliferating cells. Gene expression levels in proliferating cells are significantly lower ($p < 10^{-11}$, Wilcoxon test) for activated genes associated with induced DHSs (right) than for activated genes with no such association (left). Red bar, level of expression of *NeuroD4* gene. Data distribution represented as box with median and first and third quartiles; whiskers, ±1.5 × IQR; notches, ±1.58 × $IQR/n^{1/2}$).

(E) Frequency of motif occurrence at high occupancy sites found within differentiation-induced DHSs by Digital Genomic Footprinting (over-representation ratio indicated between brackets).

(F) Comparison of Ascl1 BEs at t = 30 min (left) or t = 18 hr (right) with the DNase-seq profile. Color shows the proportion of Ascl1 BEs by cumulative bins of increasing p value (bin = 1,842), which fall within regions of open chromatin (DHSs) in proliferating (top) or differentiating (bottom) NS cells.

To understand how Ascl1 binding may relate to the observed changes in chromatin compaction, we compared the genomic distribution of Ascl1 BEs with that of DHSs before and after neuronal differentiation (Figure 5F). Ascl1 ChIP-seq and DNase-seq data sets show a high degree of overlap (e.g., 80.3% of Ascl1 BEs with $p < 10^{-18}$ at t = 30 min fall within DHSs in proliferating cells), indicating that a large fraction of BEs, but not all, occur in regions of open chromatin in proliferating NS cells (Figure 5F). Strikingly, this overlap increases significantly under differentiation conditions (to 91.05% after differentiation, in the aforementioned case; Figure 5F). Altogether, a comparison between the Ascl1 ChIP-seq and DNase-seq suggests that (1) the Ascl1 binding profile remains constant at the two stages analyzed, (2) a large fraction of Ascl1 BEs occurs in regions of open chromatin in proliferating cells, with a subset falling within closed chromatin, and (3) binding of Ascl1 to closed chromatin precedes the appearance of new DHSs during differentiation.

Visualization of aligned Ascl1 ChIP-seq and DNase-seq data suggests that many differentiation-induced DHSs overlap with Ascl1 BEs (Figure 6A), as exemplified by those in the vicinity of genes activated during differentiation such as *NeuroD4*, *Ap3b2*, *Mcf2l*, and *Nrxn3* (Figure 6B). Validation of changes in chromatin compaction at the selected Ascl1 binding sites was performed by FAIRE-PCR using chromatin extracted from NS5 cells expressing full-length Ascl1 under the regulation of a doxycycline inducible promoter, before and after Ascl1 induction (Figure 6C). Although not all DHSs that arise de novo during

OPEN ACCESS
CellPress

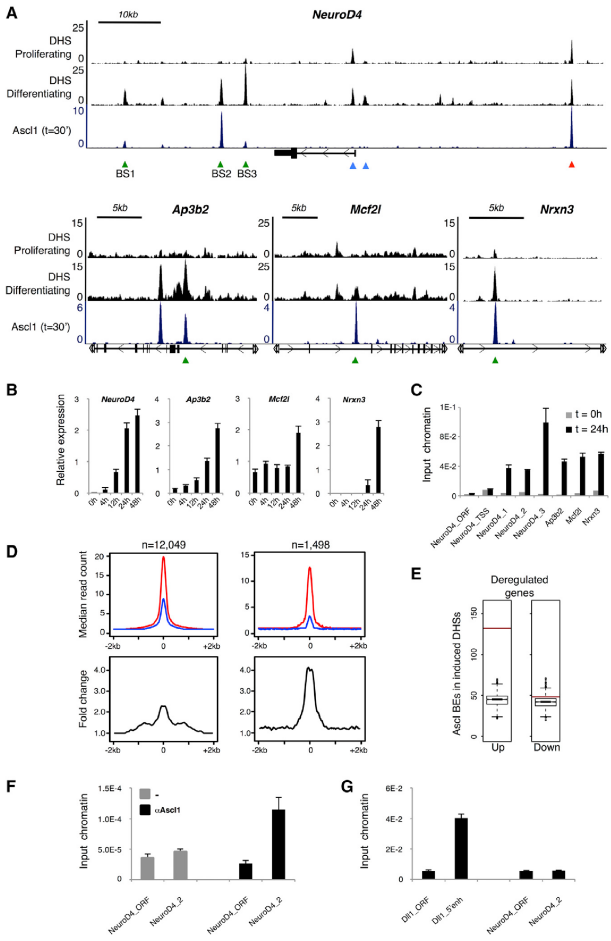

Figure 6. Ascl1 Binds Closed Chromatin and Promotes Chromatin Accessibility

(A) Visual representation of ChIP-seq and DNase-seq enrichment profiles in the vicinity of various Ascl1 targets. Examples are shown of differentiation-induced and constant DHSs localized at Ascl1 binding sites (green and red arrows, respectively) and DHSs with no apparent association with Ascl1 binding (blue arrows).

(B) Induction of expression of genes upon Ascl1-induced differentiation as quantified by real-time PCR. Data are represented as mean ± SD.

(C) FAIRE-PCR validation of differentiation-induced DHSs at Ascl1 binding sites (green arrows in A). Bars show quantification of genomic DNA obtained from proliferating and differentiating NS cells (before and 24 hr after induction, respectively). Data are represented as mean ± SD.

(D) DNase-seq signal profile at genome-wide Ascl1 BEs at t = 30 min (top left) or restricted to BEs falling within differentiation-induced DHSs (top right). Profile determined as the median read count of DNase-seq reads mapped to the 4-kb regions centered at the peak summits in proliferating (blue) and differentiating cells (red). (Bottom) Corresponding fold change for the median profiles.

(E) Ascl1 BEs located at differentiation-induced DHSs are significantly associated with clusters of activated genes (left) and not with clusters of repressed genes (right). Red bars, total number of Ascl1 BEs annotated to each set of genes; boxplots, distribution of Ascl1 BEs associations with 1,000 random sets of genes. Test data represented as box with median of test and first and third quartiles; whiskers, ±1.5 × IQR. See also Figure S6.

(F) In vivo binding of Ascl1 to the NeuroD4 regulatory region assessed by ChIP-PCR using chromatin extracted from mouse ventral telencephalon. Data are represented as mean ± SD.

(G) Chromatin structure analysis by FAIRE-PCR of *NeuroD4* and *Dll1* regulatory regions bound by Ascl1, in mouse ventral telencephalon. Data are represented as mean ± SD.

differentiation are associated with an Ascl1 BE, as not all Ascl1 BEs overlap with changes detected by DNase-seq, the vast majority of Ascl1 BEs fall within DHSs in differentiating cells (91.05% or 91.27% with $p < 10^{-18}$, at t = 30 min or t = 18 hr, respectively; Figure 5F).

To investigate the correlation between Ascl1 binding and changes in chromatin compaction on a large scale, we quantified the DNase-seq signal from both time points centered on Ascl1 peak summits. Confirming previous observations, the overall DNase-seq profile at Ascl1 peak summits is consistent with many BEs occurring in regions of already open chromatin at t = 30 min (Figure 6D). Nevertheless, a significant increase is observed when comparing profiles before and after differentiation (2.33 increase of median read count) at Ascl1 peak summits genome-wide (Figure 6D). This increase is amplified when focusing our analysis on Ascl1 peaks that fall within differentiation-induced DHSs (4.37 increase of median read count; Figure 6D). Ascl1 BEs co-localizing with differentiation-induced DHSs are strongly associated with gene activation and not with gene repression ($p < 6.8 \times 10^{-32}$; Figure 6E), targeting a total number of 98 genes during differentiation. Overall, the integration of Ascl1 location analysis, DNase-seq results, and expression profiling demonstrate Ascl1 promotes genome-wide changes in chromatin compaction at its target sites during

OPEN ACCESS
CellPress

neuronal differentiation and the appearance of new DHSs associated with activation of gene expression.

Our results are in agreement with the observation that Ascl1 can bind to nucleosomal DNA when overexpressed in fibroblasts (Wapinski et al., 2013). To verify that Ascl1 can bind to closed chromatin in a physiological context, we focused on the Ascl1-bound regulatory region identified immediately downstream the *NeuroD4* promoter (BS2 in Figure 6A), a target gene of Ascl1 in our cellular system that is not expressed in ventral telencephalon. We reasoned that binding to closed chromatin to *NeuroD4* may still occur in this embryonic brain region at the neurogenic period, even in the absence of gene expression. Indeed, we detected strong binding of Ascl1, as compared with a negative control region within the *NeuroD4* locus by ChIP-PCR in chromatin extracted from mouse ventral telencephalon (Figure 6F). However, in contrast to our previous findings with differentiating NS cells in culture, a lack of enrichment for non-nucleosomal DNA assessed by FAIRE-PCR shows this Ascl1 target site is found within closed chromatin in ventral telencephalon (Figure 6G, compare with Ascl1 site in *Dll1*). Thus, our results with the NeuroD4 regulatory region demonstrate that endogenous Ascl1 can bind to closed chromatin in an in vivo context.

Finally, we wished to analyze the accessibility of chromatin at Ascl1 target sites in the absence of Ascl1 expression. For this, we used chromatin extracted from ventral telencephalon of Ascl1-null embryos and probed Ascl1-bound regions associated with previously validated Ascl1 target genes (*Dll1*, *Fbxw7*, and *Stk33*) in this embryonic structure (Castro et al., 2006). Ascl1 null embryos show a very significant reduction of FAIRE-PCR signal relative to WT chromatin at all tested Ascl1 binding sites, as compared with pairwise control regions, which is consistent with the results above and in support of a role for Ascl1 in regulating chromatin compaction in vivo (Figure S6).

DISCUSSION

In spite of its pivotal role during neurogenesis, little is known on how Ascl1 functions to regulate gene expression. Here we investigated the reciprocal interactions between Ascl1 and the chromatin landscape when promoting the neuronal differentiation of NS cells in culture. We found that Ascl1 can bind to and promote the opening of closed chromatin regions in its native context. Below we discuss our findings and their implications to the mechanisms that govern the temporal progression of the Ascl1 transcriptional program.

Our work resulted in a fine-grained characterization of a differentiation program driven by Ascl1. In spite of displaying a wide range of biological roles, Ascl1 target genes are remarkably enriched in two categories. The first consists of genes encoding transcriptional regulators, an observation consistent with the master regulator function of Ascl1 in this developmental process. Importantly, the activation of some TFs may define feedback loops that modulate Ascl1 activity. This is the case of Id1, an inhibitor of bHLH activity that functions by sequestering E-proteins (Ruzinova and Benezra, 2003), and Cbfa2t2/MTGR1, a zinc-finger protein that has been shown to function as a co-repressor of proneural proteins, including Ascl1 (Aaker et al., 2010). Other examples, suggesting positive feedback mechanisms, are TFs previously linked to a relief of Notch inhibition by counteracting the activity of Hes1 (Hes6), repressing Notch1 (Prox1), or by as yet unknown mechanisms (MyT1) (Bellefroid et al., 1996; Gratton et al., 2003; Kaltezioti et al., 2010). These regulatory events define a less well-understood role of Ascl1 in modulating Notch signaling cell autonomously, of putative importance to the progression of differentiation. The second most prominent group of Ascl1 target genes encodes cytoskeleton-related proteins. The abundance of this group of genes is likely to result from its recognized role in many cellular functions, from signal transduction (where it may serve as a scaffold for components of signaling pathways) to cell shape change and locomotion, activities that are essential to the neurogenic differentiation program (Forgacs et al., 2004).

It was recently shown that Ascl1 promotes sequentially the proliferation and differentiation along the neuronal lineage, with the concomitant activation of distinct target genes (Castro et al., 2011). Our study focused on the transcriptional program activated by Ascl1 when promoting neuronal differentiation. Comparing the identity and molecular determinants for target gene specificity associated with both cellular functions will likely require the characterization of Ascl1 binding profile in an oscillatory versus sustained mode of expression. Nevertheless, the observation that overexpressed Ascl1 can readily access the full complement of its differentiation sites at the onset of differentiation suggests these may already be accessible to this TF in proliferating cells, an important observation in the context of the dynamics of Ascl1 function along the neuronal lineage.

It was previously shown that overexpressed Ascl1 can bind to closed chromatin in fibroblasts (as assessed by FAIRE-PCR), defining it as a pioneer TF (Wapinski et al., 2013), results that the present study validates for the first time in a neural context. Moreover, our analysis of binding of Ascl1 to the *NeuroD4* locus in ventral telencephalic progenitors that do not express this gene allowed for the dissociation between binding and opening of chromatin, revealing binding of endogenous Ascl1 to closed chromatin in vivo. Altogether, our study supports the idea that Ascl1 displays its pioneer activity when regulating gene expression in its native context.

Our analysis of chromatin states suggests that most Ascl1 binding in our differentiation model occurs within enhancer regions that are already active in proliferating NS cells as shown by their enrichment for both H3K4me1 and H3K27ac. This may be due to the fact that many genes upregulated by Ascl1 during differentiation are already expressed in proliferating NS cells. Alternatively, it may reflect the trivalent mark (H3K4me1, H3K27ac, and H3K9m3) identified at Ascl1 binding sites in various cell types permissive to Ascl1-mediated reprogramming (Wapinski et al., 2013). Most importantly, Ascl1 promotes DNase I accessibility to regions of closed chromatin at a smaller but significant number of its target sites associated with the activation of a differentiation-specific component of its transcriptional program. Our results cast light into a previously unknown function of Ascl1 and establish the first link between the chromatin landscape at Ascl1-bound regulatory regions and the temporal pattern of the Ascl1 program along the neuronal lineage. Moreover, they suggest that the hierarchical model

OPEN ACCESS
CellPress

recently proposed for the reprograming paradigm (Wapinski et al., 2013) may also be representative of the neurogenesis process and that opening of chromatin regions at Ascl1 target sites may be important to allow subsequent binding of other TFs in differentiating cells. Finally, it is tempting to speculate that the broad effect of Ascl1 in promoting chromatin accessibility described in this study will be important for the reprogramming capacity of this TF upon its ectopic expression in various cell types.

EXPERIMENTAL PROCEDURES

Plasmids and Virus Production

Ascl1-ERT2 encodes full-length mouse Ascl1 in frame with the modified ligand binding domain of the human estrogen receptor (ERT2) and an N-terminal Flag/HA tag sequence. For virus production, Ascl1-ERT2 was subcloned into pMX-IRES-GFP or pBABE-IRES-GFP-puro. Replication-incompetent retroviruses were produced from HEK293T cells transiently transfected with retroviral, viral envelope-, and VSVG-pseudotyping plasmids. Retroviral particles were concentrated from supernatant by ultracentrifugation at 90,000 *g* for 90 min. Viral titers were typically 10^5–10^6 infectious particles/ml.

Culture and Infection of NS5 Cells

NS5 cells were cultured as previously described (Conti et al., 2005) using laminin as media supplement (20 μg/ml). NS5 Ascl1-ERT2 cells were generated upon infection with pBABE-Ascl1-ERT2-IRES-GFP-puro, followed by selection in complete medium containing 1-μg/ml puromycin (Calbiochem). For differentiation, NS5 Ascl1-ERT2 cells were plated at 28,000 per cm^2 of density and induced with 50-nM 4-Hydroxytamoxifen, while reducing EGF concentration to 5 ng/ml.

Quantification of Ascl1 Protein Levels

All experiments were carried out upon approval and following the guidelines of the ethics committee of Instituto Gulbenkian de Ciência.

Quantification of Ascl1 (endogenous + Ascl1-ERT2) done by parallel immunostaining with anti-Ascl1 antibody in acutely cultured primary ventral telencephalon progenitors from E14.5 mouse embryos and NS5 Ascl1-ERT2 cells (three replicates each). A total of 939 and 751 cells for embryonic and NS5 progenitors, respectively, was imaged with identical exposure and images thresholded and normalized—mean fluorescence per cell x (mean fluorescence of all cells in picture/mean fluorescence of all cells per sample)—to define positive cells. Fluorescence intensity was measured with ImageJ.

Expression Analysis of NS5 Ascl1-ERT2 Cells

Extraction of mRNA and cDNA synthesis performed as previously described (Castro et al., 2011). Quantitative real-time PCR (qRT-PCR) was performed according to the manufacturer using SYBR Green super-mix (Quanta BioSciences) on an ABI7500 machine (Applied Biosystems). For microarray analysis, quality of total RNA from biological triplicates was assessed using Agilent Bioanalyser, and samples were processed according to the Illumina Whole-genome Gene Expression Direct Hybridization Assay Guide, using Illumina TotalPrep-96 RNA Amplification kit (Life Technologies). Quality control was performed on labeled cRNA, and 750 ng of labeled cRNA was hybridized to Mouse Ref-8v2 arrays and scanned by BeedStudio v.3.1.3 (quantile normalization with background correction). Normalization among arrays and significant analysis were performed using GeneSpring X (Agilent). Further details of data processing, including gene clustering, are described in Supplemental Information.

ChIP-seq

For Ascl1 ChIP-seq, NS5 Ascl1-ERT2 cells were fixed sequentially with 2 mM di(N-succimidyl) glutarate and 1% formaldehyde in PBS and then lysed, sonicated, and immunoprecipitated with anti-HA antibody, as previously described (Castro et al., 2011). DNA libraries were prepared from 10 ng of immunoprecipitated DNA according to the standard Illumina ChIP-seq protocol and sequenced with Illumina GAIIx. Raw reads were mapped to the mouse genome (NCBI37/mm9) with Bowtie 0.12.7 (Langmead et al., 2009). Uniquely mapped reads data (~11.5 million for both Ascl1 ChIP and input chromatin samples) were then subsampled before peak calling with MACS 1.4.1 (Zhang et al., 2008). For histone marks ChIP-seq, Ascl1-ERT2 cells were fixed in 1% formaldehyde in PBS, prepared as described above and immunoprecipitated with anti-H3K27ac and anti-H3K4me1 antibodies. Libraries were sequenced with Illumina HiSeq 2000. Raw reads were mapped as above (25 million uniquely mapped reads for all samples) and data processed with MACS 2.1.0. For chromatin state characterization, we used a Hidden Markov modeling of chromatin enrichment software—ChromHMM (Ernst and Kellis, 2012). Further details of data processing are described in Supplemental Information.

FAIRE-PCR

Chromatin preparation was done with a single fixation with 1% formaldehyde, from NS5 Ascl1-ERT2 cells, or when indicated with NS5 cells infected with a doxycycline inducible lentivirus expressing WT Ascl1 (Wapinski et al., 2013). Three rounds of phenol/chloroform extraction were followed by isopropanol precipitation of the DNA. Quantification of genomic regions was done using a standard curve generated with decross-linked input chromatin by qRT-PCR as above.

DNase-seq

DNase-seq samples from differentiating NS5 Ascl1-ERT2 cells or proliferating NS5 cells were prepared as previously described (Song et al., 2011). Libraries were generated as previously described (Boyle et al., 2008; Song and Crawford, 2010) with a slight modification to the linkers to increase ligation efficiency (Song et al., 2011) and then sequenced with Illumina GAIIx. Mapping was done as for ChIP-seq, resulting in 165.9 and 168.7 millions of unique reads for proliferating and differentiating conditions, respectively. Genomic location of DHSs was identified with MACS version 1.4.1, following a protocol described in Supplemental Information.

For oligonucleotides used in this study, see also Table S10.

ACCESSION NUMBERS

The ChIP-seq dataset for Ascl1-ERT2 (t=30') was submitted to the ArrayExpress database (www.ebi.ac.uk/arrayexpress) and is publicly available under the accession number E-MTAB-2384.

The DNase-seq datasets were submitted to the ArrayExpress database (www.ebi.ac.uk/arrayexpress) and are publicly available under the accession number E-MTAB-2270.

The ChIP-seq datasets for H3K4me1 and H3K27ac were submitted to the ArrayExpress database (www.ebi.ac.uk/arrayexpress) and are publicly available under the accession number E-MTAB-3104.

SUPPLEMENTAL INFORMATION

Supplemental Information includes Supplemental Experimental Procedures, six figures, and ten tables and can be found with this article online at http://dx.doi.org/10.1016/j.celrep.2015.02.025.

AUTHOR CONTRIBUTIONS

A.A.S.F.R. did the bioinformatics analysis. F.F.V. and D.D. designed research and performed experimental work, except electrophysiology tests performed by B.B. D.S.C. and A.A.S.F.R. wrote the manuscript, which was read and approved by all others. All other authors contributed with reagents and analytical tools.

ACKNOWLEDGMENTS

We thank Daniel Sobral and the IGC Bioinformatics Unit for expert assistance and Abdul Sesay and the NIMR high-throughput sequencing facility for ChIP-seq library preparation and sequencing. This study was funded by FCT grants

OPEN ACCESS
CellPress

(PTDC/SAU-NEU/100208/2008 and PTDC/NEU-NMC/0315/2012 to D.S.C.), Marie Curie CIG (303644 to D.S.C.), Wellcome Trust (WT095908 and WT098051 to P.F.), the European Community (FP7-223210 to P.F, L.E. and F.G.), and an FCT doctoral fellowship to F.F.V. DSC is supported by the FCT investigator program.

Received: June 2, 2014
Revised: January 14, 2015
Accepted: February 5, 2015
Published: March 5, 2015

REFERENCES

Aaker, J.D., Patineau, A.L., Yang, H.-J., Ewart, D.T., Nakagawa, Y., McLoon, S.C., and Koyano-Nakagawa, N. (2010). Interaction of MTG family proteins with NEUROG2 and ASCL1 in the developing nervous system. Neurosci. Lett. *474*, 46–51.

Alvarez-Rodríguez, R., and Pons, S. (2009). Expression of the proneural gene encoding Mash1 suppresses MYCN mitotic activity. J. Cell Sci. *122*, 595–599.

Bellefroid, E.J., Bourguignon, C., Hollemann, T., Ma, Q., Anderson, D.J., Kintner, C., and Pieler, T. (1996). X-MyT1, a Xenopus C2HC-type zinc finger protein with a regulatory function in neuronal differentiation. Cell *87*, 1191–1202.

Bergstrom, D.A., Penn, B.H., Strand, A., Perry, R.L., Rudnicki, M.A., and Tapscott, S.J. (2002). Promoter-specific regulation of MyoD binding and signal transduction cooperate to pattern gene expression. Mol. Cell *9*, 587–600.

Berninger, B., Costa, M.R., Koch, U., Schroeder, T., Sutor, B., Grothe, B., and Götz, M. (2007a). Functional properties of neurons derived from in vitro reprogrammed postnatal astroglia. The Journal of neuroscience, *27* (*32*), 8654–8664.

Berninger, B., Guillemot, F., and Götz, M. (2007b). Directing neurotransmitter identity of neurones derived from expanded adult neural stem cells. Eur. J. Neurosci. *25*, 2581–2590.

Bertrand, N., Castro, D.S., and Guillemot, F. (2002). Proneural genes and the specification of neural cell types. Nat. Rev. Neurosci. *3*, 517–530.

Borromeo, M.D., Meredith, D.M., Castro, D.S., Chang, J.C., Tung, K.-C., Guillemot, F., and Johnson, J.E. (2014). A transcription factor network specifying inhibitory versus excitatory neurons in the dorsal spinal cord. Development *141*, 2803–2812.

Boyle, A.P., Davis, S., Shulha, H.P., Meltzer, P., Margulies, E.H., Weng, Z., Furey, T.S., and Crawford, G.E. (2008). High-resolution mapping and characterization of open chromatin across the genome. Cell *132*, 311–322.

Burk, O., and Klempnauer, K.H. (1991). Estrogen-dependent alterations in differentiation state of myeloid cells caused by a v-myb/estrogen receptor fusion protein. EMBO J. *10*, 3713–3719.

Casarosa, S., Fode, C., and Guillemot, F. (1999). Mash1 regulates neurogenesis in the ventral telencephalon. Development *126*, 525–534.

Castro, D.S., Skowronska-Krawczyk, D., Armant, O., Donaldson, I.J., Parras, C., Hunt, C., Critchley, J.A., Nguyen, L., Gossler, A., Göttgens, B., et al. (2006). Proneural bHLH and Brn proteins coregulate a neurogenic program through cooperative binding to a conserved DNA motif. Dev. Cell *11*, 831–844.

Castro, D.S., Martynoga, B., Parras, C., Ramesh, V., Pacary, E., Johnston, C., Drechsel, D., Lebel-Potter, M., Garcia, L.G., Hunt, C., et al. (2011). A novel function of the proneural factor Ascl1 in progenitor proliferation identified by genome-wide characterization of its targets. Genes Dev. *25*, 930–945.

Conti, L., Pollard, S.M., Gorba, T., Reitano, E., Toselli, M., Biella, G., Sun, Y., Sanzone, S., Ying, Q.L., Cattaneo, E., and Smith, A. (2005). Niche-independent symmetrical self-renewal of a mammalian tissue stem cell. PLoS Biol. *3*, e283.

Ernst, J., and Kellis, M. (2012). ChromHMM: automating chromatin-state discovery and characterization. Nat. Methods *9*, 215–216.

Forgacs, G., Yook, S.H., Janmey, P.A., Jeong, H., and Burd, C.G. (2004). Role of the cytoskeleton in signaling networks. J. Cell Sci. *117*, 2769–2775.

Geoffroy, C.G., Critchley, J.A., Castro, D.S., Ramelli, S., Barraclough, C., Descombes, P., Guillemot, F., and Raineteau, O. (2009). Engineering of dominant active basic helix-loop-helix proteins that are resistant to negative regulation by postnatal central nervous system antineurogenic cues. Stem Cells *27*, 847–856.

Gratton, M.O., Torban, E., Jasmin, S.B., Theriault, F.M., German, M.S., Stifani, S., and Stifani, S. (2003). Hes6 promotes cortical neurogenesis and inhibits Hes1 transcription repression activity by multiple mechanisms. Mol. Cell. Biol. *23*, 6922–6935.

Imayoshi, I., Isomura, A., Harima, Y., Kawaguchi, K., Kori, H., Miyachi, H., Fujiwara, T., Ishidate, F., and Kageyama, R. (2013). Oscillatory control of factors determining multipotency and fate in mouse neural progenitors. Science *342*, 1203–1208.

Kaltezioti, V., Kouroupi, G., Oikonomaki, M., Mantouvalou, E., Stergiopoulos, A., Charonis, A., Rohrer, H., Matsas, R., and Politis, P.K. (2010). Prox1 regulates the notch1-mediated inhibition of neurogenesis. PLoS Biol. *8*, e1000565.

Karow, M., Sánchez, R., Schichor, C., Masserdotti, G., Ortega, F., Heinrich, C., Gascón, S., Khan, M.A., Lie, D.C., Dellavalle, A., et al. (2012). Reprogramming of pericyte-derived cells of the adult human brain into induced neuronal cells. Cell Stem Cell *11*, 471–476.

Kriegstein, A., and Alvarez-Buylla, A. (2009). The glial nature of embryonic and adult neural stem cells. Annu. Rev. Neurosci. *32*, 149–184.

Langmead, B., Trapnell, C., Pop, M., and Salzberg, S.L. (2009). Ultrafast and memory-efficient alignment of short DNA sequences to the human genome. Genome Biol. *10*, R25.

Littlewood, T.D., Hancock, D.C., Danielian, P.S., Parker, M.G., and Evan, G.I. (1995). A modified oestrogen receptor ligand-binding domain as an improved switch for the regulation of heterologous proteins. Nucleic Acids Res. *23*, 1686–1690.

Martínez-Cerdeño, V., Noctor, S.C., Espinosa, A., Ariza, J., Parker, P., Orasji, S., Daadi, M.M., Bankiewicz, K., Alvarez-Buylla, A., and Kriegstein, A.R. (2010). Embryonic MGE precursor cells grafted into adult rat striatum integrate and ameliorate motor symptoms in 6-OHDA-lesioned rats. Cell Stem Cell *6*, 238–250.

Natarajan, A., Yardimci, G.G., Sheffield, N.C., Crawford, G.E., and Ohler, U. (2012). Predicting cell-type-specific gene expression from regions of open chromatin. Genome Res. *22*, 1711–1722.

Ohsawa, R., Ohtsuka, T., and Kageyama, R. (2005). Mash1 and Math3 are required for development of branchiomotor neurons and maintenance of neural progenitors. J. Neurosci. *25*, 5857–5865.

Park, P.J. (2009). ChIP-seq: advantages and challenges of a maturing technology. Nat. Rev. Genet. *10*, 669–680.

Piper, J., Elze, M.C., Cauchy, P., Cockerill, P.N., Bonifer, C., and Ott, S. (2013). Wellington: a novel method for the accurate identification of digital genomic footprints from DNase-seq data. Nucleic Acids Res. *41*, e201.

Pollard, S.M., Conti, L., Sun, Y., Goffredo, D., and Smith, A. (2006). Adherent neural stem (NS) cells from fetal and adult forebrain. Cereb. Cortex *16* (*Suppl 1*), i112–i120.

Rheinbay, E., Suvà, M.L., Gillespie, S.M., Wakimoto, H., Patel, A.P., Shahid, M., Oksuz, O., Rabkin, S.D., Martuza, R.L., Rivera, M.N., et al. (2013). An aberrant transcription factor network essential for Wnt signaling and stem cell maintenance in glioblastoma. Cell Rep. *3*, 1567–1579.

Roemer, K., and Friedmann, T. (1993). Modulation of cell proliferation and gene expression by a p53-estrogen receptor hybrid protein. Proc. Natl. Acad. Sci. USA *90*, 9252–9256.

Ruzinova, M.B., and Benezra, R. (2003). Id proteins in development, cell cycle and cancer. Trends Cell Biol. *13*, 410–418.

OPEN ACCESS
CellPress

Song, L., and Crawford, G.E. (2010). DNase-seq: a high-resolution technique for mapping active gene regulatory elements across the genome from mammalian cells. Cold Spring Harbor Protoc. *2010*, pdb.prot5384.

Song, L., Zhang, Z., Grasfeder, L.L., Boyle, A.P., Giresi, P.G., Lee, B.K., Sheffield, N.C., Gräf, S., Huss, M., Keefe, D., et al. (2011). Open chromatin defined by DNaseI and FAIRE identifies regulatory elements that shape cell-type identity. Genome Res. *21*, 1757–1767.

Thurman, R.E., Rynes, E., Humbert, R., Vierstra, J., Maurano, M.T., Haugen, E., Sheffield, N.C., Stergachis, A.B., Wang, H., Vernot, B., et al. (2012). The accessible chromatin landscape of the human genome. Nature *489*, 75–82.

Vasconcelos, F.F., and Castro, D.S. (2014). Transcriptional control of vertebrate neurogenesis by the proneural factor Ascl1. Front. Cell. Neurosci. *8*, 412.

Vierbuchen, T., Ostermeier, A., Pang, Z.P., Kokubu, Y., Südhof, T.C., and Wernig, M. (2010). Direct conversion of fibroblasts to functional neurons by defined factors. Nature *463*, 1035–1041.

Wapinski, O.L., Vierbuchen, T., Qu, K., Lee, Q.Y., Chanda, S., Fuentes, D.R., Giresi, P.G., Ng, Y.H., Marro, S., Neff, N.F., et al. (2013). Hierarchical mechanisms for direct reprogramming of fibroblasts to neurons. Cell *155*, 621–635.

Wilkinson, G., Dennis, D., and Schuurmans, C. (2013). Proneural genes in neocortical development. Neuroscience *253*, 256–273.

Zaret, K.S., and Carroll, J.S. (2011). Pioneer transcription factors: establishing competence for gene expression. Genes Dev. *25*, 2227–2241.

Zhang, Y., Liu, T., Meyer, C.A., Eeckhoute, J., Johnson, D.S., Bernstein, B.E., Nusbaum, C., Myers, R.M., Brown, M., Li, W., and Liu, X.S. (2008). Model-based analysis of ChIP-Seq (MACS). Genome Biol. *9*, R137.

Cell Reports

Supplemental Information

Ascl1 Coordinately Regulates Gene Expression and the Chromatin Landscape during Neurogenesis

Alexandre A.S.F. Raposo, Francisca F. Vasconcelos, Daniela Drechsel, Corentine Marie, Caroline Johnston, Dirk Dolle, Angela Bithell, Sébastien Gillotin, Debbie L.C. van den Berg, Laurence Ettwiller, Paul Flicek, Gregory E. Crawford, Carlos M. Parras, Benedikt Berninger, Noel J. Buckley, François Guillemot, and Diogo S. Castro

Supplemental Data

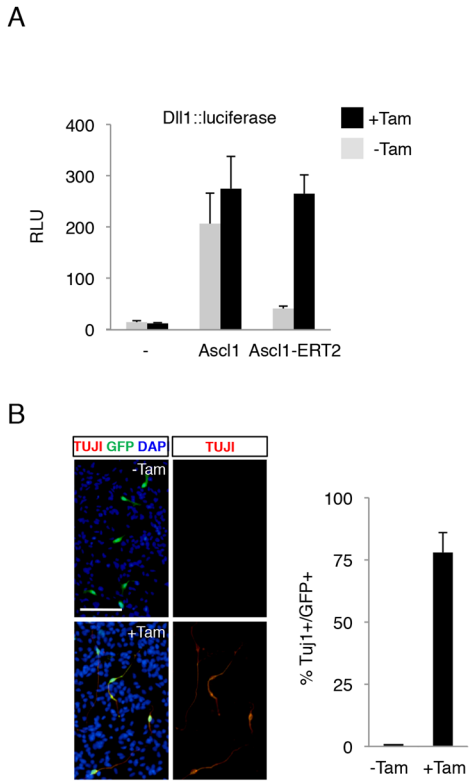

Figure S1. Generation of an inducible version of Ascl1 (related to Figure 1).
A. Induction of a *Dll1* enhancer by Ascl1 and Ascl1-ERT2 in a reporter gene assay in transfected NS5 cells, in the presence and absence of tamoxifen.
B. Differentiation of NS5 cells transduced with an adenovirus vector expressing Ascl1-ERT2, assessed by expression of the neuronal marker TUJ1. Infected cells are labeled with GFP (green). Values: mean±SD. Scale bar: 200μm.

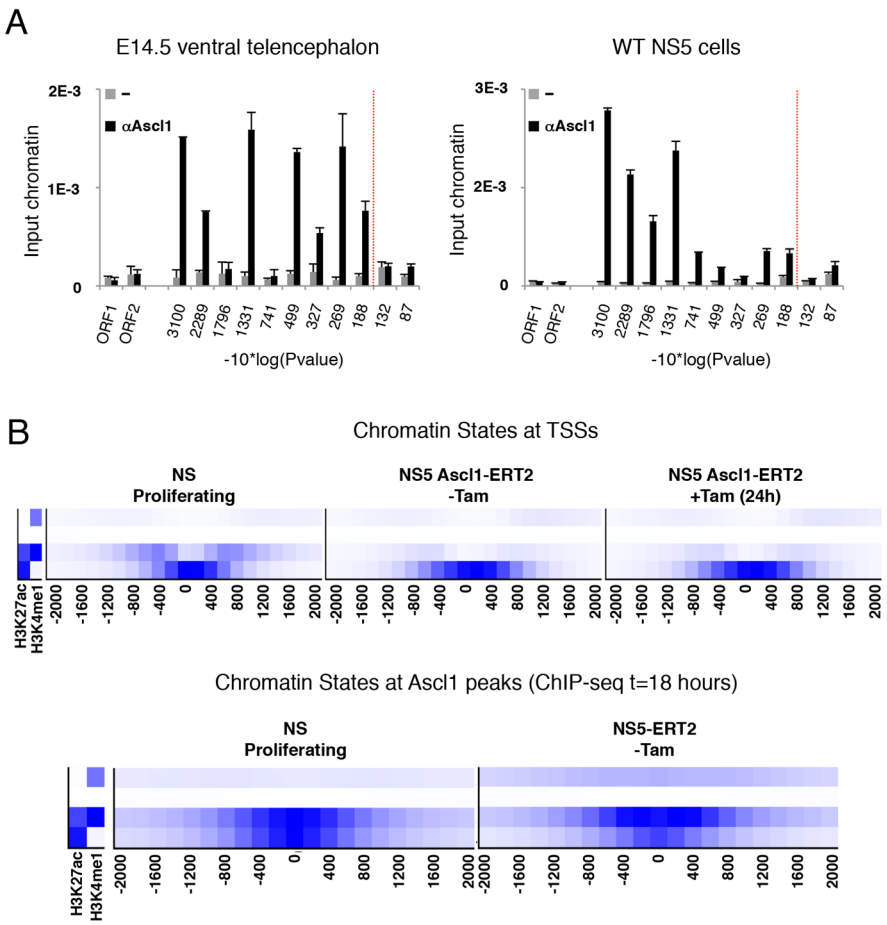

Figure S2. ChIP-PCR validation of genome-wide Ascl1 binding and characterization of chromatin states by ChromHMM in NSCs (related to Figure 2).

A. Validation of Ascl1-ERT2 binding events at various P values by ChIP-PCR against wild type Ascl, using chromatin extracted from embryonic E14.5 ventral telencephalic progenitors (left), and wild type proliferating NS5 cells (right). Red line marks threshold limit for validation ($P<10^{-18}$). Values: mean±SD.

B. *Top*: Heat maps of chromatin states for H3K27ac and H3K4me1 within ±2kb of TSSs in proliferating NS cells (*NS*, data sets from Creyghton, 2010; and Stadler, 2011) and non-induced NS5 Ascl1-ERT2 cells (*-Tam*), or in differentiating NS5 Ascl1-ERT2 cells 24 hours after induction (*+Tam*). *Bottom*: Heat maps of chromatin states for H3K27ac and H3K4me1 within ±2kb of Ascl1-ERT2 (peaks at t=18h), determined by ChromHMM in proliferating NS cells (*NS*, data sets from Creyghton, 2010; and Stadler, 2011) and in non-induced NS5 Ascl1-ERT2 cells (*-Tam*).

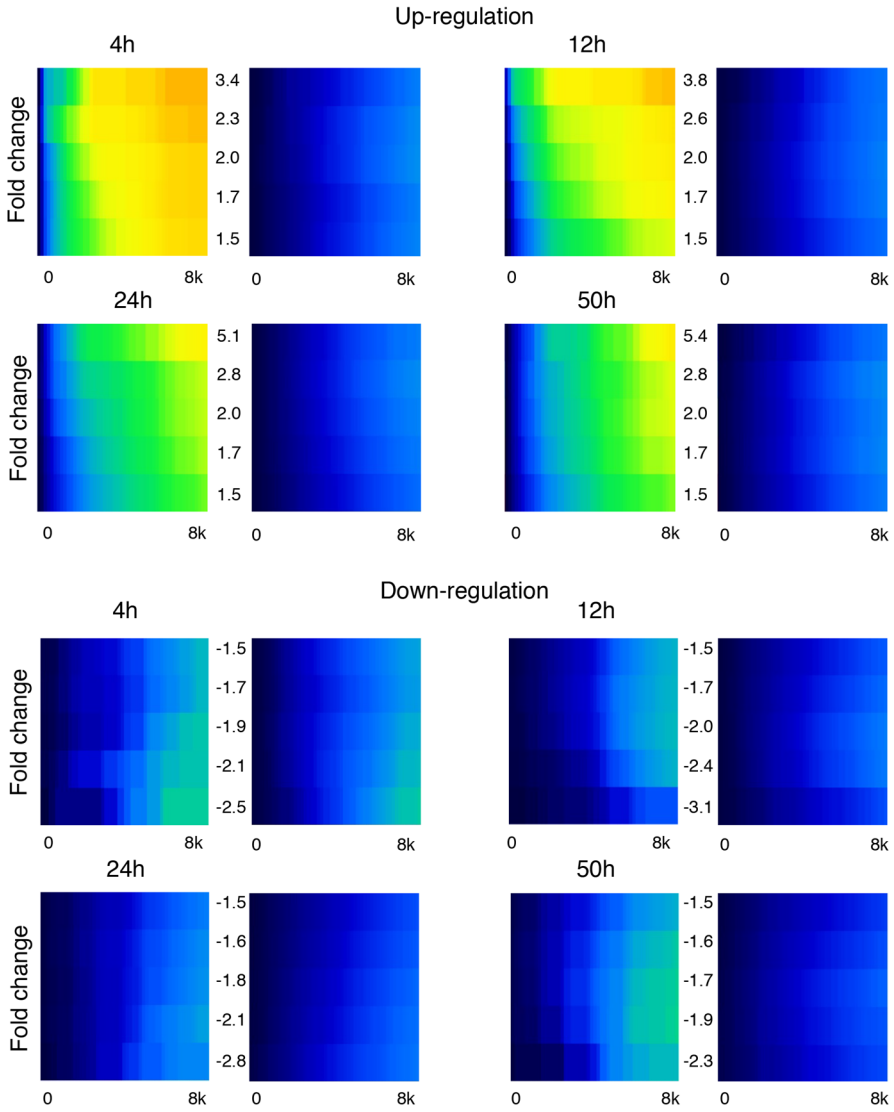

Figure S3. Ascl1 functions as a transcriptional activator at a genome-wide level (related to Figure 3). Heat maps displaying the cumulative fraction of deregulated genes at 4, 12, 24, and 50 hours after induction of differentiation. Bins defined as in main figure 3: deregulated transcripts (up – top panels; down – bottom panels) are divided in bins of equal size, with indicated fold change cutoffs. Ascl1 BEs are divided in bins of 166 peaks, with increasing P value. As control, comparisons were made against 100 randomized sets of binding events (right panels, where the average fraction is shown).

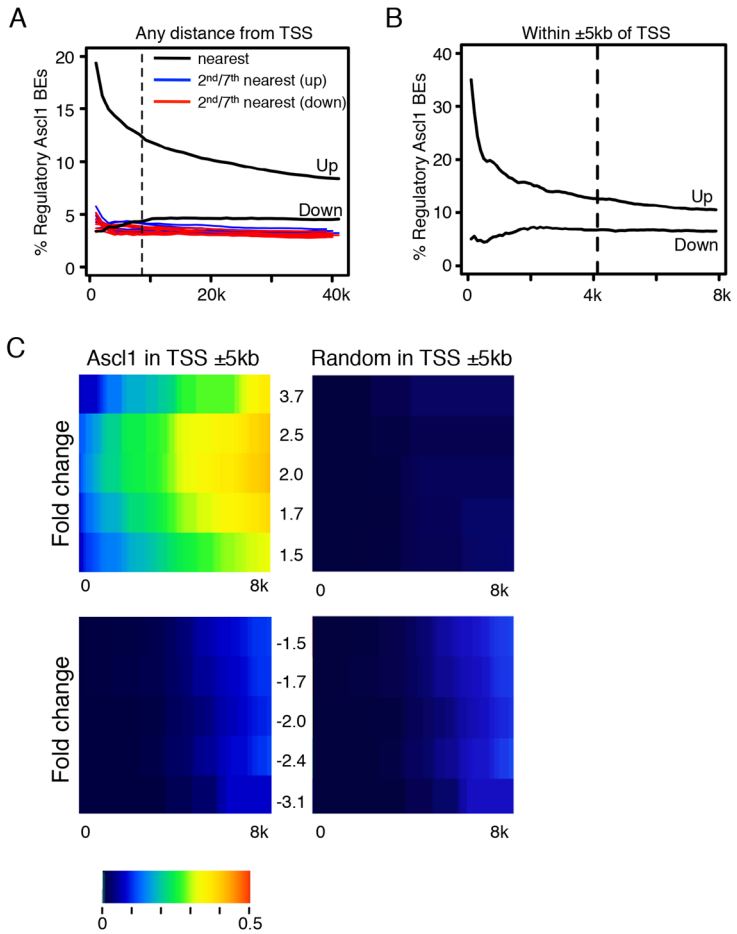

Figure S4. Integration of binding and regulation data using alternative annotation methods (related to Figure 3).

A. Fraction of Ascl1 BEs considered regulatory when peaks are annotated to the nearest TSSs (black), or 2nd to 7th nearest TSSs (red/blue).

B. Fraction of Ascl1 BEs considered regulatory when peaks are annotated to the nearest TSSs (maximum 5kb distance). Bin=100 BEs, dashed line: $P< 10^{-25}$.

C. Heat maps displaying the cumulative fraction of deregulated genes that are directly bound by Ascl1 at 12 hours after induction of differentiation (nearest gene annotation with maximum 5kb distance). Bins defined as in main figure 3: deregulated transcripts (up – top panels; down – bottom panels) are divided in bins of equal size, with indicated fold change cutoffs. Ascl1 BEs are divided in bins of 166 peaks, with increasing P value. As control, comparisons were made against 100 randomized sets of binding events (right panels, where the average fraction is shown).

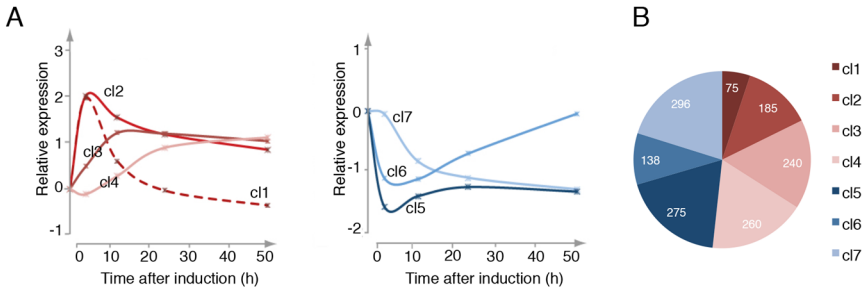

C

Cluster 2	P value
Cell communication	1.37E-3
Signal transduction	2.10E-3
Phospholipid metabolic process	2.72E-3
Small GTPase regulator activity	9.30E-4

Cluster 3	
Transcription	2.09E-5
Transcription factor activity	1.56E-4
Establishment or maintenance of chromatin architecture	7.55E-3
Transcription cofactor activity	7.02E-3
Notch signaling pathway	1.90E-3

Cluster 4	
Structural constituent of cytoskeleton	3.05E-5
Notch signaling pathway	1.29E-4
Nervous system development	3.92E-4
Developmental process	7.88E-4
Transmembrane receptor protein kinase activity	2.10E-3
Axon guidance mediated by Slit/Robo	4.62E-3

Figure S5. Temporal patterning of the Ascl1 transcriptional program (related to Figure 3).
A. Average profile of temporal clusters of genes associated with gene activation (red, left) or repression (blue, right).
B. Composition of clusters according to number of genes.
C. Enrichment of Gene Ontology biological process terms, amongst direct Ascl1 target genes that belong to clusters 2-4, and associated P value.

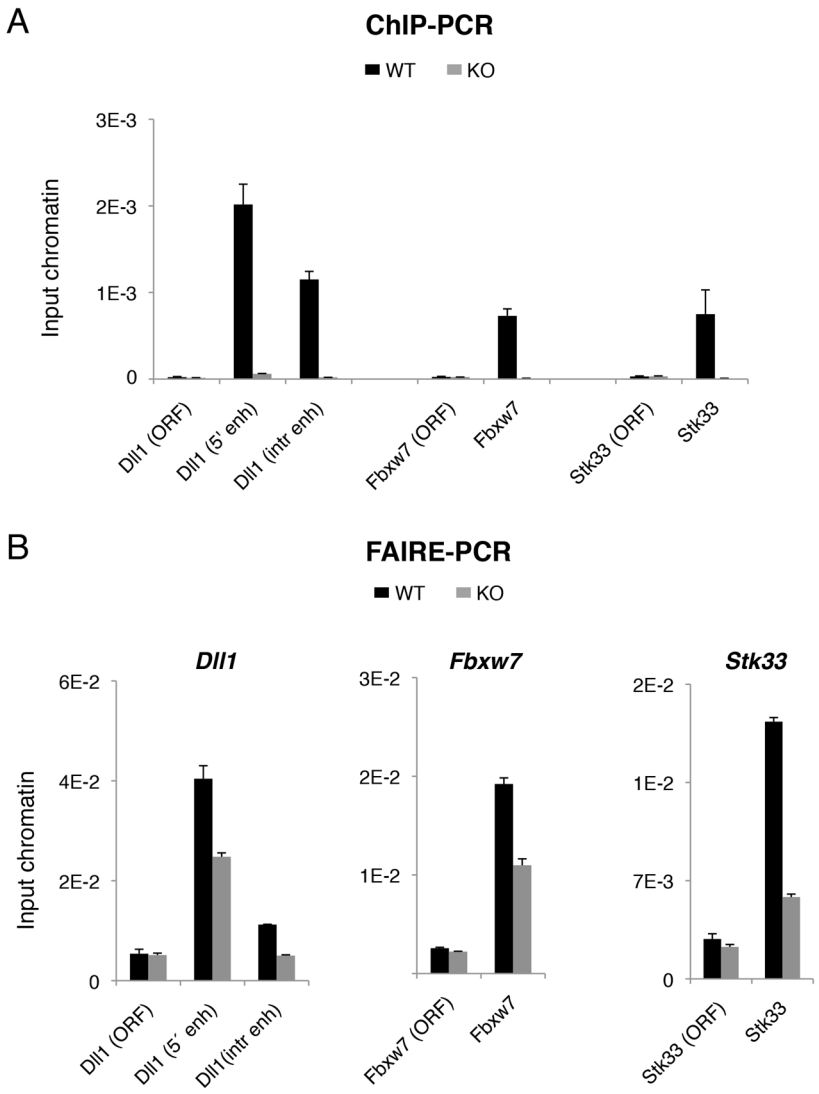

Figure S6. Analysis of Ascl1 bound regions by ChIP- and FAIRE-PCR in chromatin from Ascl1 null embryos (related to Figure 6).
A. ChIP-PCR with αAscl1 for Ascl1-bound regions associated with *Dll1*, *Fbxw7*, and *Stk33* genes, using chromatin extracted from ventral telencephalon of E14.5 wild type (WT) or Ascl1 null embryos (KO). Values: mean±SD.
B. Quantification of nucleosome-depleted chromatin by FAIRE-PCR at Ascl1-bound regions, using chromatin extracted from ventral telencephalon of E14.5 wild type (WT) or Ascl1 null embryos (KO).
In parallel with Ascl1-bound sites, one negative control region within the gene open reading frame (ORF) was tested for each locus. Values: mean±SD.

Supplemental Tables

S1: Expression profiling data set, related to Figure 1

S2: List of Ascl1 binding events at t=18h, related to Figure 2

S3: Segregation of deregulated genes in clusters, related to Figure 3

S4: List of Ascl1 direct targets, related to Figure 3

S5: DHSs in proliferating NS, related to Figure 5

S6: DHSs in differentiated NS, related to Figure 5

S7: DHS specific to differentiated NS, related to Figure 5

S8: Occupied sites identified by DGF, related to Figure 5

S9: List of Ascl1 binding events at t=30', related to Figure 4

S10: Oligonucleotides used in this study, related to Experimental Procedures

Datasets generated in this study

The dataset ChIP-seq Ascl1-ERT2 (t=30') was submitted to the ArrayExpress database (www.ebi.ac.uk/arrayexpress) and are publicly available under the accession number E-MTAB-2384.

The DNase-seq datasets were submitted to the ArrayExpress database (www.ebi.ac.uk/arrayexpress) and are publicly available under the accession number E-MTAB-2270.

The datasets ChIP-seq for H3K4me1 and H3K27ac were submitted to the ArrayExpress database (www.ebi.ac.uk/arrayexpress) and are publicly available under the accession number E-MTAB-3104.

Publicly available datasets used

ChIP-seq Ascl1-ERT2, t=18h: Walpinski OL et al, SRX323564, GSM1187228, GSE43916, PMID:24243019

ChIP-seq Ascl1-ERT2, input: Walpinski OL et al, SRX323563, GSM1187227, GSE43916, PMID:24243019

ChIP-seq H3K4me1: Stadler, M.B. et al. SRX095620, PMID: 22170606.

ChIP-seq H3K27ac: Creyghton, M.P. GSE24164, GSM94585, PMID: 21106759.

Supplemental Experimental Procedures

Reporter gene assays

Reporter gene assays were performed as previously described (Castro et al., 2006), after transfection with Lipofectamine Plus (Invitrogen). DeltaM-Luc encodes the Ascl1 specific enhancer of the mDll1 gene in frame with luciferase and beta-Glob minimal promoter (Castro et al., 2006).

List of primary antibodies used

Primary antibodies used were against Tuj1 (MMS-435P, Babco), Gadd65/67 (G5163, Sigma), GFP (ab16901, Chemicon), Ascl1 (556604, BD Pharmingen), HA-tag (ab1424, Abcam), H3K27ac (ab4729, Abcam) and H3K4me1 (ab8895, Abcam).

ChIP-PCR

Chromatin extractions and ChIP-PCR for Ascl1 in NS5 or embryonic progenitors was performed as previously described (Castro et al., 2011)

Electrophysiology studies

Electrophysiological properties of neurons derived from NS5-Ascl1-ERT2 cells were analyzed 14 d following onset of differentiation. Single perforated patch-clamp recordings were performed at room temperature with amphotericin-B (Calbiochem) for perforation (Heinrich et al., 2010). Micropipettes were made from borosilicate glass capillaries (Garner, Claremont, CA, USA). Pipettes were tip-filled with internal solution and back-filled with internal solution containing 200 μg/mL amphotericin-B. The electrodes had resistances of 2–2.5 MΩ. The internal solution contained 136.5 mM K-gluconate, 17.5 mM KCl, 9 mM NaCl, 1 mM $MgCl_2$, 10 mM HEPES, and 0.2 mM EGTA (pH 7.4) at an osmolarity of 300 mOsm. The external solution contained 150 mM NaCl, 3 mM KCl, 3 mM $CaCl_2$, 2 mM $MgCl_2$, 10 mM HEPES, and 5 mM glucose (pH 7.4) at an osmolarity of 310 mOsm. The recording chamber was continuously perfused with external solution at a rate of 0.5 mL/min. GFP-positive cells were visualized with an epifluorescence microscope (Axioskop2, Carl Zeiss) equipped with the appropriate filter sets. Digital pictures of the recorded cells were acquired using a digital camera (AxioCam, Carl Zeiss). Signals were sampled at 10 kHz with an Axopatch 200B patch-clamp amplifier (Axon Instruments, Foster City, CA, USA), filtered at 5 kHz and analyzed with Clampfit 9.2 software (Axon Instruments). For assessing a cell's excitability, cells received hyper- and depolarizing step-current injections in current clamp mode.

Expression profiling data analysis

Data analysis was performed using GeneSpring X software (Agilent). Normalization was done as follows: (i) Threshold raw signals were set to 1.0. (ii) 75th percentile normalization was chosen as normalized algorithm. (iii) Baseline was transformed to median of all samples. For significance analysis, one-way ANOVA with subsequent P value correction by Benjamini-Hochberg post-hoc correction were used. Significantly de-regulated probes were defined as probes with a corrected P value ≤0.05 and a fold change ≥1.5 relative to non-induced cells (t=0) for at least one time point in a volcano plot analysis. To assign probe sets to genes, probe coordinates previously published (Barbosa-Morais et al., 2010) were used, after annotation to the corresponding gene using ENSEMBL mm9/NCBI37 genome assembly annotation data.

Clustering of regulated genes

In order to separate distinct sets of genes with different kinetics, fuzzy c-means clustering was performed, an algorithm that relies on the same basic principles of k-means clustering. Different to K-means clustering however, fuzzy c-means does not separate entities into different clusters but instead assigns membership values for each cluster. Before clustering of expression data, variance stabilization transformation on quantile normalized “per probe” BeadStudio-output data was performed. Data for significantly deregulated probes were extracted and Z-normalized using the R/Bioconductor packages *beadarray*, *mfuzz* and *clValid*. Optimal number of clusters was pre-defined by calculating inter-cluster as well as intra-cluster connectivity of entities for a total

number of clusters ranging from 1 to 20 and chose the cluster number with the smallest intra-cluster/inter-cluster-connectivity ratio. Per-probe data was then clustered using the fuzzy c-means algorithm implemented in the cfuzz-package (parameters: number of clusters=7, fuzziness coefficient=1-25). Per-probe data was then collapsed into per-gene data using the mean membership-coefficient per cluster and gene.

Motif search and Gene Ontology analyses

We have used CisFinder (Sharov and Ko, 2009) in order to identify motifs enriched in the vicinity of Ascl1 peak summits and in DHSs. Searches were run against a control background of 100 bp genomic regions located 3kb upstream input regions, using default parameters. Gene ontology analysis of gene clusters was performed using the Panther classification system (http://www.pantherdb.org), using genes represented in Mouse Ref-8 v2 array as reference and default parameters. In addition, cluster 4 was further analyzed with GOToolBox, (http://genome.crg.es/GOToolBox/), using Hypergeometric test and the same reference control.

ChIP-seq data analysis and integration

Sequenced reads were processed after mapping with SAMTools for format conversion and removal of PCR duplicates (Li et al., 2009). Ascl1-ERT2 data sets were subsampled where necessary to balance each other for better comparison and peak-calling accuracy (Picard tools, http://picard.sourceforge.net/). Peaks for each sample were called against the input using MACS 1.4.1 (MACS 2.1.0 for histone datasets), with P value cutoff

at 10^{-10} (Zhang et al., 2008). Subsampling of the data sets confirmed that peak calling saturation was achieved with approximately 90% of sequenced reads. Peaks were then annotated to the nearest TSS using PeakAnalyzer 1.4 (Salmon-Divon et al., 2010), and annotated from 2nd to 7th nearest TSS with GREAT (McLean et al., 2010). Peak overlap with expression or DHS data calculated and plotted as heat maps with R/Bioconductor packages "genomeIntervals", "gplots", and in-house developed scripts [5,6,7]. Calculation of P values for the association between binding events and each cluster of deregulation was performed by sampling the total number of genes represented in the microarray 1000 times and assuming a normal distribution. Analysis of regions within DHSs protected from cleavage for high-resolution prediction of specific binding sites occupied by TFs at DHSs was performed with the Digital Genomic Footprinting algorithm Wellington (Piper et al., 2013).

DNase-seq data analysis and integration

Sequenced reads of 20bp for both conditions, proliferating and differentiating cells, were processed as for ChIP-seq, except subsampling. DHSs for each sample were defined with MACS 1.4.1 (P value cutoff at 10^{-5}) by extending mapped reads in 60bp as an estimation for the maximum distance between two nucleosomes (linker DNA). DHS annotation and overlap with expression data and clusters of deregulated genes were performed as described for ChIP-seq.

Density plots

Overlapping (minimum 1 bp) and non-overlapping genomic regions between datasets were determined using BEDTools (Quinlan and Hall, 2010). ChIP-seq

and DNase-seq normalized tag signals were calculated using a 10bp sliding window over the ± 2kb region around each peak summit to generate the occupancy profiles (in-house developed algorithm). These were plotted as heat maps of signal density using R/Bioconductor packages (http://www.R-project.org/ and http://CRAN.R-project.org/package=gplots) or used to determine the median of occupancy around peak summits.

Supplemental References

Barbosa-Morais, N.L., Dunning, M.J., Samarajiwa, S. a, Darot, J.F.J., Ritchie, M.E., Lynch, A.G., and Tavaré, S. (2010). A re-annotation pipeline for Illumina BeadArrays: improving the interpretation of gene expression data. Nucleic Acids Res. *38*, e17.

Castro, D.S., Skowronska-Krawczyk, D., Armant, O., Donaldson, I.J., Parras, C., Hunt, C., Critchley, J. a, Nguyen, L., Gossler, A., Göttgens, B., et al. (2006). Proneural bHLH and Brn proteins coregulate a neurogenic program through cooperative binding to a conserved DNA motif. Dev. Cell *11*, 831–844.

Castro, D.S., Martynoga, B., Parras, C., Ramesh, V., Pacary, E., Johnston, C., Drechsel, D., Lebel-Potter, M., Garcia, L.G., Hunt, C., et al. (2011). A novel function of the proneural factor Ascl1 in progenitor proliferation identified by genome-wide characterization of its targets. Genes Dev. *25*, 930–945.

Li, H., Handsaker, B., Wysoker, A., Fennell, T., Ruan, J., Homer, N., Marth, G., Abecasis, G., and Durbin, R. (2009). The Sequence Alignment/Map format and SAMtools. Bioinformatics *25*, 2078–2079.

McLean, C.Y., Bristor, D., Hiller, M., Clarke, S.L., Schaar, B.T., Lowe, C.B., Wenger, A.M., and Bejerano, G. (2010). GREAT improves functional interpretation of cis-regulatory regions. Nat. Biotechnol. *28*, 495–501.

Piper, J., Elze, M.C., Cauchy, P., Cockerill, P.N., Bonifer, C., and Ott, S. (2013). Wellington: a novel method for the accurate identification of digital genomic footprints from DNase-seq data. Nucleic Acids Res. *41*, e201.

Quinlan, A.R., and Hall, I.M. (2010). BEDTools: a flexible suite of utilities for comparing genomic features. Bioinformatics *26*, 841–842.

Salmon-Divon, M., Dvinge, H., Tammoja, K., and Bertone, P. (2010). PeakAnalyzer: genome-wide annotation of chromatin binding and modification loci. BMC Bioinformatics *11*, 415.

Sharov, A. a, and Ko, M.S.H. (2009). Exhaustive search for over-represented DNA sequence motifs with CisFinder. DNA Res. *16*, 261–273.

Zhang, Y., Liu, T., Meyer, C. a, Eeckhoute, J., Johnson, D.S., Bernstein, B.E., Nusbaum, C., Myers, R.M., Brown, M., Li, W., et al. (2008). Model-based analysis of ChIP-Seq (MACS). Genome Biol. *9*, R137.